FATIGUE OF GLASS REINFORCED PLASTIC PIPES AND JOINTS FOR OFFSHORE APPLICATIONS

A thesis submitted in accordance with the requirements of
the University of Newcastle upon Tyne
for the Degree of Doctor in Philosophy

by

Fang Zong Hu

February 1997

To Xiaotong

PREFACE

This dissertation presents the results of research studies carried out in the Department of Mechanical, Materials and Manufacturing Engineering of the University of Newcastle upon Tyne between June 1992 and July 1995. The content is original, except where specific reference is made to the work of others, and includes nothing which is the outcome of work done in collaboration.

No part of this dissertation has been submitted for a degree at any other university.

Fang Zong HU

Department of Mechanical,
Materials and Manufacturing
Engineering
University of Newcastle upon Tyne

February 1997

ABSTRACT

In this thesis the static and fatigue characteristics of glass filament wound plastic pipes and joints are examined by experiments and numerical analysis. A hydraulic fatigue test rig, capable of exerting static or cyclic pressures of up to 70 MPa, was designed and built to enable pressure tests to be carried out on glass reinforced epoxy and glass reinforced vinyl ester composite pipes incorporating various joints. Static weepage and burst tests were performed on tubular specimens with and without rubber liners to determine their weepage and burst strengths under internal hydraulic pressure and to investigate the influence of the joints.

Fatigue weepage tests were performed to determine the fatigue life and failure modes of glass fibre/epoxy and glass fibre/vinyl ester pipes and joints. For each material system, three types of specimen were tested. These were plain pipes, pipes with coupler-bonded joints (or laminate joints in the case of vinyl ester resin based pipes) and pipes with spigot/socket bonded joints. All specimens were commercial products with nominal diameters of two inches (50 mm). A family of curves showing pressure versus life was obtained. It was observed that weepage mostly occurred close to the pipe joints when pipes were subjected to internal pressure. Optical microscopy was used to investigate the damage initiation and propagation mechanisms in the specimens after testing.

Finally, two-dimensional and three-dimensional finite element analyses were carried out to calculate the stress and strain distributions, to predict the strength, to interpret the experimental results and to examine the failure modes of the specimens. Ply-by-ply stress analysis and the Tsai-Wu failure criterion were employed for the strength prediction.

ACKNOWLEDGEMENTS

I first would like to thank British Gas plc, Engineering Research Station, for providing financial support for this project. I would also like to thank Ameron, of the Netherlands, and Sarplast, of Italy, for supplying the GRP pipes and joints.

In particular, I would like to thank my supervisor, Professor A.G. Gibson, for his guidance during the course of this research. I would also like to thank Dr. P.J. Boothby and Dr. P.S. Hill of the Engineering Research Station of British Gas plc for their helpful discussions and advice.

I am grateful to Dr. D. Foster and Dr. B. Keneghan for reading the draft thesis and their helpful suggestions.

Finally, the friendship and encouragement received from my colleagues in the Centre for Composite Materials Engineering at the University of Newcastle upon Tyne are gratefully acknowledged, and many thanks are due to the technical staff for their support.

CONTENTS

LIST OF SYMBOLS AND ABBREVIATIONS

C01,C02,...	Codes for coupler connected pipe specimens in Chapter 5.
CFRP	Carbon fibre reinforced plastics.
e_c	Elastic tensile static failure strain of a composite.
e_m	Fatigue strain limit of matrix.
F_{1t}, F_{2t}, F_{3t}	Tensile strength of unidirectional lamina in principal material directions.
F_{1c}, F_{2c}, F_{3c}	Uniaxial compressive strengths of unidirectional lamina in principal material directions.
f_{12}, f_{13}, f_{23}	Interaction coefficients in the Tsai-Wu failure criterion.
FRP	Fibre reinforced plastics.
GFRP	Glass fibre reinforced plastics.
GRE	Glass reinforced epoxy.
GRP	Glass reinforced plastics.
GRVE	Glass reinforced vinyl ester.
J01,J02,...	Codes for socket/spigot connected pipe specimens in Chapter 5.
N	Number of load cycles.
P	Internal pressure.
P01,P02,...	Codes for plain pipe specimens in Chapter 5.
R	Ratio of the minimum load to the maximum load of a constant amplitude fatigue loading.
S	Fatigue strength.
S_{12}, S_{13}, S_{23}	Shear strengths of unidirectional lamina in material principal material directions.
S_A	Stress amplitude.
S_E	Fatigue strength.
S_M	Mean stress.
S_U	Static ultimate strength.
UEWS	Ultimate elastic wall stress.
VB01,VB02,...	Codes for vinyl ester based socket/spigot bonded pipe specimens in Chapter 6.
V_f	Fibre volume fraction.
VL01,VL02,...	Codes for vinyl ester based laminate jointed pipe specimens in Chapter 6.
V_m	Matrix volume fraction.
VP01,VP02,...	Codes of vinyl ester based plain pipe specimens in Chapter 6.
W_f	Fibre weight fraction.
ΔT	Temperature change.
$\Delta\sigma$	Stress range.
ρ	Specific gravity of the pipe wall material.
ρ_f	Specific gravity of glass fibre.
θ	Filament wound angle to the pipe axis.
σ_t	Transverse stress in unidirectional lamina.
τ	Shear stress.

LIST OF TABLES

LIST OF FIGURES

Figure 7.29 Suggested modification for socket/spigot (taper to taper) adhesively bonded joint.

Figure 7.30 Shear stress distributions in the adhesive layers of the socket/spigot joints with or without modification.

CHAPTER ONE

INTRODUCTION

Glass fibre reinforced plastic (GRP) materials are now well-established in certain areas of the marine, oil, chemical and process industries. Their advantages include high corrosion resistance, low weight, low maintenance costs, long service life and easy installation compared to traditional metallic materials [1-5]. The most commonly used composite components are GRP pipes and fittings, which can transport a variety of fluids [3-9].

In recent years, composite materials have attracted considerable interest within the offshore industry, in particular for applications on platform topsides [10-17]. Initially, water pipes for fire-fighting systems were the main area of applications. A more extensive use of these materials has been hindered by the lack of documentation relevant to offshore applications. Fatigue, impact and fire performance are the main properties which need to be assessed.

Since all structures are subjected to varying loads under normal working conditions, fatigue is a common cause of damage and failure during service. Designing against fatigue failure and predicting fatigue life are difficult and complex processes due to the many, and often not well-understood, influencing parameters. Fatigue behaviour can be influenced by microstructure and material properties, dimensions and geometry, production aspects, loading conditions and load history, environment and lastly by the interaction of all these parameters. To determine the influence of these parameters on the fatigue behaviour of

materials and structural components, laboratory tests on small standard specimens and large scale structural components must be undertaken.

Research on the fatigue performance of advanced composites began at the end of the 1960's, soon after their introduction, with glass, carbon and boron fibre composites [18-20]. These early works served as a basis for the later understanding of the complex fatigue behaviour of polymer matrix composites. A number of materials and testing parameters were studied during these early investigations, and it was soon recognised that carbon fibre composites had an excellent fatigue behaviour with almost flat stress-life curves and a low strength degradation rate. However, glass fibre composites, which have a lower modulus, had a relatively poor fatigue performance characterised by steeper stress - life curves and higher strength degradation rates. With the advent of more effective non-destructive and destructive testing methods it became possible to understand basic damage mechanisms and to assess damage development. This resulted in a better understanding of the different fatigue behaviours of carbon fibre composites and glass fibre composites.

In this thesis, Chapter 2 gives a description of the materials, manufacture and properties of GRP pipes and joints, and Chapter 3 reviews the current understanding of fatigue performance and fatigue mechanisms in composite materials and structures. This review concentrates on the most common reinforcing fibre materials, glass and carbon, when used in organic resin matrices. Chapter 4 describes the main experimental techniques utilised in the present work. Chapter 5 presents the results of static and fatigue tests on glass reinforced epoxy pipes and joints. Chapter 6 describes the experimental study of glass reinforced vinyl ester pipes and joints. At the end of Chapter 6, there is a discussion and comparisons are made between the experimental results for the two material systems.

Chapter 7 presents the results of finite element analyses on the specimens tested. Finally, Chapter 8 draws some conclusions from this research and makes suggestions for future work.

REFERENCES

[1] Smith,C.S., Design of Marine Structures in Composite Materials, Elsevier Applied Science, 1990.

[2] Kelly,J., Spero,A., Dorr,J. and Corona,K., Development of Organic Matrix Composites for Transport, Aircraft, Marine and Civil Structures, Proc. of Ninth Int. Conf. on Composite Materials (ICCM/9), Vol.VI, pp.283-290, Madrid, 12-16 July, 1993.

[3] Frost,S.R. and Cervenka,A., Glass Fibre Reinforced Epoxy Matrix Filament Wound Pipes for Use in the Oil Industry, Proc. of Ninth Int. Conf. On Composite Materials, Vol.IV, pp.63-73, Madrid, 12-16 July, 1993.

[4] Wilhelm,G.F. and Schab,H.W., Glass Reinforced Plastic (GRP) Piping for Shipboard Applications, Naval Engineers Journal, Vol.89, No.2, 1977, pp.139-159.

[5] Glass Reinforced Plastic Vessels and Pipework for the Chemical and Process Industries, A joint one day symposium sponsored by UMIST, the Institution of Mechanical Engineers and the Institution of Chemical Engineers, UMIST, 22 Sept. 1983.

[6] Eckold,G.C., A Design Method for Filament Wound GRP Vessels and Pipework, Composites, Vol.16, No.1, 1985, pp.41-47.

[7] Eckold,G.C., A Performance-Based Design Methodology for Glass-Reinforced Plastic Pipework and Fittings, Proceedings of the Institution of Mechanical Engineers, Part E: Journal of Process Mechanical Engineering, Vol.209, No.E1, 1995, pp.41-50.

[8] Grim,G.C., Shipboard Use of GRP Pipe - a Uuser's Experience, Conference on Maritime and Offshore Use of Fibre Reinforced Composites, 2nd and 3rd June 1992, Gateshead, England.

[9] Cheremisinoff, N. P. and Cheremisinoff, P. N., FRP Pipe Products and Applications, Chapter 3, Fiberglass-Reinforced Plastics Deskbook, Ann Arbor Science Publishers Inc., 1983.

[10] Gibson, A.G., Composite Materials in the Offshore Industry, Metals and Materials, Vol.5, No.10, 1989, pp.590-594.

[11] Gibson, A.G., Composites in Offshore Structures, Composite Materials in Marine

Structures, Volume 2: Practical Considerations, Edited by Shenoi,R.A. and Wellicome,J.F., Cambridge University Press, 1993, pp.199-226.

[12] UKOOA GRP Work Group, Marinetech NW Programme, The Cost Effective Use of Fibre Reinforced Composites Offshore, Progress Reports, 1995.

[13] Ciaraldi,S.W., Safety Philosophy for Use of Composite Materials Offshore, pp.319-326; Composite Materials for Offshore Operations: Proceedings for the First International Workshop, Houston, Texas, October 26-28, 1993, NIST Special Publication 887, edited by S.S.Wang and D.W.Fitting.

[14] McDonnell,P. and McNamara,J.F., Evaluation of GRP Composite Pipelines for High Performance Offshore Applications, Key Engineering Materials, Vol.99-1, 1995, pp.11-18.

[15] Grove,S., (ed.), Fibre Reinforced Plastics Offshore. A Introduction to Applications, Materials and Manufacture. Advanced Composites Manufacturing Centre, Polytechnic South west, Sept. 1991.

[16] Boothby, P.J., Glass Reinforced Plastics for Offshore Topside Sea Water Pipework - The Current Position, Report, British Gas Engineering Research Station, 1991.

[17] Medlicott,P.A.C., The Role of High Performance Composites in Oil Industry Applications Offshore, Conference on Maritime and Offshore Use of Fibre Reinforced Composites, 2nd and 3rd June 1992, Gateshead, England.

[18] Boller, K.H., Fatigue Characteristics of RP Laminates Subjected to Axial Loading, Modern Plastics, Vol.41, 1964, pp.145-188.

[19] Owen, M.J., Smith, T.R. and Dukes, R., Fatigue of Glass-Reinforced Plastics, with Special Reference to Fatigue, Plastics and Polymers, Vol.37, No.129, 1969, pp.227-233.

[20] Dew-Hughes, D. and Way, J.L., Fatigue of Fibre-Reinforced Plastics: A Review, Composites, Vol.4, No.4, 1973, pp.167-173.

CHAPTER TWO

GRP PIPES AND JOINTS

2.1 GRP PIPES AND THEIR MANUFACTURE

Glass Reinforced Plastics (GRP) are composite materials which comprise a polymeric matrix reinforced with glass fibres. Methods of composite manufacture include hand lay-up, spray-up, compression moulding, filament winding, centrifugal casting, pultrusion, resin injection moulding and transfer moulding. Filament winding is the method most commonly used to produce GRP pipes, one reason for this being the high fibre contents, and hence the high levels of mechanical properties, that can be achieved. Filament winding is a highly mechanised process, ideally suited to the accurate and consistent production of hollow cylindrical components (i.e., pipes and vessels) [1]. Furthermore, the angle of the reinforcement winding can be adjusted to give the required balance of axial and hoop properties. Depending on the assumptions made, the optimum winding angle for the case of simple biaxial loading arising due to the internal pressurisation of a close-end pipe is approximately $\pm 55^0$ to the pipe axis. Adjustment of the filament tension during winding is used to control the glass fibre content of the composite, which is generally 20 to 60% of the total volume.

Filament winding is illustrated in Figure 2.1. The fibre tows are impregnated with resin and wound onto a rotating mandrel. The mandrel must be coated with a wax release agent before the winding. When manufacturing pipes with resin-rich liner, the mandrel is coated with resin and a liner material, usually C-glass scrim. The winding angle, θ, is determined by the relative speeds of the lateral movement of the winding head and the mandrel rotation and by the diameter of the mandrel. Careful control of the winding process is required to ensure that the impregnated fibre bundles are laid up alongside each other. The fibre bundles should be wound in such a way that the mandrel is completely covered and the

product has a constant wall thickness. For example, a fibre bundle with a bandwidth W given by the expression:

$$W = \frac{\pi d}{\tan\theta} \tag{2.1}$$

should be used to give full wrap for a small pipe with diameter d.

Table 2.1 lists the main manufacturers of commercial GRP pipes and fittings. To match every pipe system for a certain pressure rating, there must be a complete range of fittings with different sizes and configurations. The most common fittings include couplings, nipples, flanges, tees, elbows, crosses, end caps and so on. These are manufactured either by moulding or filament winding, depending on the application. The glass reinforced epoxy (GRE) specimens tested in the present work were supplied by Ameron and the glass reinforced vinyl ester (GRVE) specimens by Sarplast.

At present, there are mainly two British Standards relating to GRP pipes and fittings: BS 6464 [2] and BS 7159 [3]. These specify the requirements for the materials, properties, design, manufacture, joining, inspection and testing of GRP pipes and fittings for the chemical and process industries. A guideline for the use of GRP pipes on offshore structures is recently developed by UKOOA GRP Work Group [4]. It consists of five parts: Part 1- Philosophy and Scope; Part 2 - Components and Manufacture; Part 3 - Systems Design; Part 4 - Fabrication and Installation and Part 5 - Operation. Other standards relating to GRP pipes are API specifications [5, 6], ASME/ANSI B31.3 [7] and ASTM standards [8-30]. In the absence of detailed guidance on GRP pipes for offshore applications, manufacturers and offshore operators have produced their own specifications, which are heavily based upon the ASTM, BS and API standards.

2.2 GRP PIPE MATERIALS

The GRP pipes used in most industrial applications are generally made with thermosetting resins. Four types of thermosetting resins predominate in GRP manufacture: polyester,

vinyl ester, epoxy and phenolic. Epoxies are the dominant matrix materials because they have the best combination of strength, toughness and chemical resistance, although they tend to be somewhat more expensive than the other resin types. Phenolics, despite their excellent fire resistance, tend not to be used for GRP pipes due to processing difficulties.

There are several different types of glass fibre used for reinforcement, as shown in Table 2.2. E-glass is the most common reinforcement for GRP pipe. S-glass has a higher Young's modulus, but is approximately five times more expensive than E-glass and is therefore not used in the manufacture of the low to medium pressure pipes required for the majority of marine and offshore applications. C-glass is supplied in a tissue form designed to give a low overall fibre content when mixed with resin. This confers a high resistance to chemical attack since the performance of the resin matrix in this respect is superior to that of the glass fibres. Therefore, C-glass is often used in the inner resin-rich liner in the manufacture of GRP pipe and fittings. The resin-rich liner is used as a diffusion barrier to prevent fluid from reaching the glass fibres. It also allows the pipe bore to be smooth and to have less resistance to the movement of the fluid.

2.3 PROPERTIES OF GRP PIPES

The properties of GRP pipes are generally dependent on the type, morphology, orientation and proportion of the glass reinforcement, and also on the resin type. Typical mechanical and physical properties of GRP pipes are given in Table 2.3 [31], which shows the properties of glass fibre, epoxy resin and steel. GRP has a low density, approximately 23% of that of steel, and therefore a high specific strength. GRP pipes are anisotropic in terms of mechanical properties and have different values in the hoop and axial directions. Furthermore, GRP has a low modulus of elasticity, which makes GRP pipes susceptible to flexure and vibration due to pressure fluctuation. Consequently, support spacing needs to be shorter for GRP piping than for steel.

Unlike metallic material, GRP is a strain-limited material which does not yield and can accommodate minimal plastic deformation before damage occurs in the form of matrix micro-cracking. This gives GRP only a small capacity for energy absorption and therefore

a relatively poor performance when subjected to impact loading. As a result, special care must be taken when designing a composite structure which will be subjected to impact loading. More discussion on the mechanical properties of GRP pipes will be given in next Chapter, Section 3.5.

2.4 JOINTING METHODS

A range of methods are available for joining GRP pipe and fittings. These include the use of adhesive joints, mechanical 'O'-ring joints, laminated joints, flanged joints and threaded joints.

An adhesive bonded joint comprises a socket and spigot arrangement which is bonded by adhesive, as shown in Figure 2.2. The adhesive bonded joint is called the 'QuickLock joint' by Ameron [32] and the 'Cement joint' by Wavin [33]. Three types of joint structures can be used for this method. The first type involves a conical socket and cylindrical spigot, as shown in Figure 2.2(a). In the second type shown in Figure 2.2(b), both socket and spigot are conical. This is often referred to as a 'Taper/Taper' joint. The third type features a cylindrical socket and spigot (Figure 2.2(c)). The advantages of adhesive bonded joints are their easy-manufacture, high strength and good sealing. However, they are permanent connections which cannot be dismantled and reassembled.

Mechanical O-ring joint also involves a socket and spigot arrangement, as shown in Figure 2.3(a). The spigot end has a machined groove into which the O-ring seal (usually formed from nitrile butadiene rubber) is mounted. The simplest arrangement of this type is the non-restrained joint, which allows for axial movement of the spigot in the socket and for some angular deflection. This is referred to by Wavin as the rubber seal joint. In the restrained joint, a flexible thermoplastic locking strip is inserted through an opening in the socket end and occupies a groove between socket and spigot. This referred to as the 'KeyLock' joint by Ameron and as the 'rubber seal lock joint' by Wavin. This arrangement provides axial restraint. For higher pressure applications, more than one O-ring and locking ring may be used. One attraction of the O-ring type joint is its tolerance to angle deflection, which typically has values of 1° to 3° depending on the pipe diameter and

the joint structure (with or without locking ring). A further feature is that, unlike the adhesive bonded joint, the mechanical O-ring connection can be dismantled and reassembled to accommodate changes in piping design. However, the socket of the mechanical O-ring joint is more heavily reinforced than that of the adhesive bonded joint, and the assembly can be more difficult in confined spaces.

The laminated joint is a butt joint which requires resin impregnated reinforcing fibres to be wrapped manually around the abutting pipe ends, as shown in Figure 2.3(b). When correctly carried out, the laminated joint offers optimum joint performance. However the technique requires skilled labour and is time-consuming. Consequently, the joints can be prone to fabrication faults and are also costly.

Threaded joints tend to be used for high pressure piping applications and are generally restricted to the smaller pipe sizes. The most common type is a simple threaded socket and spigot connection which may include an O-ring seal. Some threaded connections are designed to be used in conjunction with an adhesive. Composite pipes and tubular components often incorporate threaded steel inserts which are integrally wound into the ends of the components during manufacture.

GRP flanges are produced in a number of forms, including hubbed, hubless (for heavy duty) and loose ring (Van stone type). Pipes and fittings supplied with integral flanges can be connected with steel piping and allow for easy assembly and disassembly. Alternatively flanges can be incorporated into adhesively bonded or mechanical O-ring joint systems.

The most widely used jointing method is the adhesive bonded joint, which offers the advantages of easy installation and high strength, particularly for pipe systems with small diameters ($\leq$ 800 mm). In the present work, four types of joints are investigated. These are the straight socket/ spigot bonded (QuickLock) joint and straight coupler bonded joint manufactured by Ameron, discussed in Chapter 4, and the socket/spigot (taper/taper) joint and laminated joint manufactured by Sarplast, discussed in Chapter 5.

REFERENCES

[1] Shen,F.C., A Filament-Wound Structure Technology Overview, Materials Chemistry and Physics, Vol.42, No.2, 1995, pp.96-100.

[2] BS6464: British Standard Specification for Glass Reinforced Plastic Pipes. British Standards Institution, 1984.

[3] BS7159: British Standard Code of Practice for Design and Construction of Glass Reinforced Plastic (GRP) Piping Systems for Individual Plants or Sites. British Standards Institution, 1989.

[4] UKOOA GRP Work Group, Specifications and Recommended Practice for the Use of GRP Piping Offshore, 1994.

[5] API 15LR, Specification for Low Pressure Fibreglass Line Pipe, API Specification 15LR(Spec 15LR), Sixth Edition. American Petroleum Institute. Sept.1990.

[6] API 15HR, Specification for High Pressure Fibreglass Line Pipe, API Specification 15HR (Spec 15HR). American Petroleum Institute. Sept.1990.

[7] ASME/ANSI B31.3: 1987 Chemical Plant and Petroleum Refinery Pipes.

[8] ASTM D648, Standard Test Method for Deflection Temperature of Plastics under Flexural Load.

[9] ASTM D695, Standard Test Method for Compressive Properties of Rigid Plastics, Approved 1990.

[10] ASTM D695M, Standard Test Method for Compressive Properties of Rigid Plastics [Metric], Approved 1990.

[11] ASTM D696, Standard Test Method for Coefficient of Linear Thermal Expansion of Plastics, 1988.

[12] ASTM D1599, Standard Test Method for Short-Time Hydraulic Failure Pressure of Plastic Pipe, Tubing and Fittings, Approved 1988.

[13] ASTM D2105, Standard Test Method for Longitudinal Tensile Properties of Reinforced Thermosetting Resin Pipe and Tube, Approved 1985.

[14] ASTM D2143, Standard Test Method for Cyclic Pressure Strength of Reinforced, thermosetting Plastic pipe, Reapproved 1987.

[15] ASTM D2290, Standard Test Method for Apparent Tensile Strength of Ring or Tubular Plastics and Reinforced Plastics by Split Disk Method, Reapproved 1982.

[16] ASTM D2310, Standard Classification for Machine-made Reinforced Thermosetting-Resin Pipe, Reapproved 1986.

[17] ASTM D4024, Standard Specification for Reinforced Thermosetting Resin (RTR) Flanges, Approved 1981.

[18] ASTM D2343, Standard Test Method for Tensile Properties of Glass Fiber Strands, Yarns and Rovings Used in Reinforced Plastics, Reapproved 1985.

[19] ASTM D2393, Standard Test Method for Viscosity of Epoxy Resins and Related Components, Approved 1986.

[20] ASTM D2412, Standard Test Method for External Loading Properties of Plastic Pipe by Parallel-Plate Loading, Approved 1977.

[21] ASTM D2444, Standard Test Method for Impact Resistance of Thermoplastic Pipe and Fittings by Means of a Tup (Flatting weight), Approved 1984.

[22] ASTM D2471, Standard Test Method for Gel Time and Pack Exothermic Temperature of Reacting Thermosetting Resins, Approved 1988.

[23] ASTM D2563, Standard Practice for Classifying Visual Defects in Glass-Reinforced Plastic Laminate Parts, Reapproved 1987.

[24] ASTM D2583, Standard Test Method for Indentation Hardness of rigid Plastics by Means of a Barcol Impressor, Approved 1987.

[25] ASTM D2924, Standard Test Method for External Pressure Resistance of Reinforced Thermosetting-Resin Pipe, Approved 1986.

[26] ASTM D2925, Standard Test Method for Beam Deflection of Reinforced Thermosetting Plastic Pipe Under Full Bore Flow, Reapproved 1976.

[27] ASTM D2992, Standard Method for Obtaining Hydrostatic Design Basis for Reinforced Thermosetting Resin Pipe and Fittings, Reapproved 1977.

[28] ASTM D2996, Standard Specification for Filament-Wound "Fiberglass" (Glass-Fiber-Reinforced Thermosetting-Resin) Pipe, Approved 1988.

[29] ASTM D3567, Standard Practice for Determining Dimensions of Reinforced Thermosetting Resin Pipe (RTRP) and Fittings , Approved 1985.

[30] ASTM D3681, Standard Test Method for Chemical Resistance of Reinforced Thermosetting Resin Pipe in a Deflected Condition , Approved 1983.

[31] Ameron, Bondstrand Product Data: Bondstrand 2000 Fibreglass Pipe and Fittings for General Industrial Service, 1985.

[32] Ameron, Bondstrand Fiberglass Pipe and Fittings for Offshore Drilling and Production Applications, 1987.

[33] Wavistrong Engineering Guide, Wavin Epoxy Pipe System, April 1990.

Table 2.1 Main commercial manufacturers of filament wound GRP pipes and fittings.

Manufacturer	Location	GRP products	Diameter range mm
Ameron	Holland, USA & Singapore	Bondstrand series epoxy pipe and fittings.	50-914
Sarplast (Vetroresina)	Italy	Marpi 150&200, Marcop 150 & 200 polyester and vinyl ester pipe and fittings.	80-1000
Wavin	Holland	Wavistrong T & E type epoxy pipe and fittings.	25-1200
Smith Fiberglass	USA	Blue streak, Red thread, and Green thread polyester, vinyl ester and epoxy pipe and fittings.	37-1200
Deutsche Fibercast	Germany	F1222 Fiberdur vinyl ester pipe and fittings.	25-750
OY Muotekno	Finland	Muotekno IP polyester and vinyl ester pipe and fittings.	50-600
Sipap	France	Series E110^0 epoxy pipe and fittings.	50-400

Table 2.2 Reinforcing glass fibre types.

Material	Main characteristics for offshore applications
E-glass	Electrical grade, most common, low cost.
S-glass	High strength grade, 20% stronger than E-glass, higher price.
C-glass	Chemical grade, improved corrosion resistance.
D-glass	Low dielectric grade, low dielectric constant, less strength than E-glass.
ECR-glass	Good corrosion resistance, good resistance to strain corrosion. A little more expensive than E-glass.

Table 2.3 Physical and mechanical properties of Ameron Bondstrand® 2000 GRE pipe [31] compared with those of its components and steel.

	GRP pipe		Glass fibre	Epoxy resin	Steel
	Hoop	Axial			
Tensile strength (MPa)	165	58.6	2400	81	450
Elastic modulus (GPa)	25.2	11	76	3.3	210
Poisson's ratio	0.56 ($\nu_{hoop,axial}$)	0.37 ($\nu_{axial,hoop}$)	0.20	0.40	0.29
Density (kg/m^3)	1,800		2,550	1,400	7,860
Thermal expansion coefficient (10^{-6}/ °C)	18		5	60	15
Thermal conductivity (W/(m· °C)	0.33		1.05	0.1	63 (mild steel) 150 (stainless steel)

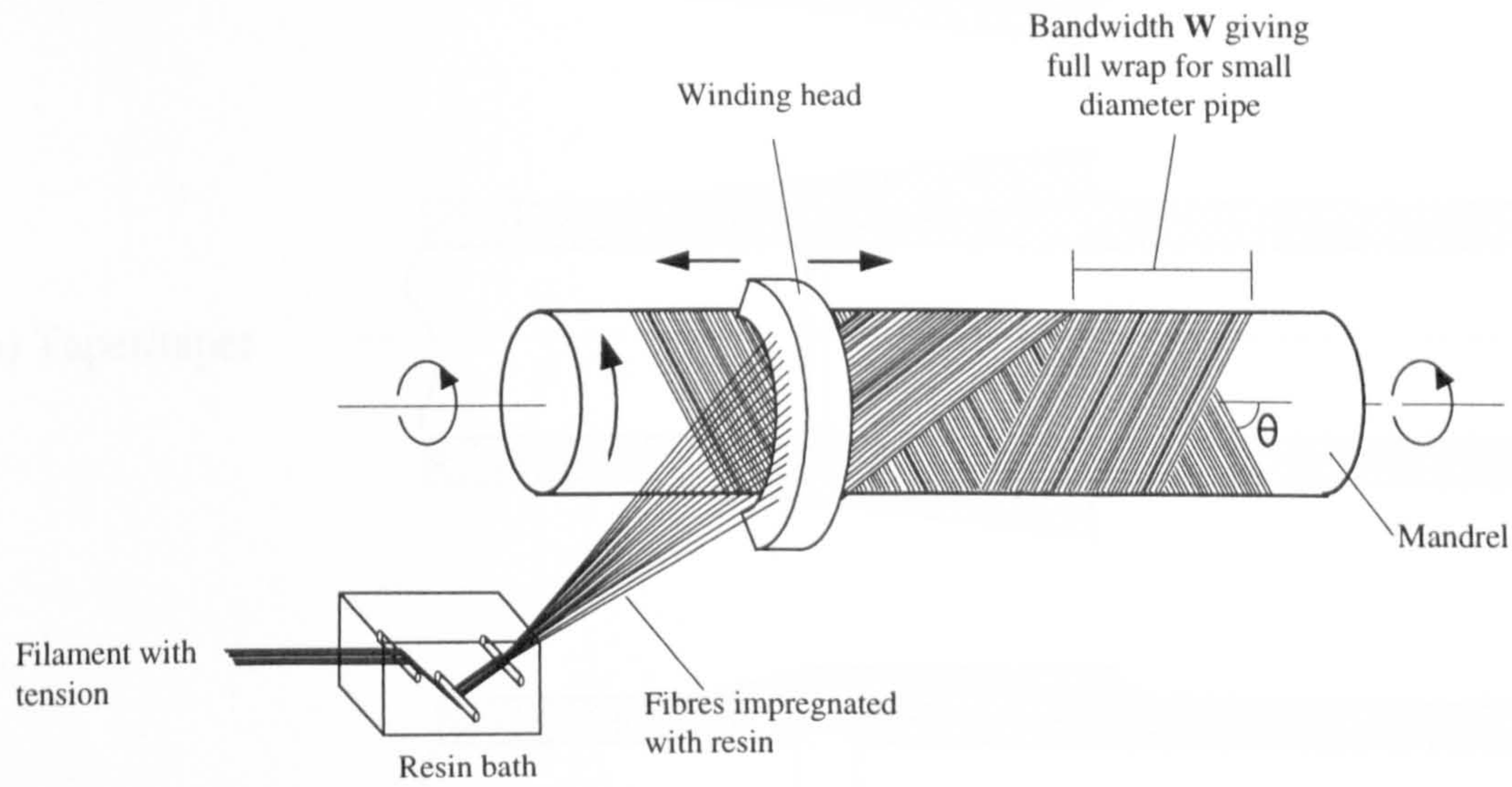

Figure 2.1 Schematic view of a filament winding machine making angle-ply GRP pipes. The winding angle θ is determined by the relative speeds of the lateral movement of the winding head and of the mandrel rotation and by the diameter of the mandrel.

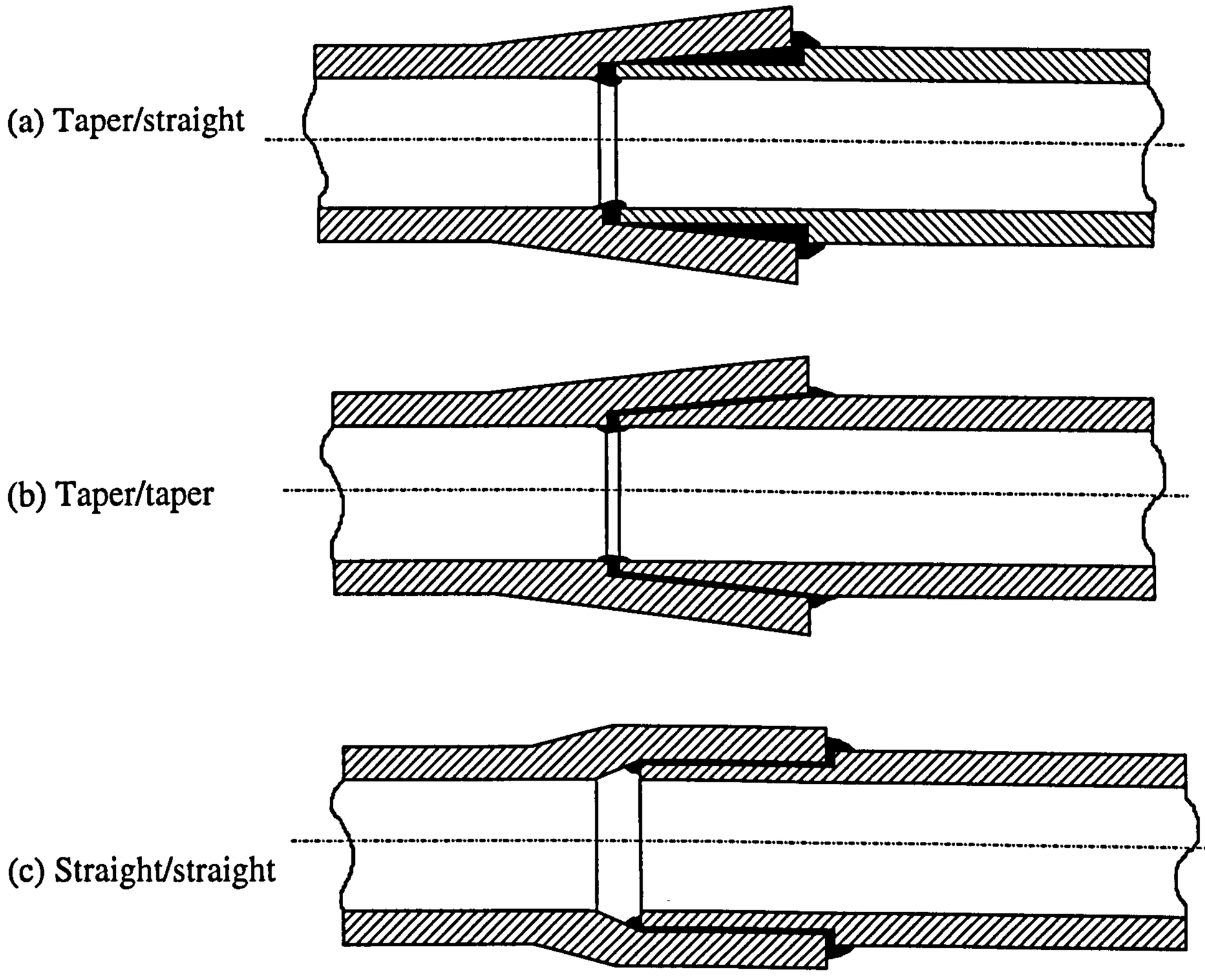

Figure 2.2 Adhesively bonded socket and spigot joints.

(a) Mechanical O-ring joint

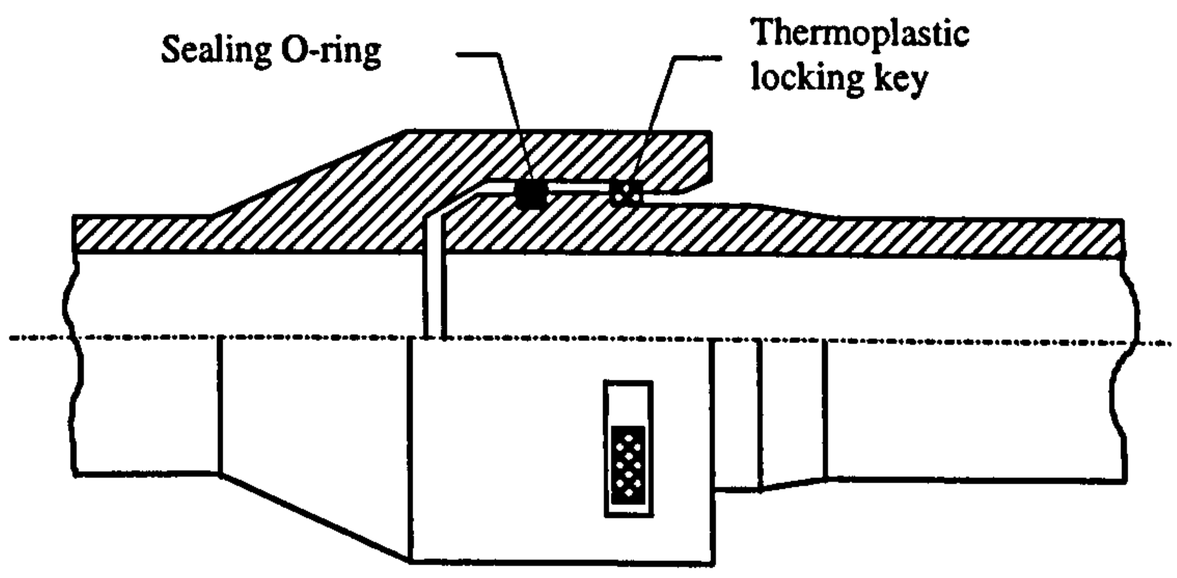

(b) Laminated joint

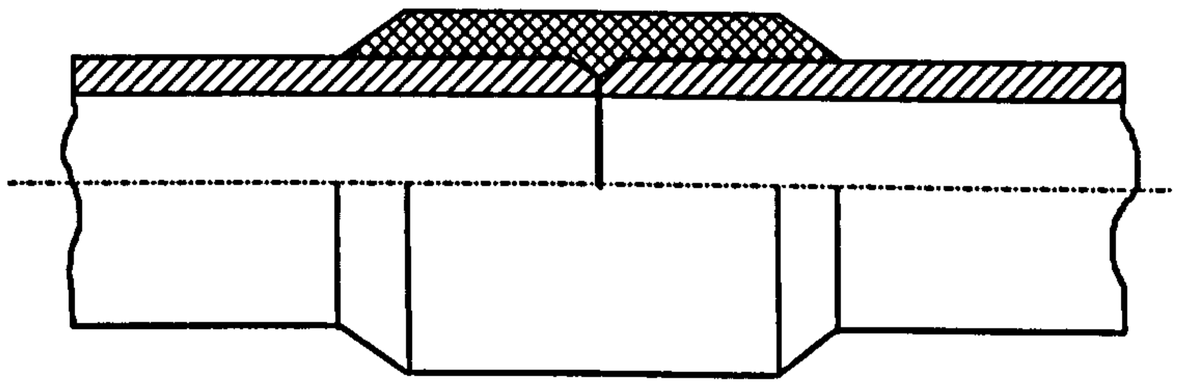

(c) Flanged joint

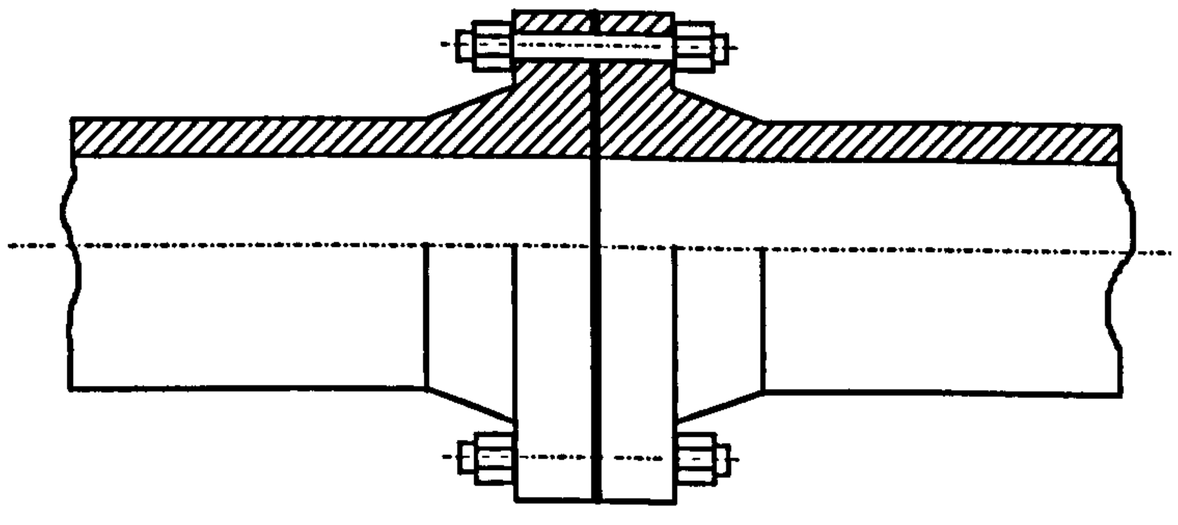

Figure 2.3 Various GRP pipe joints.

CHAPTER THREE

LITERATURE REVIEW

The earliest work on the fatigue of composites was conducted in the late 1960s and early 1970s by Boller [1] and Owen et al [2]. This work on glass and carbon fibre reinforced plastics laid the ground for our current understanding of fatigue mechanisms in composites.

In order to investigate effectively the fatigue characteristics of filament wound glass reinforced plastic pipes and joints, this Chapter provides a brief review of the relevant literature. The review covers mainly the fatigue of composite materials and structures, including GRP pipes and bonded joints. Only the most common reinforcing fibres, glass and carbon, incorporated in organic resin matrices are discussed. More extensive and detailed reviews of this subject have been carried out by Scholte [3], Konur and Matthews [4] and Curtis [5].

Firstly, the fatigue characteristics of general composite materials are discussed, including fatigue mechanisms and the influences of various material, structural and loading parameters. Then, the rules of cumulative damage and approaches to life prediction are reviewed. Finally the main points are summarised, as these were helpful in the preparation of the test programme and in the interpretation of the fatigue results presented in later Chapters. First of all, some basic concepts of fatigue are described as follows.

BASIC CONCEPTS OF FATIGUE

Fatigue can be described as a process which causes damage in materials and structures under fluctuating loads of a magnitude much less than the short term ultimate

strength. The accumulated damage may result in a gradual and significant decrease in mechanical properties such as strength and stiffness, crack growth and finally complete failure or collapse. Glass reinforced plastics of all kinds have been found to be susceptible to failure under fatigue loading [6,7].

The speed of the fatigue process is governed primarily by the magnitude of the fluctuations of the load or deformation cycles, commonly referred to as the stress or strain range. Another load effect parameter is the height of the mean or peak level of the load cycle, although this is of less importance than the stress range.

The main concepts associated with fatigue are endurance (or fatigue life), fatigue strength and fatigue limit.

- Fatigue life is the total number of load cycles of a given stress range which can be endured by the material or structure before fatigue failure occurs. Fatigue failure can be defined either as total collapse or as loss of strength or stiffness.
- Fatigue strength is the maximum cyclic load or stress range that a material or structure can withstand for a given fatigue life.
- Fatigue limit is the maximum cyclic load that can be resisted indefinitely without failure.

The relationship between the fatigue strength and the fatigue life is most commonly presented as S-N or Wohler curves for constant amplitude loading, as shown in Figure 3.1. The horizontal axis gives the number of cycles **N**, and is normally presented on a logarithmic scale. The vertical axis gives the fatigue strength **S** and may be plotted on a logarithmic or a linear scale. The fatigue strength is usually presented in the form of a stress range $\Delta\sigma$ or a double amplitude. However, sometimes the fatigue strength is represented by the load amplitude or even by the maximum of the load cycle.

The most interesting and useful part of the curves, between 10^3 and 5×10^6 cycles, can often be represented by a straight line of the expression:

$$log\,(\Delta\sigma) = c_1 - c_2\,log\,N \qquad (3.1)$$

or:
$$\Delta\sigma = c_1 - c_2\ log\,N \qquad (3.2)$$

where c_1 and c_2 are constants.

Normally, the first formula provides the best fit for test results of high cycle fatigue, whilst for low cycle, high stress fatigue levels the second formula may be preferred. A series of such curves must be produced for loadings with different levels of mean stress.

There is usually a considerable scatter of results in fatigue testing. S-N curves commonly represent mean fatigue strengths with a 50/50 chance of failure corresponding to certain fatigue lives. A component designed on the basis of a mean curve therefore has an equal chance of failure or survival at its service life. Since a greater chance of survival is usually required as a basis for practical design, so called design S-N curves need to be constructed below the mean curve.

3.1 FATIGUE MECHANISMS IN COMPOSITE MATERIALS

The mechanism of the fatigue process in fibre reinforced composite materials is quite different from that in metals, and depends on the properties of both the matrix and the reinforcement as well as on the interaction between the two [8-11]. Due to the inhomogeneity and the anisotropy of fibre reinforced composites, crack paths are highly complex, and the crack itself is not the only manifestation of structural damage.

Talreja [11,12] proposed fatigue damage mechanisms for unidirectional fibre composites based on the strain-life diagram shown in Figure 3.2, which illustrates the relationship between fatigue damage and fatigue loading. For cycles with short life at high strain amplitudes, catastrophic fibre damage is dominant and failures occur within the scatter band of the static tensile failure strain e_c. For intermediate cycles, progressive damage mechanisms become dominant, while at high cycles below the matrix fatigue limit e_m , only matrix micro-cracking is seen [13] and the fibre dominated strength does not reduce any further. The applicability of fatigue life diagrams such as this has been discussed extensively in the literature [14,15].

Generally, there are three basic fatigue failure mechanisms in unidirectional fibre composite materials. They are interfacial debonding, matrix cracking and fibre breakage. These basic failure mechanisms and their interactions are described extensively by Talreja [14], as illustrated in Figure 3.3. For multidirectional fibre reinforced composites, a fourth basic failure mechanism resulting from matrix cracking and interfacial debonding is called delamination. This causes debonding between adjacent layers of reinforcement.

Damage mechanisms in unidirectional composites using various fibres are widely discussed in the literature in terms of the fibre deformation characteristics and matrix resin fatigue limit relations [16-23]. Progressive fatigue damage has been observed in the experiments of GFRP and CFRP composites by Curtis and Moore [16] and

Lorenzo and Hahn [17,18]. The observed damage is in the form of matrix cracking and longitudinal splitting, which initiates from interfacial debonding and early matrix cracking. It was found that more extensive damage took place in glass fibre composites than in carbon fibre composites.

Some experimental work has been done on crossply laminates [24-30], angle-ply laminates [31] and chopped strand mat reinforced composites [2,32]. It was found that the damage mechanisms for crossply, angle-ply and CSM composites were different from those in unidirectional composites.

Basic damage mechanisms in crossply laminates are:

- transverse ply cracking,
- edge and internal delaminations,
- longitudinal cracks,
- interfacial debonding and fibre fracture.

Failures in angle-ply laminates are developed in the following order:

- interfacial debonding started in the ply with a maximum angle to the loading,
- resin cracking,
- delaminations,
- fibre fracture.

Damage development in CSM composites appears to be in the following sequence:

- adhesion failures between fibres and resin,
- resin cracking,
- fractures of single fibres,
- total failure caused by a propagating macroscopic crack surrounded by numerous sub cracks.

More discussions on the angle-ply laminates are in Section 3.5 where the failure of GRP pipes composed of curved angle-ply laminate is extensively discussed.

Although the foregoing descriptions of progressive fatigue damage mechanisms are based in particular on tests of composites with unidirectional, crossply and CSM reinforcement, these may be considered as applicable to all fibre reinforced plastic materials. Since damage occurs progressively from interfacial debonding to resin cracking and fibre breakage, fatigue test results for composite materials should preferably be shown as in Figure 3.4 [33]. Interfacial debonding and resin cracking occur at much lower load levels than that required for total failure. This debonding and resin cracking may result in leakage and, if the penetrating media are able to attack the fibre/resin interface and thereby weaken the composite material, can cause premature final failure.

For composite pipes and pressure vessels, the resin cracking strength is of particular concern because of the problem of media leakage caused by cracking. Unfortunately, most published data have been obtained from small coupon specimens which were broken in laboratory tests and so represent the strength of total fracture. Fatigue tests should therefore be conducted using tubular specimens containing working media (e.g. gas, water or other liquids) to obtain the resin cracking strength.

3.2 EFFECT OF MATERIAL

The fatigue behaviour of composite structures is mainly influenced by structural geometry, choice of composite materials, applied loading and environment. The effects of the composite materials are influenced by the choice of composite components, the lay-ups and the production process.

3.2.1 Effect of Matrix

The early work on the effect of matrix properties on the fatigue behaviour of advanced polymer matrix composites was carried out by Boller [1] and Davis et al [34]. They studied the comparative fatigue performance of laminates of epoxy, silicone, polyester and phenolic matrices reinforced with E-glass fabric, and concluded that the epoxy matrix composites gave the best results, as shown in Figure 3.5. Further investigations have, subsequently been carried out by Owen et al [35], Harris [23,30], Curtis [36], Mandell et al [31], Newaz [37] and other groups.

The resins most commonly used as matrices for GRP are polyester, epoxy and vinyl ester resins. The fatigue behaviour of epoxy resins is slightly superior to polyester, vinyl ester, phenolic and silicone resins. The superior behaviour of epoxy resins is attributed to their greater strength, better bonding to the fibres and lower shrinkage. This results in smaller residual stresses, higher strain without cracking and less exposure to fibre corrosion [8]. From cyclic flexural testing of polyester and vinyl ester resins [38,39], it was concluded that vinyl ester type resins had a significantly better fatigue behaviour than polyester resin. Isophthalic polyester was found to be somewhat better than orthophthalic polyester resin whereas little difference was observed between the standard vinyl ester and the new pre-accelerated thixotropic vinyl esters. Despite great chemical differences, the effect of the resin on the fatigue strength of FRP is rather small when compared with the effect of the different reinforcements [3].

3.2.2 Effect of Fibre

3.2.2.1 Effect of Fibre Type

The initial work on the effect of glass fibre properties on the fatigue behaviour of polymer matrix composites was carried out by Boller [40] in the early 1960's. He studied comparative fatigue performances of higher modulus S-glass and lower modulus E-glass fibre-reinforced composites for the same matrices, and found that the higher modulus composites had a superior fatigue performance. Later, Davies and Sunsdrud [41] and other workers [42,43] also compared the tensile fatigue performance of S-glass and E-glass fibre-reinforced epoxy matrix composites, again concluding that S-glass composites had a better fatigue performance.

From the early 1970's, a large number of investigations into the fatigue performance of carbon fibre-reinforced polyester and epoxy matrix composites were carried out by Owen et al [44,45], Curtis et al [16,19,36], Harris et al [23,46], Dharan [47,48], Sturgeon [49 -52] and other groups [17,18,53]. It was found that high modulus carbon fibre composites gave a superior fatigue performance, better than that of metals, E-glass and S-glass reinforced composites.

Curtis and Dorey [19], Jones et al [28,29] investigated Kevlar fibre-reinforced plastic composites and found that they had a fatigue performance intermediate between carbon fibre composites and glass fibre composites.

It has also been found that the fatigue performance of glass fibre composites is improved through hybridisation with carbon fibres [54,55]. In a similar manner, the fatigue performance of Kevlar-49 fibre composites can be improved through hybridisation with carbon fibre.

Fibre stiffness and failure strain are clearly the key parameters in determining fatigue performance. Generally, composites containing fibres with low modulus have a

steeper S-N curve than those containing fibres with high modulus. From tests by various investigators it is suggested that a ranking of fibre materials from best to worst would be [3,4]:

- High modulus carbon fibre
- High strength and low modulus carbon
- Aramid/carbon hybrid
- Aramid
- Glass/aramid hybrid
- S-glass
- E-glass

3.2.2.2 Effect of Fibre Fraction

The effect of the fibre fraction on the longitudinal properties of composites can generally be described by the rule of mixtures. This states that a composite property, X_c , is equal to the volume fraction weighted-average of the contributions from the fibre and matrix, $X_c = X_f V_f + X_m V_m$, where X_f , V_f , X_m , V_m are the properties and volume fractions of fibres and matrix respectively. As, in most cases, $X_f >> X_m$, the approximate form, $X_c = X_f V_f$, is employed. Experimental results obtained by Tanimoto and Amijima [56] confirm that an increase in fibre content results in an improvement of fatigue strength in GRP laminates. The properties of the matrix are used to predict the transverse and shear performance of the composite.

3.2.2.3 Effect of Fibre Orientation

For UD fibre reinforced specimens with fibres aligned at a specific angle to the loading axis, the fatigue strength is found to decrease as the fibre alignment angle increases. Specimens with an aligned angle of 0^0 provide the highest fatigue strength and other properties in the load direction, whereas an angle of 90^0 gives the lowest fatigue properties.

3.2.2.4 Effect of Fibre Length

Composites reinforced with short fibres generally have much lower initial and fatigue strengths than those reinforced with long fibres. GRP containing short fibres (0.2 mm) has only 20% of the ultimate strength of continuous fibre GRP. The reason for this is that in short fibre composites the load must be transferred from one fibre to another by the matrix between them. This results in a higher stress level in the resin and especially in an increase of the shear forces at the interface between fibre and resin.

3.2.2.5 Effect of Fabric

Many tests have been done on the effects of fabric construction [1,5,38,57-60]. The construction and orientation of the reinforcement plays a critical role in fatigue performance. In general, if more fibres are aligned with the main loads, then the fatigue strengths for a given number of cycles are higher and the S-N curves are flatter.

Thus fatigue strength of laminates decreases in the following order: laminates with UD reinforcement in the loading direction, with non-woven reinforcement, with woven fabrics or with random short fibre mats are in order of providing better fatigue strengths [38,57]. This ordering can be explained largely by the differences in the fraction of fibres orientated parallel to the loading direction. Other factors which influence the modulus of elasticity of the laminate and thus the fatigue behaviour will be the continuity of the fibres and the amount of stretching. Unidirectional fibres are continuous and capable of relatively good stretching, resulting in a rather high modulus of elasticity. The same applies for the non-woven fabrics, although not all fibres are oriented parallel to the loading direction, resulting in a smaller load carrying fibre-volume fraction and thus a lower modulus and a lower fatigue strength.

Woven composites are widely used in industry because they offer significant advantages in handling and fabrication over conventional non-woven materials. However, their mechanical properties, particularly in fatigue loading [5], are generally poorer than the equivalent non-woven material, mainly because of the inevitable distortion of the fibres, but also because of the difficulties associated with achieving high fibre volume fractions in woven composites.

3.2.3 Effect of Interface

By definition [61, 62], an "interface", or in a more generalised concept, an "interphase" exists from some point in the fibre where the local properties begin to change from the fibre's bulk properties, through the actual interface into the matrix. Interface thickness varies from a few to thousands of μm. The exact nature of the interface region and its effect on composite performance is unclear [4].

The interface effects on fatigue performance of advanced composites have been studied by Sih and Ebert [63,64], Harris [9,23], Curtis [36] and other researchers. The interface may have a significant effect on crack initiation as well as on crack propagation, depending on the bonding strength of the interface and the orientation of fibres and principal stresses. On the one hand, stress concentrations at the interface can lead to rapid crack initiation and thus drastically reduce the life of a matrix. On the other hand, the presence of interfaces may considerably slow down crack propagation by effectively blocking and changing the propagation direction of the crack. In addition, friction developed between fibre and matrix can absorb energy needed for crack propagation.

A comparison has been made in [3] of the fatigue strengths of laminates with various fabric constructions under flexural loading and under axial loading [3,38,57]. The fatigue strengths under flexural loading are always smaller than those under axial loading[3, page 191]. The reason for this is probably the comparatively large stress gradient through the thickness of the laminate under flexural bending, which results in considerable shear stresses in the interface between fibres and resin.

3.2.4 Effect of Production Process

In addition to the factors previously discussed, the fatigue behaviour may also be affected by the production process and quality control. The curing and hardening processes can affect the properties of the resin and the interface. During the laminating process air bubbles may be entrapped in the fabric weave or in the surface layer. Such voids may result in a fatigue strength reduction factor of up to 1.3 or 1.4 for the onset of resin cracking [65]. The distribution of the resin, the saturation of the reinforcement and the stretching of the fibres are determined by the laminating process. Inhomogeneous distribution of the resin and slack in the fibres may result in an overall or local influence on stiffness and fatigue strength.

Resin additives may affect the fatigue behaviour of the resin and of the laminate in an adverse sense. Since the fatigue damage process starts with the onset of debonding between fibres and resin, much attention should be paid to the quality of the interface. Depending on the selected coupling agent, the static bond strength of polyester to glass may increase by a factor of 4 or 5 [8]. It can be expected that this will also affect the fatigue life at lower stress levels.

3.3 EFFECT OF TYPE OF LOADING

3.3.1 Effect of the Mean Stress

Fatigue data in the form of S-N curves do not show clearly the effect of the mean stress on the fatigue behaviour. However, for design purposes this information may be essential, in which case further S-N curves for different mean stresses are needed. From these curves it is possible to construct a Smith diagram [66] or a master diagram in which the stress amplitude is plotted against mean stress for chosen lives. Where there have been insufficient test results to produce a master diagram, it has sometimes been suggested that an approximation of the diagram can be produced, using a linear relationship between the stress amplitude S_A , the mean stress S_M , the fatigue strength S_E at zero mean stress for a given life and the static ultimate strength S_u of the material:

$$S_A / S_E = 1 - S_M / S_u \tag{3.3}$$

This relationship is known as the modified Goodman law and is applicable to many common metals. Regarding GRP, the use of S_c may be preferred to S_u. S_c is the stress rupture strength for the time corresponding to the cyclic endurance. However, investigations into the suitability of this law, or of alternative relationships for GRP, have shown a restricted area of applicability and a rather poor accuracy of representation of the material properties in fatigue [66].

3.3.2 Effect of Frequency

For GRP tested in the fibre direction, the frequency of the fatigue loading affects the properties significantly; the greater the rate of loading, the greater the strength. For most other continuous fibre composites (CFRP and KFRP) tested in the fibre direction, however, the effect is negligible, as long as hysteresis heating is also negligible [67]. The reason for this is not entirely clear, but it is believed to be due to the environmental sensitivity of the glass fibres rather than any visco-elastic effect [68]. The composites with no fibres in the testing direction, where the resin matrix has visco-elastic behaviour, will also often exhibit a significant rate effect.

When collecting fatigue data on composite materials, it is important to carry out the static tests at the same rate as the fatigue tests, or the static strengths may be artificially low. The best policy with GRP, as well as with laminates showing marked hysteresis heating, is to carry out all fatigue tests at a constant rate of stressing [1]. Thus low load tests are performed at relatively high frequencies and high load tests at low frequencies.

As a general consideration for fatigue testing of composite materials, the test frequency should be chosen so as to minimise the hysteresis heating of the materials, or at least to limit the temperature rise to no more than a few degrees centigrade above ambient. The source of this heating effect is hysteresis in the resin and perhaps at the fibre/matrix interface. Generally composites dominated by continuous fibres mainly in the test direction show lower strains and little hysteresis heating, and test frequencies of around 10 Hz or more are suitable. However, resin-dominated laminates, with few or any fibres in the test direction, show larger strains and marked hysteresis heating; as a guide, frequencies of 5 Hz or less are suitable [68].

3.3.3 Effect of Compressive Loading

Under compression load, the buckling strength of the fibre and shear forces in the interface between fibre and resin may come to dominate the fatigue behaviour. Although the fibres remain the principal load bearing elements, they must be supported by the matrix and the fibre/matrix interface to prevent them becoming locally unstable and undergoing a microbuckling type of failure (Curtis [69-71] and Soutis [72-73]). Thus, the integrity of the matrix and the interface is far more important in compressive fatigue loading than in tensile loading. Matrix and interfacial damage develops for much the same reasons as in tensile loading, but because of the greater demands on the matrix and the interface, compressive fatigue loading generally has a greater effect on the strength of composite materials than tensile loading [74]. In addition, local resin and interfacial damage in compressive loading leads to fibre instability which is more severe than the fibre isolation mode that occurs in tensile loading. Generally, much less information is available on the compressive fatigue of composites, mainly because the compressive testing of these materials presents many problems. Not least of these are the need to support the specimens from undergoing macrobuckling, and the limitations imposed on specimen geometry by the anisotropic nature of the materials.

Ultimately, the worst fatigue loading condition for composite materials is fully reversed axial fatigue, or tension - compression loading. The poorer behaviour of composite materials in reversed axial loading compared with tensile loading results from the inter-ply damage which develops in many of the laminate plies which lack fibres in the test direction. This causes local layer delamination at relatively short lifetimes. In tensile loading this is less serious, since the layers containing fibres aligned along the test direction continue to support the majority of the applied load. In compression, however, tensile-induced damage of this type can lead to local layer instability and layer buckling, potentially taking place before resin and interfacial

damage within the layers has initiated fibre microbuckling. Thus, for the same maximum loading, fatigue lives in reversed axial loading are usually shorter than for zero-compression or zero-tension loading.

In composites typical damage consists of interlayer damage and reduced support for the fibres with a consequent loss in compressive strength, with the result that they are more sensitive to compressive loading than tensile loading.

3.3.4 Effect of Environmental Conditions

The effect of the environment on fatigue behaviour depends on the sensitivity of the laminate to the matrix properties, since it is usually the matrix or fibre-matrix interface that is affected by absorbed moisture. Thus carbon fibre laminates, having a strong fibre-matrix interface, show little sensitivity to moisture content [75-76] when tested at room temperature. The laminate lay-up is also important; generally laminates with a large percentage of fibres in the loading direction are little affected, whereas those with few fibres in the loading direction may show a significant deterioration in properties [5,77]. In addition, composites in modes such as compression or shear, which impose significant stresses in the matrix, can also cause deteriorations in properties when combined with environmental exposure, regardless of the laminate configuration.

For offshore structures, fatigue life may be reduced considerably due to the environmental conditions such as sea water, especially if the surrounding medium can penetrate into the laminate along surface cracks and debonded fibres. The reduction of the fatigue strength is considerable at high load amplitudes, but small at lower stress levels [33, 77, 78]. In this respect it must be realised that, under a random load distribution, resin cracking and penetration by the sea water may occur at a very early stage and thus affect the fatigue strength during subsequent low load cycles more strongly than in the case of a constant amplitude loading. This shows the importance of a tough surface layer. Data on fatigue tests in sea water are restricted in number. Whilst tests in air are themselves limited in the applied frequency to about 5 Hz, this limitation is much more serious in sea water since time is needed for the deterioration of the laminate by the environment. The test frequency in sea water should therefore not exceed the frequency under working conditions or, at most, 0.2 Hz [3]. A test of up to 1 million cycles can be done performed in 2.5 days at 5 Hz, but a frequency of 0.2 Hz results in a test period of 2 months, which is expensive and time consuming.

Fatigue data on composite materials tested at elevated temperature are scarce, but do suggest that steeper S-N curves are obtained, even for CFRP, when tested wet and hot in fatigue [79].

3.4 EFFECT OF STRUCTURES

Fatigue data are usually obtained from laboratory tests carried out on small specimens. However, certain features in composite structures can cause them to be more susceptible to fatigue damage than the base compiste materials. For example, bonded or bolted joints, ply drop-offs used for tapering sections and the complex stressing around attachment points could have significant effects on fatigue life. Once such fatigue behaviours are understood, their effects can be minimised by careful design and fabrication.

Fatigue testing on composite structures indicates that fatigue damage, comprising resin cracking and fibre-debonding at stress-raisers such as holes and hatch corners, usually remains very localised with negligible effect on overall structural behaviour. However, fatigue is more likely to lead to serious problems at bonded structural connections, which are widely used in the offshore pipeline system. The weakness is caused by the absence of load-bearing fibres across the bonded interfaces and by the low interlaminar tensile and shear strength in combination with the inevitable occurrence of stress concentrations associated with joint geometry and bond imperfections. In many cases the occurrence of loads perpendicular to the plane of the laminate aggravates the problem. Purely theoretical estimates of joint strength seem unacceptable. Reference must therefore be made to test data, and the development of a new high-performance design should include a thorough programme of tests on all important joints with evaluation of static and fatigue strength [3].

3.4.1 Effect of Stress Concentrators

There are many stress concentrators such as holes, notches, fasteners and other imperfections in composite structures. Boller [80] found that, in general, notches had little effect on fracture strength (final failure) because of the large number of debonding sites already present in the material. He also showed that small holes had

no effect on long-life fatigue behaviour, presumably because progressive damage quickly removed the stress concentration due to the hole.

In contrast the results presented by Owen and Bishop [81] showed that holes are fully effective in initiating fatigue damage, although they do not always affect final failure. They found that a circular hole acts as a stress concentrator at the onset of damage, with reduction of the fatigue strength by a factor of between 2 and 4 in most GRP materials and up to 10 in unidirectional GRP.

Shutz and Gerharz [82] showed that the notch sensitivity of $(0_2/\pm45/0_2/\pm45/90)_S$ carbon/epoxy laminates changed during cycling in such a way as to eliminate the stress concentration effect almost completely, whereas the opposite effect occurs during fatigue cycling of metals. The accompanying reduction in notch sensitivity can even lead to fractures away from the cross-section containing the notch. This effect has also been observed in random short-fibre composites by Harris et al [83].

Studies of the notch sensitivity of woven GRP in the low cycle region ($N<10^3$) have been carried out by Prabhakaran and Sridhar [84]. They observed rapid decreases of the fatigue strength reduction factor K_f for $1<N<10$ followed by smaller reductions during continued cycling to about 500 cycles.

Summarising the above discussion, stress concentrators generally have less effect on fatigue strength than they do on static strength. At low cycles, stress concentrators may significantly reduce the fatigue strength of composite structures, but after a large number of load cycles the fatigue strengths approach those of the plain composites. In addition, they mainly affect the matrix cracking strengths and have little effect on fibre breaking strength. Since the main concern for GRP pipes is their matrix cracking strength at weeping, and since offshore fire systems experience low cycles of pressure, the stress concentrators may significantly influence the fatigue strength of GRP pipes used for offshore applications.

3.4.2 Effect of Edge-Induced Stresses

Edge-induced stresses can be a problem in many types of testing, and especially so in fatigue. Both shear and normal stresses can develop at the coupon edges, arising from the mismatch of properties between the layers [5,85-87]. The layer stacking sequence is a critical variable and the magnitude of edge stresses varies greatly with the relative positions of the layers. Laminates with thin and evenly-distributed layers generally lead to the lowest edge stresses.

The magnitude of edge-induced stresses will change both with temperature, since layers have different expansion coefficients, and with moisture content, since layers expand to different extents on absorbing external moisture [88]. The sign of the external loading may also influence the significance of the edge effects. For example, a laminate that is insensitive to edge effects in tensile loading may develop severe edge-induced damage in compressive loading. Edge-induced damage usually grows with increasing numbers of fatigue cycles. In the worst cases, the layers can become completely delaminated, leading to potential environmental attack and , certainly, to serious losses in compressive strength.

The pipe ends of GRP pipe joints in offshore fire systems are submerged in sea water. The edge effects and sea water penetration may cause the pipe system to leak prematurely.

3.5 GRP PIPES AND BONDED JOINTS

3.5.1 GRP Pipes

GRP pipes are the most commonly used composite structural components. Their fatigue behaviour is different to that of the common laminates, because of their large flexure and multi-axial loading. In this section, a special discussion is carried out on the performance of GRP pipes and their joints. Before discussing their fatigue behaviour, the static results are reviewed.

3.5.1.1 Static Behaviours

Extensive investigations on the static and fatigue behaviours of GRP pipes were conducted by Soden et al [89-96], Hull et al [97-99], Cowling et al [100, 101], Owen et al [102, 103], Frost et al [104-108] and other groups [109-115].

(a) Testing Methods

Hull et al [97] investigated the failure of glass/polyester filament wound pipe with the 'ideal winding angle', $54^0 44'$. Three basic methods of internal pressure testing were used, as shown in Figure 3.6. Mode 1 was the 'restrained end' test in which the pipe ends were clamped by a thick frame, hence allowing no axial strain. Mode 2 was the 'closed-end' test in which the pipe ends were clamped but were unrestrained so that the axial stress was half the hoop stress. Mode 3 was the 'free-end' test, referred to as 'open ended' test by Soden et al [89], in which the pipe ends were free to slide on 'O' ring seals and therefore the axial stress was zero. The results of 'Mode 2' tests showed that weepage occurred at a hoop stress of about 100 MPa in short term tests, but that burst occurred at a much higher hoop stress of 460 MPa. In comparison with Mode 2 tests, the 'Mode 3' tests gave a higher weepage hoop stress of about 240 MPa but a lower burst hoop stress of about 250 MPa. In Mode 2 tests, the UD laminae in

the pipe wall had a higher transverse stress than they had in Mode 3 tests, the gross pipe wall thus had a lower weepage hoop stress (therefore a lower failure pressure) than in Mode 3 tests. Since the weepage strength of the GRP pipes is of greater concern, the more critical test mode, 'closed-end test' (Mode 2), was chosen in the current test program.

The GRP pipe tests were classified as weepage tests and burst tests according to the installation of rubber liners [89,90,97]. The test fluid would escape at weepage pressure for a GRP pipe without a rubber liner, whereas the installation of a rubber liner acting as an internal seal allowed the load to reach the higher burst stresses.

(b) Effect of Winding Angle

A simple expression for the effect of winding angle was the netting analysis , in which it was assumed that all of the load was carried by the fibres [93]. With a pipe wound at $\pm\theta$ to the pipe axis, the axial stress σ_x and hoop stress σ_y are determined by,

$$\sigma_x = \sigma_f \cos^2\theta \tag{3.4}$$

$$\sigma_y = \sigma_f \sin^2\theta \tag{3.5}$$

where σ_f is the stress in the filament. Therefore, the optimum angle of the reinforcement is determined by,

$$\tan^2\theta = \frac{\sigma_y}{\sigma_x} \tag{3.6}$$

For a 'closed-end' test, where the application of internal pressure gives rise to a hoop/axial stress ratio of 2:1, the optimum winding angle is $54^0 44'$. When a "closed-end" pipe with this optimum winding angle is subjected to pure internal pressure, the strong fibres in the pipe wall will carry most of the load, the weaker matrix will suffer the least stresses and thus the pipe has the highest strength (weepage).

The same problem was analysed by the author of this thesis using laminate theory to examine the influence of the winding angle on the ply stresses. The results showed that the UD laminae had a large value of ply stress σ_1, small values of the transverse stress σ_2 and in-plane shear stress τ_{12} when the winding angle equalled 55^o. Based on the Tsai-Hill failure criterion, the pipe was predicted to have the maximum (weepage) strength when the winding angle was 55^o.

Spencer and Hull [98] conducted weepage tests using the 'closed-end' method to investigate the effect of winding angle on the weepage stresses of GRP pipes. Their

test results confirmed that the weepage stress was a maximum at a winding angle of 55°.

Fracture tests in Mode 2 and Mode 3 were also conducted by Spencer and Hull [98] to examine the effect of winding angle of GRP pipes on pipe fracture strength. Their Mode 2 tests indicated that the optimum winding angle was 55°, the same as in Mode 2 weepage tests. In Mode 3 tests, the resistance to deformation and fracture increased progressively with increase in winding angle.

Therefore, most of the commercial GRP pipes (Table 2.1) are using winding angle of 55° except some products for special purposes. However, according to the experimental results on $\pm 55^0$ GRE pipes under biaxial loads [89], shown in Figure 3.7, the maximum hoop stress to weepage was achieved with a hoop/axial stress ratio R=3.3/1, whereas at R=2/1 the weepage hoop stress was relatively low. The optimum winding angle of practical GRP pipes therefore may not always agree with that predicted by netting analysis [104-105] and further investigation is required.

In the current tests, all pipes were commercial products manufactured by Ameron and Sarplast, wound at winding angles of $\pm 55^0$. It is important to note that the netting analysis is only valid when the applied loads combine to act in the direction of the fibres. That the winding angle $\pm 55^0$ is the optimum configuration is valid only for a pipe with a 2:1 ratio of hoop to axial stresses, see Eq.(3.6). In practice, however, pipe systems can be subjected to any other load ratio.

(c) Failure Modes

In Mode 2 tests, Hull et al [97] observed that weepage was associated with debonding of fibre/matrix interface and matrix cracking in the transverse direction. The final failure of pipe with rubber liner involved in fibre breakage. Jones and Hull [99] examined the microscopic failure mechanisms of GRP pipes and found that weepage in Mode 2 tests was governed by the occurrence and interaction of transverse cracks,

as shown in Figure 3.8. These cracks initiated and propagated along the interface under the influence of transverse stress normal to the fibre direction.

With Mode 3 tests, weepage occurred at very high stresses, close to the burst stress [97]. Resin shear predominates in the early stages of deformation so that no weepage paths in the form of interface and resin cracks were produced. Weepage occurred in association with delamination effects.

Frost and Cervenka [104,105] conducted axial tensile, hoop and internal pressure tests on 3 inch commercial GRE pipes. They observed that the failure mechanism was matrix cracking and that the fibres remained intact. The matrix cracks ran through the ply thickness and were parallel to the fibres. The ply stresses controlling the failure were the transverse and shear stresses. Therefore, a failure criterion based on the transverse and shear ply stresses was proposed to fit the experimental data for 45^0, 55^0 and 75^0 GRE wound pipes [105-108],

$$\left(\frac{\sigma_t}{\sigma_{t,fail}}\right)^2+\left(\frac{\tau}{\tau_{fail}}\right)^2+C\left(\frac{\sigma_t\tau}{\sigma_{t,fail}\tau_{fail}}\right)=1 \qquad (3.7)$$

where $\sigma_{t,fail}$, τ_{fail} and C were the material constants.

(d) Failure Envelopes

The strengths of filament wound GRP pipes under biaxial loading were extensively studied by Soden et al [89-94], Frost [106-108] and Owen [102, 103]. Failure envelopes under biaxial stresses (hoop and axial stresses) were obtained experimentally and theoretically for GRE pipes with various winding angles, including $\pm35^0$ [92,94], $\pm55^0$ [89,92,94], $\pm72.5^0$ [94], $\pm75^0$ [90]. Figure 3.7 shows the initial failure envelope (weepage stresses) and final failure envelope (burst stresses) of $\pm55^0$ GRE pipes subjected to biaxial loads.

Based on the UMIST weepage data, Frost [107] predicted the weepage envelopes for filament wound GRE pipes with the most commonly used winding angles of 45° and 55° by the simplified quadratic failure criterion (Equation 3.7), as shown in Figure 3.9. However, the manufacturing process of filament winding and subsequent post-curing introduces residual stresses in GRE pipes. The residual stresses are generated from the differences in thermal contraction between the individual plies comprising the pipe wall and the overall composite pipe during the cool down from the maximum cure to operation temperature. The solid lines in Figure 3.9, which had taken account the influence of the thermal residual stresses, had better correlation with the experimental data than the dotted lines (no residual stresses were considered). In Figure 3.9, UMIST ultimate data from burst tests of GRE pipes fitted with rubber liners were compared with the weepage strength (tests data and predictions), showing that the weepage strength was about 50% of the ultimate strength for various hoop/axial stress ratios.

Owen et al [102, 103] used thin-walled tubular specimens to investigate the static and fatigue strength of GRP pipes under biaxial loads. Figure 3.10 shows the results for glass CSM reinforced polyester pipes. Large differences can be seen in Figure 3.10 between the different failure stages, i.e. fibre/matrix interface debonding, resin cracking and final rupture. Figure 3.11 shows the fatigue failure envelopes by burst tests of glass CSM/polyester, 0^0 and 45^0 wound glass fabric/polyester pipes under various values of the axial/hoop stress ratio *R*. Comparing Graph (a) with (b) and (c), glass fabric/polyester pipes had higher static and fatigue strengths than glass CSM/polyester pipes. When R=0.5 , i.e. hoop stress was two times axial stress (so called "closed-end" tests), the glass fabric/polyester pipes had a burst pressure of 260 MPa, about 3 times higher than the glass CSM/polyester pipes.

3.5.1.2 Fatigue Behaviours

The fatigue behaviour of glass/polyester composites under biaxial loads was investigated by Owen et al [102,103]. A large number of fatigue tests were conducted on thin-walled tubes under combined axial loading and internal pressure. The fatigue envelopes for the final rupture of off-axis angle $\alpha=0^{\circ}$ and $\alpha= 45^{\circ}$ glass fabric/polyester, glass CSM/polyester pipes are shown in Figure 3.11. Owen et al did not, however, report weepage fatigue envelopes for these composites.

Recently, fatigue pressure tests were conducted on 3-inch commercial filament wound GRE pipes by Frost and Cervenka [104,105] under cyclic internal pressure with a mean pressure of 200 bar and pressure ranges of 100 - 300, 125 - 175 and 150 - 250 bar; and with a mean pressure of 150 bar and ranges of 50 - 250, 125 - 175 and 100 - 200 bar. In all tests pipes failed by weepage, undergoing a practically uniform seepage of water along the pipe length. S-N curves for various cyclic fatigue tests with different mean and amplitude of the pressure cycle [104-106] were presented as a plot of scaled hoop stress against the logarithm of cycles to failure, as shown in Figure 3.12. The scaled stress was defined as,

$$scaled\ hoop\ stress = \sqrt{1-R^2}\ *maximum\ hoop\ stress \qquad (3.8)$$

where R is the ratio of the minimum cyclic pressure to the maximum pressure.

Cyclic failure envelopes in the form of hoop stress against axial stress of GRE pipes are presented in Figure 3.13, and were deduced from Tsai-Wu failure criterion (static failure) and the regression curve in the S-N diagram (fatigue failure) [104, 105]. However, these cyclic failure envelopes still require experimental verification.

It was found that the main failure mechanism of the GRE pipes is matrix cracking. These matrix cracks ran through the ply thickness and were parallel to the fibres. The ply stresses controlling failure were therefore the transverse and shear stresses to the fibre direction. A simplified failure criterion was subsequently developed by Frost [107], based on a polynomial representation of the transverse and shear ply stresses in the pipe wall. The failure criterion is of the form

$$\left(\frac{\sigma_t}{\sigma_{t,fail}}\right)^2+\left(\frac{\tau}{\tau_{fail}}\right)^2+C\left(\frac{\sigma_t\tau}{\sigma_{t,fail}\tau_{fail}}\right)=k \qquad (3.9)$$

where the failure coefficient k equals unity for static strength prediction. This criterion then was generalised to fatigue failure by the introduction of a normalised failure coefficient $k=k(N)$, which was given in the form of scaled stress against cycles to failure. In another paper [108], Frost applied the damage mechanics to GRP pipes to obtain the equivalent stiffness matrix of the damaged materials. The normalised failure coefficient k was therefore presented as the function of the damage density s (or the spacing of matrix cracks).

Foral and Gilbreath [115] found that delamination was a potentially important failure mode in filament-wound tubes with a small winding angle (θ=20°) when tested under axial tension.

3.5.2 Adhesively Bonded Composite Joints

(a) Lap Joint

By definition, a bonded joint consists of adherends and adhesive, which can be arranged in various configurations. The most commonly used bonded joint types are single lap joints, double lap joints, stepped lap joints and scarf joints, as shown in Figure 3.14. Extensive research on their static behaviours has been carried out by

Hart-Smith [116-119], Adams [120], Liechti et al [121], Pickett and Hollaway [122]. Figure 3.15 shows the relative strengths and failure modes of various bonded joint types. Obviously, the simplest single-lap joint gives the lowest strength whereas the complex scarf joint has 100% load transferring capability.

The failure modes of bonded composite joints are very complicated. The position of crack initiation, the subsequent growth rate and the crack path in a joint depend on the joint geometry, loading and the properties of both the adherends and the adhesive. In particular, since the matrix of FRP laminates may be weaker than the structural adhesives, failure may occur within the composite by delamination or inter-ply fracture, rather than by debonding. Furthermore, inevitable defects in the adhesive layer can lead to crack initiation and environment attack.

The amount of research carried out on fatigue has, however, been very limited [123-125]. Robson and Matthews [125] performed tension-tension fatigue tests on carbon fibre reinforced epoxy composite repair joints. It was observed that delamination initiated at the edges of the joint and propagated inwards. Fatigue limits were lower than those of virgin CFRP. Tiu and Sage [123,124] predicted the fatigue strengths of bonded lap joints by applying finite element analysis. The first step of this method was to calculate the stress concentration in both the adhesive and the composite adherends. The second was to obtain the fatigue strength of each material. These strengths were then compared with the maximum stress from the analysis of the joint to predict its fatigue strength, using an appropriate failure criterion. It appeared possible to predict the fatigue strength of joints by such methods, although a number of investigations remain to be completed.

As has been observed, most research on adhesively bonded joints is focused on lap joints. However, the application of these techniques to tubular joints is questionable.

(b) Pipe Joint

Recently, Cowling et al [100,101] investigated the structural integrity of adhesively bonded GRE pipe joints. Static tests were conducted on taper/taper pipe joints with and without bonding defects under four loading conditions: tension, tension with internal pressure, bending and bending with internal pressure. Finite element analysis was performed for the specimens. It was found that the most defect-sensitive loading condition was bending plus internal pressure.

Fatigue tests were conducted on 1-, 3- and 6-inch diameter GRP pipes, fittings and joints under conditions of internal pressure and bending stress, by Wilhelmi and Schab [126]. Each pipe assembly included a 90° moulded GRP elbow, a filament-wound sleeve coupling and moulded GRP flanges. The results showed that all failures occurred by weepage through the pipe wall rather than in any of the joints or fittings. Strain measurements on both moulded and filament-wound GRP fittings indicated that they were operating at relatively low stress levels due to their rigidity compared to that of the piping. It was emphasised that in all 14 assemblies with different diameters there were no failures in any of the joints or fittings. But in my opinion, these results do not necessarily mean that the fatigue strengths of pipes with fittings are the same as for plain pipes themselves. The interaction between GRP pipes, joints and fittings should be examined. Fatigue strength of the GRP pipes is, to a certain extent, influenced by the presence of joints and fittings.

Couplers are widely used in GRP pipelines and have been recently investigated by different groups[127-131]. Gustafson et al [127] investigated the fatigue behaviour of adhesive bonded joints consisting of filament-wound GRE pipes and coupler subjected to water hammer loading (Figure 3.16a). Except for a few specimens in which the bond lines contained large defects such as air entrapments etc., the fatigue cracks mainly propagated through the 0/90° fabric reinforced wound coupler and caused leakage. The ±55° wound parent pipes were strong in comparison with the couplers and adhesive layers. Improvement in the bonding quality and modification of the coupler were therefore required. In my opinion, the use of ±55° wound couplers and taper/taper connections may achieve higher strengths.

Two dimensional finite element analysis on bonded tubular joints connected by straight/straight couplers was carried out by Jena and Pradhan [128] to identify the optimal geometrical parameters of the joints. The effects of defects in the adhesive layer of tubular joints were investigated by Melve and Moursund [129]. They found that a defect size amounting to 85% of the area without bonding was critical for short term strength. However, the effects in the bonding layer are much more significant under fatigue loading, where cracks initiate and propagate to cause premature failure.

Huysmans et al [130] studied a coupler which was constructed by wrapping a prepreg tape around the external pipe surface, as shown in Figure 3.16(b).

Juwono et al [131] investigated the environmental performance of flat and tubular scarf adhesive joints, as shown in Figures 3.16(c) and (d).

To summarise the discussion, generally there are four possible failure modes for adhesive bonded joints:

(1) adhesive bonded interface cracking; critical stress state with high shear and tensile stresses and imperfections in the adhesive layer may be the reasons;
(2) joints or fittings fail because of their poor design;
(3) main structural members fail in the zone influenced by the fittings because they act as stress-raisers in the structure and
(4) main structural members fail in the zone far from fittings, indicating that fittings have little effect on the fatigue strength of the structures.

3.6 CUMULATIVE DAMAGE RULES AND LIFE PREDICTION

Since test data on fatigue are normally presented in the form of S-N curves and relate to constant amplitude fatigue tests, an important aspect of safe-life design is the use of cumulative damage rules to predict fatigue life under conditions of varying or random

loading from constant amplitude fatigue data. The most widely used theory for metallic structures is the Palmgren-Miner rule i.e.:

$$\Delta = \sum\left(\frac{n_i}{N_i}\right) \tag{3.10}$$

where n_i is the current number of cycles at stress amplitudes σ_i , N_i is the number of cycles to failure at σ_i and Δ is a constant somewhat less than unity at failure. The sum is taken over all loading amplitudes. The Palmgren-Miner rule is linear and hence stress-independent and free of stress interaction. Even though the accumulation of fatigue damage in fibre reinforced plastics (FRP) is non-linear, Owen and Howe [132] found that this law gave reasonable results for FRP laminates subject to multi-stress level fatigue loading.

An alternative non-linear version of this failure criterion has been found to give improved results for CSM GRP laminates [132], i.e.

$$\Delta = \sum\left[A\left(\frac{n_i}{N_i}\right) - B\left(\frac{n_i}{N_i}\right)^2\right] \tag{3.11}$$

where A and B are material constants and Δ is equal to unity at failure. Cumulative damage expressions of the same form may also be related to initial fibre-debonding, resin cracking and fibre breakage.

The application of the fracture mechanics approach to GRP materials has been studied by Owen and Bishop [133]. They found that it is possible to apply the conventional Paris law, in which the crack growth rate da/dN is a function of the range of stress intensity factor ΔK,

$$\frac{da}{dN} = C(\Delta K)^m \tag{3.12}$$

3.7 SUMMARY

(1) There are three basic fatigue damage mechanisms in unidirectional fibre composites: interfacial debonding, matrix cracking and fibre breakage. A fourth failure mechanism for multi-directional reinforced composites is delamination which is the result of matrix cracking and interfacial debonding.

(2) Fatigue damage in glass reinforced plastics propagates progressively from the initial damage in the form of interfacial debonding and matrix cracking to the final failure of the structures by fibre breakage. With GRP pipes and pressure vessels, the matrix cracking strengths are of major concern because they become unserviceable when matrix cracks penetrate the pipe wall. However, most published data were obtained from small coupon specimens in laboratory tests. Therefore, fatigue tests should be conducted using pipes containing working medium (e.g. gas, water or other liquids) to obtain their fatigue strength when the weepage occurs.

(3) Since fatigue strength of GRP materials is dependent on the loading rate, a low test frequency should be chosen to minimise the hysteresis heating of the materials for GRP fatigue tests. The best policy is to carry out all the tests at a constant rate of stressing. For composites subjected to fatigue loading combined with environmental conditions, the test frequency should not exceed the frequency under working conditions or at most 0.2 Hz as the deterioration of the laminate by the environment needs time.

(4) Fatigue is more likely to lead to serious problems at bonded structural connections, in which weakness is caused by the absence of load-bearing fibres across bonded interfaces and by the inevitable bond imperfections.

(5) Although fatigue damage, comprising resin cracking and interfacial debonding at stress-raisers such as the local joint area, usually remains localised with negligible effect on overall structural fracture strength, the penetration of harmful environmental media will occur at a very early stage and may affect the fatigue strength significantly.

(6) Composite fatigue performance (final fracture) is generally better than for metallic materials. The composites have larger ratios of fatigue strength to static strength, such that at long lifetime the difference is considerable. In addition to their light weight and low maintenance cost, this superior fatigue performance is another incentive for a more extensive application of composites to offshore structures in the future. However, for composite pipes and pressure vessels where the weepage strength is concerned, further work is required on their fatigue weepage performance.

(7) Fatigue strength is not currently a serious design criterion for composite structures, but composite materials and structures are developing quickly. As static design allowable strengths are increased, fatigue behaviour is becoming more important.

(8) There is still a great need for further, systematic research on composite fatigue. This should include comparative evaluation of the fatigue damage mechanisms and modelling of fatigue damage development, leading to fatigue prediction for composite structures.

REFERENCES

[1] Boller, K.H., Fatigue Characteristics of RP Laminates Subjected to Axial Loading, Modern Plastics, Vol.41, 1964. pp.145-188.

[2] Owen, M.J., Smith, T.R. and Dukes, R., Failure of Glass-Reinforced Plastics, with Special Reference to Fatigue, Plastics & Polymers, Vol.37, No.129, 1969, pp.227-233.

[3] Scholte, H.G., Fatigue Characteristics, Composite Materials in Maritime Structures, Ed. by Shenoi, R.A. and Wellicome, J.F., 1993, pp.178-198.

[4] Konur, O. and Matthews, F.L., Effect of the Properties of the Constituents on the Fatigue Performance of Composites: A Review, Composites, Vol. 20, No. 4, 1989, pp.317-328.

[5] Curtis, P.T., The Fatigue Behaviour of Fibrous Composite Materials, Journal of Strain Analysis, Vol.24, No.4, 1989, pp.235-244.

[6] Smith, C.S., Design of Marine Structures in Composite Materials, Elsevier Science Publishers Ltd., London, 1990.

[7] Powell, P.C., Engineering with Fibre-Polymer Laminates, Chapman & Hall, First Edition, 1994.

[8] Dew-Hughes, D., Way, J.L., Fatigue of Fibre-Reinforced Plastics: A Review, Composites, Vol.4, No.4, 1973. pp.167-173.

[9] Harris, B., Fatigue and Accumulation of Damage in Reinforced Plastics, Composites, Vol.8, No.5, 1977, pp.214-220.

[10] Reifsnider, K., Fatigue Behaviour of Composite Materials, Int. J. Fracture, 16, (1980), pp.563-583.

[11] Talreja, R., Fatigue of Composite Materials and Fatigue-Life Diagram, Proc. Royal Soc. Lond A378, 1981, pp.461-475.

[12] Telreja, R., A Conceptual Framework for Interpretation of Fatigue Damage Mechanisms in Composites, J. Comp. Tech. Res., Vol. 71, 1985, pp.25-29.

[13] Dharan,C.K.H., Fatigue Failure in Glass Fibre Polymer Composites, J. Mater. Sci., Vol.10, 1975, pp.1665-1670.

[14] Talreja, R., Fatigue of Composite Materials, Technomic Publishing: Lancaster, Pennsylvania 17604, USA, 1987. ISBN 87762-516-6.

[15] Talreja, R., ed., Damage Mechanics of Composite Materials, Composite Materials Series, Volume 9, Series Editor: R.B.Pipes, Elsevier Science Publishers Ltd., 1994.

[16] Curtis,P.T. and Moore,B.B., A Comparison of Plain and Double Waisted Coupons for Static and Tensile Testing of UD GRP and CFRP, Proceedings of Second International Conference on Composite Structures, Paisley, Scotland, UK, September 1983, Elsevier Applied Science Publishers, London, 1983, pp.383-398.

[17] Lorenzo,L. and Hahn, H.T., Fatigue Failure Mechanisms in Unidirectional Composites, ASTM STP907, 1987, pp.210-232.

[18] Lorenzo,L., Fatigue Failure Characterisation of a Unidirectional Composite and its AE Characterisation, Ph.D thesis, Washington University, St. Louis, MO, USA, 1985.

[19] Curtis,P.T. and Dorey, G., Fatigue of Composite Materials, Proceedings of International Conference on Fatigue and Engineering Materials and Structures, I. Mech. E., London, 1986, pp.297-306.

[20] Stinchcomb,W.W. and Reifsneider,K.L., Fatigue Damage Mechanisms in Composite Materials: A Review, ASTM STP 675, 1979, pp.762-787.

[21] Hahn,H.T., Fatigue Behaviour and Life Prediction of Composite Laminates, ASTM STP 674, 1979, pp.383-417.

[22] Agarwal,B.D. and Broutman,L.J., Analysis and Performance of Fibre Composites, John Wiley, New York, USA, 1980, pp.223-246.

[23] Harris, B., Engineering Composite Materials, Chapter 5: Fatigue Behaviour of Fibre Composites, The Institute of Metal, 1986.

[24] Stinchcomb,W.W., NDE of Damage Accumulation Process in Composite Materials, Composite Science and Technology, Vol.25, No.2, 1986, pp.103-118.

[25] Reifsnider,K.L., Schulte,K. and Duke,J.C., Long Term Fatigue Behaviour of Composite Materials, ASTM STP 813, Ed. By O'Brien,T.K., 1983, pp.136-159.

[26] Schulte,K., Damage Development Under Cyclic Loading, Proceedings of European Symp. on Damage Development and Failure Process in Composite Materials, Leuven, Belgium,1987, pp.35-54.

[27] Talreja,R., Fatigue Reliability of Composite Materials, Technical University of Denmark, 1986.

[28] Jones,C.J., Dickson,R.F., Adam,T., Reiter,H. and Harris,B, The Environmental Fatigue Behaviour of Reinforced Plastics, Proc.R.Soc.London. Vol.A396, No.1811, 1984, pp.315-338.

[29] Jones,C.J., Dickson,R.F., Adam,T., Reiter,H. and Harris,B., The Environmental Fatigue Behaviour of Reinforced Plastics, Composites, Vol.14, No.3, 1983, pp.288-293.

[30] Mandell,J.F., Huang,D.D. and McGarry,F.J., Tensile Fatigue Performance of Glass Fibre Dominated Composites, Comp. Tech. Rev., Vol.3, 1981, pp.96-102.

[31] Sturgeon,J.B., Fatigue of Multi-Directional Carbon Fibre-Reinforced Plastics, Composites, Vol.8, 1977, pp.221-226.

[32] Owen,M.J. and Howe,R.J., The Accumulation of Damage in a Glass-Reinforced Plastic under Tensile and Fatigue Loading, J.Phys. D.: Appl. Phys., Vol.5, 1972, pp.1637-1649.

[33] Malmo, J., Fatigue Properties of Glass Fibre Reinforced Polyester, Proc. Symp. Use of Reinforced Plastics in the Petroleum Industry, The French Petroleum Institute, Paris, 15th-16th June 1978.

[34] Davis,J.W., McCarthy,J.A. and Schurb,J.N., Fatigue Resistance of Reinforced Plastics, Mater. Des. Engng, 1964, pp.87-91.

[35] Owen,M.J. and Rose,G., Polyester Flexibility versus Fatigue Behaviour of Fibre Reinforced Plastics, Modern Plastics, Vol.47, No.11, 1970, pp.130-138.

[36] Curtis,P.T., An Investigation of Tensile Fatigue Behaviour of Carbon Fibre Composite Laminates, Proceedings of ICCM6, Imperial College of Science and Technology, London, UK, 1987, Elsevier Applied Science Publishers, Vol.4, pp.54-64.

[37] Newaz,G.M., Influence of Matrix Material on Flexural Fatigue Behaviour of Unidirectional Composites, Composites Science and Technology., Vol.24, 1985, pp.199-214.

[38] Greene,E., Marine Composites: Investigations of Fibreglass Reinforced Plastics in Marine Structures, Ship Struct. Cttee., USCG, Rep. SSC-360, September 1990.

[39] Burrel, et al, Cycle Test Evaluation of Various Polyester Types and a Mathematical Model for Projecting Flexural Fatigue Endurance, Proc. 41st Annual Conf. Society of the Plastics Industry, 1986.

[40] Boller,K.H., Fatigue Fundamentals for Composite Materials, ASTM STP 460, 1969, pp.217-235.

[41] Davis,J.N. and Sundsrud,G.J., Fatigue Data on a Variety of Nonwoven Glass Composites for Helicopter Rotor Blades, ASTM STP 674, 1979, pp.137-148.

[42] Salkind,M.J., Fatigue of Composite Materials, ASTM STP 497, 1982, pp.143-169.

[43] Giavotto,V., Wagner.V., Caslini,M. and Zanotti,C., Consideration of Early Fatigue Damage on Damage Accumulation and on Delamination Mechanism in Composite Materials Structures, Proc. 14th ICAF Conf., 1987, pp.503-535.

[44] Owen,M.J. and Morris,S., Assessment of Potential of CFRP as Fatigue Resistant Materials, Proc. of 25th SPI Annual Tech. Conf., Washington DC, USA, February 1970, paper 8-E.

[45] Owen,M.J., Fatigue of Carbon Fiber Reinforced Plastics, Composite Materials Volume 5, Fatigue and Fracture, L.J.Broutman (ed.), Academic Press, New York, 1974, pp.341-369.

[46] Beaumont,P.W.R. and Harris,B., The Effect of Environment on Fatigue and Crack Propagation in Carbon Fibre Reinforced Epoxy Resin, Proc. Int. Conf. On Carbon Fibres, Their Composites and Applications, Plastics Institute, London, UK, 1971, paper 49.

[47] Dharan,C.K.H., Fatigue Failure Mechanisms in Unidirectinally Reinforced Composite Materials, ASTM STP 569 , 1975, pp.171-188.

[48] C.K.H.Dharan, Fatigue Failure in Fibre Reinforced Materials, Proceedings of ICCM1, Geneva, Switzerland and Boston, MA, USA, April 1975, pp.830-839.

[49] Sturgeon,J.B., Fatigue and Creep Testing of CRFP, Proceedings of 28th Annual Conf., Society of Plastics Industry, Washington DC, Feb. 1973, Paper 12-B.

[50] Moore,B.B. and Stugeon,J.B., Zero-Tension Fatigue Tests on High Modulus CFRP, RAE TM MAT 155, Royal Aircraft Establishment, Farnborough, UK, 1972.

[51] Sturgeon,J.B., Fatigue testing of CFRP, RAE TR 75135, Royal Aircraft Establishment, Farnborough, UK, 1975.

[52] Sturgeon,J.B., Tensile Fatigue of 0, +/-30 and +/-60° Angleplied Glass Fibre Epoxy Resin, RAE TR 80151, Royal Aircraft Establishment, Farnborough, UK, 1980.

[53] Favre,J.P. and Vidal,G., In-plane and Interlaminar Shear Fatigue Characterization of Unidirectional GFRP and CFRP, Including Moisture Effects, Int. Conf. On Testing, Evaluation and Quality Control of Composite Materials, University of Surrey, UK, Sept. 1983.

[54] Sturgeon,J.B., Some Fatigue Results on Carbon Fibre/Glass Fibre Epoxy Hybrid Composites, RAE TM MAT 235, Royal Aircraft Establishment, Farnborough, UK, 1975.

[55] Hofer,K.E., Bennett,L.C. and Stander,M., Effect of Moisture and Fatigue on Residual Mechanical Properties of S-glass/Graphite/Epoxy Hybrid Composites, ASTM STP 636, 1977, pp.103-122.

[56] Tanimoto,T. and Amijima,S., Progressive Nature of Fatigue Damage of Glass Fiber Reinforced Plastics, J. Comp. Mater., 9(4), 1975, pp.380-90.

[57] Engineers' Guide to Composite Materials, American Soc. Metals, Metals Park, Ohio, 1987.

[58] Smith,C.S., Design of Marine Structures in Composite Materials, Elsevier Science Publishers Ltd., London, 1990.

[59] Agarwal, B.D., Broutman, L.J., Analysis and Performance of Fiber Composites, Wiley, New York, 1980.

[60] Howe,R.J. and Qwen, M.J., Accumulative Damage in Chopped Strand Mat/Polyester Resin Laminates, Proc. 8th Intl. Reinf. Pl. Congr. BPF, London, 1972.

[61] Drzal,L.T., Composite Interphase Characterisation, SAMPE J., Vol.19, Sept./Oct. 1983, pp.7-13.

[62] Drzal,L.T. and Rich,M.J., Effect of Graphite Fibre/Epoxy Adhesion on Composite Fracture Behaviour, ASTM STP 864, 1985, pp.16-26.

[63] Shih,G.C., Basic Role of Interface on Fatigue Performance of Unidirectional Fibre Glass Reinforced Composites, Ph.D thesis, Case Western Reserve University, 1985.

[64] Shih,G.C. and Ebert, L.J., Effect of Interface on Fatigue Performance of Unidirectional Fiber Glass Composites, Comp. Sci. Tech., 28(1987), pp.137-161.

[65] Owen,M.J. and Griffiths,J.R., Evaluation of Biaxial Stress Failure Surfaces for a Glass Reinforced Polyester Resin under Static and Fatigue Loading, J. Materials Science, 13(1978), 1521-1537.

[66] Smith,T.R. and Owen,M.J., Fatigue Properties of RP, Modern Plastics, Vol.46, April 1969, pp.124-132.

[67] Jones,C.J., Dickson,R.F., Adam,T., Reiter,H. and Harris,B., The Environmental Fatigue Behaviour of Reinforced Plastics, Proc.R.Soc.London. A396, pp.315-338, 1984.

[68] Curtis,P.T., The Fatigue of Organic Matrix Composite Materials, Chaper 10, pp.331-367, Advanced Composites, ed. by I.K.Partridge, Elsevier Applied Science, 1991.

[69] Curtis,P.T. and Moore,B.B., A Comparison of the Fatigue Performance of Woven and Non-Woven CFRP, Proceedings of the fifth International Conference on Composite Materials, San Diego, 1985.

[70] Curtis,P.T. and Moore,B.B., A Comparison of the Fatigue Performance of Woven and Non-Woven CFRP, RAE TR85059, 1985.

[71] Purslow,D., Some Fundamental Aspects of Composites Fractography, Composites, Vol.12, 1981, p.241.

[72] Soutis,C., Curtis,P.T. and Fleck,N.A., Compressive Failure of Notched Carbon Fibre Composites, Proc. R. Soc. London, A(1993)440, pp.241-256.

[73] Soutis,C., Measurement of the Static Compressive Strength of Carbon Fibre-Epoxy Laminates, Composites. Science and Technology, Vol.42, pp.373-392, 1992.

[74] Rosenfield,M.S. and Gause,L.W., Compression Fatigue Behaviour of Graphite/Epoxy in the Presence of Stress Raisers, ASTM STP 723, 1981, p.174.

[75] Curtis,P.T. and Moore,B.B., The Effect of Environmental Exposure on the Fatigue Behaviour of CFRP Laminates, RAE TR84027, 1984.

[76] Curtis,P.T. and Moore,B.B., The Effect of Environmental Exposure on the Fatigue Behaviour of CFRP Laminates, Composites, Vol.14, 1983, pp.294-300.

[77] McGarry et al, Marine Environment Effects on Fatigue Crack Propagations in GRP Laminates for Hull Construction, Report No. MITSG 73-16, MIT, Boston, 1973.

[78] Dixon, R.H., Ramsey, B.W. and Usher, D.J., Design and Build of the Hull of HMS Wilton, Proc. Intl. Symp. GRP Ship Construction, RINA, London, October 1972.

[79] Webb,J.N., Fatigue and Damage Tolerance Data for Carbon Fibre Reinforced Plastics, Progress Note Issued under MOD Contract A93b/458 with BAe Warton Division, 1985/86.

[80] Boller,K.H., Fatigue Properties of Fibrous Glass-Reinforced Plastics Laminates subjected to Various Conditions, Modern Plastics, Vol .34, No.10, 1975, p163-186.

[81] Owen,M.J. and Bishop,P.T., Fatigue Properties of Glass-reinforced Plastics Containing a Stress Concentrator, J.Phys. D: Appl. Phys., Vol.6, 1973, pp.2057-2069.

[82] Shutz,D. and Gerharz,J.J., Fatigue Strength of a Fibre-Reinforced Material, Composites, Vol.8, 1977, pp.245-250.

[83] Harris,B., Ankara,A.O., Cawthorne,D. and Bye,S.M.T., Cyclic Loading and the Strength of Dough Moulding Compounds, Composites, Vol.8, 1977, pp.185-189.

[84] Prabhakaran,R. and Sridhar,M.K., Proc. 30th Annual Tech. Conference of Reinforced Plastics/Composites Institute of SPI, paper D-9, 1975.[H1-ref]

[85] Pagano,N.J. and Pipes,R.B., The Influence of Stacking Sequence on Laminate Strength, Journal of Composite Materials, Vol.5, 1971, pp.50-57.

[86] Curtis,P.T., The Effect of the Edge Stresses on the Failure of (0,45,90) CFRP Laminates, RAE TR 80054, 1980.

[87] Curtis,P.T., The Effect of the Edge Stresses on the Failure of (0,45,90) CFRP Laminates, Journal of Composite Materials, Vol.19, 1980, pp.167-182.

[88] Curtis,P.T., Residual Strains and the Effects of Moisture in Fibre Reinforced Laminates, RAE TR 80045, 1980.

[89] Soden,P.D., Kitching,R. and Tse,P.C., Experimental Failure Stresses for $\pm 55^0$ Filament Wound Glass Fibre Reinforced Plastic Tubes under Biaxial Loads, Composites, Vol. 20, No. 2, 1989, pp.125-135.

[90] Highton,J., Adeoye,A.B. and Soden,P.D., Fracture Stresses for ±75 Degree Filament Wound GRP Tubes under Biaxial Loads, Journal of Strain Analysis, Vol.20, No.3, 1985, p.139-150.

[91] Soden,P.D., Kitching,R., Tse,P.C., Tsavalas,Y. and Hinton,M.J., Influence of Winding Angle on the Strength of Filament Wound Composite Tubes Subjected to Uniaxial and Biaxial Loads, Composites Science and Technology, No.46, 1993, pp.363-378.

[92] Soden,P.D., Leadbetter,D., Griggs,P.R. and Eckold,G.C., The Strength of a Filament Wound Composite under Biaxial Loading, Composites, Vol.9, No.4, 1978, pp.247-250.

[93] Eckold,G.C., A Design Method for Filament Wound GRP Vessels and Pipework, Composites, Vol.16, No.1, 1985, pp.41-47.

[94] Eckold,G.C., Leadbetter,D., Soden,P.D. and Griggs,P.R., Lamination Theory in the Prediction of Failure Envelopes for Filament Wound Materials Subjected to Biaxial Loading, Composites, Vol.9, No.5, 1978, pp.243-246.

[95] Lee,J., Soden,P.D., Kitching,R. and Tse,P.C., Strength of Filament Wound GRP Tubes with Axisymmetric Steps, Composites, 1989, Vol.20, No.3, pp.234-243.

[96]Highton,J. and Soden,P.D, End Reinforcement and Grips for Anisotropic Tubes, Journal of Strain Analysis, Vol.17, No.1, 1982, pp.31-43.

[97] Hull,D, Legg,M.J. and Spencer,B., Failure of Glass/Polyester Filament Wound Pipe, Composites,Vol.9, No.1, 1978, pp.17-24.

[98] Spencer,B. and Hull,D., Effect of Winding Angle on the Failure of Filament Wound Pipe, Composites, Vol.9, No.5, 1978, pp.263-271.

[99] Jones,M.L.C. and Hull,D., Microscopy of Failure Mechanisms in Filament-Wound Pipe, Journal of Materials Science, Vol.14, 1979, pp.165-174.

[100] Cowling,M.J., Hashim,S.A., Winkle,I.E. and Lafferty,S., Structural Integrity of Bonded Connections between Polymer Composite Components in Marine Applications, Project Report CP304, Glasgow Marine Technology Centre, Glasgow University, May 1996.

[101] Cowling,M.J., Hashim,S.A., Smith,E.M. and Winkle,I.E, Adhesive Bonding for Marine Structural Applications, Proc. 3rd Int. Conf. On Polymers in a Marine Environment, London, I.Mar.E., October, 1991.

[102] Owen,M.J. and Griffiths,J.R., Evaluation of Biaxial Stress Failure Surfaces for a Glass Reinforced Polyester Resin under Static and Fatigue Loading, J. Materials Science, Vol.13, 1978, pp.1521-1537.

[103] Owen, M.J., Designing against Fatigue in Glass Reinforced Plastics, Conference Sponsored by the Materials Technology Section of the Applied Mechanics Group of the Institution of Mechanical Engineers, London, 27-28th Sept. 1977.

[104] Frost,S.R. and Cervenka,A., Glass Fibre Reinforced Epoxy Matrix Filament Wound Pipes for Use in the Oil Industry, Proc. of Ninth Int. Conf. on Composites Materials (ICCM/9), Vol.V, pp.684-691, Madrid, 12-16 July, 1993.

[105] Frost,S.R. and Cervenka,A., Glass Fibre Reinforced Epoxy Matrix Filament Wound Pipes for Use in the Oil Industry, Composites Manf., 1994, No.5, pp.73-81.

[106] Frost,S.R., The Impact Behaviour and Damage Tolerance of Filament Wound Glass Fibre/Epoxy Matrix Pipes, 6th Int. Conf. on Fibre Reinforced Composites (FRC'94), University of Newcastle upon Tyne, UK. 29-30 March 1994.

[107] Frost,S.R., Designing Composite Pipelines for Use in the Oil Industry, Paper in Conference Proceedings: Composite Materials for Offshore Use, Nov. 1994.

[108] Frost,S.R., Predicting the Long Term Fatigue Behaviour of Filament Wound Glass Fibre/Epoxy Matrix Pipes, to be published, 1995.

[109] Uemura,M. and Fukunaga,H., Probabilistic Burst Strength of Filament Wound Cylinders under Internal Pressure, J. Composite Materials, 1981, Vol.15, pp.462-480.

[110] Mistry,J., Theoretical Investigation into the Effect of the Winding Angle of the Fibers on the Strength of Filament Wound GRP Pipes subjected to Combined External-Pressure and Axial-Compression, Composite Structures, 1992, Vol.20, No.2, pp.83-90.

[111] Xue,M.D,.Lu,Q.H., Zhuang,Z.Z. and Xue,Y.D., Stress and Strength Analysis by FEM of Fiber-Reinforced Plastic Pipe Tees Subjected to Internal-Pressure, Int. J. of Pressure Vessels and Piping, Vol.67, No.1, 1996, pp.11-15.

[112] Griffen,S.A., Pang,S.S. and Yang,C., Strength Model of Adhesive Bonded Composite Pipe Joints under Tension, Polymer Engineering and Science, Vol.31, No.7, 1991, pp.533-538.

[113] McDonnell,P. and McNamara,J.F., Evaluation of GRP Composite Pipelines for High-Performance Offshore Applications, Key Engineering Materials, Vol.99, No.1, 1995, pp.11-18.

[114] Fahrer,A., A Study of the Failure of Key-Lock Joints in Glass Fibre Reinforced Plastic Pipework, M.Sc Thesis, University of Twente, The Netherlands, May 1994.

[115] Foral,R.F. and Gilbreath,D.R., Delamination Failure Modes in Filament-Wound Composite Tubes, Composite Materials: Fatigue and Fracture, Second Volume, ASTM STP 1012, 1989, pp.313-325.

[116] Hart-Smith,L.J., Further Developments in the Design and Analysis of Adhesive-Bonded Structural Joints, Joining of Composite Materials, Ed. by Kedward,K.T., ASTM STP 749, 1981, pp.3-31.

[117] Hart-Smith,L.J., Analysis and Design of Advanced Composite Bonded Joints, NASA Contractor Report CR 2218, 1974.

[118] Hart-Smith,L.J., Adhesive Bonded Joints for Fibrous Composite Structures, Douglas Paper 7740 - Presented at International Symposium, Joining and Repair of Fibre Reinforced Plastics, Imperial College, 1986.

[119] Hart-Smith,L.J., Adhesive Bonded Scarf and Stepped Lap Joints, NASA Contractor Report CR 112237, 1973.

[120] Adams,R.D., Theoretical Stress Analysis of Adhesively Bonded Joints, Joining Fibre-Reinforced Plastics, Ed. by F.L.Matthews, Elsevier Applied Science Publishers Ltd., 1987, pp.185-226.

[121] Liechti,K.M., Johnson,W.S. and Dillard,D.A., Experimentally Determined Strength of Adhesively Bonded Joints, Joining Fibre-Reinforced Plastics, Ed. by F.L.Matthews, Elsevier Applied Science Publishers Ltd., 1987, pp.105-184.

[122] Pickett,A.K. and Hollaway,L., The Analysis of Elastic Adhesive Stresses in Bonded Lap Joints in FRP Structures, Composites Structures, Vol.3, No.1, pp.55-79, 1985.

[123] Tiu,W.P. and Sage,G.N., Fatigue Strength of Bonded Joints in Carbon Fibre Reinforced Plastics, Int. Conf. on Structural Adhesives in Engineering, The University of Bristol, 2-4 July 1986.

[124] Sage,G.N. and Tiu,W.P., The Effect of Glue-line Voids and Inclusions on Fatigue Joints in Composites, Composites, 1982, Vol.13, No.3, pp.228-232.

[125] Robson,J.E., Matthews,F.L. and Kinloch,A.J., The Fatigue Behaviour of Bonded Repairs to CFRP, Proc. of 2nd Int. Conf. on Deformation and Fracture of Composites, 29-31, March 1993.

[126] Wilhelmi,G.F. and Schab,H.W., Glass Reinforced Plastic (GRP) Piping for Shipboard Applications, Naval Engineers Journal, Vol.89, No.2, 1977, pp.139-159.

[127] Gustafson,C.G., Semb,G. and Moursund,B., Fatigue from Waterhammer on Filament Wound GRE-Pipes and Adhesive Bonded Joints, Proc. of 9th Int. Conf. on Composite Materials (ICCM/9), Vol.IV, pp.63-73, Madrid, 12-16 July, 1993.

[128] Jena,B. and Pradhan,B., Analysis and Optimization of Bonded Joints with FRP Composite Tubes, Proc. of Ninth Int. Conf. on Composite Materials (ICCM/9), Vol.IV, pp.82-88, Madrid, 12-16 July, 1993.

[129] Melve,B. and Moursund,B., Critical Defects in Adhesive Tubular Joints of GRP Process Pipes Determined with Acoustic Emission, Proc. of Ninth Int. Conf. on Composite Materials (ICCM/9), Vol.IV, pp.36-46, Madrid, 12-16 July, 1993.

[130] Huysmans,G., Marsol,J-F., Verpoest,I., Roeck,G.D., Ridder,L.D. and Vansant,J., A Friendly Rigid Composite Coupler for GRP Pipes, 7th European Conference on Composite Materials (ECCM-7), 14-16 May 1996, London.

[131] Juwono,A.L., Leong,K.H. and Strafford,K.N., Performance of Flat and Tubular Adhesive Joints in Hostile Environments, 7th European Conference on Composite Materials (ECCM-7), 14-16 May 1996, London.

[132] Owen,M.J. and Howe,R.J., The Accumulation of Damage in a Glass-Reinforced Plastic under Tensile and Fatigue Loading, J. Phys. D: Appl. Phys., Vol.5, 1972, pp.1637-1649.

[133] Owen,M.J. and Bishop,P.T., Crack-growth Relationships for Glass-Reinforced Plastics and Their Application to Design, J. Phys. D: Appl. Phys., Vol.7, 1974, pp.1214-1224.

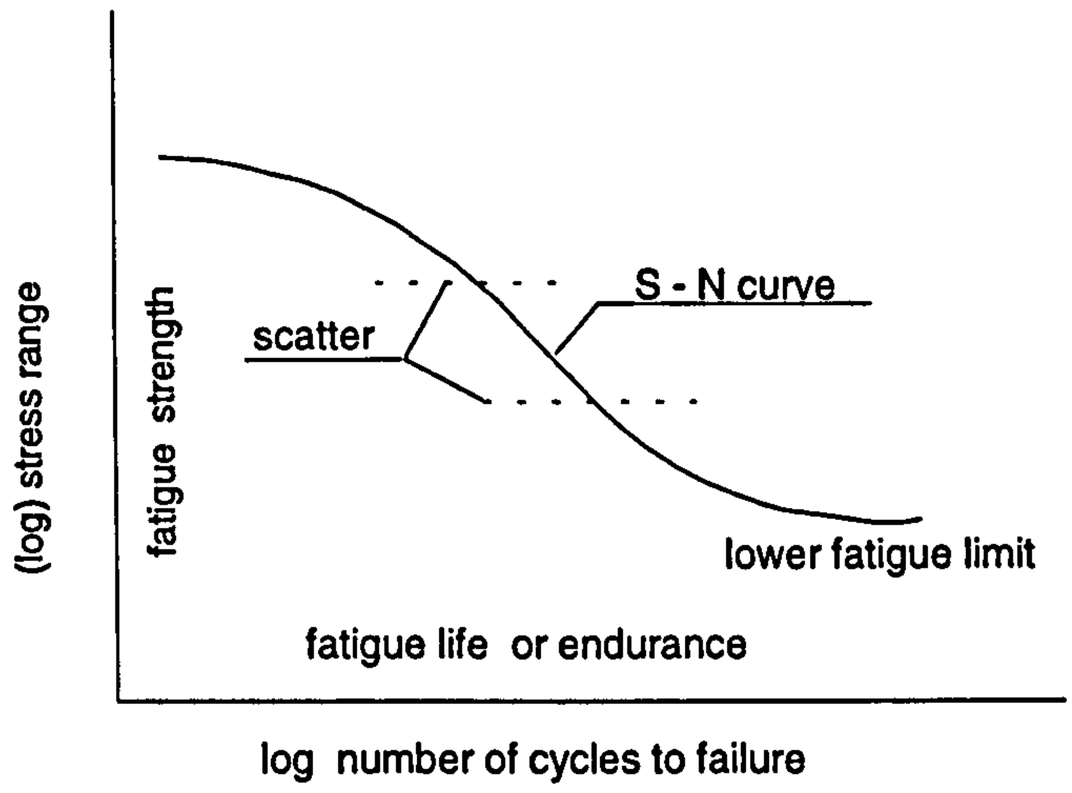

Figure 3.1. Fatigue life (S-N) curve.

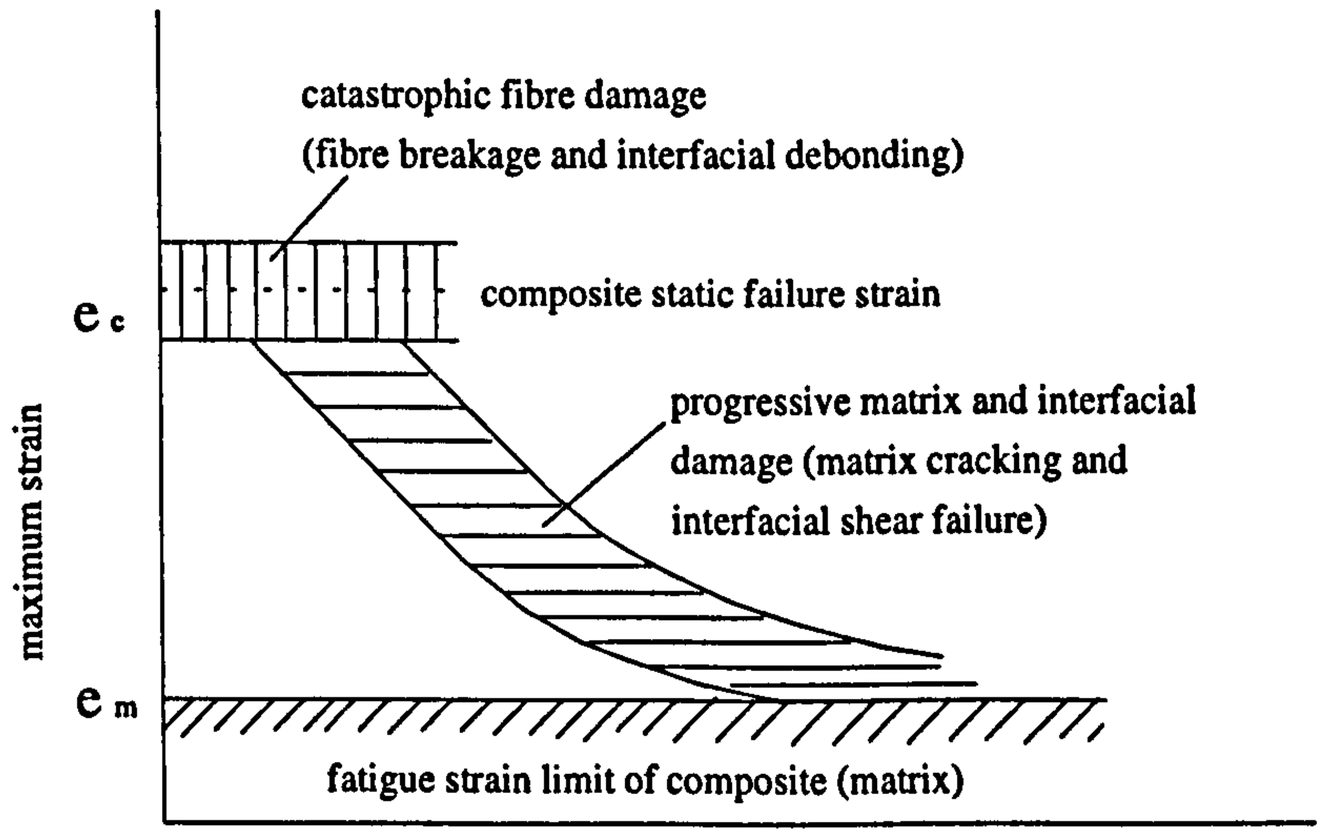

Figure 3.2 Strain-life diagram for unidirectional fibre composites showing the dominant regions of tensile fatigue damage mechanisms, based on the so-called fatigue-life diagrams proposed by Talreja [11].

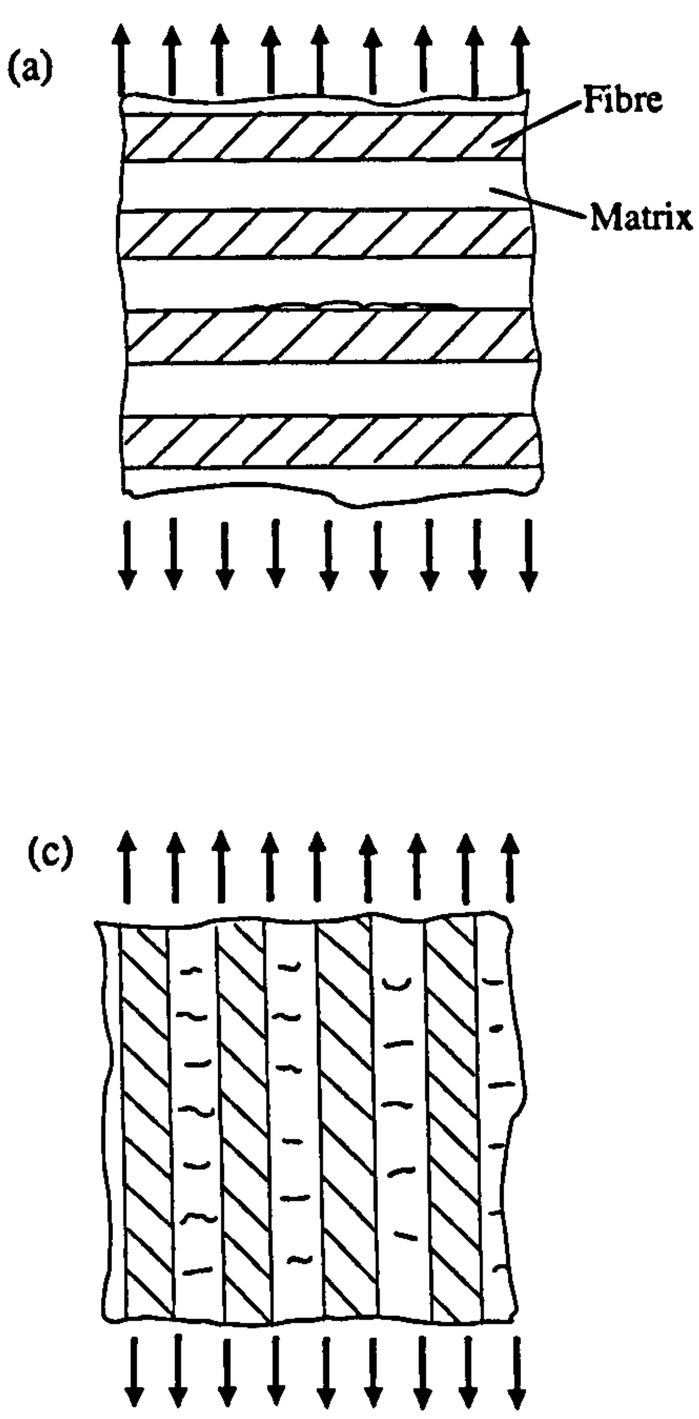
(a)
Fibre
Matrix

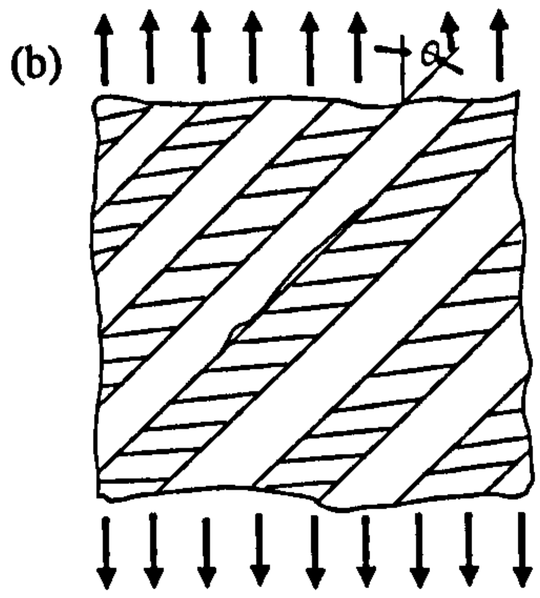
(b)
θ

(c)

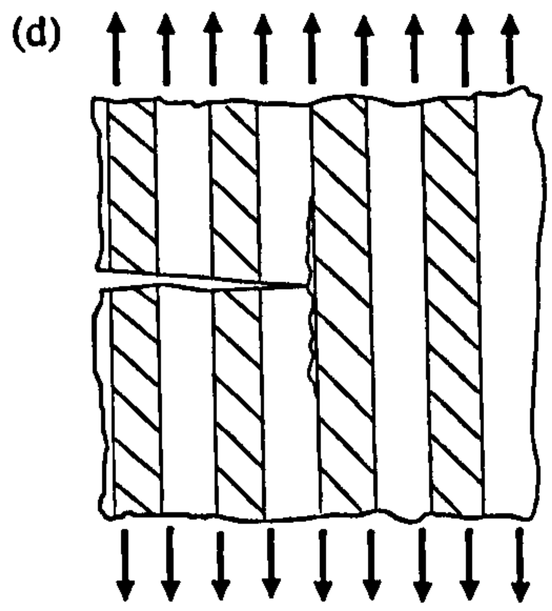
(d)

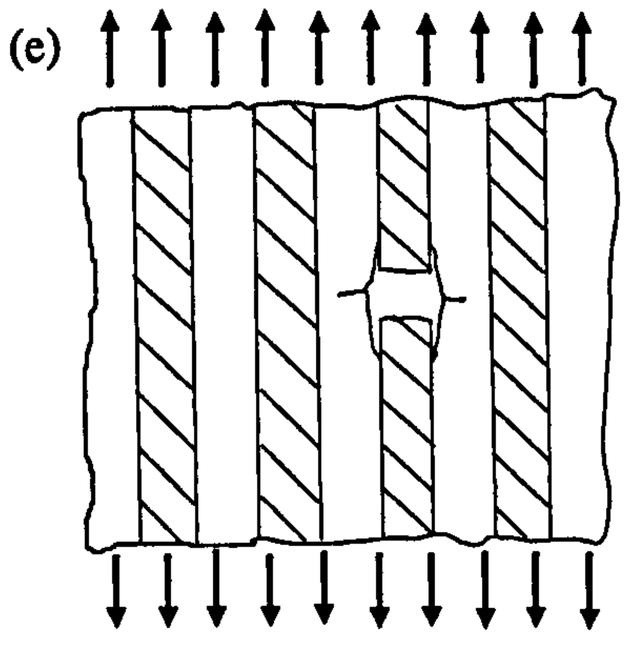
(e)

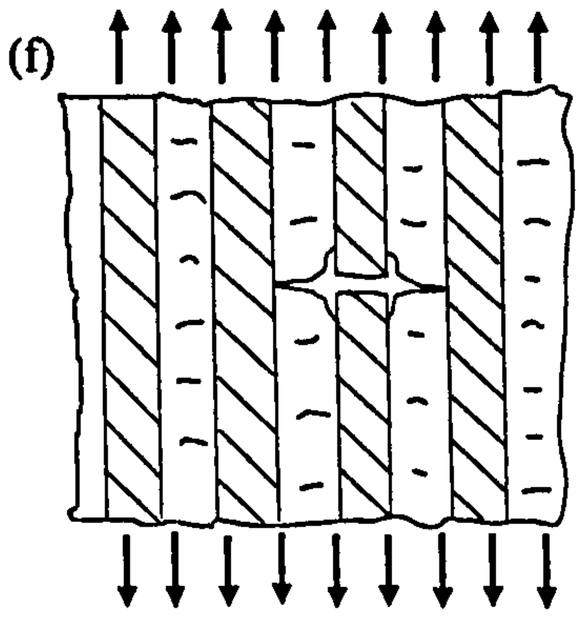
(f)

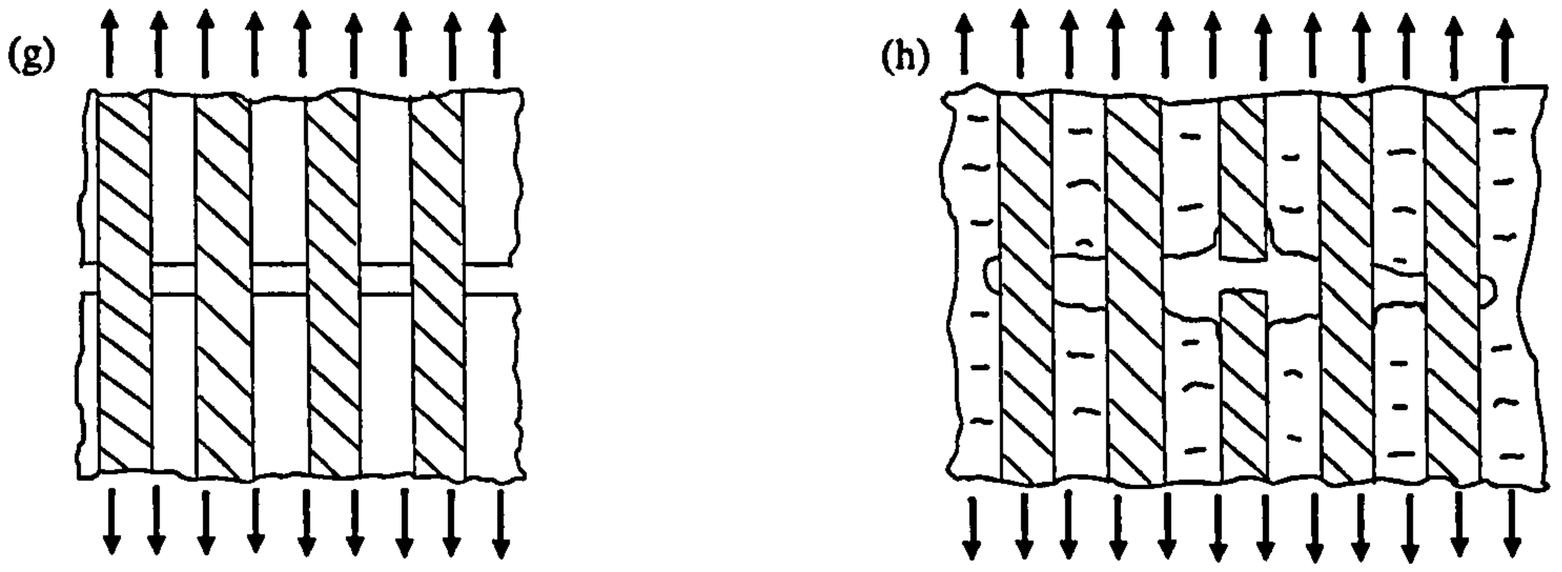

Figure 3.3 Fatigue damage mechanisms in unidirectional fibre reinforced composite [14]

Matrix and interfacial cracking under off-axis fatigue of unidirectional composites:

(a) Opening mode crack growth (transverse fibre debonding), $\theta = 90^{o}$,

(b) Mixed (opening and sliding) mode crack growth, $0 < \theta < 90^{o}$.

Ductile (polymer) matrix damage:

(c) Dispersed failure mode: cracks confined to matrix only,

(d) Localised failure mode: cracks grow by fibre breakage and, at later stages, by interfacial failure.

Fibre damage:

(e) Fibre break causing interfacial debonding,

(f) Fibre break causing matrix cracking,

(g) Fibres bridging a matrix crack,

(h) Combination of (e), (f) and (g).

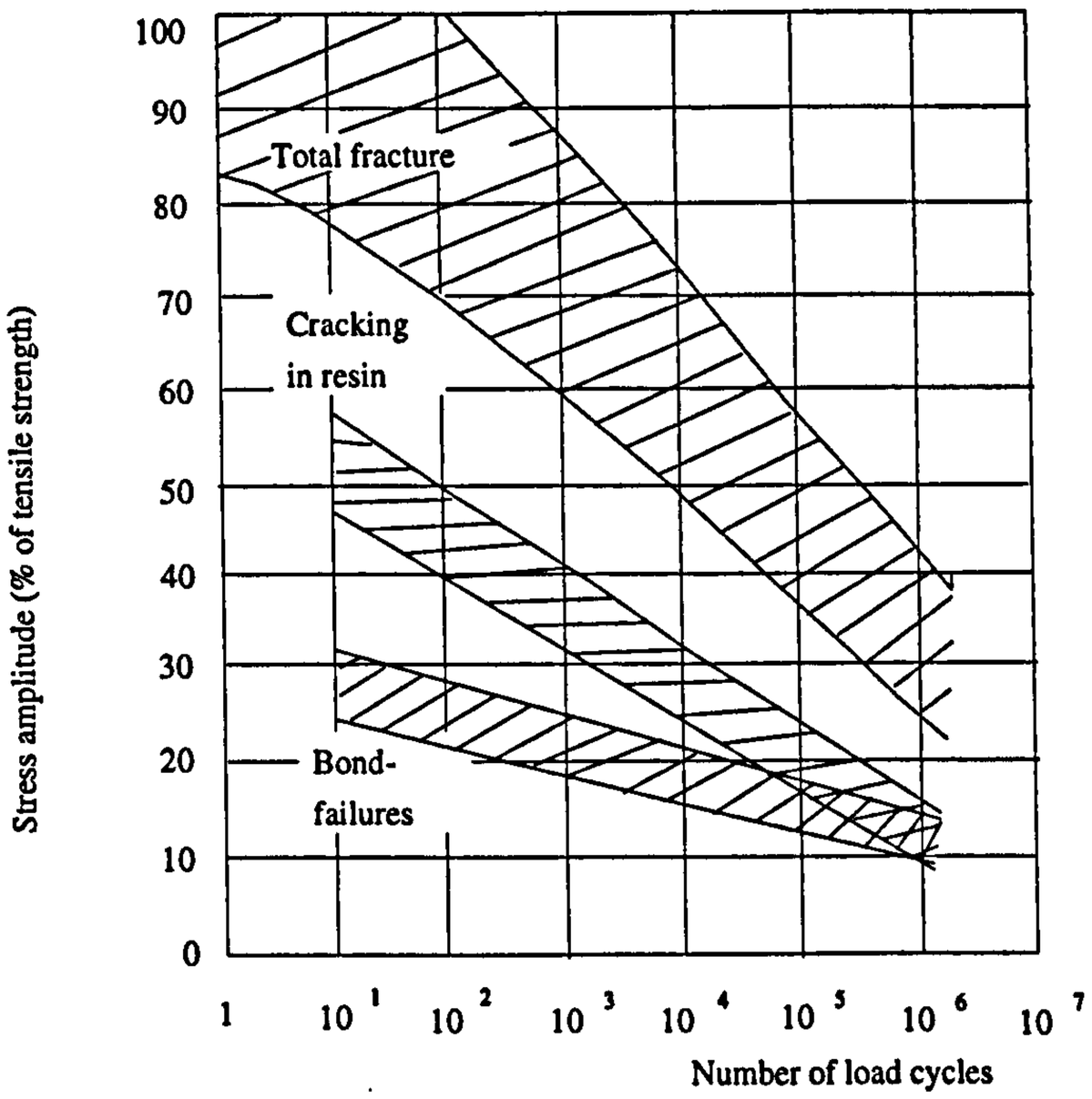

Figure 3.4 S-N curve for glass fibre reinforced polyester under alternating tension/ compression loading. (Ratio of maximum loading to minimum loading: R= -1, frequency: 100 cycles per minute) [33]

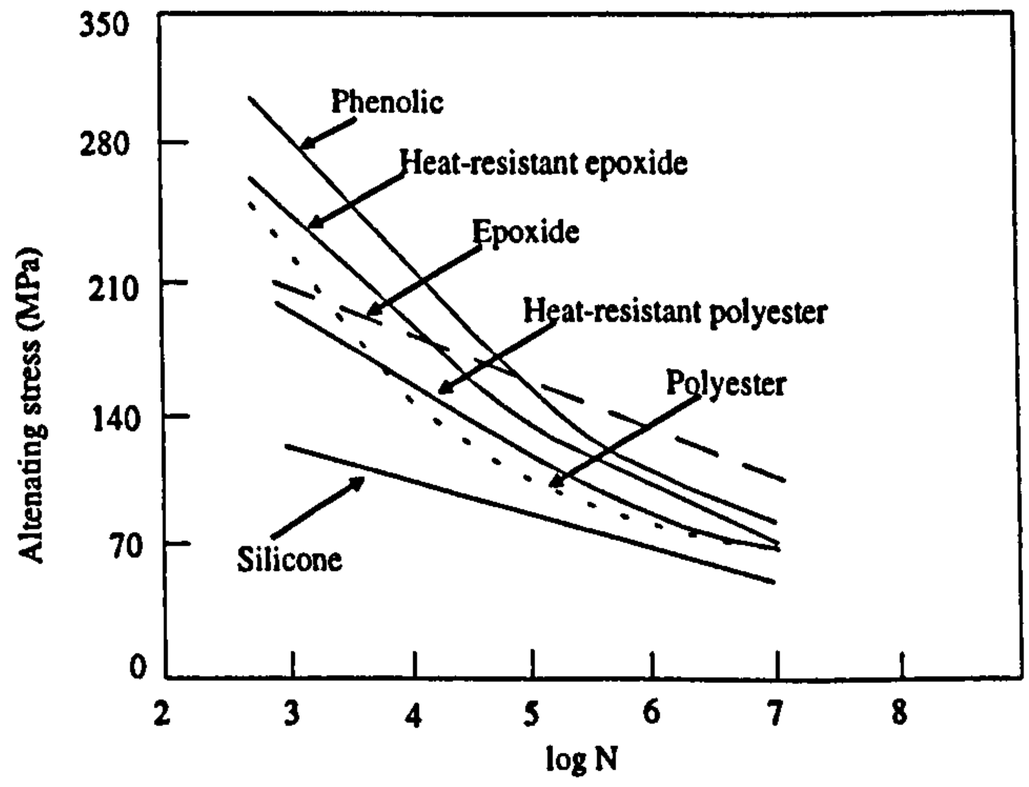

Figure 3.5 S-N curves for E-glass fibre composites with a number of matrices, showing the effect of matrix type [1].

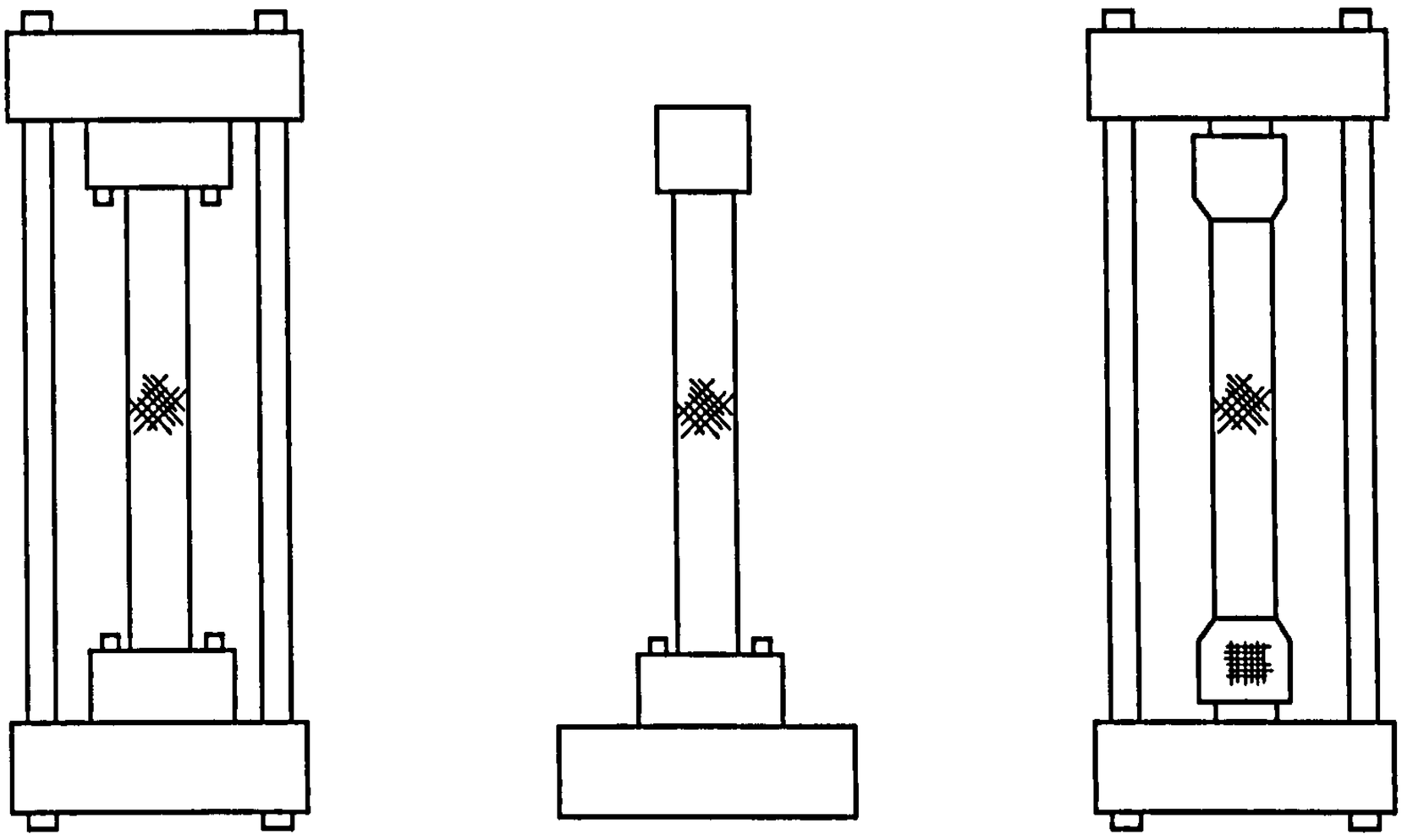

Mode 1 Mode 2 Mode 3

Figure 3.6 Schematic diagram of three methods of internal pressure testing; in Mode 1 the ends of the pipe are sealed and clamped to the thick end plates and tie bars hence allowing no axial strain; in Mode 2 the ends are clamped and sealed but are unrestrained so that the axial stress is half the hoop stress; in Mode 3 the ends of the pipe are free to slide on 'O' ring seals and therefore the axial stress is zero.

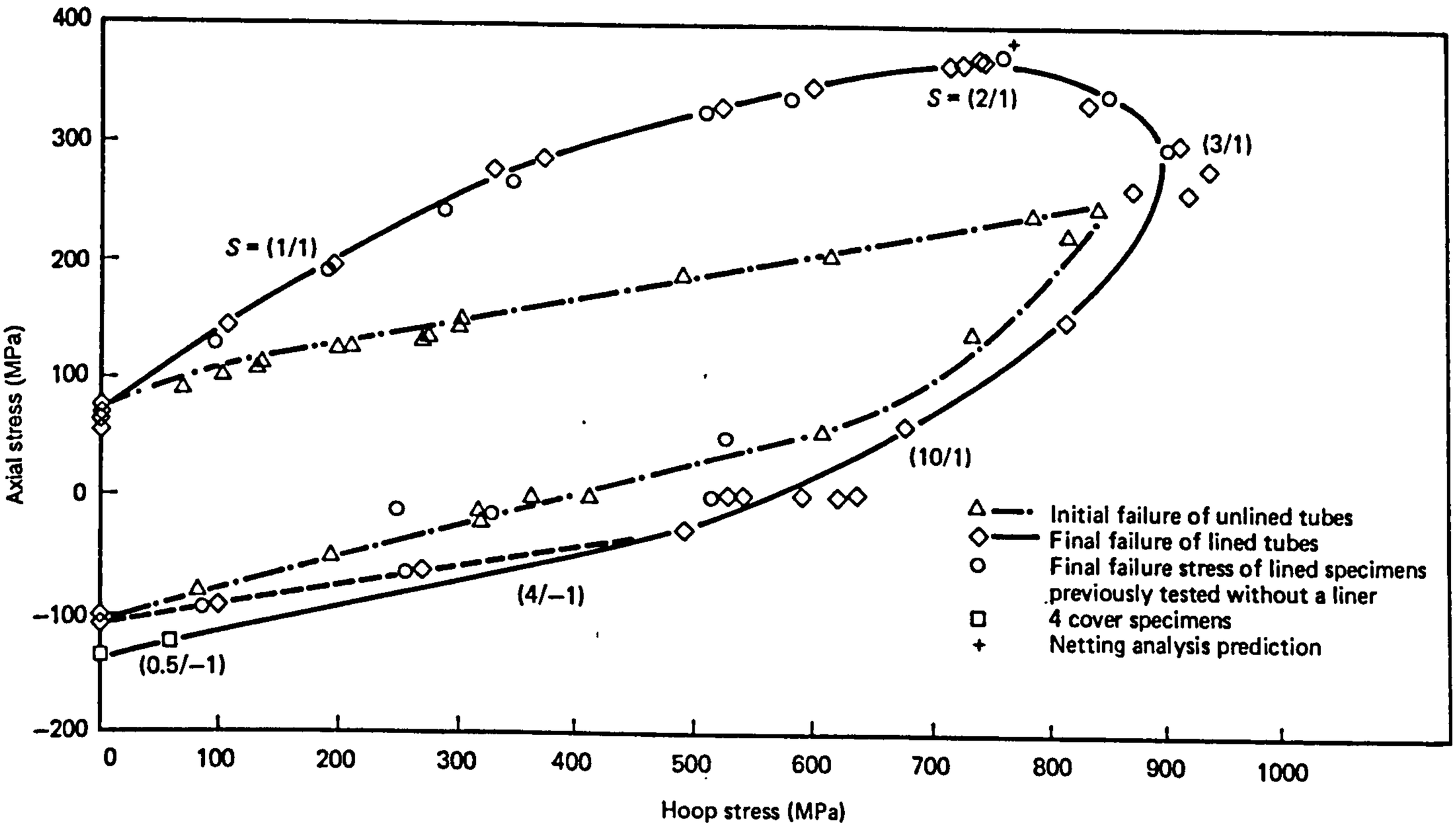

Figure 3.7 Initial failure (weepage stresses) and final failure (burst stresses) envelopes for $\pm 55^0$ filament wound E-glass/epoxy pipes subjected to biaxial loads, obtained by Soden et al [89].

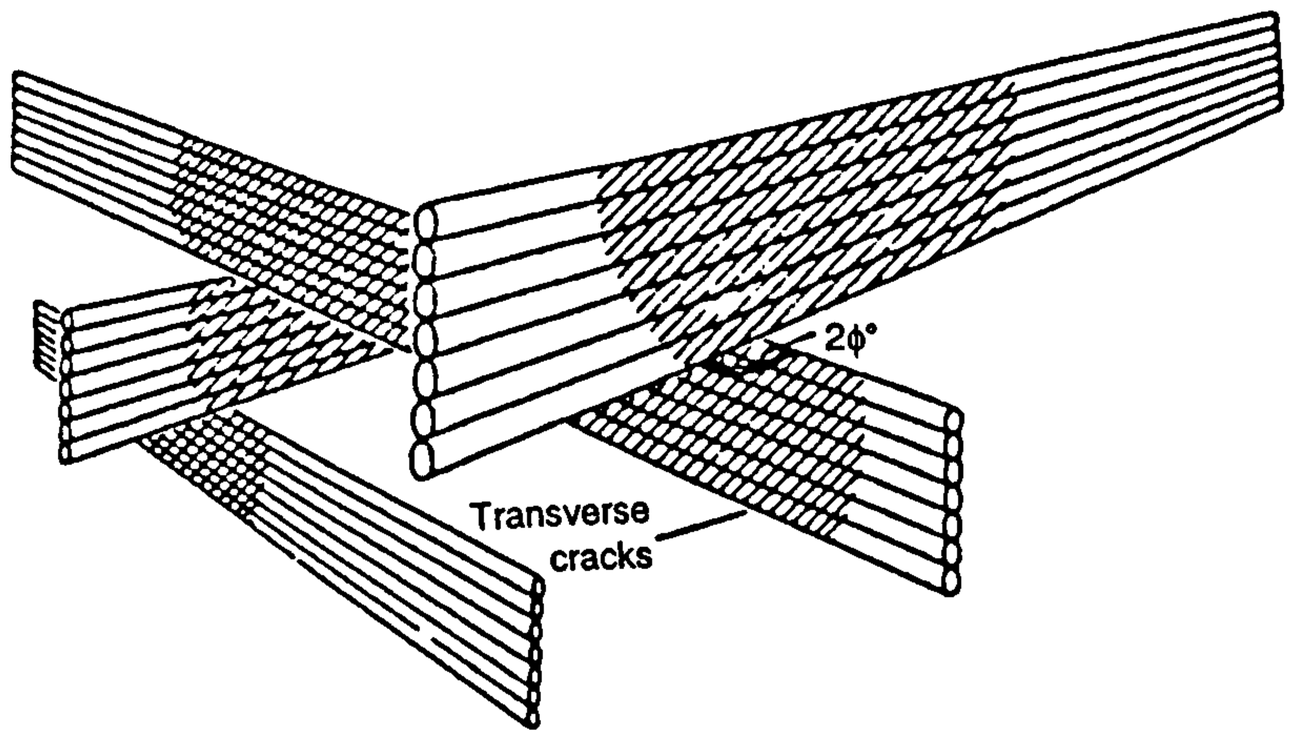

Figure 3.8 Schematic illustration showing formation of a weepage path through the pipe wall by the intersection of transverse cracks. The flow of liquid is restricted to the three contact points [99].

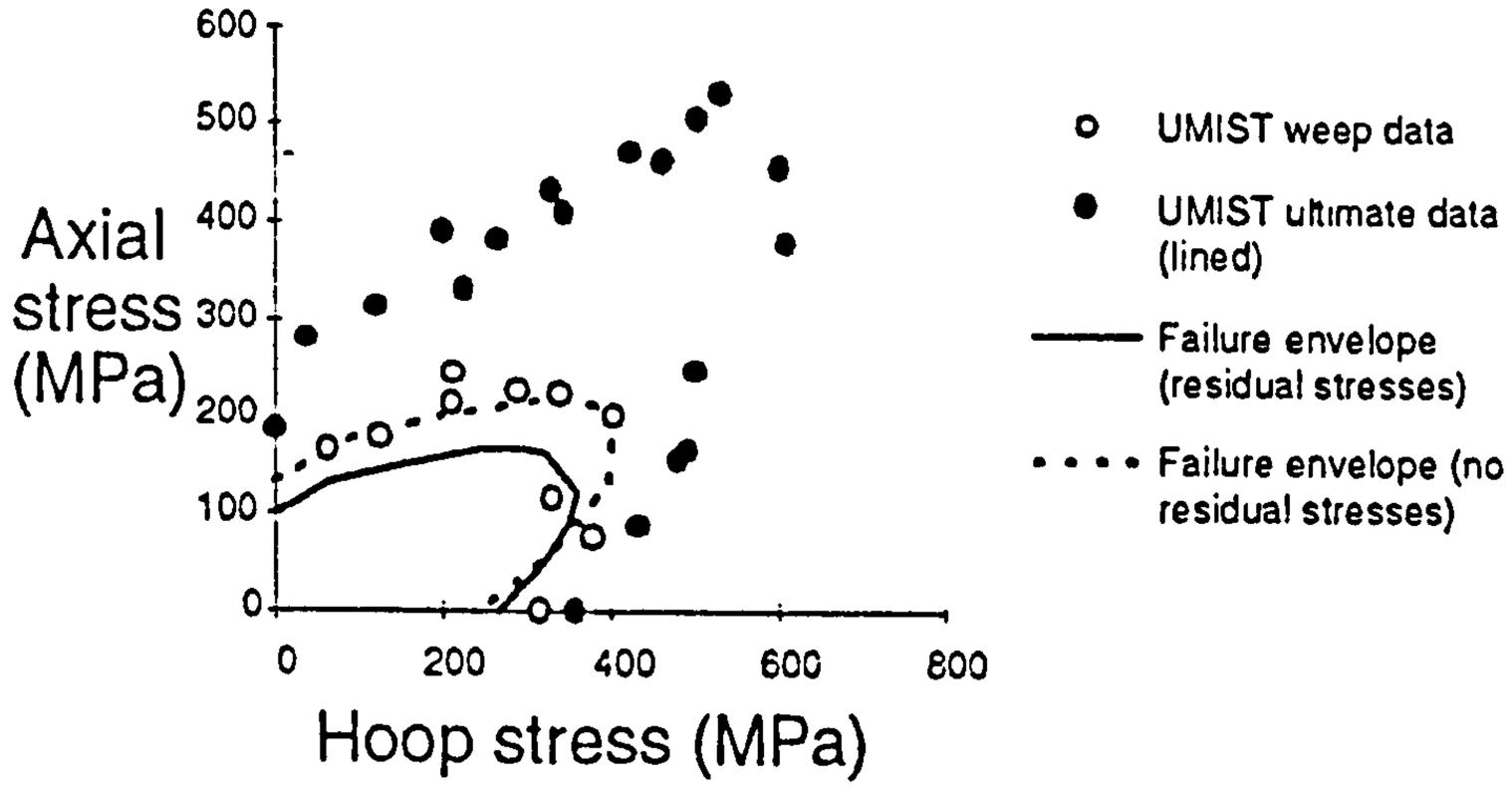

(a) 45^0 wound GRE pipes

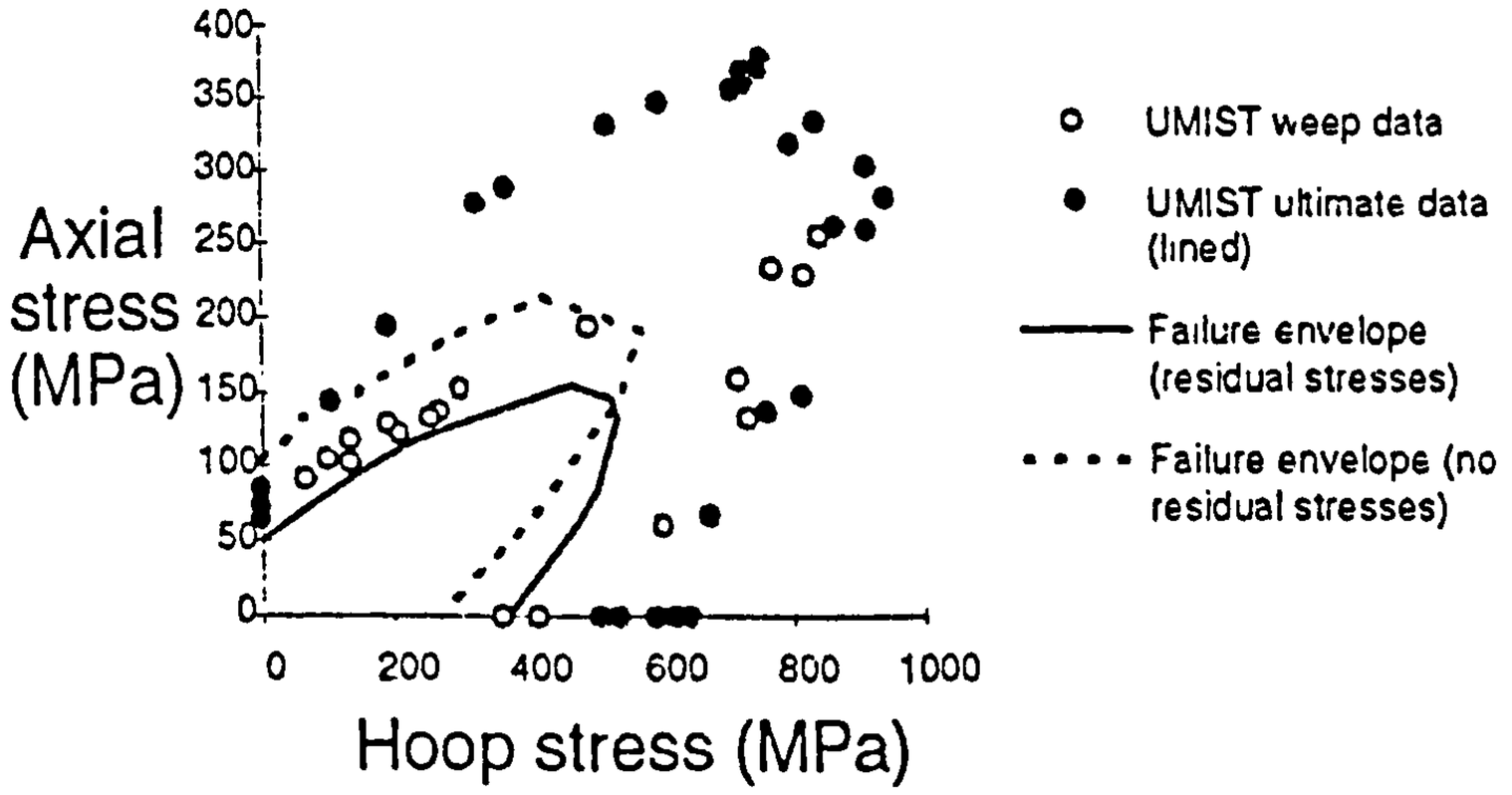

(b) 55^0 wound GRE pipes

Figure 3.9 Weepage envelopes for filament wound GRE pipes, calculated by Frost [107].

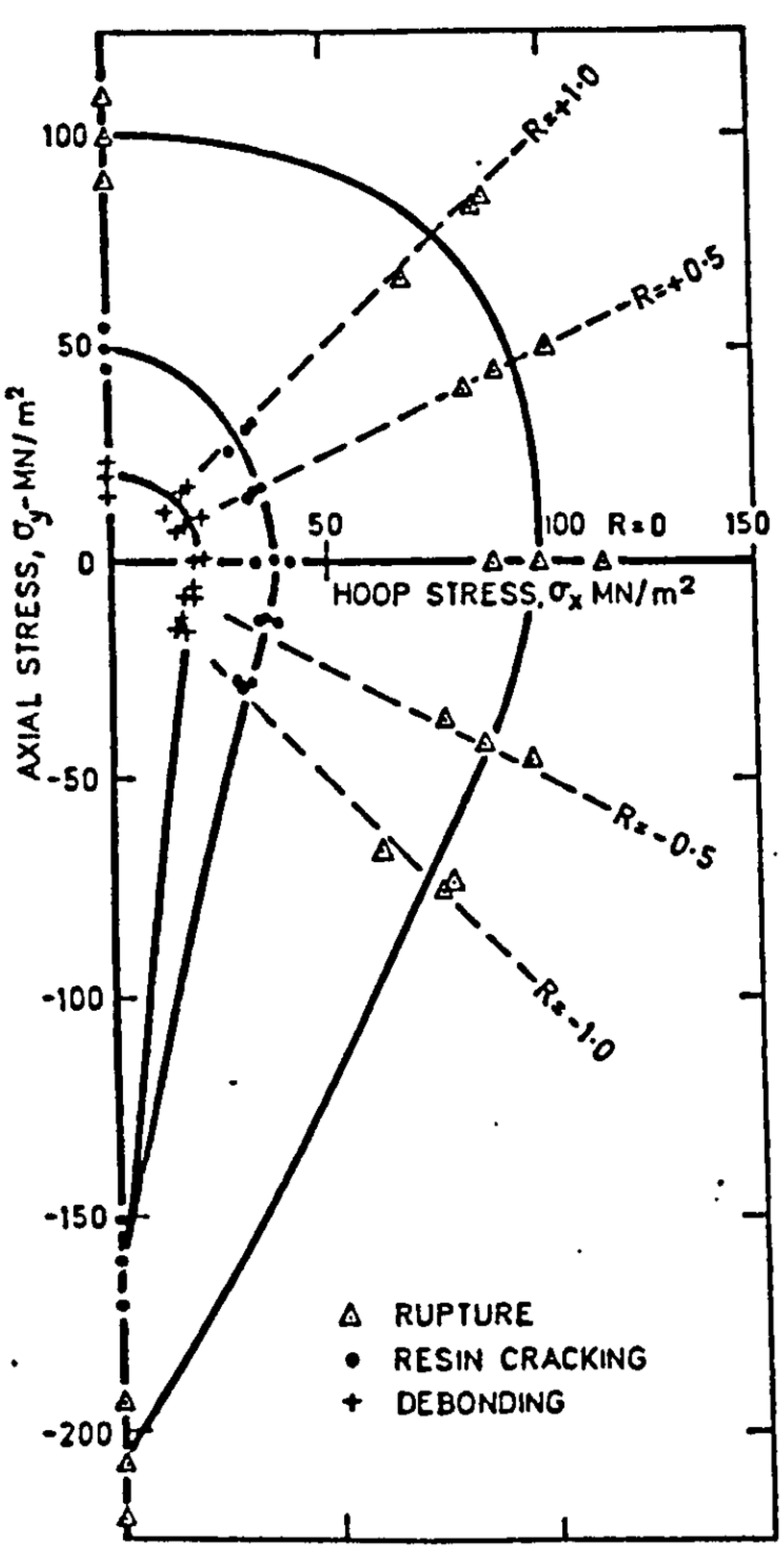

Figure 3.10 Static failure envelopes of glass CSM/polyester thin-walled pipes at different failure stages, obtained by Owen[103]

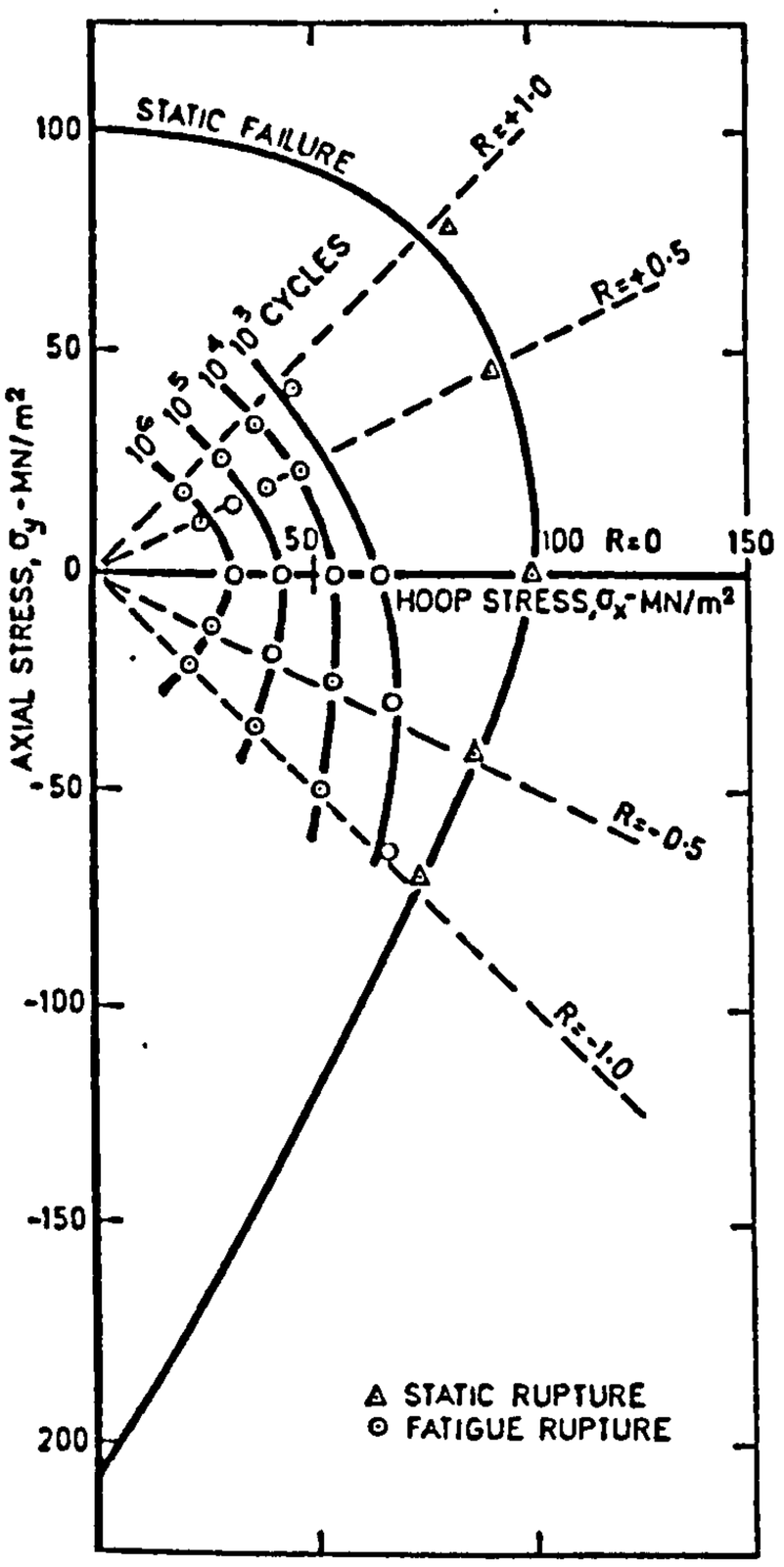

(a) glass CSM/polyester [103].

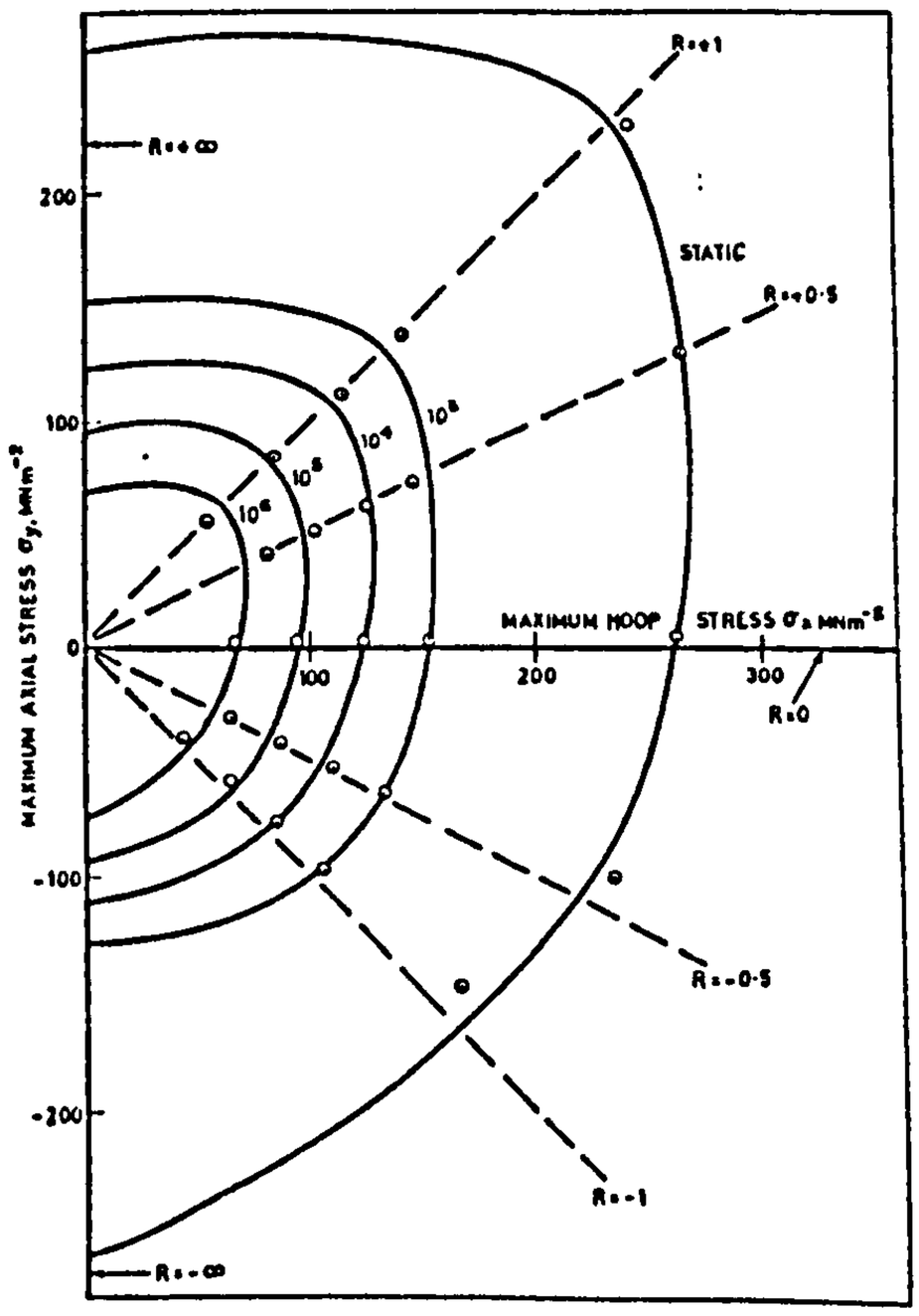

(b) α=0°, glass fabric/polyester [102]

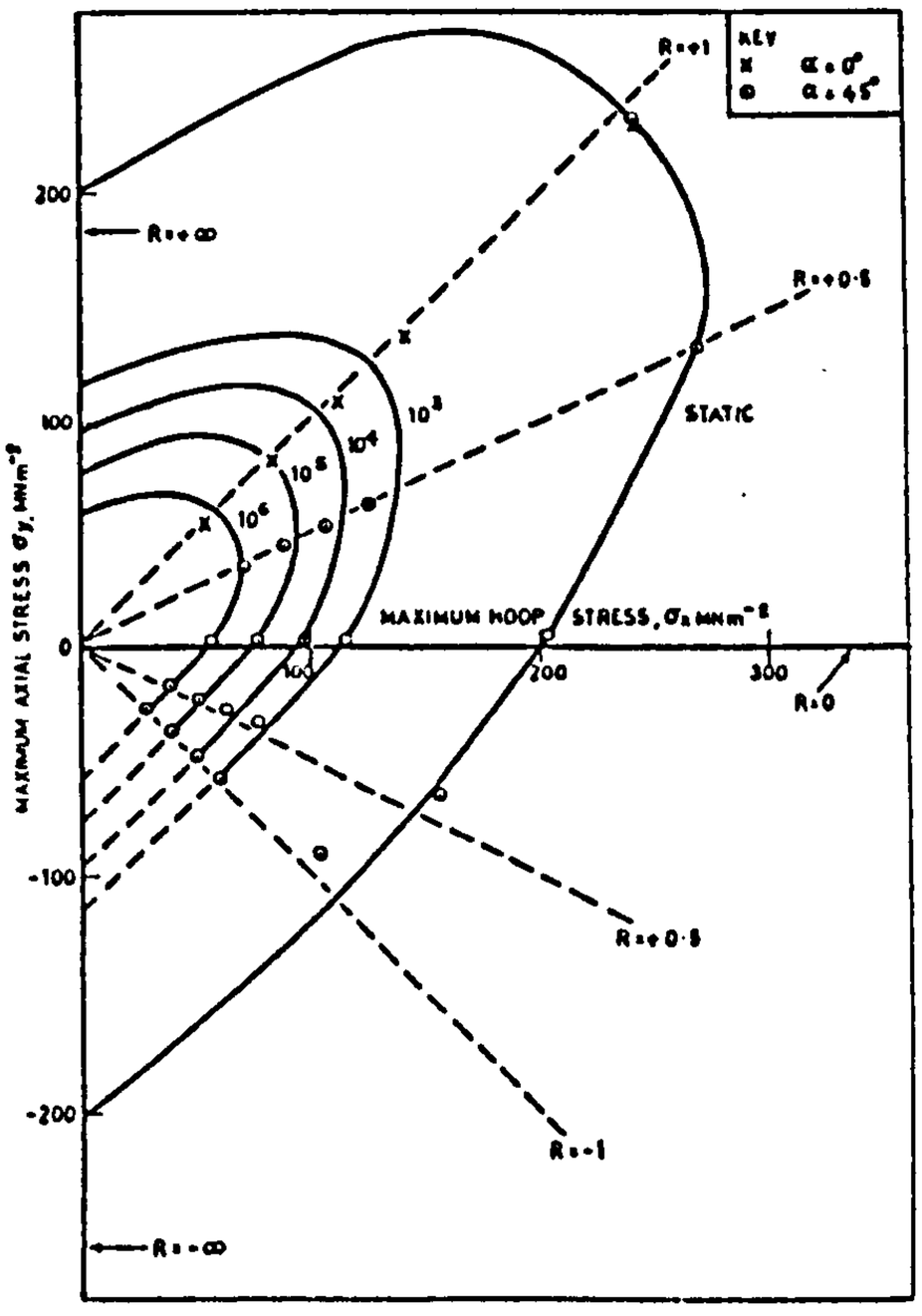

(c) α=45°, glass fabric/polyester [102]

Figure 3.11 Fatigue envelopes for rupture of thin-walled pipes (α is off axis angle, R= axial stress/hoop stress).

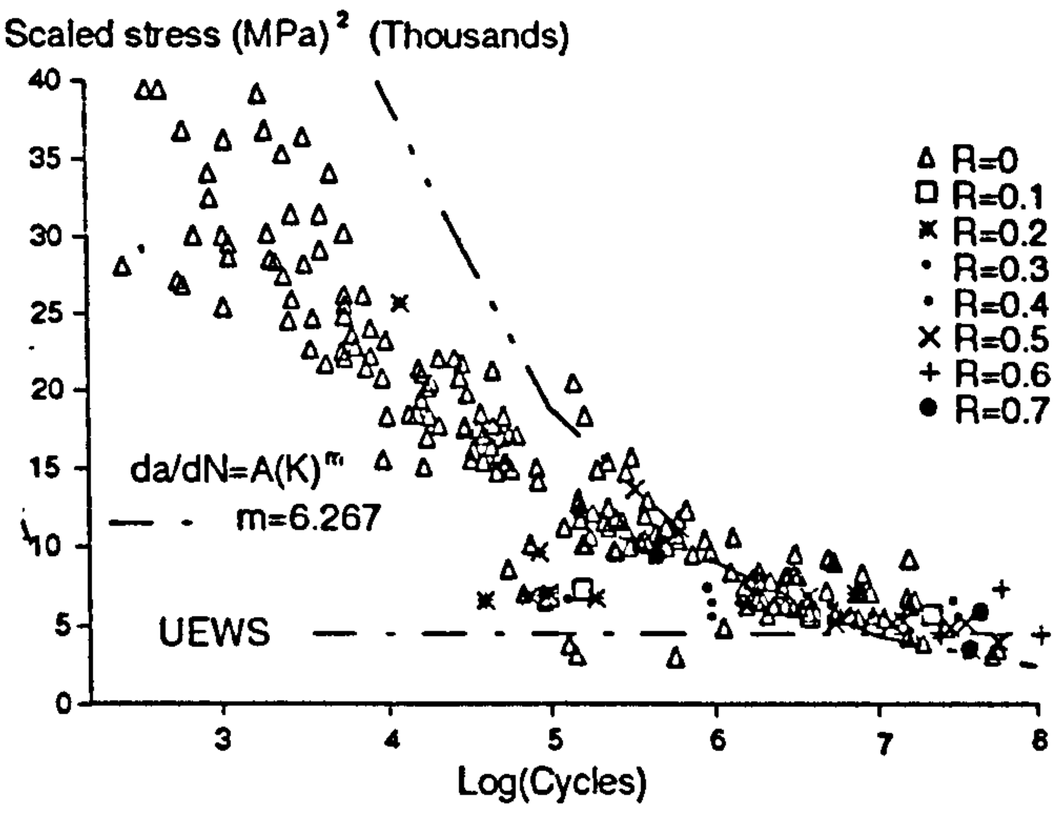

Figure 3.12 Scaled S-N curves for 55^0 wound GRE pipes subjected to cyclic internal pressure with different minimum/maximum pressure ratio R [106,107].

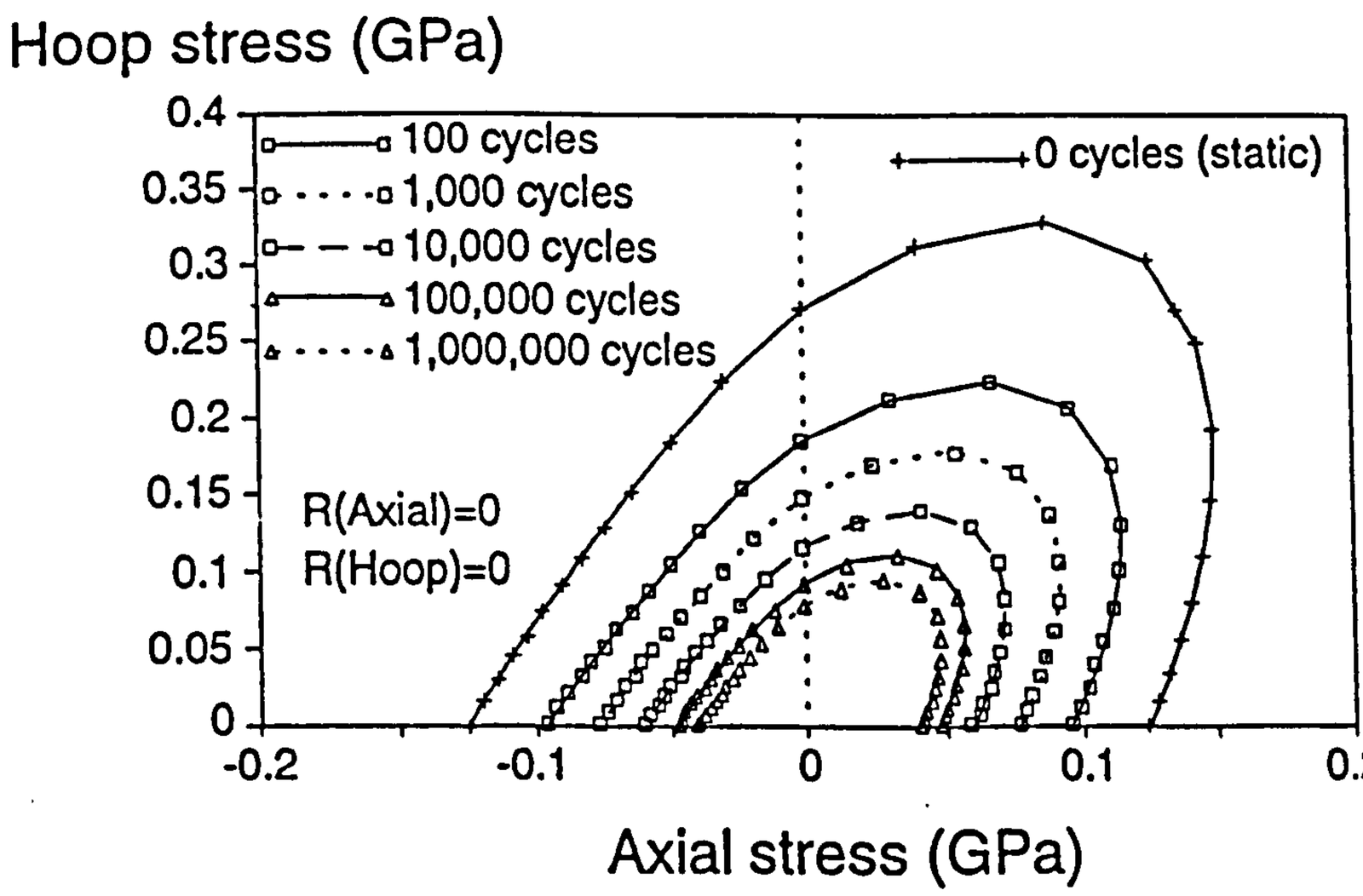

Figure 3.13 Predicted fatigue envelopes for 55^0 wound GRE pipes based on Tsai-Wu criterion [104,105].

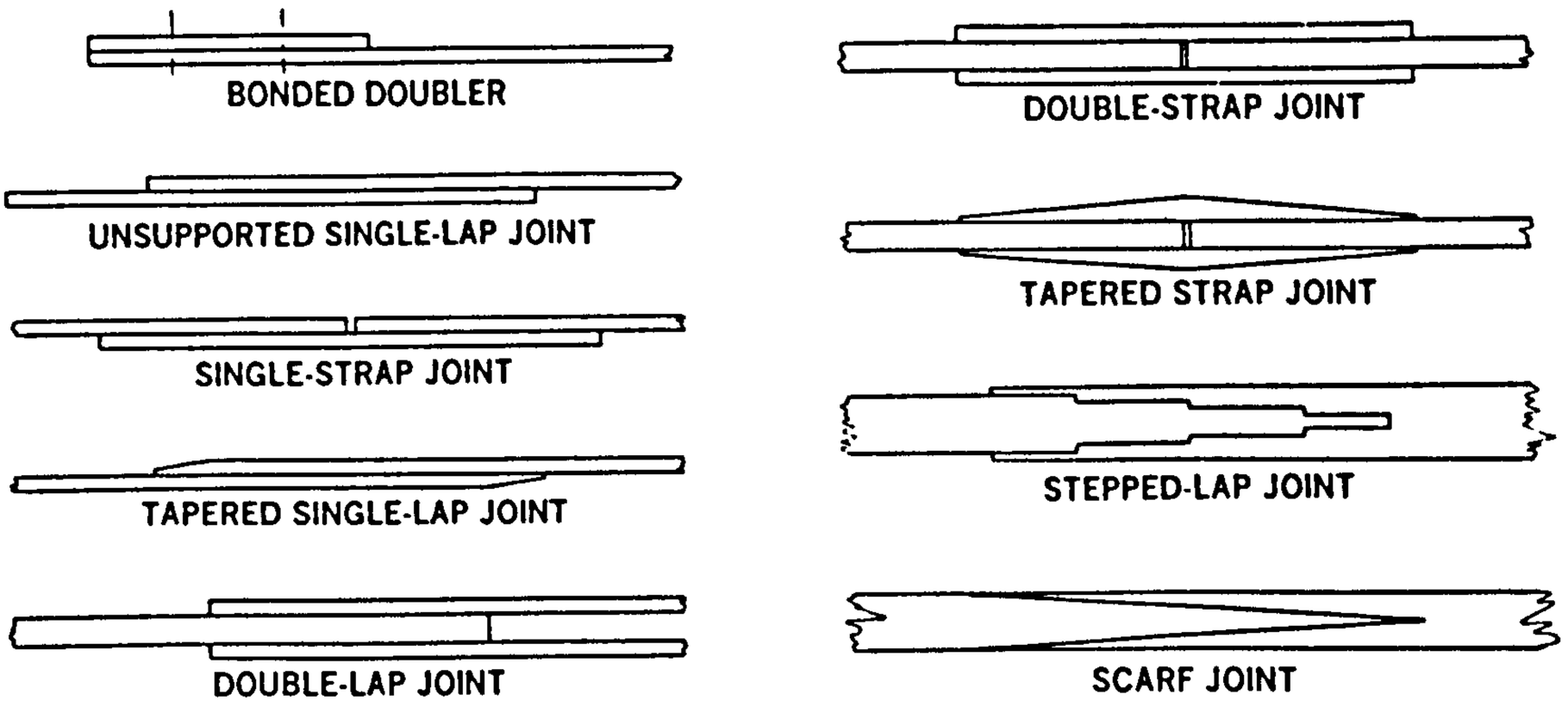

Figure 3.14 Adhesively bonded joint types.

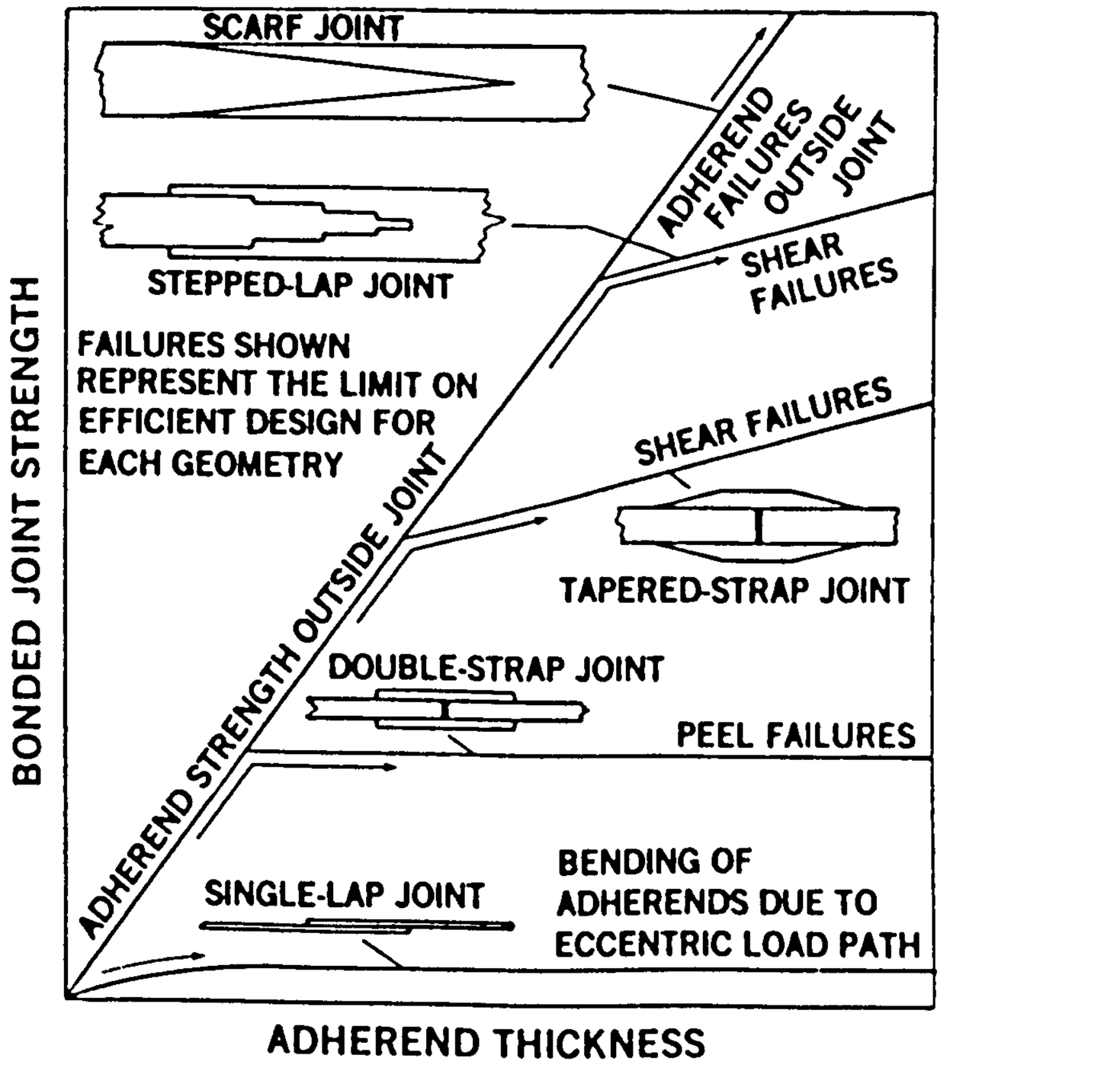

Figure 3.15 Relative failure strengths and mechanisms of different bonded joint types [118].

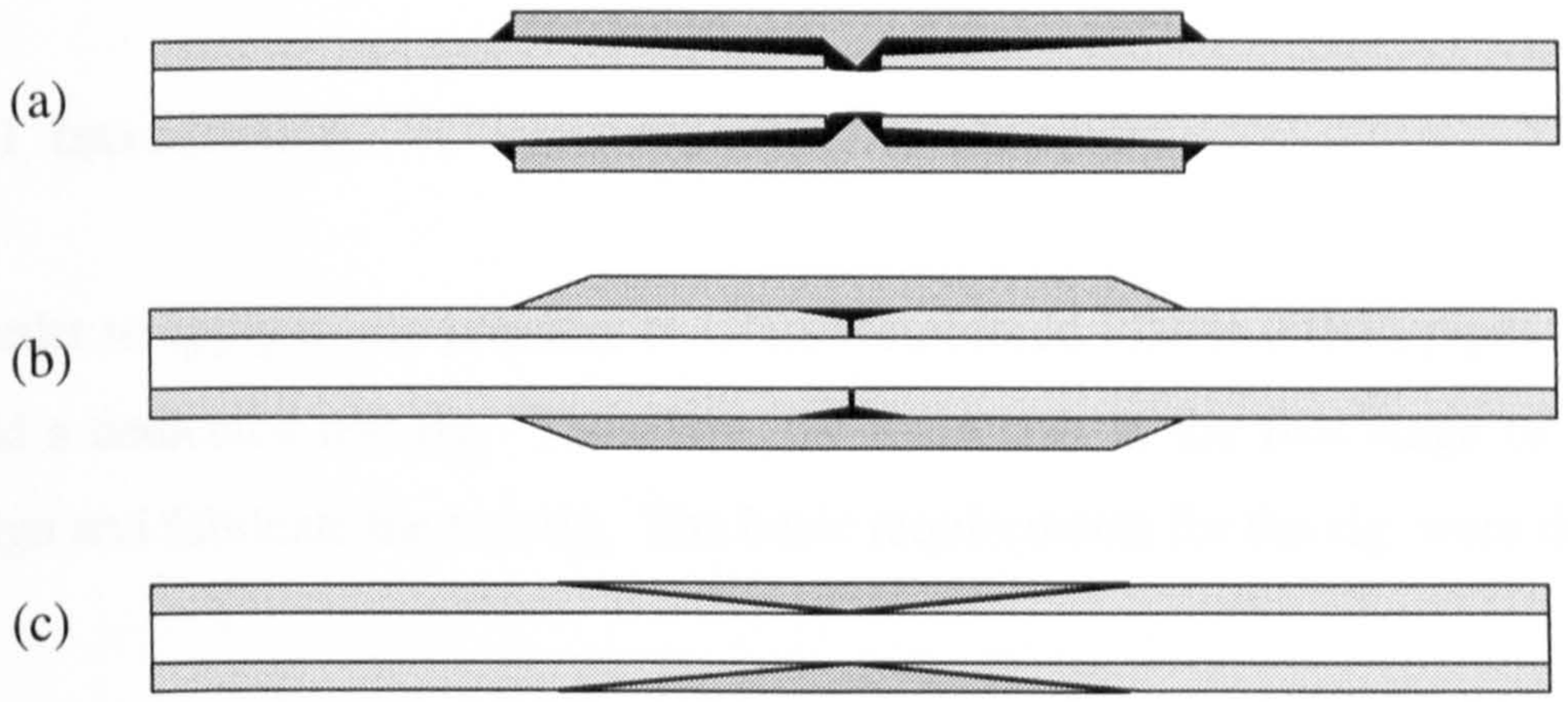

Figure 3.16 Typical coupler-connected joints.

CHAPTER FOUR

EXPERIMENTAL TECHNIQUES

4.1 FATIGUE TEST RIG

4.1.1 Introduction

In order to apply cyclic pressure to Glass Reinforced Plastic (GRP) pipes it was necessary to build a dedicated test rig. Therefore, the main task in the first stage of this project was to design and fabricate the test rig. The basic requirements for the rig were that:

(a) it should be fatigue resistant with respect to the fatigue life of the GRP pipes to be tested;
(b) it should be capable of generating pressures of up to at least 70 MPa statically and cyclically and remain safe for operators and equipment around;
(c) it should be able to record the pressure history of the specimen tested during a fatigue or static test.

4.1.2 Functions

The rig used in this project, shown in Figure 4.1, was designed and built by the author. It has the following functions:

(a) It can produce hydraulic pressures, using natural sea water, of up to 70 MPa (≈10,000 psi).

(b) It can carry out static tests on pressure vessels, e.g. various tanks and pipes, subjected to internal or external pressure.

(c) It can perform fatigue tests on various pressure vessels under cyclic internal or external pressure. The test frequency can be controlled by varying the pressurisation speed, and is

generally not higher than 20 cycles per minute depending on the cyclic pressure level.

(d) It can perform static fatigue tests on various pressure vessels under a constant internal or external pressure.

(e) It can perform tests on various vessels under pressure in combination with high temperature and corrosive solutions. The hydraulic system was made of stainless steel parts, allowing the hydraulic media to contain additions of corrosive materials.

4.1.3 Construction and Working Principles

The construction of the rig was based on the ASTM standard test method D2143 [1], which gives guidelines and suggestions for GRP pipe testing and rig construction. Figure 4.2 shows schematically the construction of the rig. This consisted of two main systems; the pressure system, as shown in Figure 4.3, to generate high pressures in a hydraulic media by an air-operated pump, and the control and data acquisition system to control the pressure cycle and to display and store the pressure data within the system.

The principle of the rig is shown schematically in Figure 4.4. There are three circuits in the figure; the electrical circuit, the pneumatic circuit and the hydraulic circuit. In the diagram, E1 to E7 are the electric parts in the electrical circuit, A1 to A7 are the pneumatic parts and H1 to H7 are the hydraulic parts, as described in Table 4.1.

(a) Pressurisation

The hydraulic pump (H1), model SC 10-400-12.5, was manufactured by SC Hydraulic Engineering Corporation. It can produce a hydraulic pressure of 20,000 psi (138 MPa) which is almost twice the required maximum working pressure. The pump is driven by compressed air with a pressure in the range of 10 to 100 psi. The output of the hydraulic pressure of the pump is approximately proportional to the input pneumatic pressure, as shown in Figure 4.5. A start pressure of 0.3 bar (≈4 psi) is required to start the pump, thus the line in Figure 4.5 is shifted a little bit to the left. Adjusting the air pressure by altering regulator (A1) caused a change in the hydraulic pressure output by the rig.

The pressure gauge, isolator valves, pressure transducer, stainless elbows, tees and other hydraulic parts were also manufactured by the same company and are rated in 10,000 psi (≈70 MPa). The pressure transducer (H4) was connected to a digital indicator (E3), type K9010, which was supplied by Intersonde Limited. A full range calibration of the transducer was carried out at a laboratory temperature of 21°C. The K9010 digital indicator is a microprocessor-based process indicator and alarm controller. It displays the pressure in the system and sets off an alarm when the pressure becomes higher or lower than the preset values. A system pressure higher than the preset 'high pressure level' caused the alarm relay E4 to switch, whereas a system pressure lower than the preset 'low pressure level' caused the alarm relay E5 to switch. These alarm relays were useful for producing cyclic pressure during fatigue tests and were very important for setting a maximum safe pressure during static tests.

An air-operated relief valve (H5) was connected to the rig to allow the release of pressure when it reached the maximum value during a fatigue test or when it reached the safe pressure level during static tests. Two 3-way solenoid valves (A2 and A6) were mounted in the air inlets of the pump and of the relief valve. Raising or lowering of the hydraulic pressure was achieved by switching these solenoid valves on or off.

The solenoid shuttle valve A6 was controlled by the high pressure level alarm relay (E4) and the solenoid shuttle valve A2 was controlled by the low pressure level alarm relay (E5). When the system pressure reached the preset HIGH level , the alarm relay E4 switched on and E5 switched off, causing the relief valve H5 to switch on and the pump off. Conversely, when the system pressure reached the preset LOW level , the alarm relay E4 switched off and E5 on, causing the relief valve H5 to switch off and the pump on. As a result, a "saw-tooth" type pressure cycle was generated in the system and the sea water automatically cycled in the hydraulic circuit. In each pressure cycle, system pressure firstly increased at a constant speed from the preset minimum to the maximum pressure and then decreased to the minimum rapidly at very high pressure release speed. Therefore, the pressure wavaform was normally a right triangle with a constant pressurisation speed. The frequency of the fatigue load was controlled by the pressurisation speed of the pump and could be changed by adjusting the input air pressure through regulator A1.

(b) Data-Logging System

The voltage signals from the pressure transducer (H4) and strain gauges were recorded by an RM Nimbus PC-386/25 computer through a data acquisition and control board PC30AT manufactured by Amplicon Liveline Limited. A Basic program was written for data acquisition and the transformation of the voltage signal into pressure. A linear relation existed between the output voltage of the board PC30AT and the hydraulic pressure shown in the indicator (E3), up to 70 MPa. The system had 16-channel 12-bit A/D (analog/digital) input and 2-channel 12-bit D/A (digital/analog) output facilities.

4.1.4 Test Types

GRP pipe specimens with carefully designed end-caps (see section 4.2) were tested under static or cyclic internal pressure. Load was applied using natural sea water as the hydraulic medium. According to the load type and rubber liner installation, three types of tests were performed:

(a) Static weepage test: The specimen was subjected to static internal pressure without the installation of a rubber liner, to measure its water weepage strength;

(b) Fatigue weepage test: The specimen was subjected to cyclic pressure, without the installation of a rubber liner, to measure its fatigue weepage strength;

(c) Static burst test: The specimen was installed with a rubber liner and subjected to static internal pressure to measure its burst strength.

No fatigue tests were carried out for specimens with rubber liners.

4.1.5 Definition of Failure

For each type of test, a consistent definition of failure for all specimens was made as follows:

(a) Failure during static weepage test

The general failure mode of commercial GRP pipes in static tests was weepage in the form of a sudden spout of water through the pipe wall or the adhesive interface of a joint. This occurred as resin in the pipe wall cracked. Weepage generally caused the system pressure to drop rapidly to no more than 30% of the maximum pressure. Increasing the pumping speed of the rig failed to produce a higher pressure which would have allowed the test to continue.

During the test, the computer data logging system was used to identify the pressure at which weepage first occurred. Once the weepage occurred, the specimen was deemed to have failed.

(b) Failure during fatigue weepage test

During the fatigue weepage test, the entire system was automatically pressure-cycled. The smallest detectable leak (seapage or weepage) was taken to constitute failure. This occurred in the GRP pipe as a result of the formation of small matrix cracks, usually parallel to the fibre reinforcement, which allowed leakage as the pressure reached its maximum value. Normally, when the load returned to its minimum, the leakage would stop, even when the pressure did not reach zero. In most cases, leakage amounted to only a few drops and the system still maintained pressure. Both types of weepage tests made only the surroundings of the test rig wet and were generally safe.

(c) Failure during static burst test

In order to measure the ultimate pressure strength, pipes were lined with rubber tubes to prevent leakage of the pressurising fluid on resin cracking. For these lined pipes, matrix cracking did not constitute the failure of the pipe. System pressure was further increased until the final burst took place. At the moment when the burst occurred, system pressure

disappeared suddenly with a big 'BANG'. A large proportion of the fibres were broken and an obvious crack or hole appeared on the pipe wall. Unlike the weepage tests, the burst tests could be very dangerous when the burst occurred.

The rubber tube should provide a perfect seal and leakage should never occur before the final burst. Furthermore, the burst location should be in the gauge area of the pipe and at a reasonable distance from the pipe ends, such as at least 2 to 3 times the pipe diameter. The results for pipes failing near their ends should be discarded as they are affected by the end caps.

4.1.6 Experimental Procedure

With each test, the operation procedure specified below was strictly followed:

(a) The specimen was visually examined to inspect for defects which may have arisen during fabrication and transportation. The specimen's dimensions, including internal and external diameters, wall thickness and so on, were measured at several locations.

(b) The ends of the specimen were reinforced, tapered (by machining), bonded to aluminium collars and cured (see Section 4.2). The end caps (and a rubber liner for burst tests) were then installed, ensuring that both ends were perfectly sealed.

(c) The specimen was installed in a safety enclosure and isolated from the operator and surrounding equipment. It was particularly important that, whilst one end of the pipe specimen was connected to the rig to allow sea water to be pumped into the empty specimen, the outlet at the other end of the specimen was left open to allow air to come out.

(d) The pressure high level and low level relays were set to the maximum and the minimum pressures of the required hydraulic loading cycle. For example, to apply a cyclic load of 0 - 100 bar, 100 bar and 0 were set as the maximum and minimum values in the control unit. For a static test, the maximum pressure was set to a high value, greater than the pipe static strength, and the minimum to zero. Since the design limit of the test rig was 700 bar, the

maximum pressure was normally set to 700 bar for static tests.

(e) The pump was switched on and natural sea water was pumped into the system and the specimen until water came out from the outlet of the specimen. The outlet end of the specimen was then lifted a little to assist the expulsion of the air. It is very important that all the air is eliminated from the entire system. Then the outlet of the specimen was switched off.

(f) All electric, pneumatic and hydraulic circuits were then checked over to ensure that every part was in its normal state. In particular, the pressure of the air input to the pump was set to a very low level and it was ensured that the hydraulic pressurisation speed was not too high.

(g) The test was started by switching the pump on. The required pressurisation speed and loading frequency were achieved by increasing the pneumatic pressure input.

(h) All tests were conducted under room temperature. The temperature variation was controlled in the range of 20 - 22 °C.

(i) The number of load cycles and the history of the pressure were recorded by the data logging system until the specimen failed. According to the definition of failure, the final failure was confirmed, the number of load cycles to failure (or the failure load for static tests) was recorded and failure status was also described. Consistent failure definitions were used for all specimens (see Section 4.1.5)

4.2 END-FITTINGS

4.2.1 Introduction

For the experiment on a pipe specimen subjected to internal pressure, it was necessary to fit special end grips at both ends of the specimen. With such a 'close-end' test, the axial load induced by the internal pressure is transferred to the pipe wall through the end grips. Therefore, a strong joint was used between the pipe wall and the end grips. During fatigue tests, all components of the end grips should be fatigue-resistant. Furthermore, the sealing construction between the pipe and end grips was carefully designed to prevent leakage of the liquid at high pressure, since GRP pipe with low stiffness had relatively large deformation in the radial direction. This section describes the design and manufacturing process of the adhesively bonded end-fittings and their stress analysis.

4.2.2 Cast Resin End-Fittings

Soden et al [2-4] used cast resin end-fittings for quasi-static tests on a series of filament wound GRP tubes subject to biaxial loads, as shown in Figure 4.6. The ends of the specimens were sanded, cleaned and then reinforced with circumferentially wound E-glass fibres and epoxy resin. The reinforced ends were then mounted in aluminium alloy grips using cast epoxy resin.

In the work carried out by Soden et al, this design of end fittings was successful for thin walled GRE tubes having 100 mm diameter and 1 mm wall thickness. However, for weepage tests of commercial GRP pipes (e.g. Ameron Bondstrand® 2000 series GRE pipes, see Table 2.3) with 53.2 mm internal diameter and 3.6 mm wall thickness, the prevention of end leakage was found to be difficult. Because of the large radial deformation of the pipe, the 'O'-ring between the aluminium inner grip and the GRE pipe did not prevent leakage when subjected to high pressure. For static burst tests, problems were also encountered in the installation of a strong (thick) rubber liner.

An improved design was proposed out by British Gas, as shown in Figure 4.7, in which a 'V'-shaped sealing ring was introduced. The 'V' shaped ring provided a good seal over a large pressure range, and allowed a rubber tube to be fitted between the 'V' shaped ring and the GRP pipe. However, tests using this type of end fittings were also unsuccessful due to premature failure of the cast resin and end reinforcements. Further disadvantages of the cast resin end-fittings were the difficulties associated with the injection and curing of the resin, and the long period of time that it required. Therefore, a new design of end-fittings using adhesive bonding was introduced in present research.

4.2.3 Adhesively Bonded End-fittings

The construction of the adhesively bonded end-fittings is shown in Figure 4.8. In contrast with the cast resin end-fittings, the first design feature was that the pipe end was reinforced with laminated woven E-glass fibres and epoxy resin, which provided higher axial strength than circumferentially wound E-glass fibre reinforced epoxy used by Soden et al [2-4] and British Gas. For 2 inch pipe specimens, the reinforcement layer was 120 mm long and 5 mm thick, although its thickness gradually reduced to zero as the gauge length was approached. Both laminated ends were then cured for 2 hours at 130 °C using heating blankets.

The second feature was that the reinforced pipe end was machined to a shallow angle of 1° 8' in order to fit a tapered aluminium collar. After the machined ends were cleaned and dried, the tapered aluminium collars were bonded to both ends of the pipe with Ameron RP-48 two-component epoxy adhesive. The adhesive bonded joints were then cured at 130 °C for 75 minutes using an Ameron Bondstrand heating blanket.

Figure 4.9 shows all the components of the end grips. An aluminium piston was inserted into the bore of the GRP pipe end and a special 'V' shaped sealing ring was fitted on the top of the piston, allowing it to expand with the pipe under high pressure and thus ensuring a watertight seal over the entire loading range. The piston and the aluminium collar were held in contact by an aluminium clamp ring and a steel flange, bolted together by four studs. The number and the diameter of the studs were determined from calculations of their strength and

stiffness. An O-ring was installed in the groove between the piston and the flange. The flange was made of steel to ensure that there was a strong threaded joint between the flange and the hydraulic rig.

After testing, a steel plug was used to dismantle the aluminium collars, which were strongly bonded to the pipe ends, so that they could be recycled, as shown in Figure 4.10. To facilitate this, the bonded pipe end was first heated to 250 °C for 10 minutes by a heating jacket to reduce the bonding strength. A special steel plug, which fittted the pipe bore, was then used to push the collar off the pipe using a hydraulic ram.

The advantages of the adhesively bonded end-fittings were:

(a) low stress concentration;
(b) good sealing over the entire loading range;
(c) ease of fitting a rubber liner for a burst test;
(d) short preparation time;
(e) ease of manufacture;
(f) reusable;
(g) low cost.

4.2.4 Stress Analysis of the Adhesively Bonded End-fittings

In order to determine correctly the important dimensions of the end fittings, such as the bonding length, the tapering angle and the thickness of the reinforcement, simple strength calculations and complicated finite element analysis were carried out by the author (see Chapter 7, page 189). The stress analysis indicated that the stress concentration induced by the end-fittings mounting was negligible.

4.3 MEASUREMEMT OF WEIGHT AND VOLUME FRACTIONS

A knowledge of the weight and volume fractions of the fibres and matrix in the pipe wall was required for the prediction of the mechanical properties. The weight fractions were measured by means of burn-off tests carried out in accordance with BS 2782, Part 1, method 107K. Section samples measuring 10 mm by 10 mm were cut from the GRP pipe wall and the joints, and heated in a furnace at 500 °C for approximately 5 hours. After the resin was completely burnt off, the weight fractions of fibres, W_f, and of the matrix, W_m , were obtained. A minimum of five specimens were used to obtain an average value.

The volume fractions for each specimen can be calculated from the weight fractions and the density of the pipe, ρ, and of glass fibre, ρ_f, by the equation:

$$V_f = W_f \bullet \rho/\rho_f \tag{4.1}$$

For E-glass fibre, a value of $\rho_f = 2.55$ g/cm^3 was used [5].

The density ρ of the pipe wall was measured by submerging the section specimen in a mercury bath and measuring the up-thrust of the mercury,

$$\rho = (\text{weight of specimen in air } P \times \rho_{\text{mercury}})/(\text{up-thrust of mercury} + P) \tag{4.2}$$

where the density of the mercury $\rho_{\text{mercury}} = 13.56$ g/cm^3.

4.4 OPTICAL MICROSCOPY

Optical microscopy was used to examine the microstructure of the pipe wall, allowing counting of the layers and measurement of the winding angle and the thicknesses of the reinforcement layers, resin liner and the coating. Optical microscopy was also used to check the crack initiation and propagation in different stages (weepage and burst). This was helpful in the analysis of damage initiation and crack propagation.

4.5 STRAIN GAUGES

Strain gauges (5 mm single and two element rosettes, type N11-MA-5-350 and N21-MA-5-350) were used to measure the hoop and axial strain components on the outer surface of the GRP pipes and joints. The strain gauges were manufactured by SHOWA Measuring Instruments Co., Ltd.

REFERENCES

[1] ASTM D2143, Standard Test Method for Cyclic Pressure Strength of Reinforced thermosetting Plastic Pipes, Reapproved 1987.

[2] Soden,P.D., Kitcking,R. and Tse,P.C., Experimental Failure Stresses for 55 Filament Wound Glass Fibre Reinforced Plastic Tubes under Biaxial Loads, Composites, Vol.20, No.2, 1989, pp.125-135.

[3] Highton,J, Adeoye,A.B. and Soden,P.D., Fracture Stresses for ±75 Degree Filament Wound GRP Tubes under Biaxial Loads, Journal of Strain Analysis, Vol.20, No.3, 1985, pp.139-150.

[4] Highton,J and Soden,P.D., End Reinforcement and Grips for Anisotropic Tubes, Journal of Strain Analysis, Vol.17, No.1, 1982, pp.31-43.

[5] Smith, C.S., Design of Marine Structures in Composite Materials, Elsevier Applied Science, 1990, p.32.

Table 4.1 List of parts shown in the schematic drawing of the fatigue test rig (see Figure 4.4)

A1	Lubrication, filter and pressure control unit
A2	3-way solenoid shuttle valve. (normal position: upstream off, downstream vented to air; energised position: upstream connected to downstream)
A3	Manual isolator valve
A4	Air pressure gauge (0 - 7 bar)
A5	Lubrication, filter and pressure control unit
A6	3-way solenoid shuttle valve
A7	Air muffler
E1	Personal computer
E2	Data acquisition and control board
E3	Transducer indicator
E4	Pressure high level relay
E5	Pressure low level relay
E6	Counter
H1	Air operated pump
H2	Air operated relief valve (normally open)
H3	High pressure manual isolator valve
H4	Hydraulic pressure gauge (0 - 700 bar)
H5	Hydraulic pressure transducer (0 - 700 bar)
H6	Needle valve
H7	Needle valve

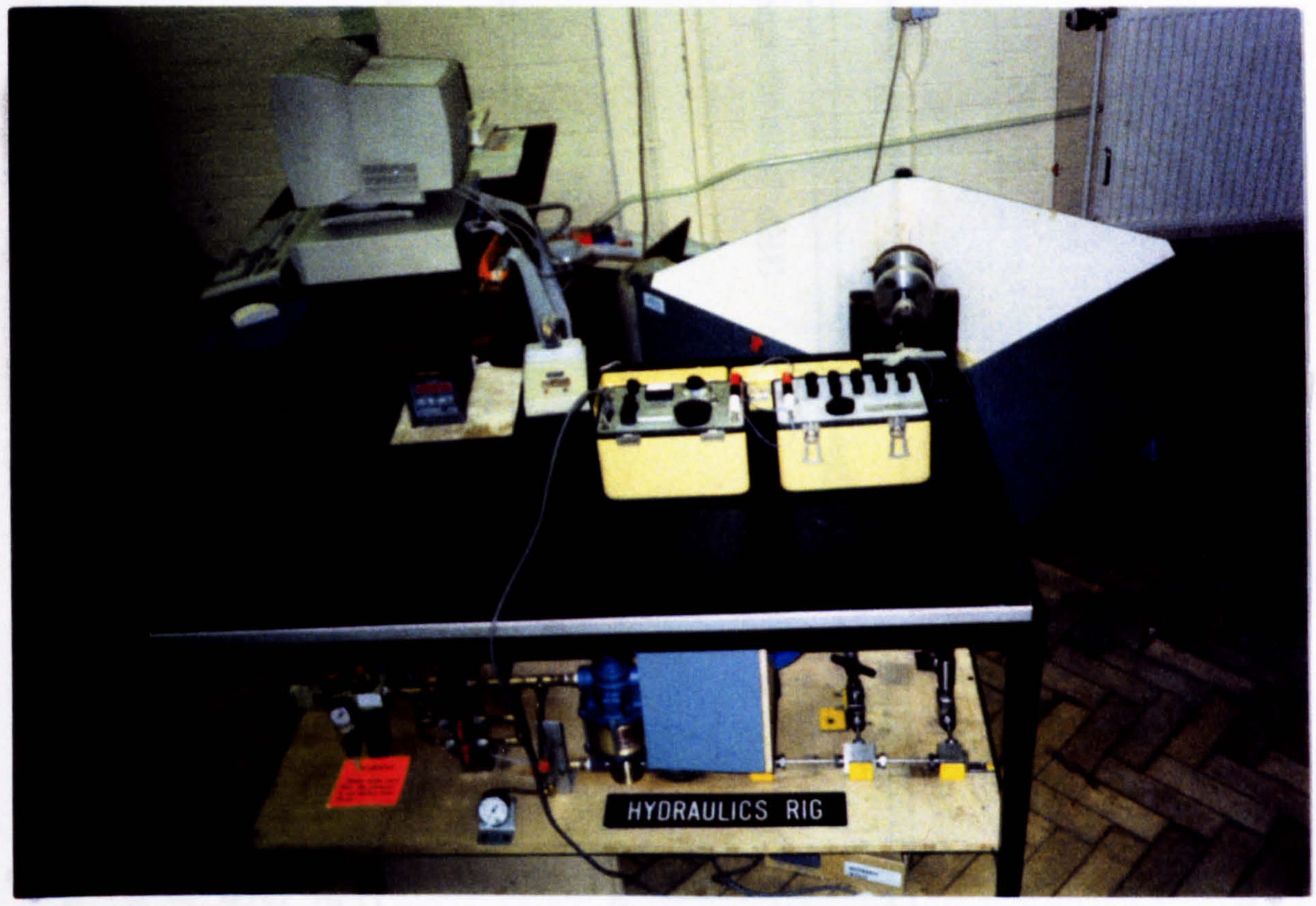

Figure 4.1 Hydraulic rig for GRP pipe fatigue testing.

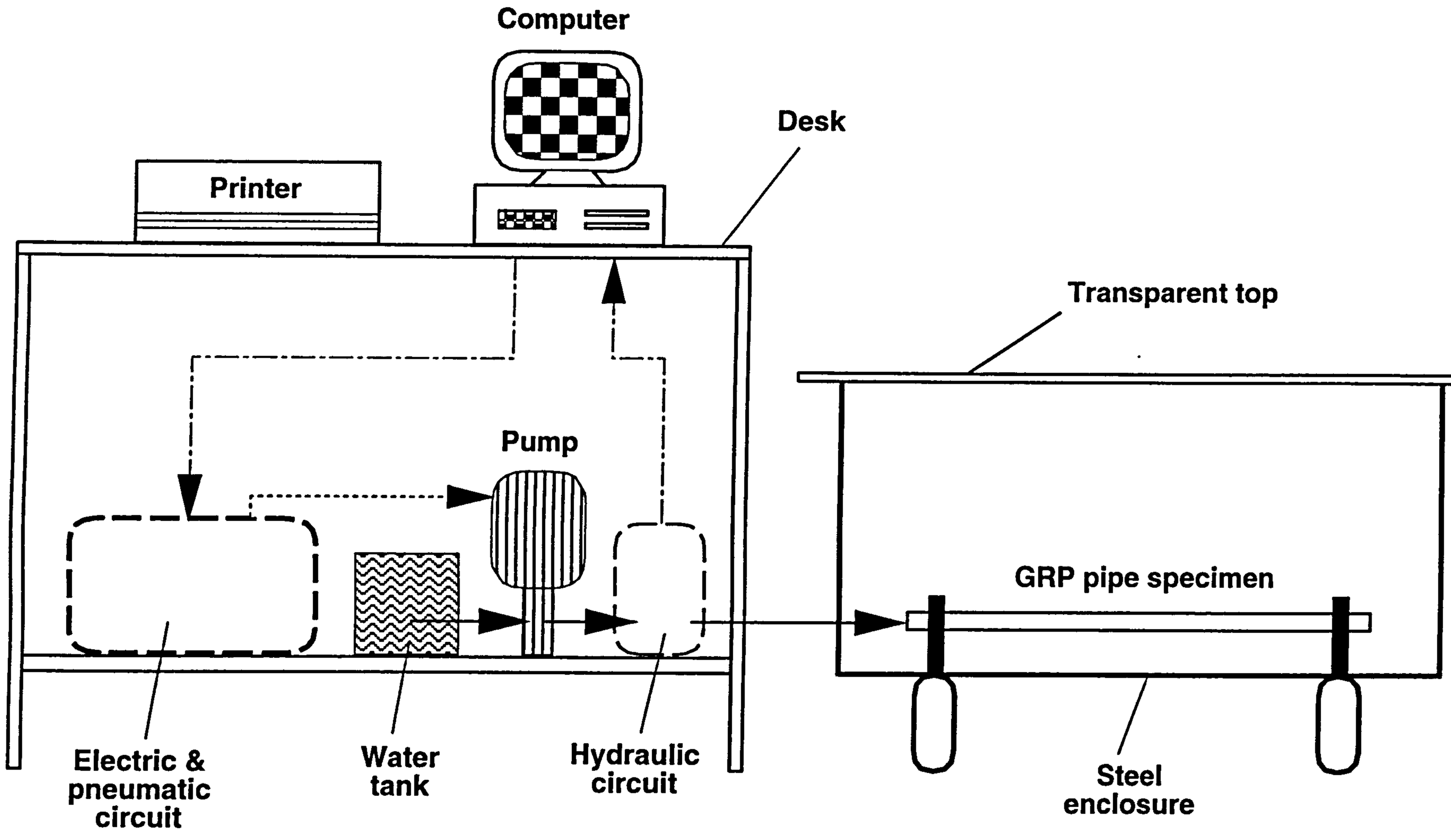

Figure 4.2 Schematic drawing of the hydraulic test rig.

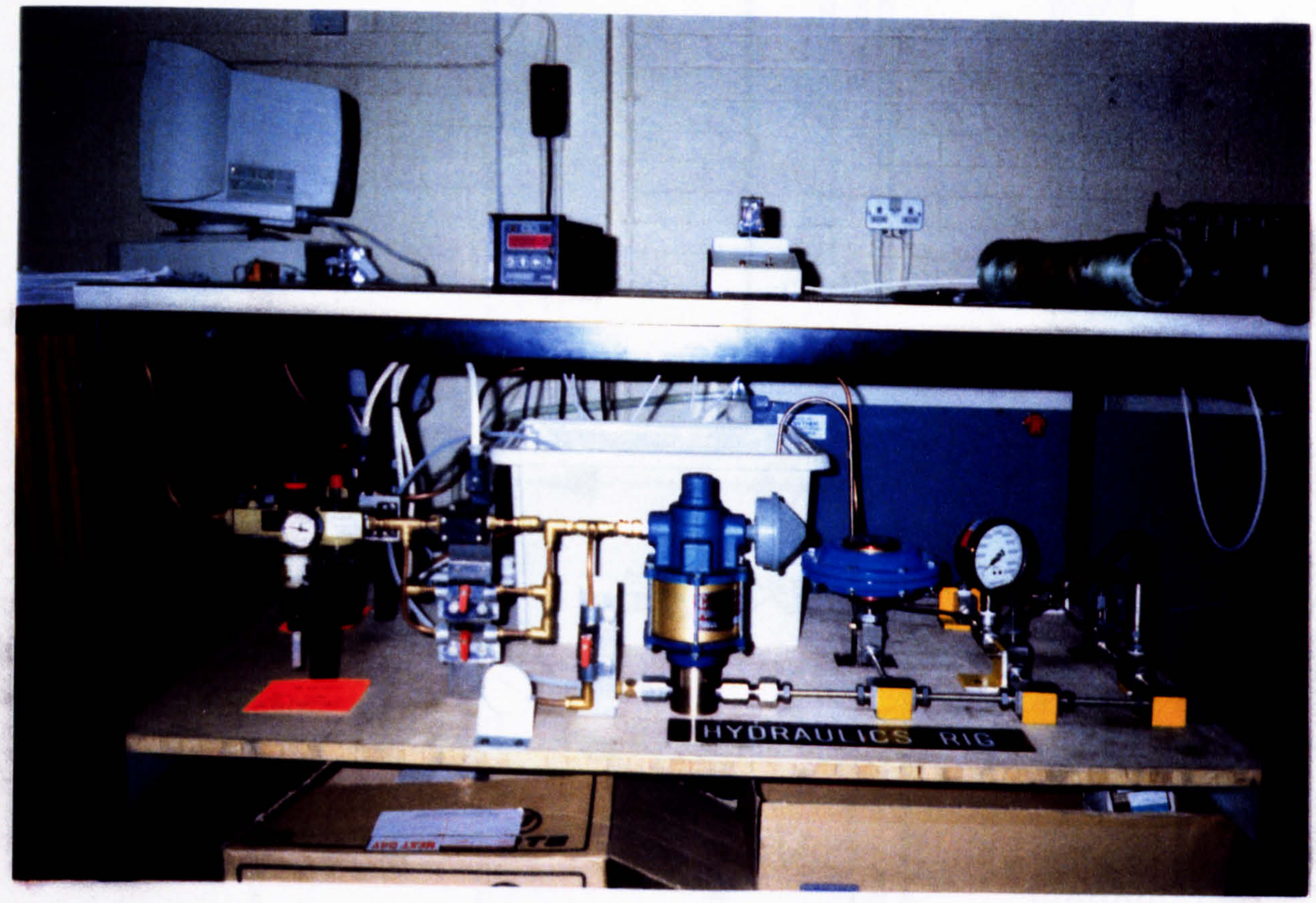

Figure 4.3 Pressurisation system of the fatigue rig.

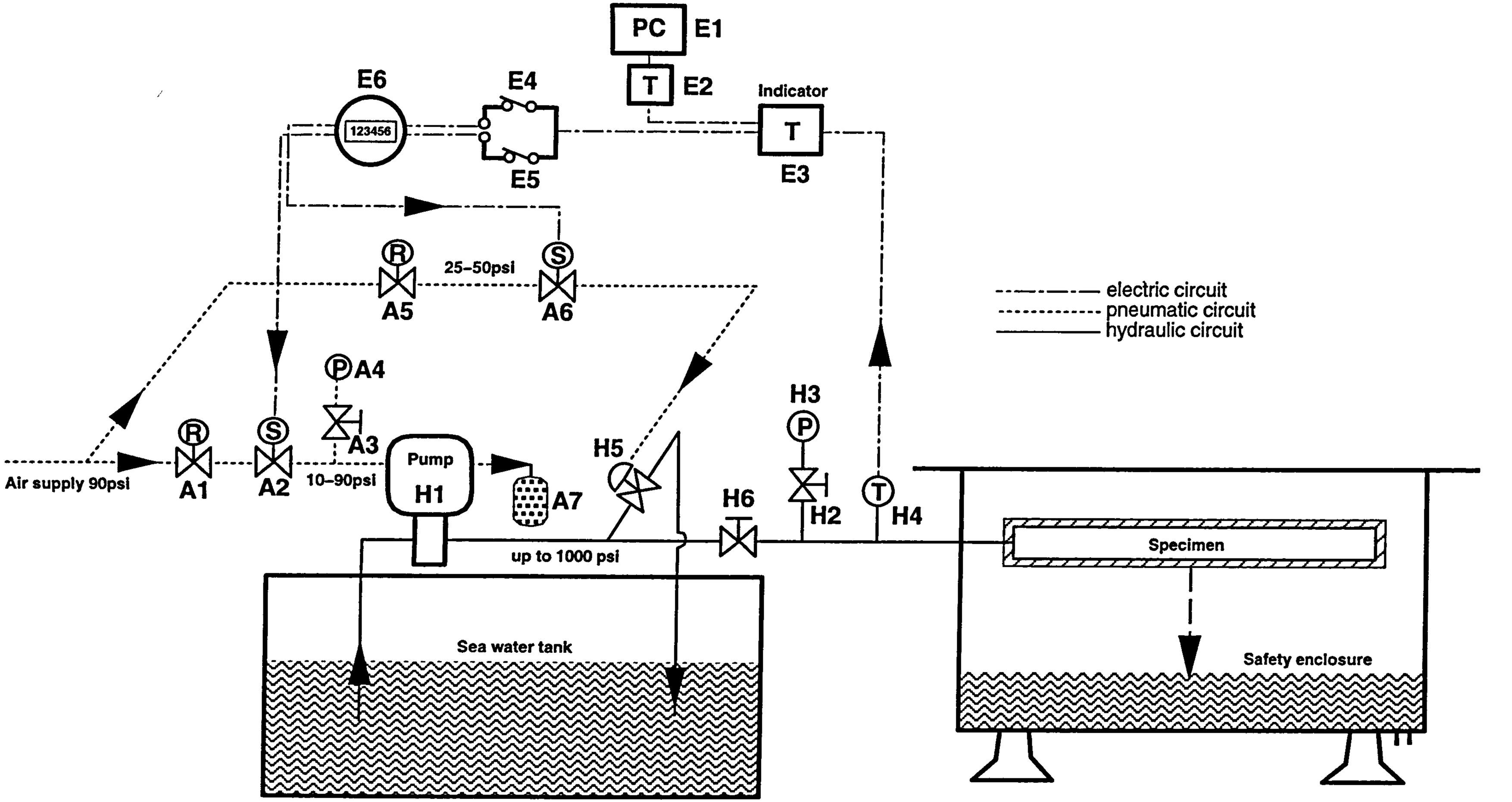

Figure 4.4 Schematic drawing showing the working principle of the fatigue test rig.

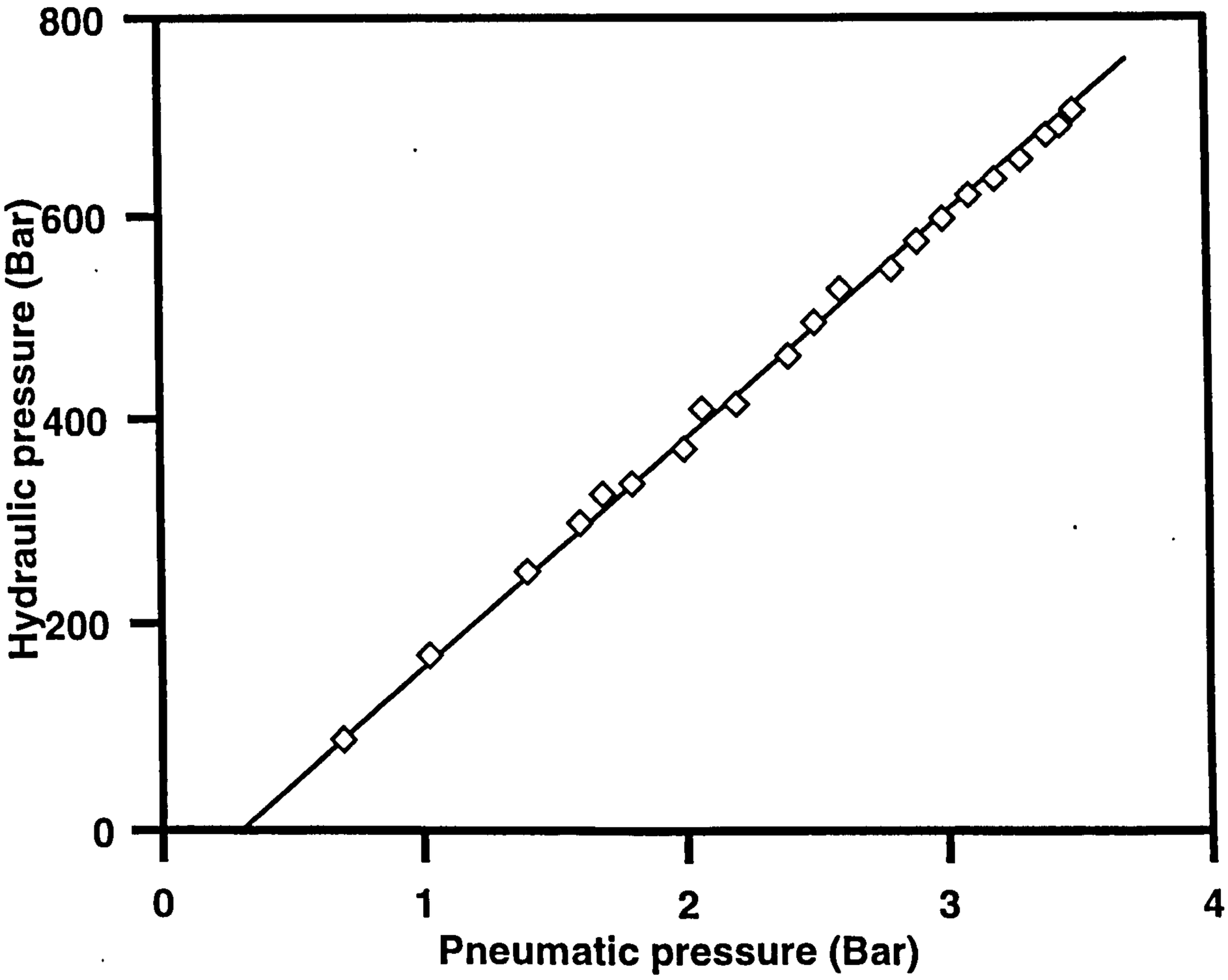

Figure 4.5 The relationship between pneumatic and hydraulic pressure in the fatigue test rig. The maximum hydraulic pressure output is approximately proportional to the input pneumatic pressure. A pneumatic pressure of 0.3 bar is needed to start the pump. Thus, the stable static pressure and the pressurisation speed can be set by adjusting the input air pressure.

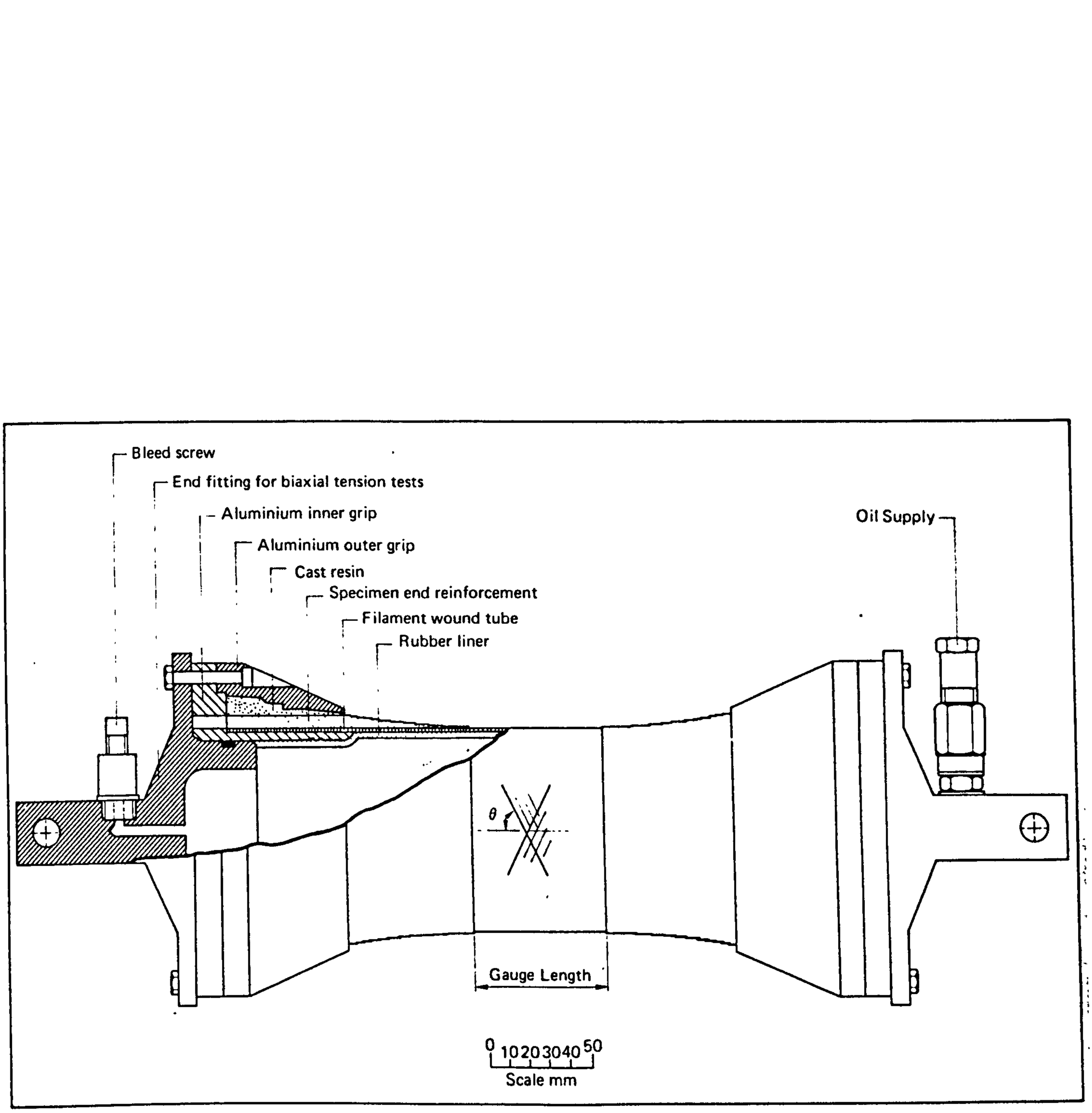

Figure 4.6 Cast resin end-fittings used by Soden et al [2].

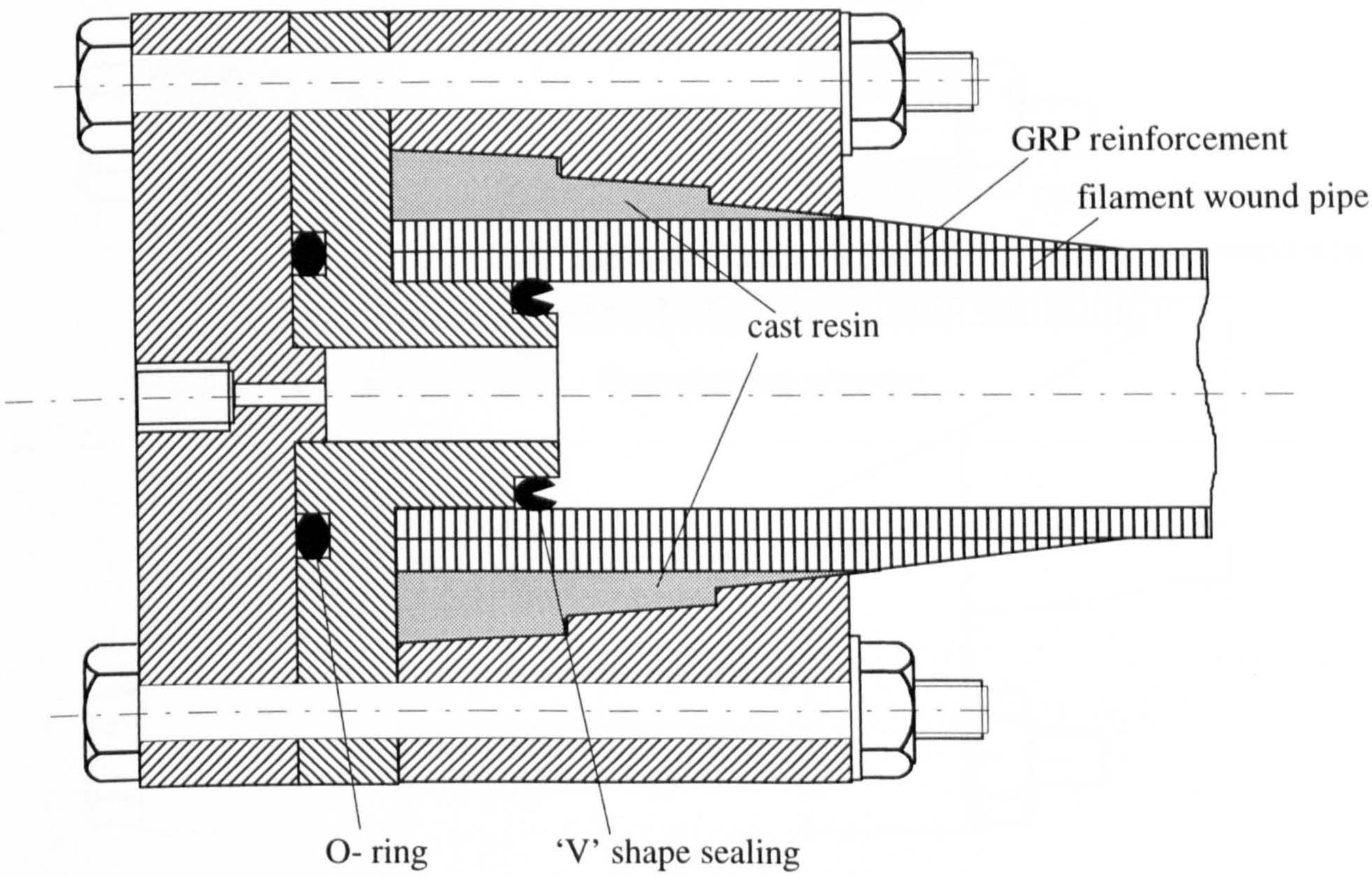

Figure 4.7 Cast resin end-fittings used by British Gas plc.

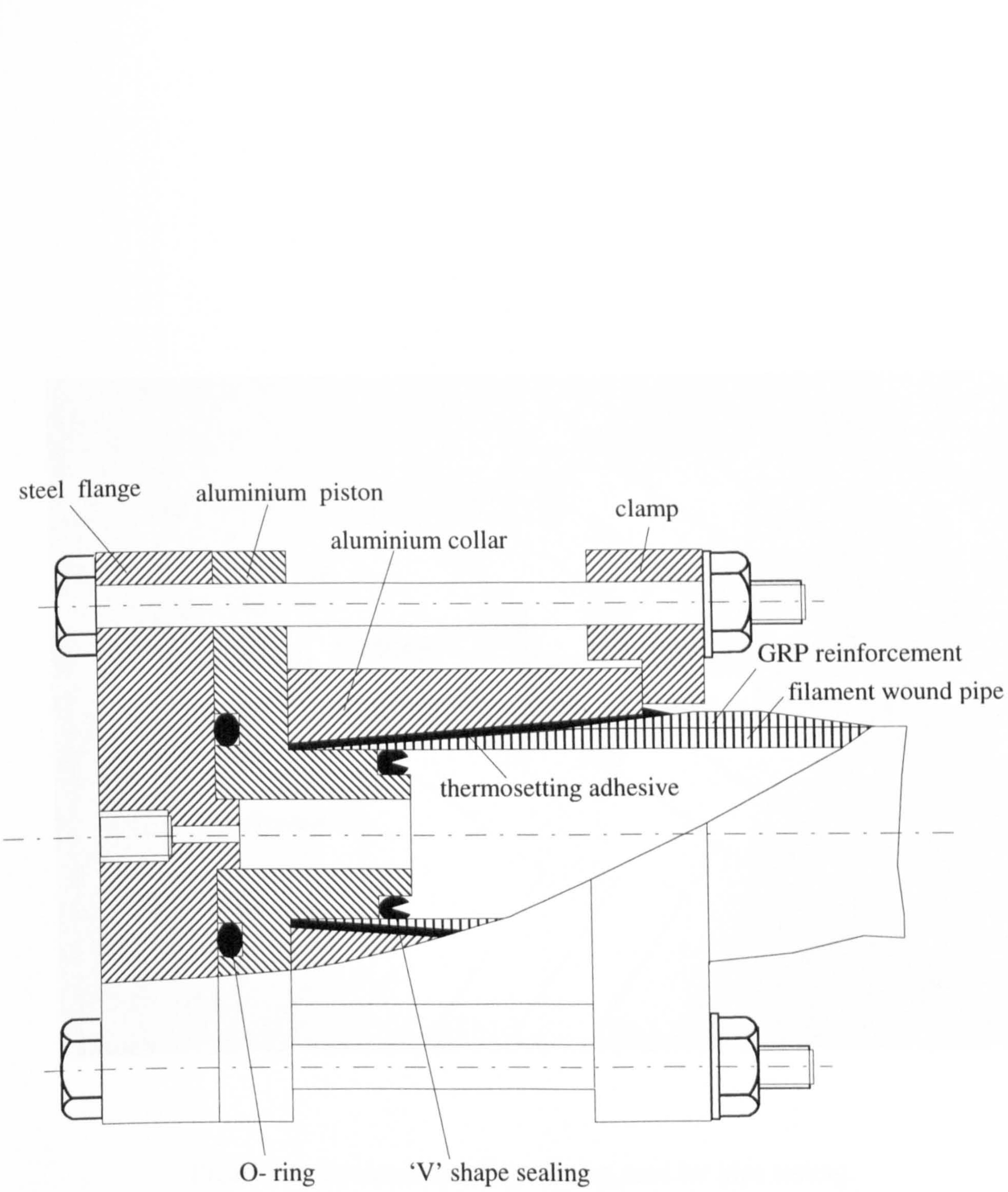

Figure 4.8 Adhesively bonded end-fittings.

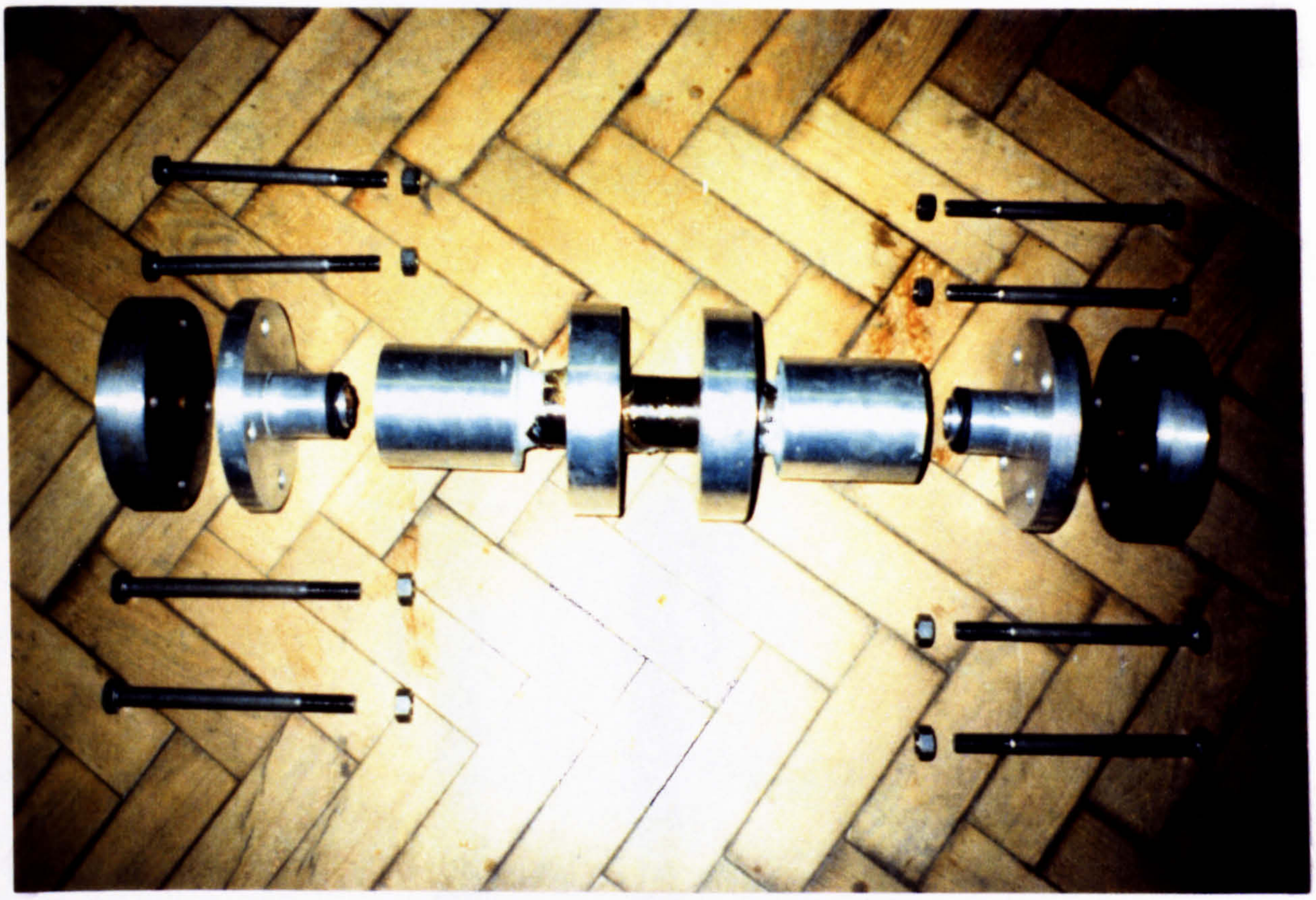

Figure 4.9 Components of end-fitting used for pipe testing.

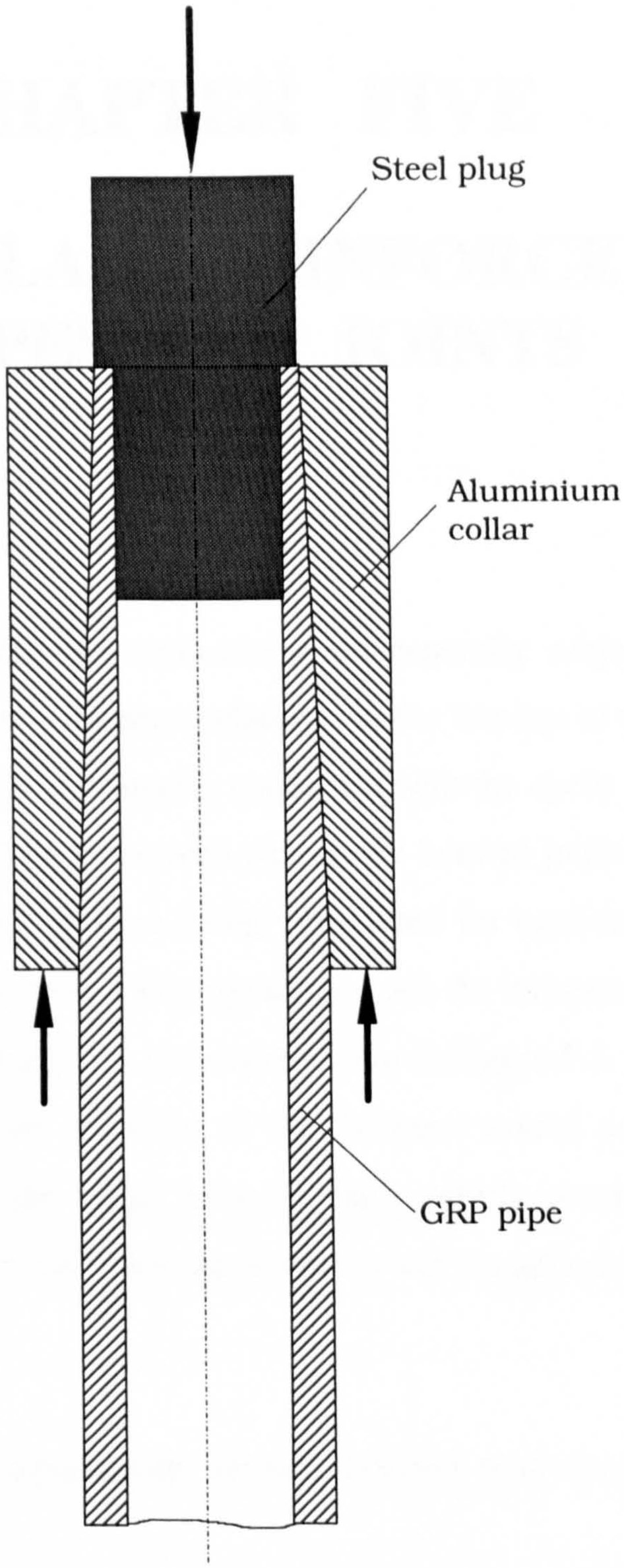

Figure 4.10 Illustration of the method of end-collar removal.

CHAPTER FIVE

TESTS ON GLASS REINFORCED EPOXY PIPES AND JOINTS

5.1 INTRODUCTION

Fire water systems in the offshore applications are generally subjected to regular tests. Thousands of pressure cycles will be accumulated over the lifetime of the offshore structures [1,2]. The present investigation is primarily concerned with the cyclic fatigue characteristics of glass reinforced epoxy (GRE) pipes with adhesively bonded joints. Two inch (50 mm) diameter pipes and fittings which were being considered for applications on offshore fire water systems were selected for the test programme. All the components were commercial products. The various pipes and joints tested are shown in Figure 5.1. The objectives of this investigation were to study the response of the filament wound composite pipework to fatigue pressure loading in the range between the working pressure and the weeping pressure, to examine the interaction between the pipes and the adhesive bonded joints and to determine the failure mode.

This chapter describes the experimental results obtained with three types of GRE pipe specimens;

plain pipes,
coupler-jointed pipes,
socket/spigot jointed pipes,

as shown in Figure 5.1(a), (b) and (c). The specimens were a set of 2-inch (50 mm) nominal diameter, 44 bar nominal pressure, filament wound E-glass reinforced epoxy resin pipes, series BS2000M, manufactured by Ameron. They included 7 plain pipes, 42 central coupler adhesively-bonded joints and 5 central socket/spigot adhesively bonded joints.

Prior to the fatigue tests, several specimens of each type were tested under quasi-static internal pressure. Several load levels for the fatigue testing were then determined once the static weepage pressure was known. At each load level, 3 to 4 specimens were tested under cyclic saw-tooth (approximately in a right triangle waveform) internal pressure. The pressure of the sea water in the specimen was increased from the minimum pressure to the maximum at an identical loading speed of 100 MPa per minute and then dropped to the minimum rapidly (in a very short time). The frequency of the cyclic pressure varied slightly with the maximum and the minimum pressures. The minimum pressure was always set to zero for all tests conducted and the maximum pressure was from 8 MPa to 14.5 MPa corresponding to a frequency range of 7 - 12 cycles per minute.

The results demonstrate that all of the pipes tested have sufficient strength for offshore applications. The fatigue strength of the specimens tested will be presented in the form of applied internal pressure versus number of cycles to failure, the P-N diagram.

Terms used in Chapter 5 and 6

Weepage test: A GRP pipe is tested by applying internal pressure using pressurised sea-water. Pipe failure is characterised by water weepage, the water seeping through cracks in the matrix material and/or adhesive. No visible fibre breakage occurs in a weepage test.

Burst test: After the weepage test, the pipe is further tested by installing a rubber liner in the pipe core and applying quasi-static internal pressure through pressurised water. Burst failure is characterised by a burst which causes a loud bang. No water weepage occurs until the final burst at the point of catastrophic fibre breakage. A burst test gives the strength of fibre breakage in the pipe wall, which is not the real strength of a GRP pipe. The burst strength shows the potentiality of the GRE pipe, which can be achieved by using a liner with a high failure strain (e.g. rubber liner and thermoplastic liner etc.).

GRE pipe: A pipe made from epoxy resin reinforced by glass fibres. The GRE pipes tested in the current work were manufactured by filament winding.

GRVE pipe: A pipe made from vinyl ester resin reinforced by filament wound glass fibres.

P - N curve: The load - life fatigue curve of a GRP pipe plotted in the form of internal pressure versus number of pressure cycles to failure. The internal pressure always cycles from the minimum pressure of 0 to the maximum of *P*. The pressure increases linearly at a identical speed of 100 MPa per minute and is released at a much higher speed producing a right triangle wave form.

Resin liner: The inside of a commercial GRP pipe normally contains a resin-rich liner which offers higher resistance to corrosive media than the reinforced pipe wall. Usually, the material of the resin liner is the same as the matrix of the pipe wall. The thickness of the resin liner varies among the various products of different companies, but is normally between 0.5 to 2.0 mm.

Rubber liner: Following weepage, a large number of cracks are present in the pipe wall, resin liner and adhesive layer. The pipe can not normally contain pressurised media unless a rubber tube is installed to prevent leakage, or unless the pressurising equipment is capable of a very high flow rate. Usually, a cycle inner tube is used as the rubber liner. This should be properly fitted between the end grips and the pipe core to ensure that no water leakage occurs at the pipe ends during a burst test.

5.2 PLAIN PIPES

5.2.1 Specimens

A total of seven plain pipe specimens were tested under static or cyclic internal pressure. These were all commercial products in the series Bondstrand 2000M, manufactured by Ameron, see Figure 5.1(c). Table 5.1 lists their geometric parameters and physical properties. The nominal diameter of the pipes was 50 mm and the nominal pressure rating was 4.4 MPa (the cyclic hydraulic design basis, ASTM Standard D2992). The actual internal diameter was 53.2 mm and the total wall thickness was 3.6 mm (Figure 5.2). The gross fibre volume fraction of the pipe wall was 44%. The pipes had a 0.1 mm topcoat and a 0.5 mm resin-rich inner liner with a C-glass mat reinforcement. The structural wall comprised a reinforcement of E-glass fibres and an epoxy resin matrix. After the top coat layer and the resin liner were removed, the volume fraction of the glass fibre in the structural wall was measured to be 49.8%. The structural wall was composed of six plies of GRE reinforced unidirectional laminae, the ply thickness being 0.5 mm and thus the total thickness of the structural wall was approximately 3.0 mm. The winding angles were ±55°. The pipe was wound with full wrap at each direction and there were no crossovers of +55° and -55° fibres. The gross length of each pipe was one metre. After the installation of the end caps, this was reduced to a gauge length of 760 mm. Table 5.2 presents the main mechanical properties of this GRE pipe[5].

5.2.2 Experimental

All seven plain pipes, numbered as P01, P02, ..., P07, were subjected to internal pressure through pressurised sea water, using the hydraulic test rig described in Chapter 4. Initially, three specimens were tested under quasi-static internal pressure until water weepage occurred. The remaining four were then tested under cyclic saw-tooth pressure, as described in Table 5.3. Two load levels were used for the four specimens in the fatigue tests. A cyclic load of 0 - 14.0 MPa was applied to P04 and P05, and 0 - 11.0 MPa to P06 and P07. The internal pressure was increased at a constant speed of 100 MPa per minute from the

minimum pressure to the maximum and then was dropped rapidly to zero. The frequencies therefore had values of between 7 to 9 cycles per minute, depending on the amplitude of the cyclic pressure. Tests were conducted under the room temperature of 20-22 °C.

It was found that water weepage occurred at a relatively low pressure due to cracking of the matrix material and the resin liner of the pipe wall. In order to allow the full strength of the pipes to be determined, pipes P01, P02, P04 and P06 were fitted with rubber liners after the weepage tests and were subjected to quasi-static internal pressure until they burst. The other specimens P03, P05 and P07 were examined by optical microscopy to study the failure mechanisms of the pipe wall.

During burst tests, special care had been taken because of the hazard associated with high pressures of up to 54 MPa (540 bar). Entrapped air was completely removed from the inside of the specimens and from the entire hydraulic system to minimise the energy stored. Specimens were enclosed inside a 1m by 1m by 0.5m safety tank which was made of 1/4 inch thick steel plate.

The experimental set-up was the same described in Chapter 4.

5.2.3 Results and Discussion

The weepage test results from the seven plain pipe specimens (P01 to P07) are shown in Table 5.3. These comprise the weepage pressures and the number of pressure cycles to weepage. The burst pressures are the results of static burst tests. Specimens P01, P02 and P03 gave quite consistent static weepage pressures. The maximum difference between P02 and P03 was 13.5%. The average static weepage pressure was 21.78 MPa. Fatigue tests on specimens P06 and P07 gave longer fatigue lives under a lower load level of 11.0 MPa than P04 and P05. Specimens P04 and P05 were subjected to fatigue pressures with higher amplitudes, and thus had fewer pressure cycles to weepage. All four fatigue-tested specimens were subjected to relatively high stresses in the 'low cycle' fatigue region. Since pipes in offshore fire systems normally experience a few thousands of tests during the service life of the offshore rig, only low cycle fatigue tests (up to 2×10^4 cycles) were carried out. According to the discussion in Chapter 3, it is more appropriate to use identical loading speed for all specimens than to use the same frequency. The loading speed depends on the pumping capability, the volume and stiffness of the specimen, and the input air pressure to the pump. The maximum pressurisation speed achieved was 100 MPa per minute using the rig described in Chapter 4 for 1 metre long and 50 mm nominal diameter GRE pipes. Thus, a uniform pressurisation speed of 100 MPa per minute was used for all pipes tested. This was equivalent to a frequency of 9 cycles per minute for cyclic pressure ranged 0 - 11 MPa. It therefore took approximately 9 hours to conduct the test on specimen P06 continuously for 4,783 cycles. For a pipe tested to 20,000 cycles under pressure 0 - 10 MPa, it took more than 33 hours. Therefore, a fatigue test lasting longer than 20,000 cycles is rather time-consuming.

The burst pressures for specimens P01, P02, P04 and P06 were also quite consistent, even though different pressures were experienced during the weepage tests. The differences were less than 4%. The weepage pressure cycles, it appears, only caused matrix damage in the pipe wall and had little influence on the burst pressures which mainly reflected the strength of the glass fibre. The fact that the glass itself appears undamaged by the fatigue process is an interesting result.

(a) Failure Modes

Different failure modes were observed in the weepage and burst tests by microscopy. In weepage tests, the original commercial pipes failed under internal pressure due to water weeping through cracks in the matrix of the pipe wall. As the internal pressure (static tests) or the number of pressure cycles (fatigue tests) increases, fibres start to debond from the surrounding matrix, cracks initiate and grow in the matrix between fibres, and finally the cracks are joined up by cracks between the plies , as shown in Figure 5.3. Little fibre breakage occurred.

The cracks in the resin-rich liner were in the axial direction of the pipe, as shown in Figure 5.4. The resin liner would be expected to have isotropic mechanical properties and thus same failure strain in the hoop and axial directions. When subjected to internal pressure, GRE pipes would be expected to show hoop strains which were larger than the axial strains, as discussed later in Section (b): Stress and Strain Analysis, Eqs.(5.7) on page 108. Due to the high level of hoop strain, the resin liner cracked in the axial direction. Figure 5.5 shows a micrograph of a crack in the resin-rich liner of a pipe inner face. The crack apparently initiated at the air bubbles, which were entrapped during the manufacturing process, and grew along the axial direction of the pipe. Like a plate with an open-hole, a void in the resin liner caused stress concentration and thus the damage initiation.

Figure 5.6 shows the microstructure of some cracks propagating in the resin-rich liner and the GRE pipe wall in the thickness direction. This is a typical image taken from the pipe cross section. The first layer from the bottom of the image is the resin-rich liner, which had little reinforcement. The C-glass fibres were randomly aligned in the resin-rich liner. Above the resin liner layer is the E-glass reinforced epoxy structural pipe wall. Fibres were aligned unidirectionally in each layer of the pipe wall at an angle of $+55^{\circ}$ or -55° to the pipe axis. Cracks propagated in the resin matrix between fibres. The fibres remained undamaged. Delaminations were observed between the $+55^{\circ}$ and -55° reinforced plies, but there were no delamination between the resin-liner and $+55^{\circ}$ reinforced ply.

Similarly, Figure 5.7 shows the microstructure of cracks crossing the GRE plies to the outer coat. In this picture, the section specimen was cut at an angle of 55° direction to the pipe axis. The plies with +55° and -55° winding angles could be easily distinguished. Matrix cracks can be seen in the -55° reinforced layers. There were also many cracks between the plies due to delamination. However, there were no cracks perpendicular to the fibres observed in the +55° plies. Thus the cracks crossed each ply by matrix cracking between fibres and the cracks in two adjacent plies were joined by delamination.

As discussed in Chapter 3.2, damage in composite materials develops progressively from fibre debonding, matrix cracking through to final fibre breakage. Corresponding to these different failure stages, the materials show very different static and fatigue strengths, as shown in Figure 3.4. The water weepage in the GRE pipes tested in the current work was caused by the matrix cracking. The weepage pressure mainly reflected the matrix-cracking strength of the pipe wall material. In order to measure the strength to fibre-breakage, GRE pipes were further tested by inserting rubber liners and applying internal pressure until they burst. The burst pressures are quite consistent and are independent of the pressure history experienced prior to weepage. This is because the damage developed before weepage resulted only in small cracks in the matrix, with no damage to the fibres. The failure mode of the burst tests was catastrophic fibre breakage, as shown in Figure 5.1(c).

However, the matrix cracking caused the stiffness reduction of materials, as shown in Figure 5.8. Owen et al [3] examined the loss of the modulus after the damage development. Thus, the relation between the internal pressure and hoop strain in the GRE pipe wall can be plotted as a curve in Figure 5.9. Before the debonding and matrix cracking start, the hoop strain is proportional to the internal pressure. As the resin matrix cracks, the gradient of the curve decreases.

Figure 5.9 explains the failure process of the GRE pipes schematically. The equivalent curve in the three graphs schematically demonstrates the relationship between the applied internal pressure and the damage stages of the materials in the pipe wall. Point A marks the start of the stage during which fibre debonding and matrix cracking occur in the GRE structural wall. When the pressure is lower than that at point A, the pipe deforms linearly.

Point B represents the stage at which the resin-rich liner cracks. Since the resin liner is usually formed from the same material as the matrix of the main pipe wall but has fewer interfaces with reinforcement, the resin liner has a higher matrix cracking strength. Thus point B usually is reached after point A. However, if the resin liner is very thin, the voids or other types of defects may already penetrate the resin liner and point B and A are the same.

Finally, point C is where the fibres break catastrophically. In Figure 5.9, graph (a) shows the failure of a pipe without a liner (neither rubber nor resin-rich liners). The pressure can only reach to point A, before water seeps through the pipe wall. This type of failure is controlled by the matrix cracking strength of the GRE material. Graph (b) shows failure of a GRE pipe with a resin liner. The pipe achieves higher strength up to point B, when the resin liner cracks after the matrix cracking in the GRE structural wall. This type of failure is controlled by the cracking behaviour of the liner material. The failure load can be predicted when the hoop strain reaches the ultimate tensile strain of the liner material. The difference between A and B is dependent on the thickness and the type of the resin liner. It is inevitable that there will be some defects, such as the small bubbles shown in Figure 5.5, in the resin liner. If the resin liner is not sufficiently thick, the defects and cracks initiating at these defects may penetrate the resin liner prematurely. Points B and A converge and no extra weepage strength will be achieved by the resin liner. Graph (c) shows the case of a burst test for a pipe fitted with an extra rubber liner which has a low elastic modulus and a high failure strain. Under these conditions, the maximum pressure will finally reach point C. This type of failure is controlled by the fibre-breaking strength. In practical terms, the strength of commercial GRE pipes corresponds to point A or B. So only a small proportion of the strength of the E-glass is used.

(b) Stress and Strain Analysis

Consider a "thin-walled" pipe which has an internal diameter D and a wall thickness t, ($t < 0.1D$), is subjected to a pure internal pressure P. Assuming that the hoop and axial stresses uniformly distribute in the pipe wall, then we can get,

$$\sigma_{hoop} = \frac{D}{2t}P$$
$$\sigma_{axial} = \frac{D}{4t}P \tag{5.1}$$

According to the Hooke's law and the orthotropy assumption, the gross elastic strains in axial and hoop directions are,

$$\varepsilon_{axial} = \frac{\sigma_{axial}}{E_{axial}} - \nu_{hoop,axial}\frac{\sigma_{hoop}}{E_{hoop}}$$
$$\varepsilon_{hoop} = \frac{\sigma_{hoop}}{E_{hoop}} - \nu_{axial,hoop}\frac{\sigma_{axial}}{E_{axial}} \tag{5.2}$$

where E_{axial}, E_{hoop}, $\nu_{axial,hoop}$ and $\nu_{hoop,axial}$ are the elastic constants of the pipe wall in axial and hoop directions.

For the $\pm\theta$ filament wound GRE pipes, the ply strains are calculated by,

$$\varepsilon_1 = \varepsilon_{axial}\cos^2\theta + \varepsilon_{hoop}\sin^2\theta$$
$$\varepsilon_2 = \varepsilon_{axial}\sin^2\theta + \varepsilon_{hoop}\cos^2\theta \tag{5.3}$$
$$\gamma_{12} = 2(\varepsilon_{hoop} - \varepsilon_{axial})\sin\theta\cos\theta$$

According to the Hooke's law, the ply stresses can be calculated from the ply strains by,

$$\sigma_1 = \frac{E_1}{1-\nu_{12}\nu_{21}}(\varepsilon_1 + \nu_{21}\varepsilon_2)$$
$$\sigma_2 = \frac{E_2}{1-\nu_{12}\nu_{21}}(\varepsilon_2 + \nu_{12}\varepsilon_1) \tag{5.4}$$
$$\tau_{12} = G_{12}\gamma_{12}$$

where E_1, E_2, ν_{12}, ν_{21} and G_{12} are the elastic constants of the unidirectional GRE lamina in the fibre and transverse directions.

The elastic constants of the UD lamina can be estimated by the rule of mixtures from the properties of fibres and matrix. A Fortran program and the equations for the calculations are given in Appendix A and B. For the E-glass/epoxy system used in the pipes tested, the modulus of fibres E_f= 76 GPa, Poisson's ratio ν_f= 0.2; the modulus of matrix E_m = 3.4 GPa, Poisson's ratio ν_m= 0.4. Therefore, from Appendix A and B, the elastic constants of the E-glass/epoxy UD lamina with fibre volume fraction V_f=50% are,

$$\begin{aligned} E_1 &= 39.7\,GPa \\ E_2 &= 7.1\,GPa \\ \nu_{12} &= 0.30 \\ \nu_{21} &= 0.054 \\ G_{12} &= 3.3\,GPa \end{aligned} \tag{5.5}$$

The elastic constants of $\pm 55^0$ wound pipes in hoop and axial directions can be calculated by the program and the equations of the laminate theory in Appendix A and C. They are,

$$\begin{aligned} E_{axial} &= 8.1\,GPa \\ E_{hoop} &= 16.1\,GPa \\ \nu_{hoop,axial} &= 0.76 \\ \nu_{axial,hoop} &= 0.38 \end{aligned} \tag{5.6}$$

From Eqs.(5.1) to (5.4), we have (when the internal pressure P and all stresses use the unit of MPa),

$$\sigma_{axial} = 0.25\left(\frac{D}{t}P\right)$$

$$\sigma_{hoop} = 0.5\left(\frac{D}{t}P\right)$$

$$\varepsilon_{axial} = 7.261713\times10^{-6}\left(\frac{D}{t}P\right)$$

$$\varepsilon_{hoop} = 19.327505\times10^{-6}\left(\frac{D}{t}P\right) \qquad (5.7)$$

$$\varepsilon_1 = 15.357981\times10^{-6}\left(\frac{D}{t}P\right)$$

$$\varepsilon_2 = 11.231237\times10^{-6}\left(\frac{D}{t}P\right)$$

$$\gamma_{12} = 11.338136\times10^{-6}\left(\frac{D}{t}P\right)$$

$$\sigma_1 = 0.644226\left(\frac{D}{t}P\right)$$

$$\sigma_2 = 0.114306\left(\frac{D}{t}P\right) \qquad (5.8)$$

$$\tau_{12} = 0.0374158\left(\frac{D}{t}P\right)$$

where P is the applied internal pressure, D is the internal diameter and t is the wall thickness of the GRE pipe.

(c) Prediction of Weepage Pressure

The weepage pressure of a GRE pipe can be roughly estimated from the basic strength properties of the UD lamina by using certain stress failure criteria. The typical fracture strength properties of E-glass/epoxy lamina (V_f = 50%) are as follows [1,2],

tensile strength in fibre direction: $\sigma_{1,t} = 1000\ MPa$

tensile strength in transverse direction: $\sigma_{2,t} = 30\ MPa$

shear strength in lamina plane: $S_{12} = 40\ MPa$

Maximum Stress Criterion

In the maximum stress criterion, the stresses in the principal material directions must be less than the respective strengths, otherwise fracture is said to have occurred, that is for tensile stresses,

$$\begin{aligned} \sigma_1 &< \sigma_{1,t} \\ \sigma_2 &< \sigma_{2,t} \\ |\tau_{12}| &< S_{12} \end{aligned} \tag{5.9}$$

Note that the shear strength is independent of the sign of τ_{12}.

With the 2-inch Ameron BS2000M GRE pipe, the internal diameter for the structural pipe wall is $D = 54.2$ mm and wall thickness $t = 3.0$ mm. Using the stresses in Eqs.(5.8) and the failure criteria (5.9), we obtain the weepage internal pressure,

$$P_{weepage} = 14.53\ MPa$$

at which the transverse stress σ_2 equals the transverse tensile strength $\sigma_{2,t}$. Hence it is assumed that failure mode is matrix cracking in transverse direction to fibres, caused by the tensile stress σ_2.

Tsai-Hill Failure Criterion

The Tsai-Hill failure criterion can be written as

$$\frac{\sigma_1^2}{\sigma_{1,t}^2} - \frac{\sigma_1\sigma_2}{\sigma_{1,t}^2} + \frac{\sigma_2^2}{\sigma_{2,t}^2} + \frac{\tau_{12}^2}{S_{12}^2} = e \quad \begin{cases} e < 1 & no\ failure \\ e \geq 1 & failure \end{cases} \tag{5.10}$$

Substituting the values of the stresses in Eqs.(5.8) and $D = 54.2$ mm, $t = 3.0$ mm of the structural pipe wall into Eq.(5.10), we obtain the weepage internal pressure,

$$P_{weepage} = 13.95\ MPa$$

Unlike the maximum stress criteria, the Tsai-Hill criterion has taken account of the interaction between the failure strengths $\sigma_{1,t}$ and $\sigma_{2,t}$, but it can not predict the failure mode.

Frost's Criterion

Based on the observation that the failure mechanism of filament wound GRE pipes was matrix cracking and fibres remained intact, Frost [4] concluded that the ply stresses controlling the failure were the transverse and shear stresses to the fibre direction. Therefore a simple criterion was proposed as,

$$\frac{\sigma_2^2}{\sigma_{2,t}^2}+\frac{\tau_{12}^2}{S_{12}^2}+C\left(\frac{\sigma_2\tau_{12}}{\sigma_{21,t}S_{12}}\right)=e \quad \begin{cases} e<1 & no\ failure \\ e\geq 1 & failure \end{cases} \tag{5.11}$$

where the interactive coefficient C was obtained by fitting the weepage data. Frost suggested C=-1.5 for the commonly used GRE pipes [4].

Substituting the values of the stresses in Eqs.(5.8) and D = 54.2 mm, t = 3.0 mm into the Frost's criterion (5.11), we obtain the weepage internal pressure for 2-inch AMERON BS2000M GRE pipes,

$$P_{weepage} = 17.46\ MPa$$

Prediction Based on Manufacturer's Data

The following gross strengths of the pipe wall of 2-inch BS2000M GRE pipes were given by the manufacturer [5],

Hoop strength: $\sigma_{hoop,fail}$=165 MPa (Test method: ASTM D1599)

Axial strength: $\sigma_{axial,fail}$=58.6 MPa (Test method: ASTM D2105)

If we treat the pipe wall as homogeneous and use a criterion similar to the maximum stress criteria by comparing the gross hoop and axial stresses with the corresponding strengths, i.e.,

$$\sigma_{hoop} < \sigma_{hoop,fail}$$
$$\sigma_{axial} < \sigma_{axial,fail} \tag{5.12}$$

Substituting the stresses in Eqs.(5.7) and D = 54.2 mm, t = 3.0 mm into the above inequalities, we get the weepage internal pressure for 2-inch AMERON BS2000M GRE pipes,

$$P_{weepage} = 12.97\ MPa$$

at which the axial stress σ_{axial} equals the axial tensile strength.

Discussion

Table 5.4 compares the results of experiments with those of the above predictions. The experiments on three specimens P01, P02 and P03, as shown in Table 5.3, give an average weepage pressure of 21.78 MPa. The four predictions are the pressures when the damage initiation occurs and are lower than the experimental result which was the average weepage pressure when the last ply failed. Nevertheless, all failure criteria give reasonably close predictions. The errors between the predicted and the measured weepage pressures are less than 41%. The classic maximum stress criteria and Tsai-Hill criterion give quite consistent results. The best prediction has been obtained by Frost's criterion for the pipes tested.

5.3 COUPLER JOINTED PIPES

5.3.1 Specimens

A total of 42 straight-coupler jointed GRE pipes were tested. The specimens were all commercial products in they series Bondstrand 2000M, manufactured by Ameron, and were nominally the same. Each specimen, as shown in Figure 5.10, was 1 metre long and had 2 inches (50 mm) nominal diameter. It comprised two 500 mm long pipes and a 100 mm long coupler, bonded with a two-part thermosetting epoxy adhesive, Ameron RP-48. The coupler and the pipe ends were carefully machined, degreased, sanded and cleaned before the epoxy adhesive was applied. The joints were then assembled and cured using a special heating blanket for one hour at 130°C. The geometry and dimensions of the joint are shown in Figure 5.11. The external diameter of the machined section of the pipes was 59.2 mm, compared with 60.4 mm for the pipe itself. A thickness of 0.6 mm, the top coat and the outer ply, was removed away. The machined length was 50 mm, 5 mm longer than the overlap with the coupler.

Both the pipes and the coupler were manufactured by filament winding. The basic geometric parameters and physical properties of the pipes and the coupler are given in Table 5.1. The coupler had an inner diameter of 60.2 mm, 1 mm greater than the external diameter of the machined pipe ends allowing a 0.5 mm thick adhesive layer to bond them together. The pipes were as described previously in Section 5.2.1.

5.3.2 Experimental

All 42 coupler-jointed specimens were tested under static or cyclic internal pressure generated using the hydraulic test rig described in Chapter 4. The specimens were numbered from C01 to C42. Before performing the fatigue tests, three specimens were tested under quasi-static internal pressure until weepage. Fatigue tests were carried out by applying cyclic saw-tooth internal pressure with maximum values of 14.5, 14.0, 13.5, 13.0, 12.8, 12.5, 12.2, 12.0, 11.8, 11.5, 11.2, 11.0, 10.5, 10.0 and 9.5 MPa respectively. In each case the minimum pressure was zero and thus R=0. An identical pressurisation speed of 100 MPa per minute was used in all the fatigue tests. The resulting frequencies were therefore between 6.9 to

10.5 cycles per minute, depending on the maximum pressure of the cycle. Low pressure tests were thus performed at relatively high frequencies and high pressure tests at low frequencies.

The same design of end-caps was used as for plain pipes (Chapter 4). Since the joints were expected to be weaker than either the pipes or the ends, no additional glass/epoxy reinforcement was needed at the specimen's ends before they were tapered by machining. Therefore, the aluminium collars had a smaller inner diameter and a taper angle to fit the shaved pipe ends. Burst tests were also conducted for coupler-jointed pipes after weepage. The experimental set-up was the same as for plain pipes described in Chapter 4.

Finite Element Stress Analysis

Finite element analysis was carried out using NISA software on the specimen subjected to internal pressure, to evaluate the significance of the stress concentration at the joint. This was found helpful in interpreting the failure modes. Details of the finite element analysis are presented in Chapter 7.

5.3.3 Results and Discussion

The results of the static tests on coupler-jointed GRE pipes are given in Table 5.5. The three specimens C01, C02, and C03 showed quite similar weepage pressures. The average weepage pressure was 19.29 MPa, slightly lower than that of the plain pipes, 21.78 MPa in Table 5.3.

After the weepage tests, C01 and C02 were fitted with rubber liners and were burst under quasi-static internal pressure. These two specimens gave quite consistent burst pressures and their difference was less than 3%. As with the average weepage pressure, the average static burst pressure of C01 and C02 was 49.39 MPa, slightly lower than the value of 53.10 MPa for the plain pipes shown in Table 5.3.

The results of fatigue tests on 37 coupled GRP pipes are plotted in the P-N diagram shown in Figure 5.12. Pipes were tested by applying cyclic saw-tooth internal pressure until water weepage or up to 20,000 cycles. Of the 37 coupled specimens, four specimens (presented

with "+") did not fail after 20,000 cycles at load levels of 0 - 9.5 and 0 - 10.0 MPa. All points fall in a small scatter band, which shows a linear relationship between the internal pressure and the logarithm of cycles, as shown in Figure 5.12. This is consistent with the equation (3.2) which was supposed to be the best fit with the test results at low cycles and high stress fatigue levels. The following equation is obtained by the least squares calculations (see Appendix D):

$$P = 21.48 - 2.86 \log N \qquad (MPa) \tag{5.13}$$

After the fatigue (weepage) tests, 17 specimens were equipped with rubber liners and burst by applying quasi-static internal pressure. The burst pressures, shown in Figure 5.12, fell in the scatter band close to a horizontal line. It appears that the weepage fatigue process had little influence on the burst pressure. The burst tests gave an average pressure of 50 MPa, almost the same as that shown in Table 5.5 for static tests.

Two specimens, C07 and C11, which had been intended for fatigue tests under cyclic pressure of 0 - 14.0 MPa, however failed by water weepage through the bonded interface at a lower pressure than the preset maximum pressure of 14.0 MPa. C07 failed at 12.70 MPa and C11 at 12.53 MPa. The premature failure appeared to have been caused by poor bonding. In the burst test after weepage failure, C07 gave a burst pressure of 53.20 MPa, which was not significantly different from specimen C01, C02 and the other specimens, despite C07 having lower weepage pressure. Therefore, the comparison of these results indicated that the burst strength was independent of the damage in the matrix and adhesive during weepage tests.

A comparison is given in Figure 5.13 between the fatigue strengths of the coupled and plain pipes. Fatigue life was plotted against nominal hoop stress in the pipe wall. The nominal hoop stress was calculated for the structural pipe wall by Eq.(5.1) or (5.7) discussed earlier, in which the values, D = 54.2 mm and t = 3.0 mm, were used. The fatigue results showed little differences between the fatigue strengths of plain pipes and coupler-jointed pipes, despite the latter gave lower static strength than the former. It indicated that the presence of couplers did not influence the fatigue weepage strength as much as it did for static strength. The reason probably was that the stress concentration in the pipe wall near the joint induced by the installation of the thick-walled coupler only affected the damage initiation. As ply

cracks and delaminations grew, the damaged plies degraded, the ply stresses were redistributed and the stress concentration was eased. The coupler worked as a stress concentrator. As discussed in Section 3.4.1 in Chapter 3, small stress concentrators in composite structures have little effect on fatigue strength as progressive damage quickly removed the stress concentration.

Fatigue life is plotted against the nominal hoop strain of the pipes in Figure 5.14 to show the permissible level of the strain. The nominal hoop strains were calculated by the Hooke's law and the nominal wall stresses. Eqs.(5.2) and (5.7) are used for the calculations. The fitted line by the least squares calculations (see Appendix D) is:

$$\varepsilon_{hoop} = 0.75 - 0.10 \log N \qquad (\%) \tag{5.14}$$

At N=10,000 and 20,000 cycles, the lower confidence limit with 5% level of significance are calculated by Eq.(D8) in Appendix D. They are:

$$\varepsilon_{hoop,LowerLimit} = 0.32\% \qquad when \quad N = 10,000 \tag{5.15}$$

and

$$\varepsilon_{hoop,LowerLimit} = 0.29\% \qquad when \quad N = 20,000 \tag{5.16}$$

That is to say, 97.5% of the expected failures will be above 0.32% at N=10,000 and above 0.29 at N=20,000.

Figure 5.15 shows the failure positions of the specimens during weepage and burst tests. Most of specimens failed in the external transition zone from the coupler to the pipe except 3 specimens failed by water weepage through bonding interface and 2 in the coupler. Burst of the rubber-lined pipes occurred consistently in the pipe wall close to the joint, mostly 30 to 50 mm away from coupler shoulder. Figure 5.16 shows six typical examples of the burst specimens. It was also observed that delamination occurred between the top ply and the second before the specimens finally burst, starting from the shaved step of the pipe end close to the coupler.

There are four possible weepage modes for the coupled specimens shown in Figure 5.17: (a) through the coupler wall, (b) through the bonded interface, (c) through the pipe wall near to the joint and (d) through the pipe wall far from the joint.

Figure 5.17 also shows the frequency of the occurrence of each weepage mode during tests. Most of the failures occurred in mode C: weepage through the pipe wall close to the joint. According to finite element analysis (Chapter 7), a stress concentration exists in this external transition zone because the thick-walled coupler restricts the pipe expansion and causes local bending. It seems that this stress concentration has caused the damage initiation and thus the dominant failures in mode C. Fewer specimens failed in other minor modes A, B and D at lower pressures. These minor failure modes appeared to be caused by various types of defect existing in the adhesive layer, the coupler wall, the pipe wall or the liner. Therefore, provided the quality of the adhesive bonding and the couplers are controlled, the bonded-coupler joints can achieve the same fatigue strength of the plain pipes.

Gustafson et. al. [6] performed fatigue tests on 4 inch diameter coupler-jointed GRE pipes, subjected to waterhammer loading. Weepage occurred predominantly through couplers which were wound with $0^{\circ}/90^{\circ}$ GRE woven fabric. In comparison with the coupler-joints tested in the current work, one possibility for the differences of their failure modes was the different designs of the couplers. The $\pm 55^{\circ}$ filament wound coupler seems stronger than the $0/90^{\circ}$ fabric wound coupler. Fibre debonding and resin cracking probably are more easily induced by internal pressure in $0^{\circ}/90^{\circ}$ fabric wound couplers. Therefore, the $\pm 55^{\circ}$ filament wound coupler appears to be a better design.

Figure 5.18 shows the cracks in the resin-rich liner inside the pipe. Cracks were predominantly distributed in the region near the coupler. The installation of the coupler induced stress and strain concentration in the pipe wall in this region. The finite element analysis (Figure 7.6 in Chapter 7) showed that the hoop strain was greater than the axial strain in the liner. As the resin-liner would be expected to have same failure strains in hoop and axial directions, the higher hoop strain had induced the liner to crack in axial direction. Figure 5.19 shows a picture of the inside of a typical specimen, where the liner cracks could be seen.

5.4 SOCKET/SPIGOT JOINTED PIPES

5.4.1 Specimens

A total of five spigot/socket jointed GRE pipe specimens were tested, all of which were commercial products of Ameron, series BS2000M, as shown in Figure 5.1(a). Each specimen comprised two 500 mm long pipes which were bonded through the spigot and socket ends by a two-part thermosetting epoxy adhesive, Ameron RP-48. The dimensions of the joint are shown in Figure 5.20. Compared with the 3.6 mm pipe wall, the thickness of socket was 5 mm. The bonding length was 40 mm, 5 mm shorter than the coupler-joint. The pipes and the manufacture of the joints were the same as the plain pipes and the coupler-joints.

5.4.2 Experimental

Two specimens, J01 and J02, were tested under quasi-static pressure until they failed by weepage. Fatigue tests were carried out on three specimens, J03, J04 and J05, under two pressure ranges: 0 - 8.0MPa and 0 - 11.0 MPa, as described in Table 5.6. The experimental set-up was the same as that described previously for coupler-jointed pipes.

5.4.3 Results and Discussion

The results for the spigot/socket jointed pipes are given in Table 5.6. Specimens J01 and J02 were tested under static pressure, equivalent to 1/2 of the load cycle (from the minimum load of zero to the weepage load). The average weepage pressure of specimens J01 and J02 was 12.6 MPa. The fatigue tests were conducted on J03, J04 and J05. Specimen J03 only withstood 75 cycles to weepage under the pressure cycles of 0 - 11.0 MPa, and J04 and J05 were 357 and 5341 cycles under 0 - 8.0 MPa. Compared with the plain pipes in Table 5.3, the socket/spigot joints showed lower static and fatigue strengths. Figure 5.21 shows a pressure - cycle (P-N) diagram, comparing the results of the socket/spigot jointed pipes with

those of plain pipes and of coupler-jointed pipes. The static and fatigue weepage pressures of the socket/spigot joints were significantly lower than the plain and coupler-jointed pipes.

Burst tests were also conducted on the socket/spigot bonded joints. The results are shown in Table 5.6. The burst pressures were significantly lower than those of the plain pipes (Table 5.3) and of coupler-jointed pipes (Table 5.5). The average burst pressure of the four specimens was 31.54 MPa. The maximum difference between specimens J03 and J05 was 37%.

Figure 5.22 shows the locations of the water weepage and the pipe burst. There were two main types of failure modes in weepage tests: the socket failure and the adhesive interface failure. Specimens J02 and J04 failed by water weepage through the adhesive interface and J01, J03 and J05 by the socket failure. Comparing the weepage pressures in Table 5.6, J02 had lower static weepage pressure than J01, and J04 had shorter fatigue life than J05 under the same cyclic pressure. This indicated the poor bonding between the socket and the spigot of J02 and J04.

Of all the four burst tests, bursts occurred consistently at the same location and there was no adhesive interface failure. Figure 5.23 shows the typical external appearances of two burst specimens. Since the defects in the adhesive had very small dimensions, they did not greatly influence the burst strength.

Figure 5.24 shows the cracks in the resin-rich liner inside a socket/spigot jointed pipe. Different from those of the plane pipes (Figure 5.4) and the coupler-jointed pipes (Figure 5.18), cracks were aligned in the hoop direction in the region close to the socket bottom. Since the resin-rich liner was expected to have isotropic mechanical properties, it was assumed that these cracks were probably caused by large axial strain in the liner. According to the finite element analysis, there were high axial strains at the socket bottom due to the local bending. Figure 5.24 is a typical picture showing the inside failure appearance of a socket/spigot joint tested.

Figure 5.26 compares the average strengths of the three types of 2-inch GRE pipes. The static burst pressures, the static weepage pressures and the fatigue weepage pressures at 10^4

cycles were plotted in the same chart. The average fatigue pressures were obtained from the fitted lines in Figure 5.21. These results showed that the plain pipes had the highest strengths, the strengths of coupler-jointed pipes were slightly lower than those of the plain pipes, and the socket/spigot jointed pipes were the weakest. For all three types of specimens, the static weepage pressures were approximately 40% of the burst strengths, and the fatigue weepage pressures at 10^4 cycles were approximately 50% of the static weepage pressures.

5.5 DISCUSSION AND CONCLUSIONS

(a) Strength

A pressure - life diagram is presented in Figure 5.21 and a bar chart in Figure 5.26 for the 2-inch filament wound GRE pipes and joints. These results show that the socket/spigot jointed pipes had the lowest strengths. The coupler-jointed pipes failed near to the joints but exhibited a strength comparable to that of the plain pipes. The installation of a thick-walled coupler did not severely influence the fatigue strength of a pipe but did affect its static strength.

In relation to the working pressure range of 3 MPa (30 bar) used in offshore fire water systems and the pressure rating of 4.4 MPa (44 bar) of these pipe products, all the pipes tested were found to have sufficient strengths. The fatigue weepage pressure (at 10^4 cycles) of the weakest socket/spigot joints was still 2.3 times higher than the working pressure required. Therefore, they are applicable for offshore fire system.

(b) Failure modes

Plain pipes failed by resin cracking. As the cracks penetrated the pipe wall, water seeped through the cracks and the pressure was released. With coupled pipes, water weepage occurred predominantly through the pipe wall close to the coupler, where stress concentration existed because of the local bending moments. The sudden change of the wall

thickness was the reason for this local stress concentration. With socket/spigot jointed pipes, weepage occurred mostly through the pipe wall near the bottom of the socket.

(c) Test rig and end caps

The rig designed and built by the author worked well and was capable of producing static and cyclic hydraulic pressures up to 70 MPa. The system was tested in the range between the 0 and 70 MPa and was verified to be safe. The computer data logging system played an important role in identifying the maximum pressure at which weepage or burst first occurred. All the specimens tested failed in gauge length or at joints with reasonable distances from their ends, indicating that the modified design of adhesively-bonded end caps was a successful one.

REFERENCES

[1] Gibson, A. G., Composites in Offshore Structures, pp.199-226, Composites Materials in Marine Structures, Volume 2: Practical Considerations, Edited by Shenoi,R.A. and Wellicime,J.F., Cambridge University Press, 1993.

[2] Boothby,P.J., Glass Reinforced Plastics for Offshore Topside Seawater Pipework - The Current Position, ERS Report 4613, March 1991.

[3] Owen,M.J., Smith,T.R. and Dukes,R., Failure of Glass-Reinforced Plastics, with Special Reference to Fatigue, Plastics and Polymers, June 1969, pp.227-233.

[4] Frost,S.R., Designing Composite Pipelines for Use in the Oil Industry, Paper in Conference Proceedings: Composite Materials for Offshore Use, November 1994.

[5] Ameron Bondstrand® Product Data, Bondstrand 2000M Fiberglass Pipe and Fittings for Marine and Offshore Service.

[6] Gustafson,C.G., Semb,G. and Moursund,B., Fatigue from Waterhammer on Filament Wound GRE-Pipes and Adhesive Bonded Joints. Proc. of Ninth Int. Conf. on Composite Materials (ICCM-9), Vol.IV, pp.63-73, Madrid, 12-16 July, 1993.

Table 5.1 Dimensions and physical properties of the GRE pipes and couplers (Ameron Bonstrand 2000M).

	GRP Pipes	Couplers
Nominal diameter (mm)	50	50
Inner diameter (mm)	53.2	60.2
Outer diameter (mm)	60.4	71.2
Wall thickness (mm)	3.6	5.5
liner (mm)	0.5	-
structural wall (mm)	3.0	5.4
topcoat (mm)	0.1	0.1
Length (mm)	1000	100
Specific gravity	1.77	1.77
Gross fibre weight fraction, w%	64	64
Gross fibre volume fraction, v%	44	44
Fibre volume fraction in structural wall , v%	50	50
Fibre orientation	±55°	±55°
Internal pressure rating (MPa) (cyclic hydraulic design basis) [ASTM Standard D2992]	4.4	5.3
Production method	Filament winding	Filament winding
Weight (kg/m)	1.2	-

Table 5.2 Typical pipe mechanical properties supplied by the manufacturer (Ameron Bonstrand 2000M). [5]

	21°C	93°C
Longitudinal tensile strength (MPa)	58.6	47.6
Longitudinal tensile modulus (MPa)	11000	8500
Poisson's ratio ($\nu_{axial,hoop}$)	0.37	0.41
Circumferential tensile stress at weeping(MPa)	165	-
Circumferential tensile modulus (MPa)	25200	22100
Poisson's ratio ($\nu_{hoop,axial}$)	0.56	0.70
Beam apparent elastic modulus (MPa)	11700	6900

Table 5.3 Experimental results for plain GRE pipes.

	Specimen identifier	Weepage pressure (MPa)		Burst pressure[1] (MPa)
		Pressure to weepage (MPa)	Cycles to weepage	Pressure to burst (MPa)
Static tests	P01	21.90	½ (static)	52.14
	P02	23.30	½ (static)	53.17
	P03	20.14	½ (static)	-
		Average: 21.78		
Fatigue tests	P04	0 - 14.0[2]	275	53.90
	P05	0 - 14.0	97	-
	P06	0 - 11.0	4,783	53.17
	P07	0 - 11.0	2,144	-
				Average: 53.10

[1] After water weepage tests, specimens P01, P02, P04 and P06 were fitted with rubber liners and subjected to quasi-static internal pressure. The load was increased gradually until they burst. Weepage failure was characterised by resin-cracking and water weepage. Burst failure was characterised by catastrophic fibre-breakage.

[2] Cyclic saw-tooth internal pressure was applied by increasing the pressure at a constant speed of 100 MPa per minute from the minimum pressure of zero to the maximum pressure of 14 MPa and then releasing the pressure rapidly (at very high pressure release rate).

Table 5.4 Comparison of predicted weepage pressures with experimental results

Test or predictions*	Static weepage pressure (MPa)	Errors to experimental data
Experimental result (average)	21.78	-
Maximum stress criteria	14.53	33.3%
Tsai-Hill failure criterion	13.95	36.0%
Frost's criterion	17.46	19.8%
Prediction based on manufacturer's data	12.97	40.4%

* Predictions carried out in Section 5.2(c)

Table 5.5 Experimental results for static tests on coupler-jointed GRE pipes.

Specimen	Weepage pressure (MPa)	Burst pressure (MPa)
C01	20.19	48.82
C02	19.05	49.96
C03	18.64	-
Average	19.29	49.39

Table 5.6 Experimental results for socket/spigot jointed GRE pipes.

	Specimen identifier	Weepage tests		Static burst tests after weepage
		Weepage pressure or cyclic pressure (MPa)	Pressure cycles to weepage	Burst pressure (MPa)
Static tests	J01	15.4	½ (static)	31.74
	J02	9.7	½ (static)	33.50
		Average:12.6		
Fatigue tests	J03	0-11.0	75	37.33
	J04	0-8.0	357	-
	J05	0-8.0	5,341	23.60
				Average: 31.54

Figure 5.1 Examples of GRP pipes tested:

(a) Adhesively bonded spigot/socket-jointed GRE pipe (Ameron BS2000M).
(b) Adhesively bonded coupler-jointed GRE pipe (Ameron BS2000M).
(c) Filament wound GRE plain pipe (Ameron BS2000M).
(d) GRE pipe with conductive fibres (Ameron BS7000).
(e) Adhesively bonded spigot/socket-jointed GRE pipe (Wavin).
(f) Adhesively bonded spigot/socket-jointed GRVE pipe (Sarplast).
(g) CSM laminate-jointed GRVE pipe (Sarplast).
(h) Filament wound GRVE plain pipe (Sarplast).

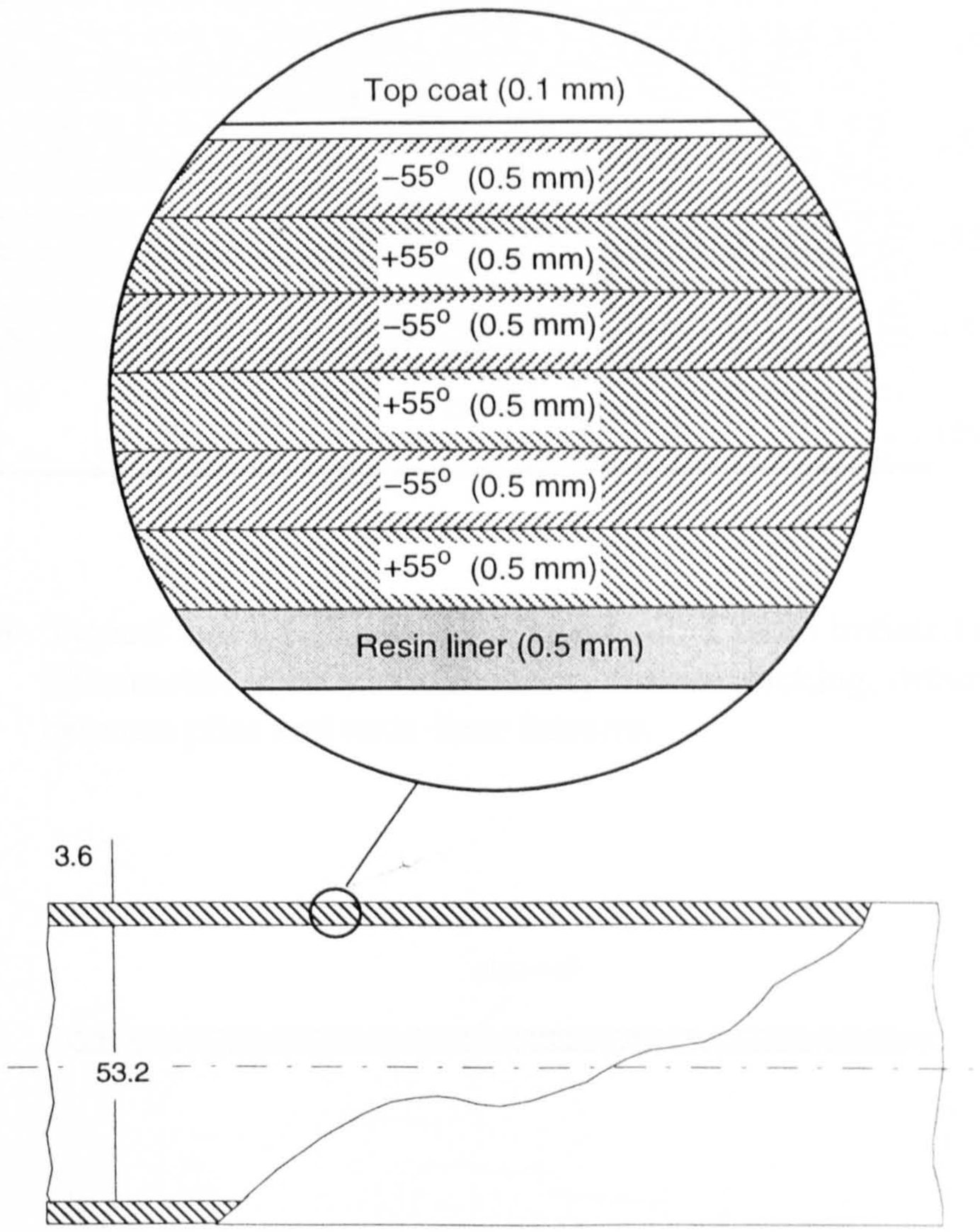

Figure 5.2 Schematic diagram of the filament wound GRE plain pipe. The internal diameter is 53.2 mm. Total wall thickness is 3.6 mm, which consists of 0.5 mm resin liner, 6 plies of $\pm 55^0$ glass fibre reinforced epoxy and 0.1 mm top coat.

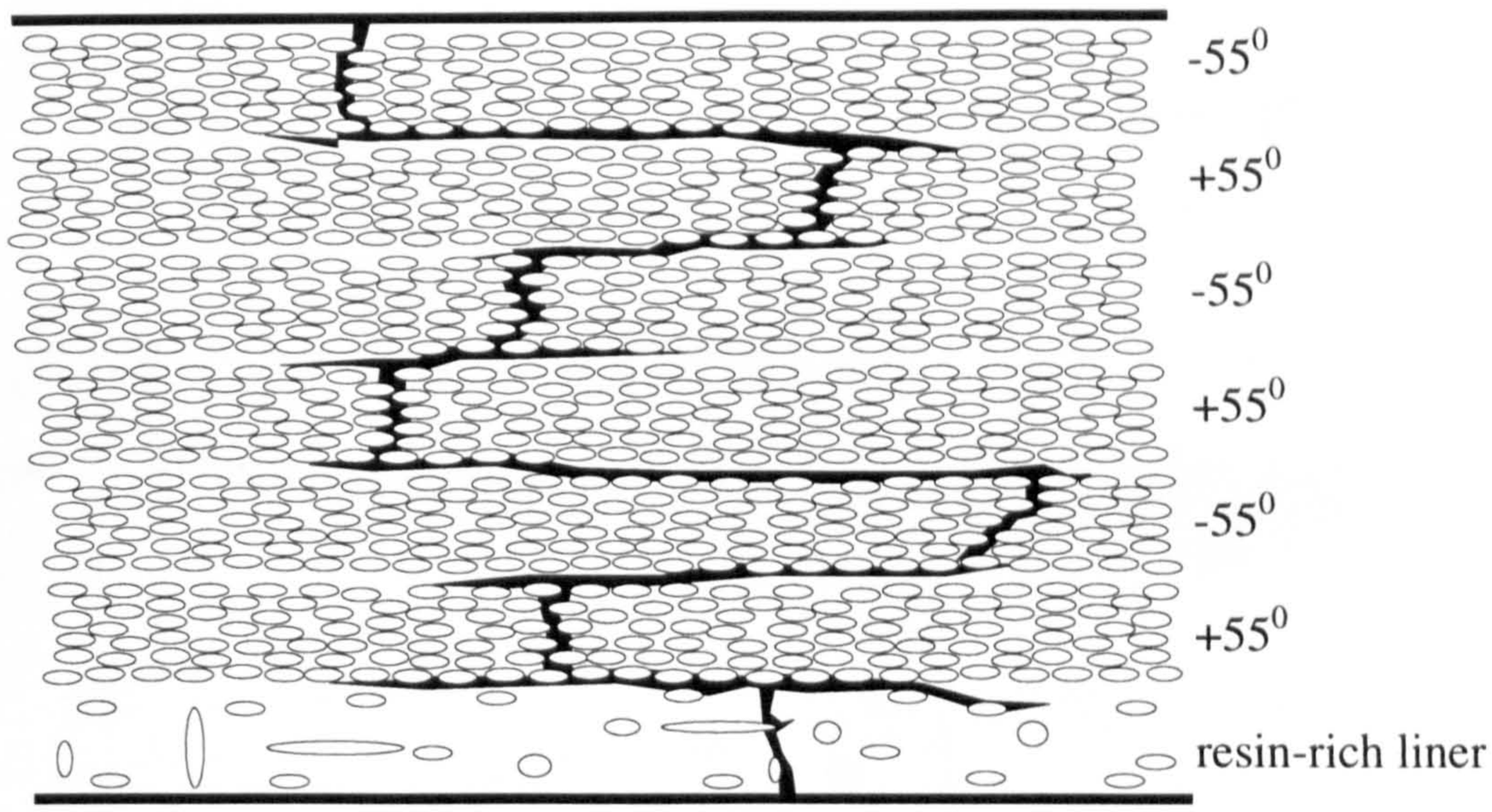

Figure 5.3 Typical crack path across the pipe wall. Cracks initiated at the fibre/matrix interface followed by matrix cracking, delamination between plies and resin-liner fracture.

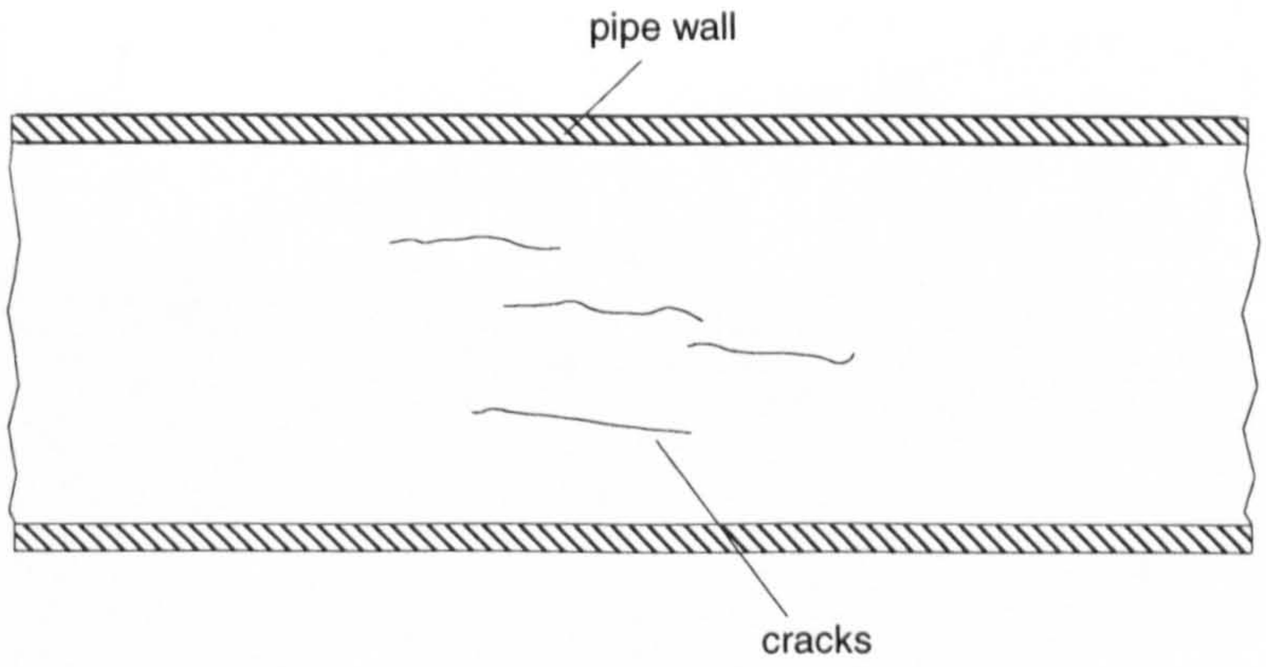

Figure 5.4 Cracks in the resin-rich liner of a plain pipe. The resin liner cracked in the gauge region along the axial direction. These cracks were induced by the hoop stress.

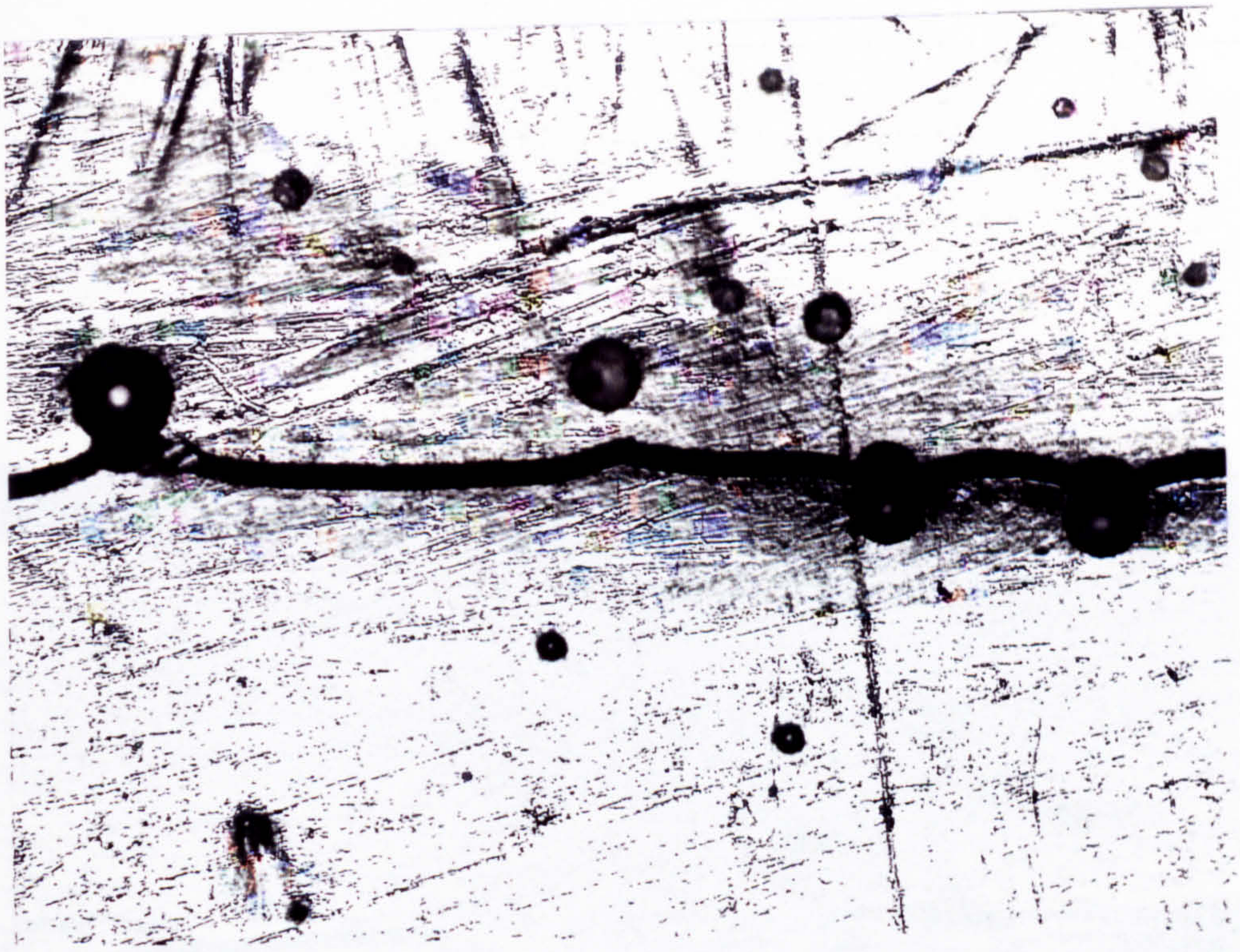

Figure 5.5 Cracks initiating from air bubbles in the resin liner of the pipe and propagating in the axial direction.

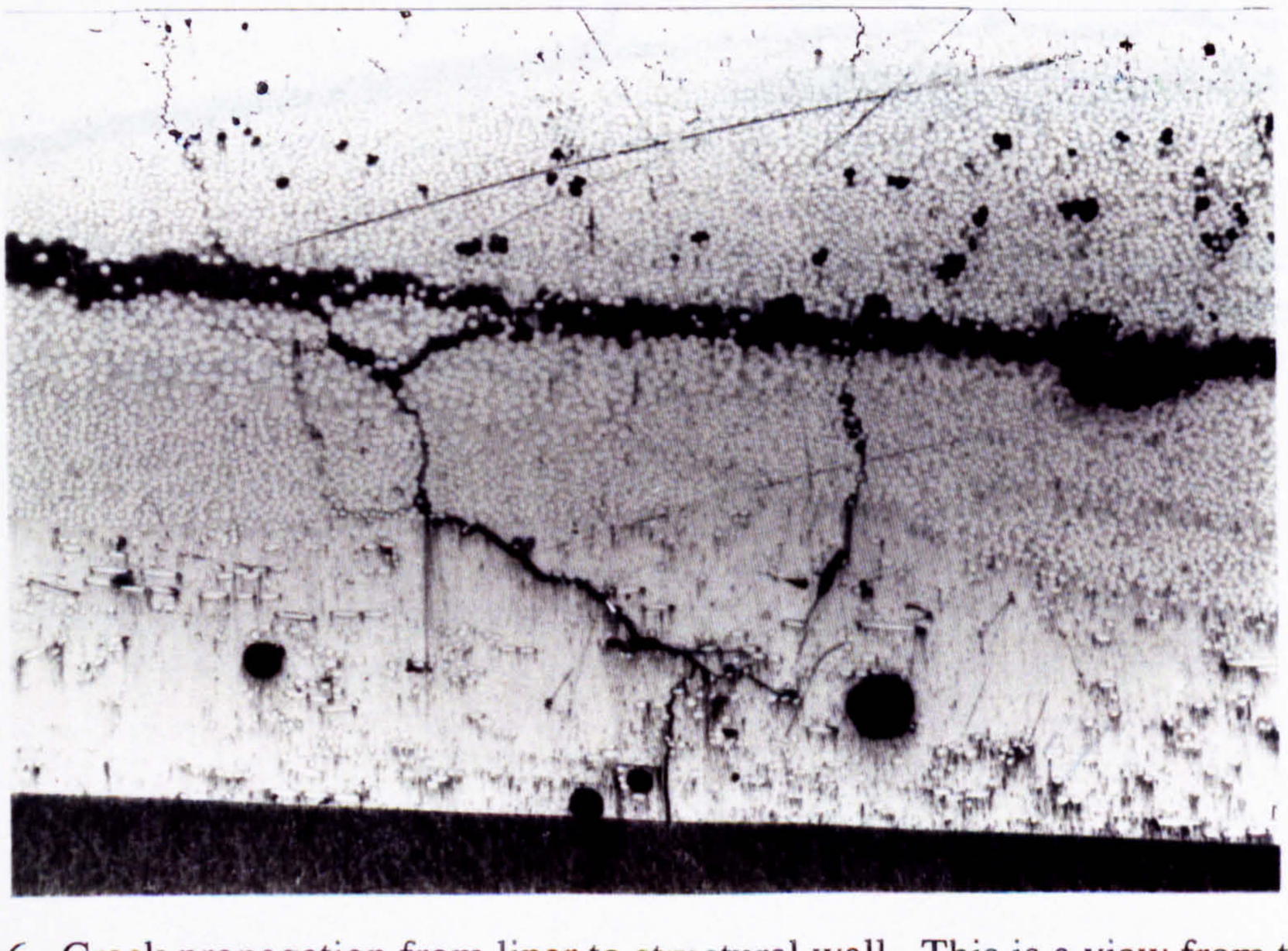

Figure 5.6 Crack propagation from liner to structural wall. This is a view from the pipe cross-section. The resin liner is cracked in the pipe axial direction due to the high hoop strain.

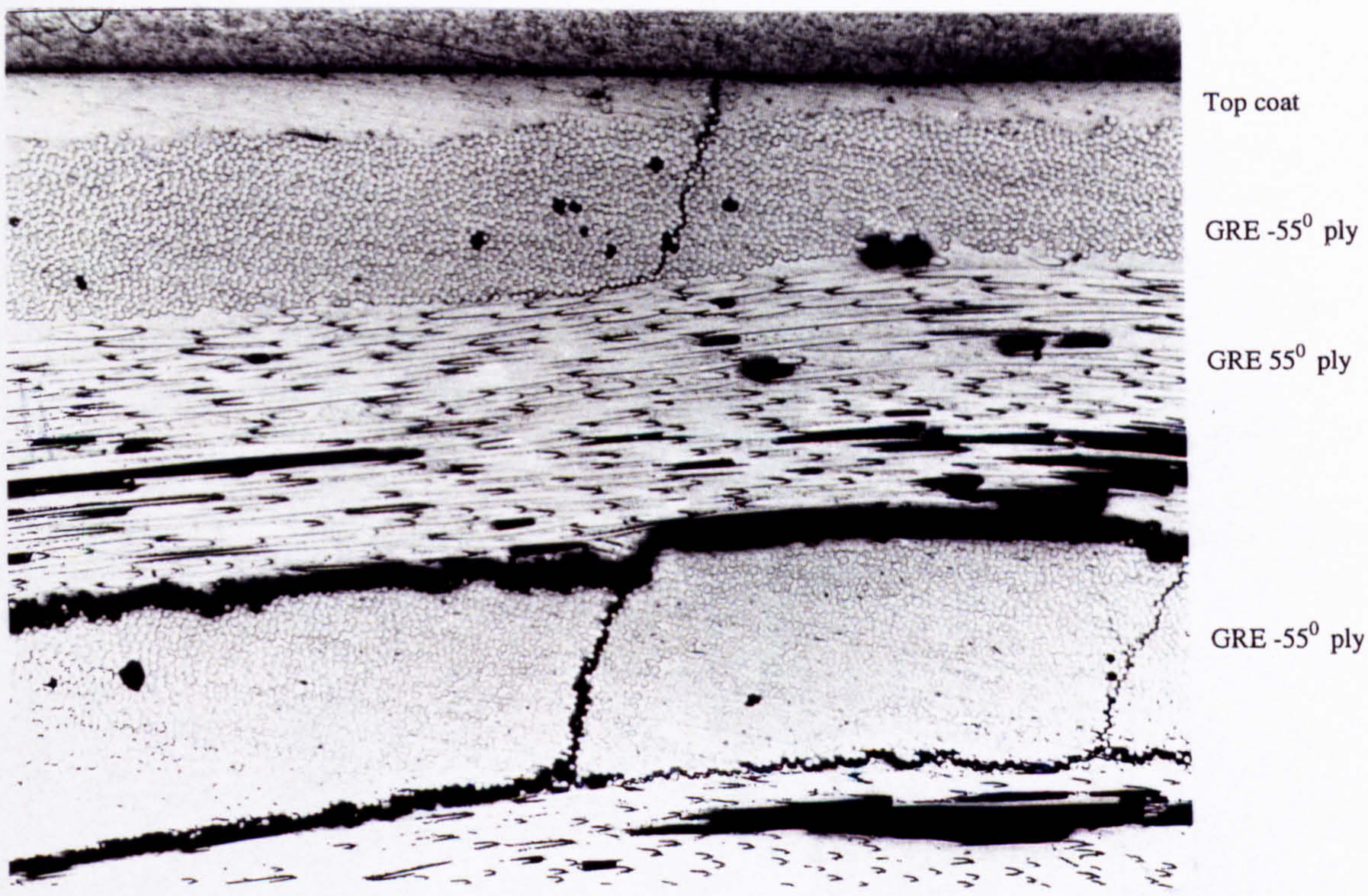

Figure 5.7 Crack propagation between ±55^o plies. The cracks propagated through each ply by fibre debonding and resin cracking, and across the interface between plies by delamination.

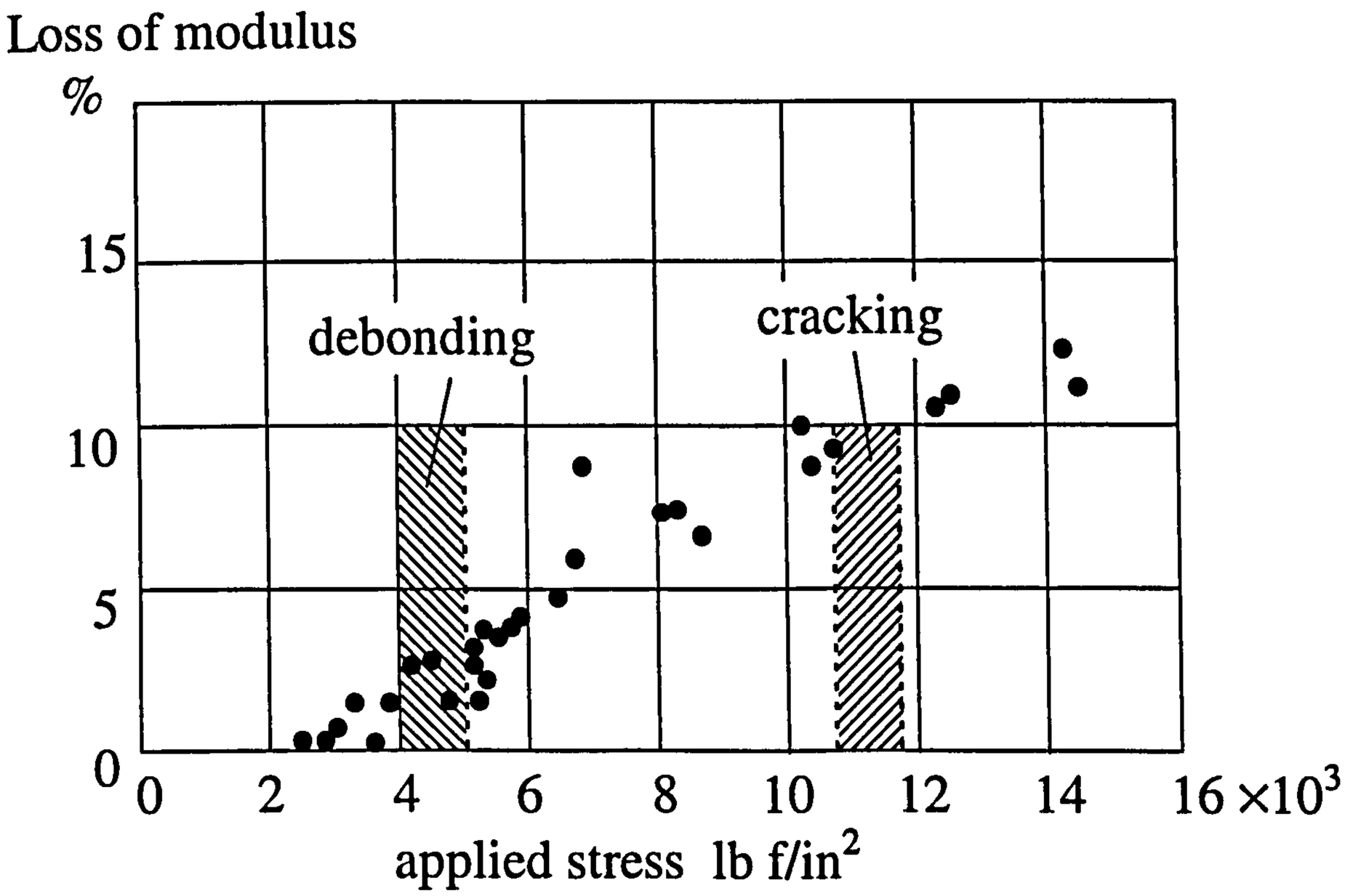

Figure 5.8 Loss of modulus after application of tensile stress to glass/polyester laminates [3]

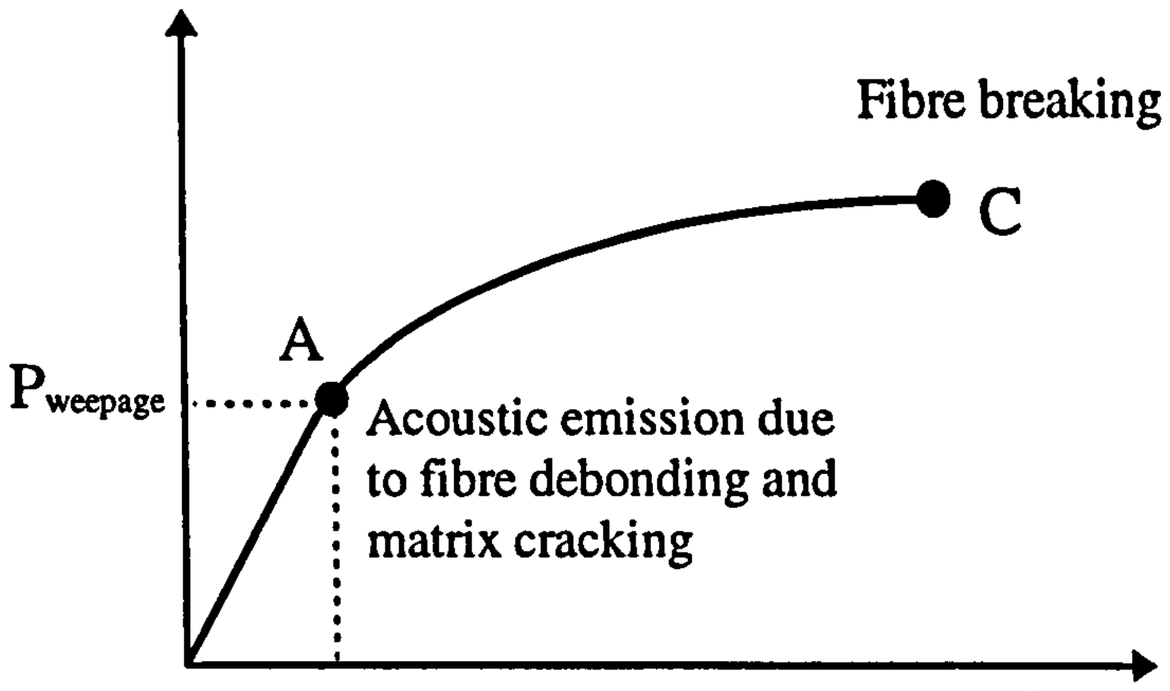

(a) GRE pipe without liner

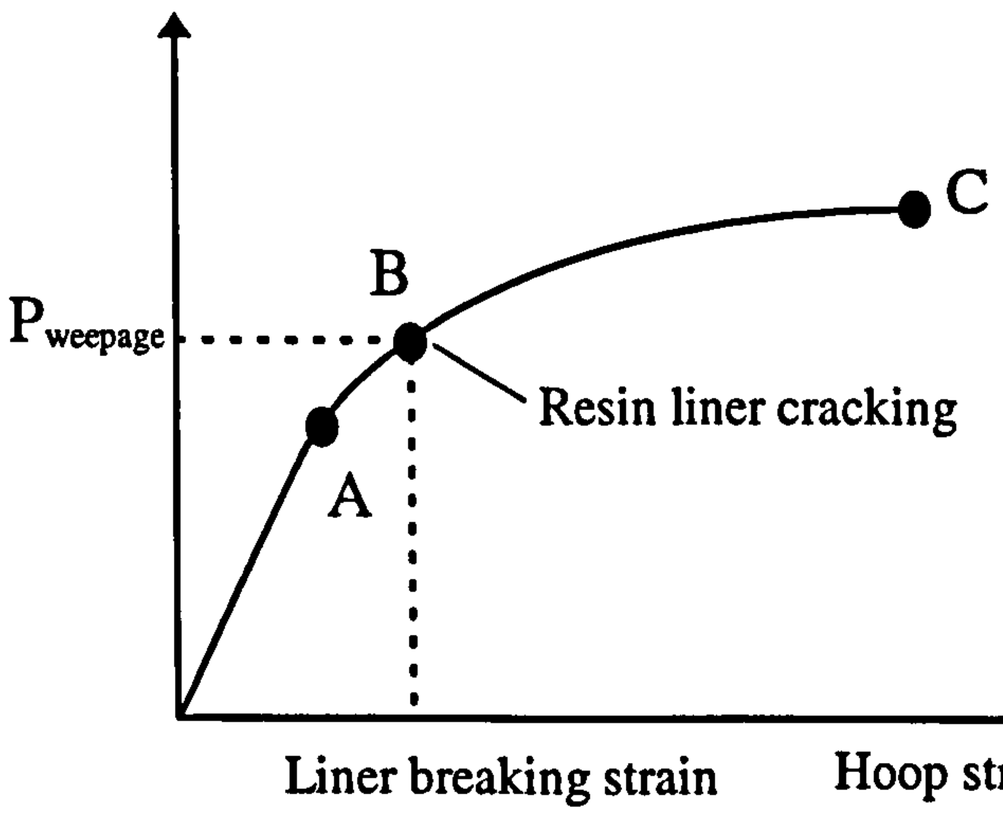

(b) GRE pipe with resin-rich liner

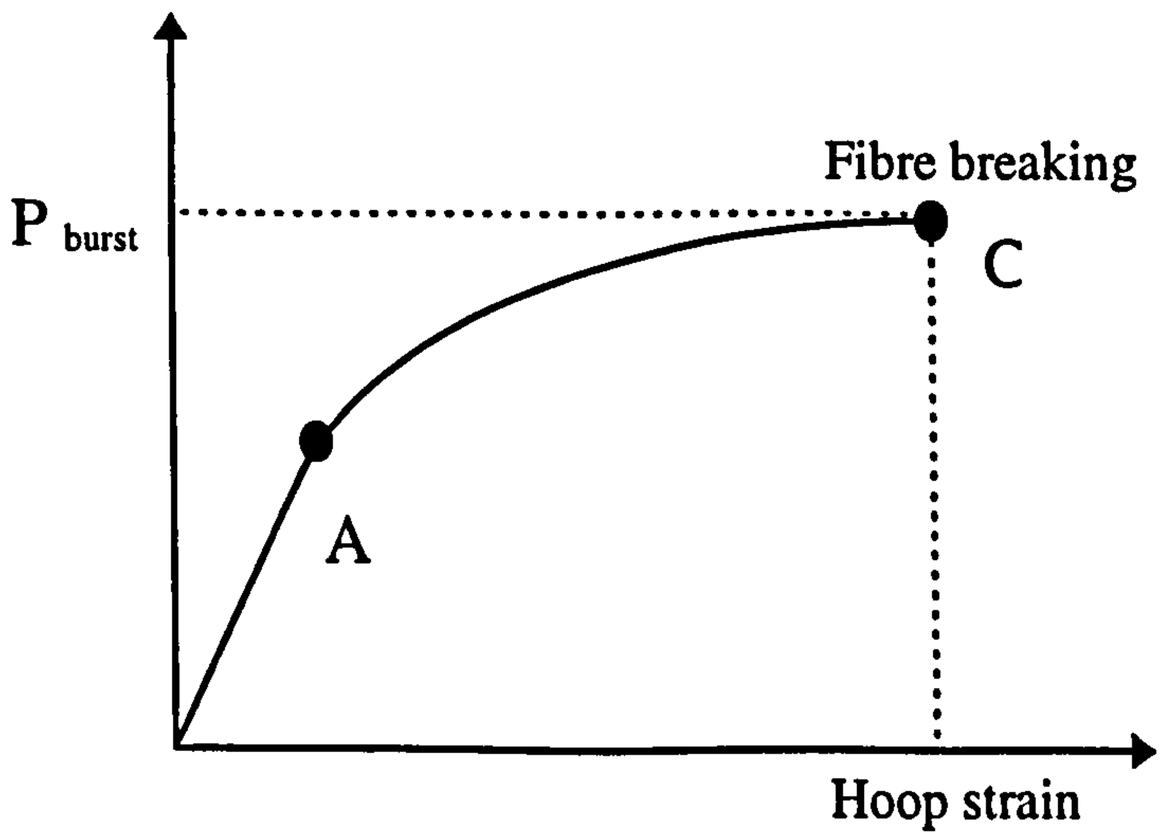

(c) GRE pipe fitted with extra rubber liner

Figure 5.9 Internal pressure - hoop strain diagrams showing failure modes for GRE pipes with or without liners.

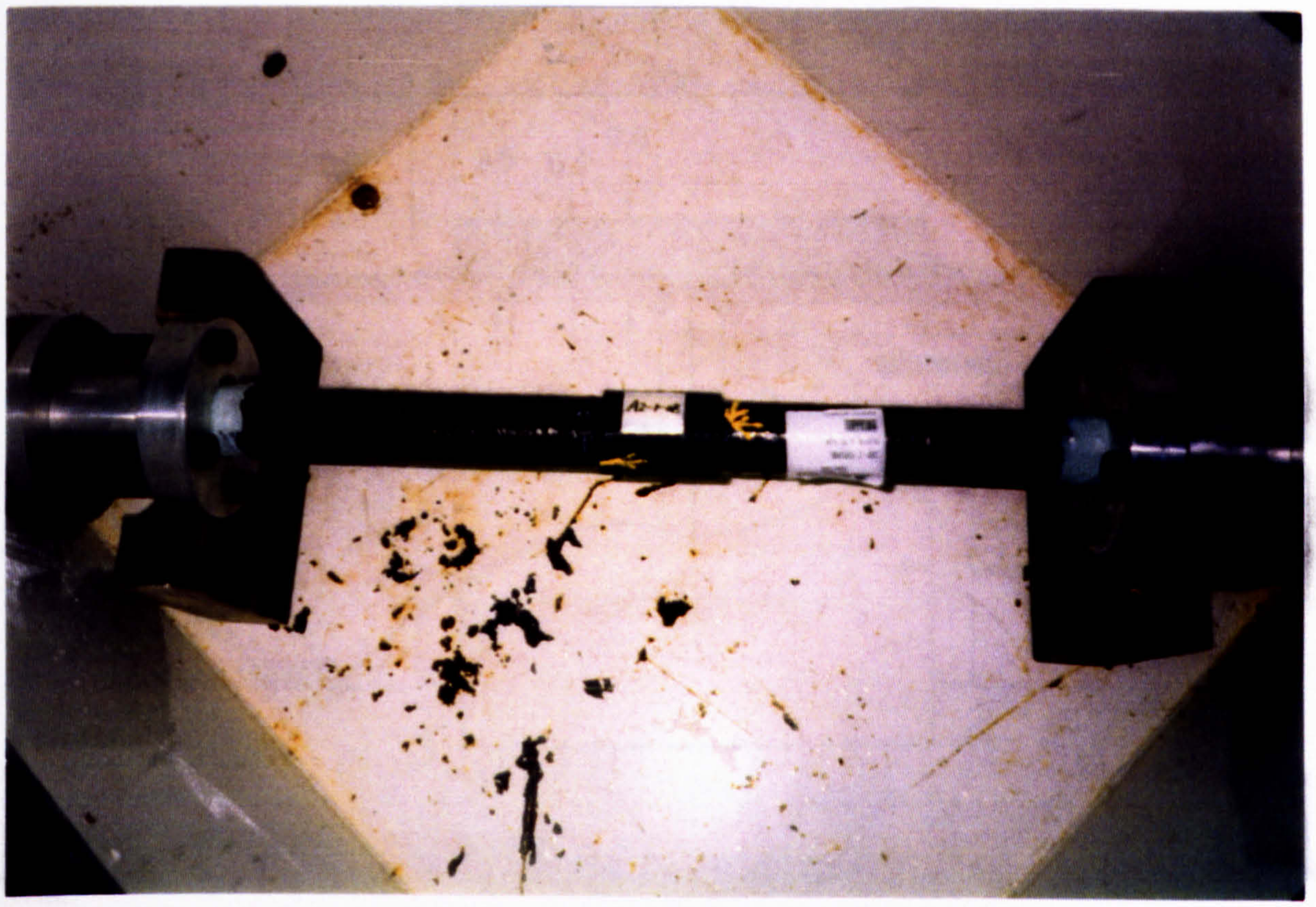

Figure 5.10 Coupler-jointed GRE pipe specimen equipped with end-caps ready to be tested.

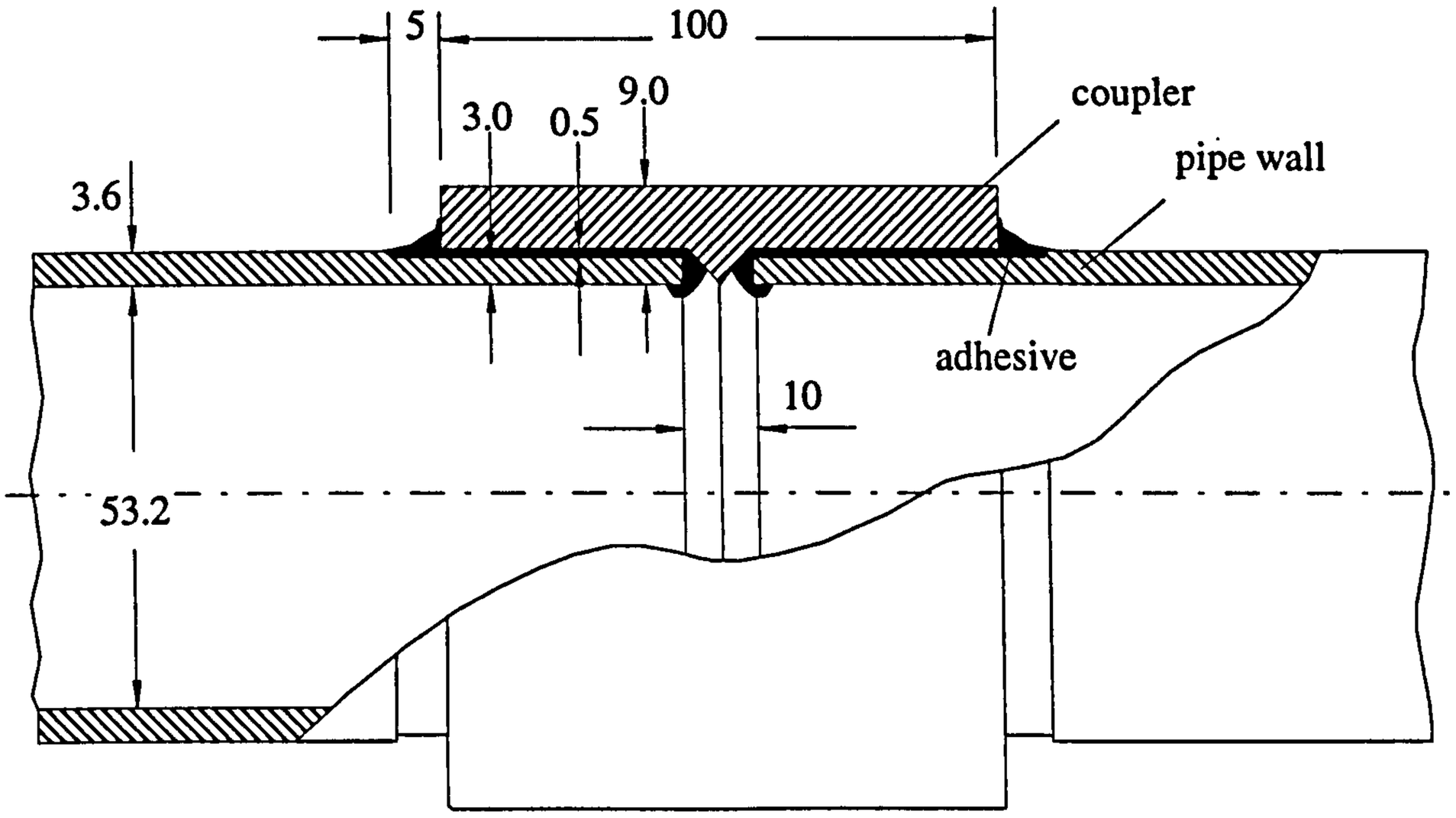

Figure 5.11 Two GRE-pipes jointed by an adhesively bonded coupler (Units of dimensions: mm). The top-coat and the outer ply of the pipe ends were machined off (0.6 mm thick).

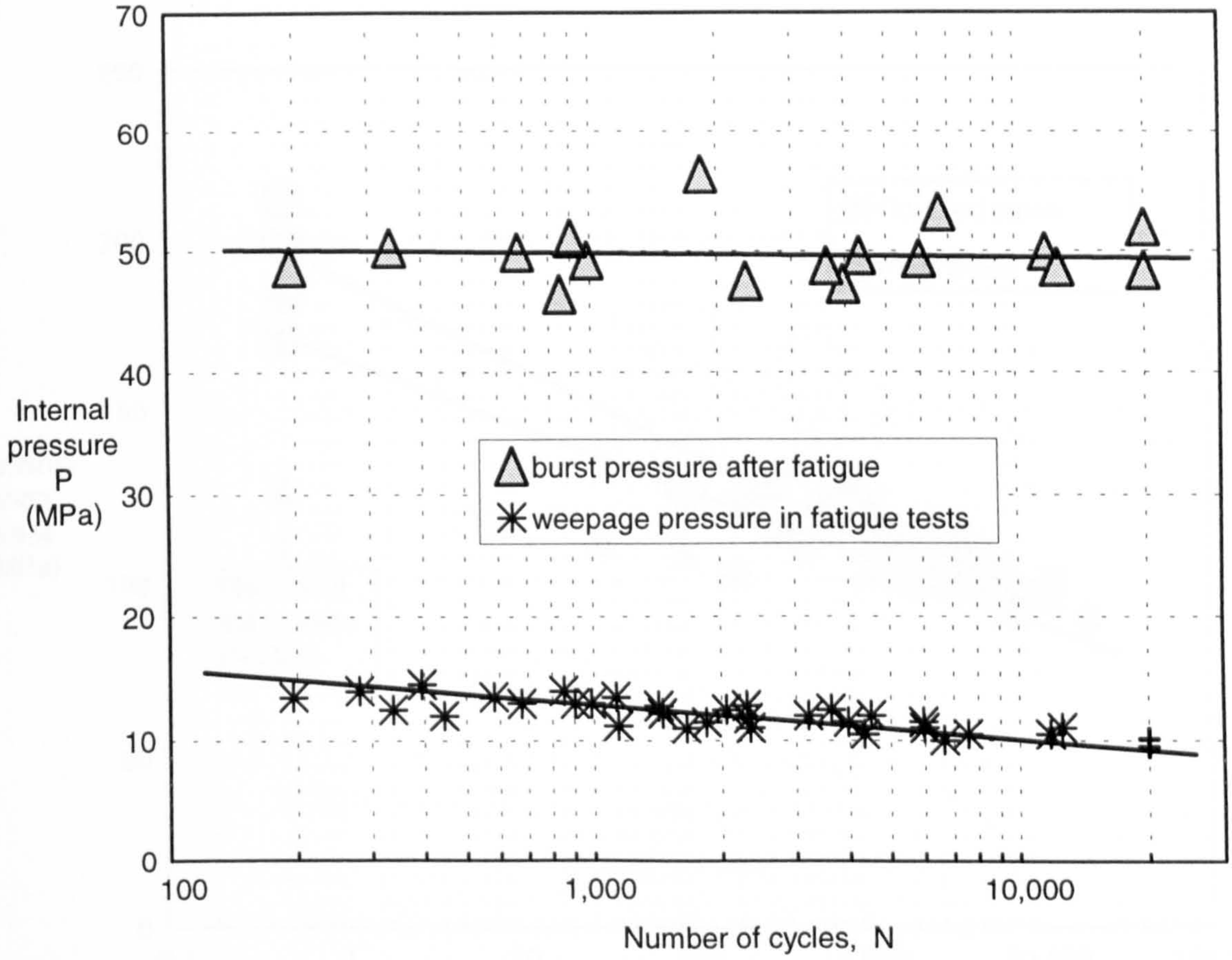

Figure 5.12 P - N diagram for coupled GRE pipes. Specimens were tested by applying a cyclic saw-tooth internal pressure until water weepage or up to 20,000 cycles. Some of the weepage-failed specimens were then installed with rubber liners and subjected to quasi-static pressure until they burst. The points (+) are the results for the pipes in which weepage did not occur after 20,000 cycles.

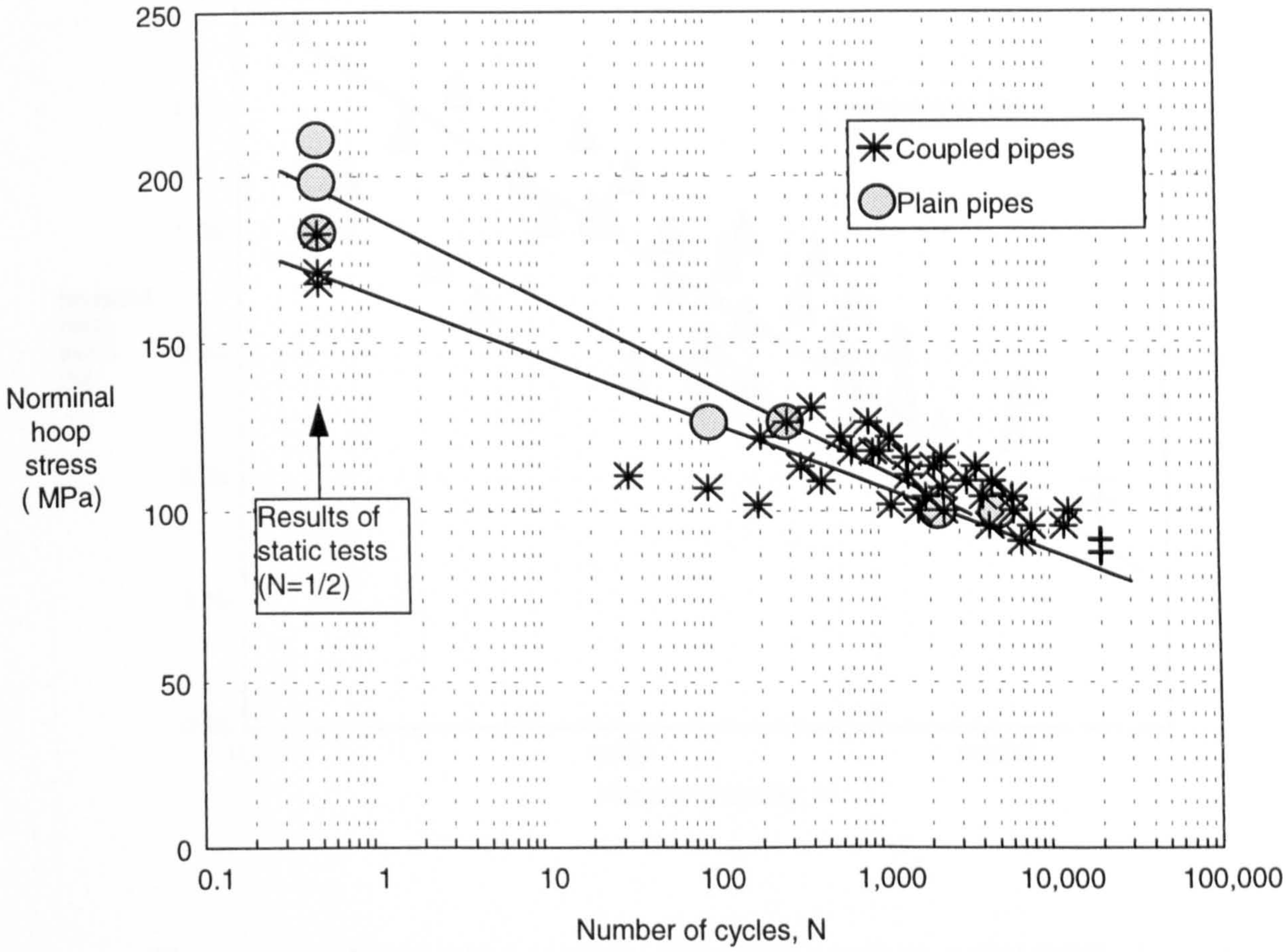

Figure 5.13 Hoop stress - life diagram for plain and coupled GRE pipes. The results of static and fatigue tests on plain pipes are compared with those for the coupled pipes. Fatigue life is plotted against nominal hoop stress in the pipe wall. Stress concentration in coupled pipes does not affect fatigue strength so severely as it affects static strength. The points (+) are the results for the pipes in which weepage did not occur after 20,000 cycles.

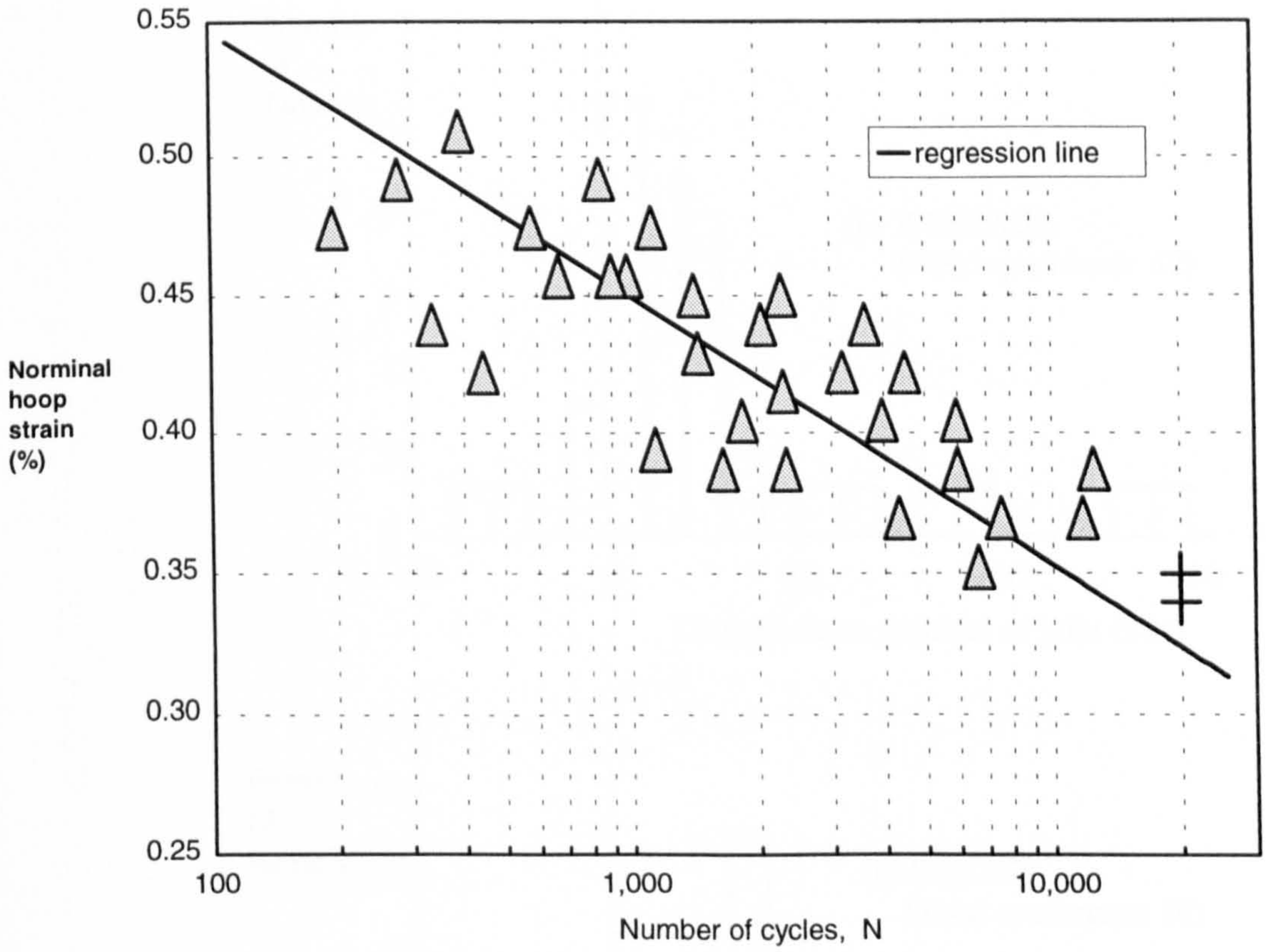

Figure 5.14 Nominal hoop strain - life diagram for coupled GRE pipes. Lower confidence limit with two-sided 5% level of significance was 0.294 at 20,000 cycles. The points (+) are the results for the pipes in which weepage did not occur after 20,000 cycles.

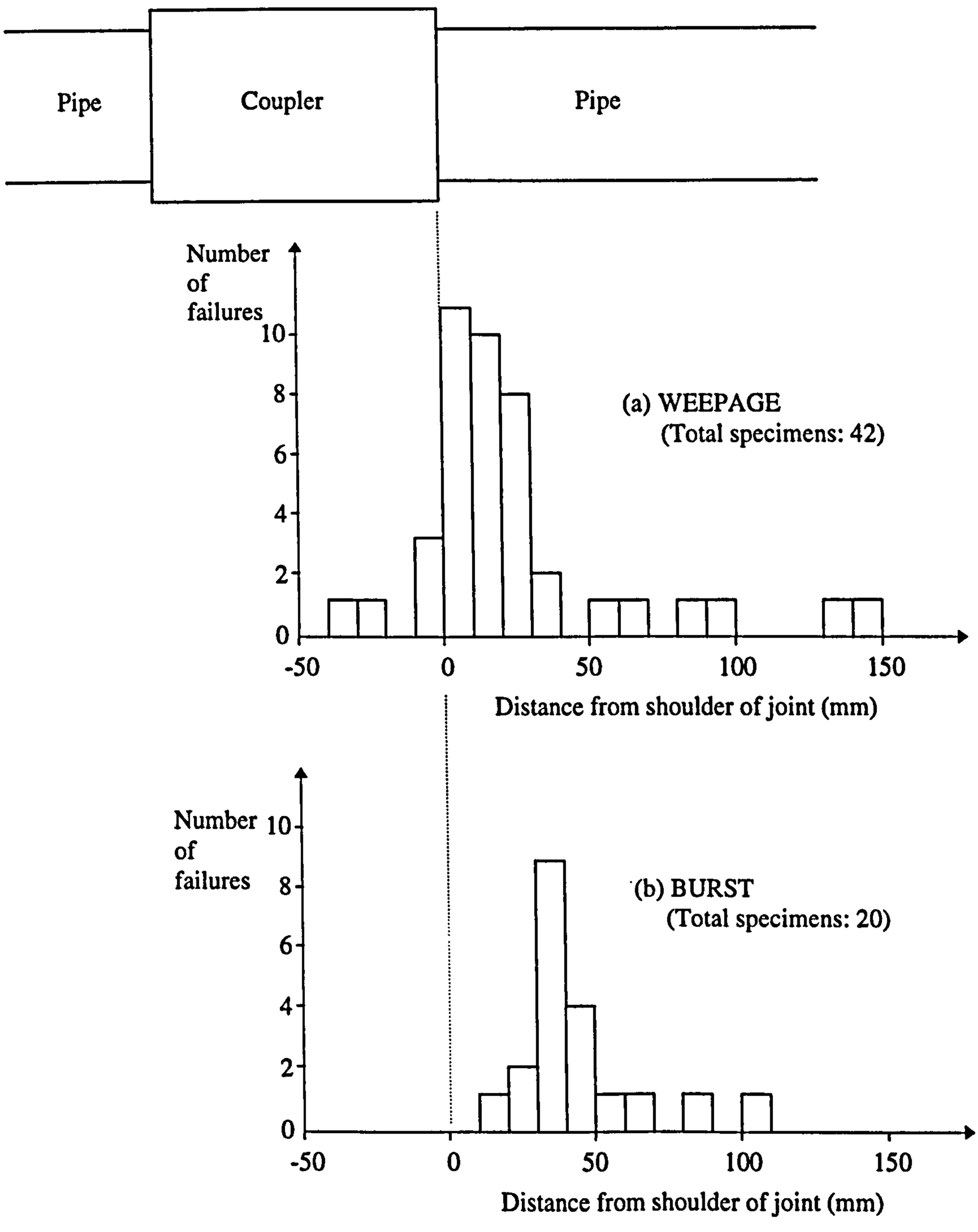

Figure 5.15 Distribution of the failure locations along the axial direction. Both the weepage points of the fatigue tests and the burst locations after fatigue tests were predominantly in the region near the coupler ends.

Figure 5.16 Examples of the failed specimens. During burst tests, pipe failure was characterised initially by whitening of the pipe wall, followed by peeling of the outer plies, and finally by a burst in the area near to the joint.

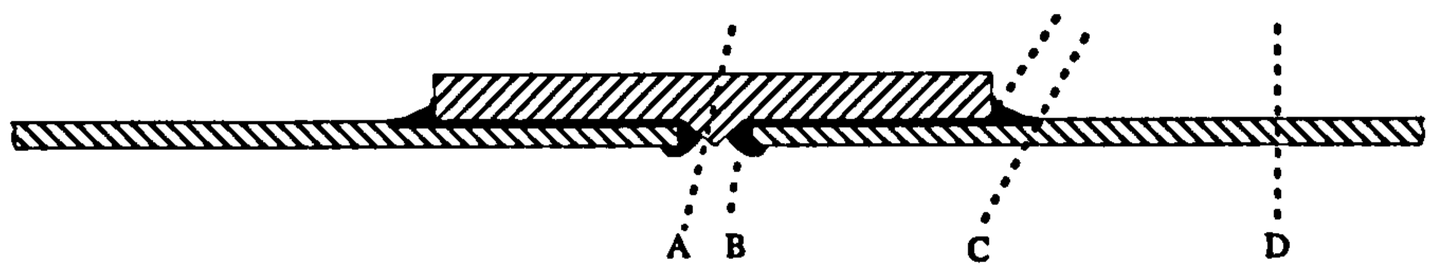

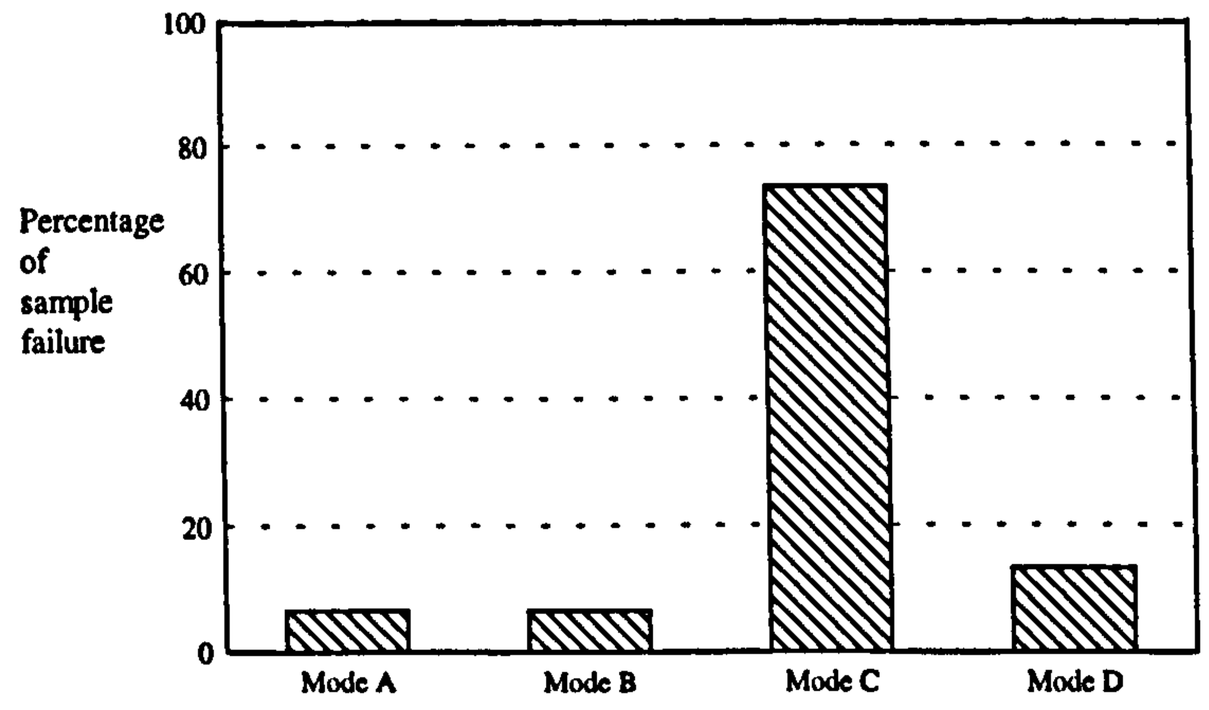

Mode A: Coupler wall,
Mode B: Bonded interface,
Mode C: Pipe wall near coupler,
Mode D: Pipe wall far from coupler.

Figure 5.17 Basic weepage modes and the frequency of pipe failure in each mode.

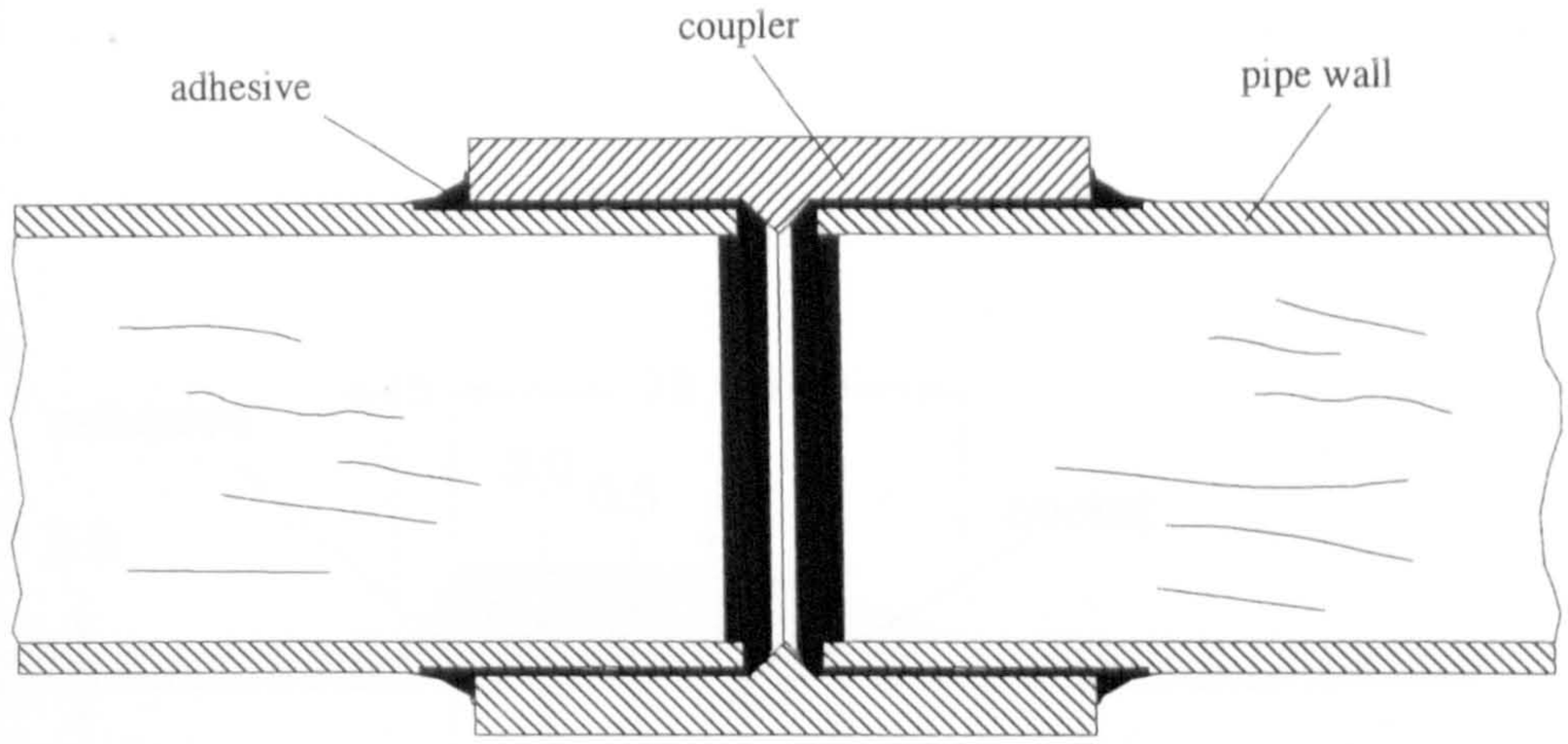

Figure 5.18 Illustration of a coupler bonded joint showing cracks initiated in the resin-rich liner of the pipes close to the joint. Hoop stresses induced the liner to crack in the axial direction.

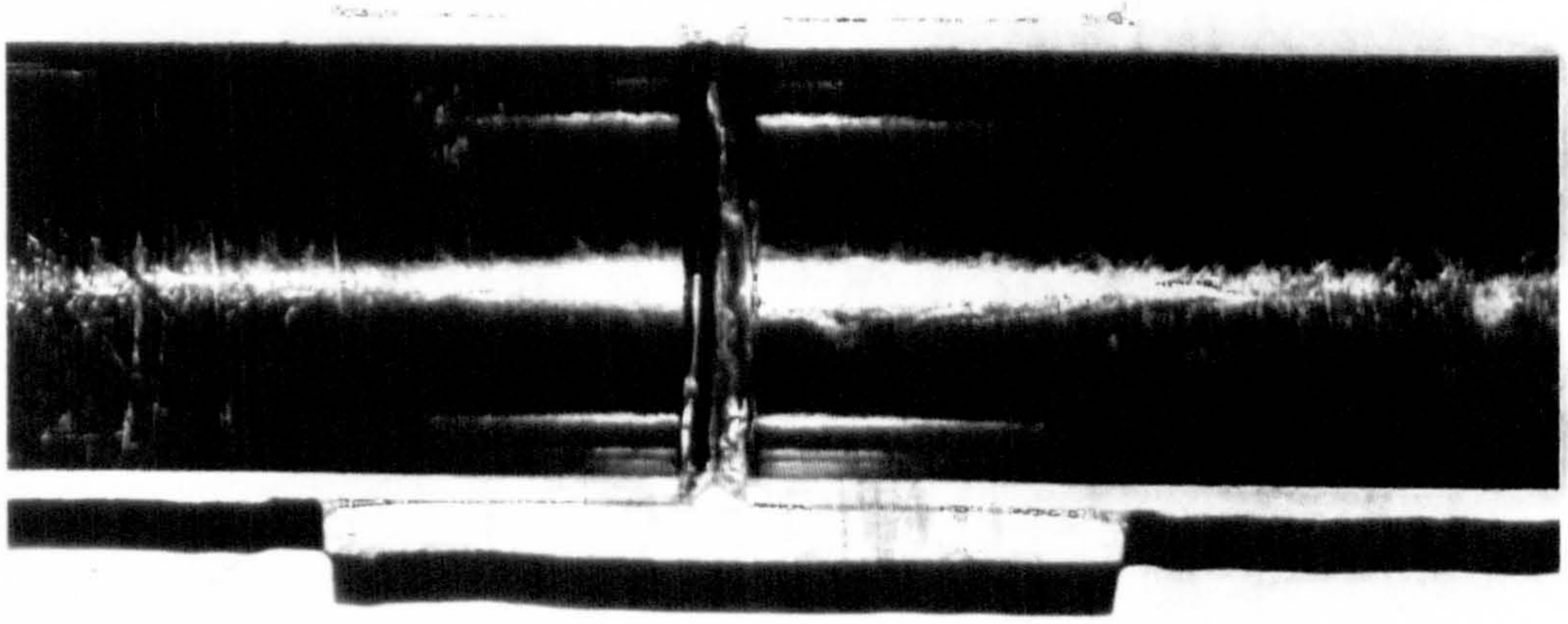

Figure 5.19 A typical example of weepage failure. Liner cracks are located in the area close to the joint and propagating in the axial direction.

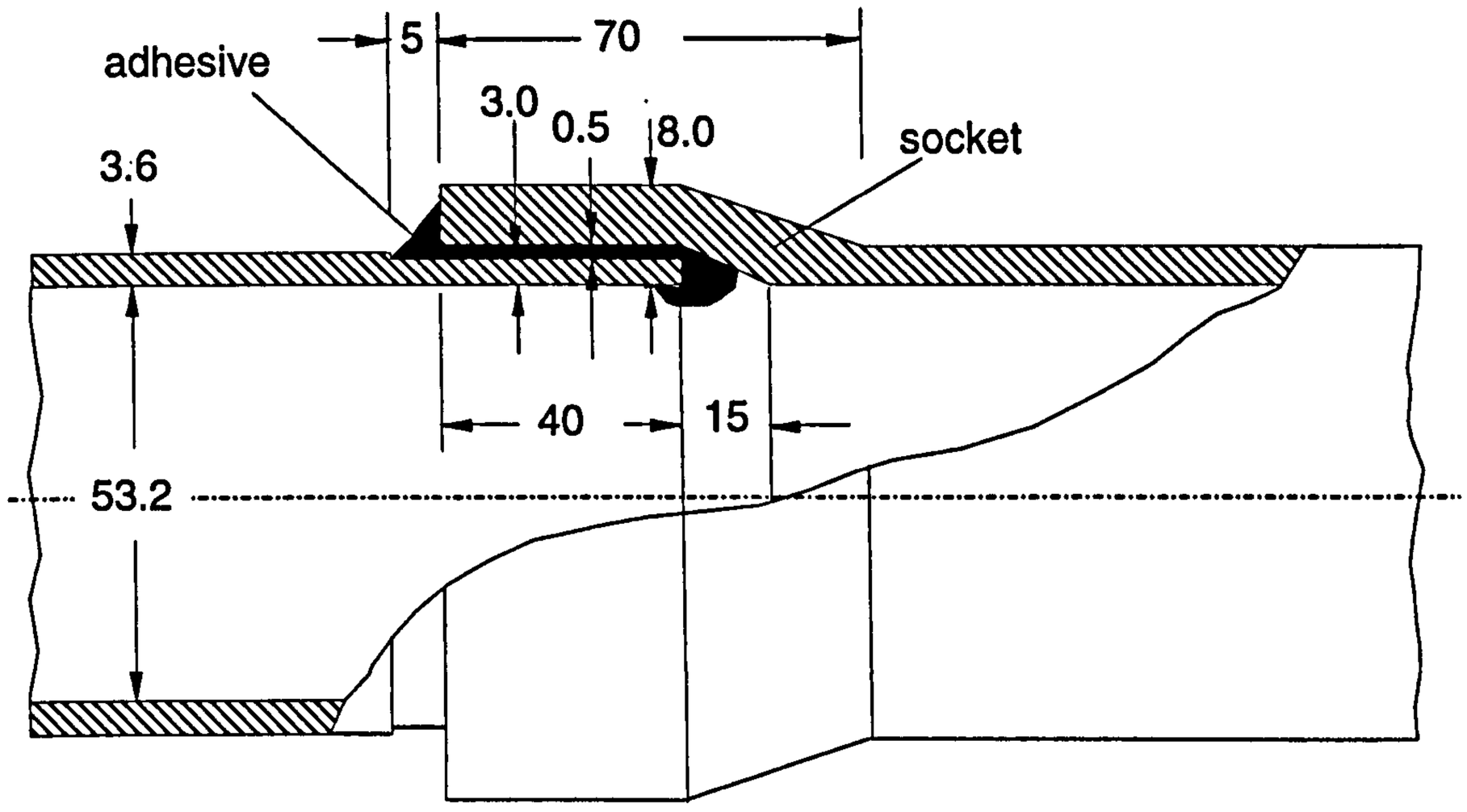

Figure 5.20 Illustration of a GRE socket and spigot connected joint (Units for dimensions: mm). A thickness of 0.6 mm (the top-coat and the outer ply) of the spigot were machined off before being bonded with the socket by adhesive. The machined length was 45 mm, 5 mm longer than the bonding length.

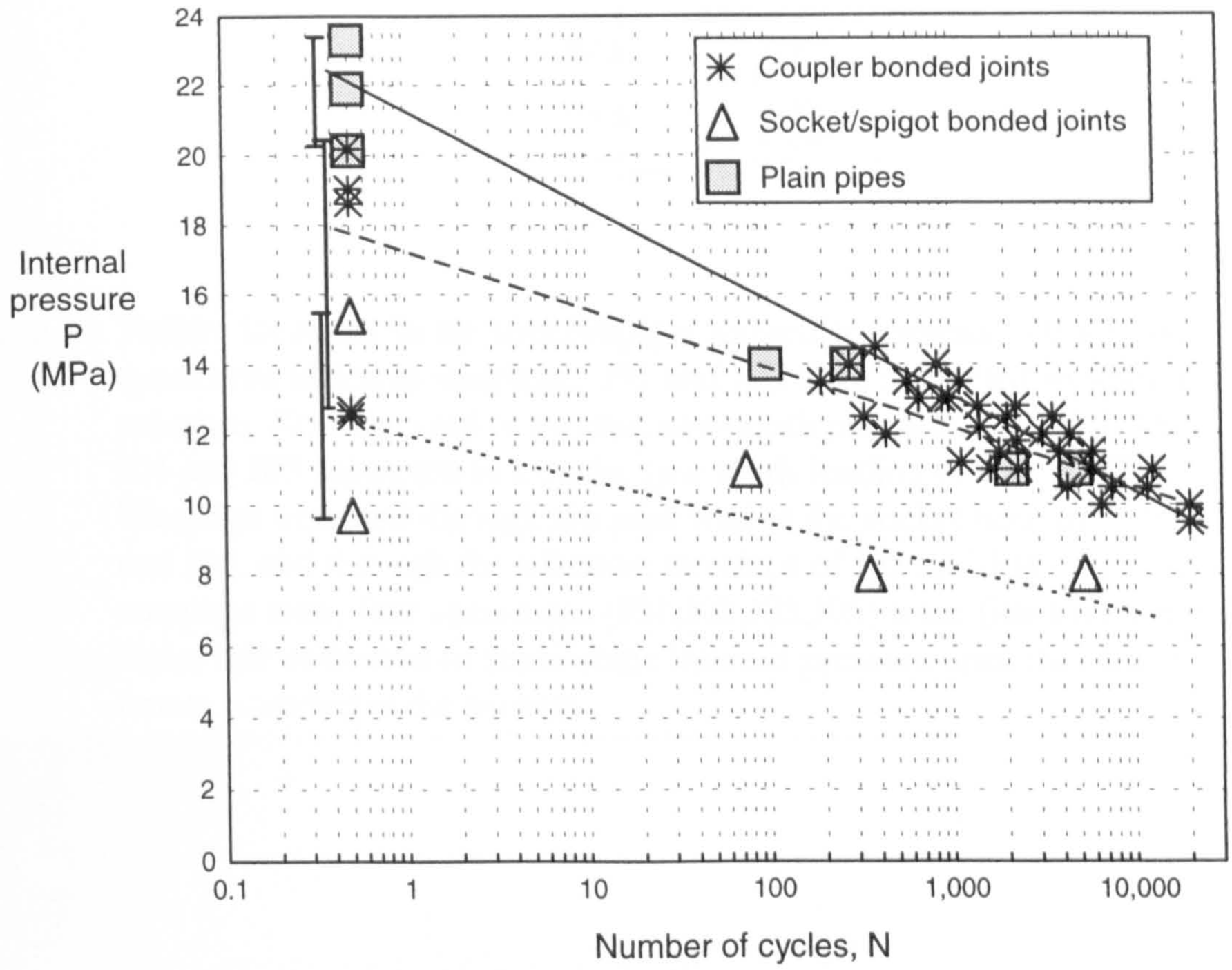

Figure 5.21 P - N diagram for filament wound GRE pipe specimens, including plain, coupler jointed and socket/spigot jointed pipes. Plain pipes had almost the same fatigue weepage pressures as the coupler-connected pipes. The weepage pressures for the socket/spigot connected pipes were apparently lower than those for the plain and coupled pipes.

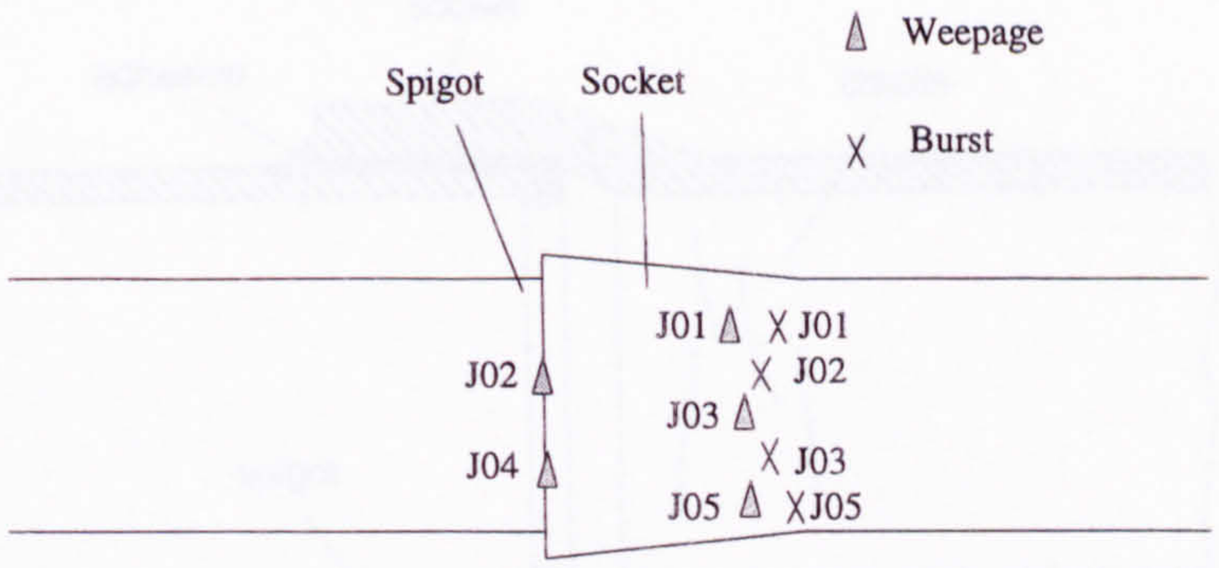

Figure 5.22 Failure locations in the socket/spigot jointed specimens. Of the five specimens tested to weepage, J01 and J02 were subjected to static internal pressure, J03 subjected to a cyclic saw-tooth pressure of 0~11.0 MPa, and J04 and J05 subjected to a cyclic saw-tooth loading of 0~8.0 MPa. Weepage occurred through the pipe wall at the socket bottom of J01, J03 and J05, and through the adhesive interface of J02 and J04. After the weepage tests, four specimens (J01,J02,J03,J05) were fitted with rubber liners and subjected to quasi-static internal pressure until they burst. All bursts occurred at the sockets.

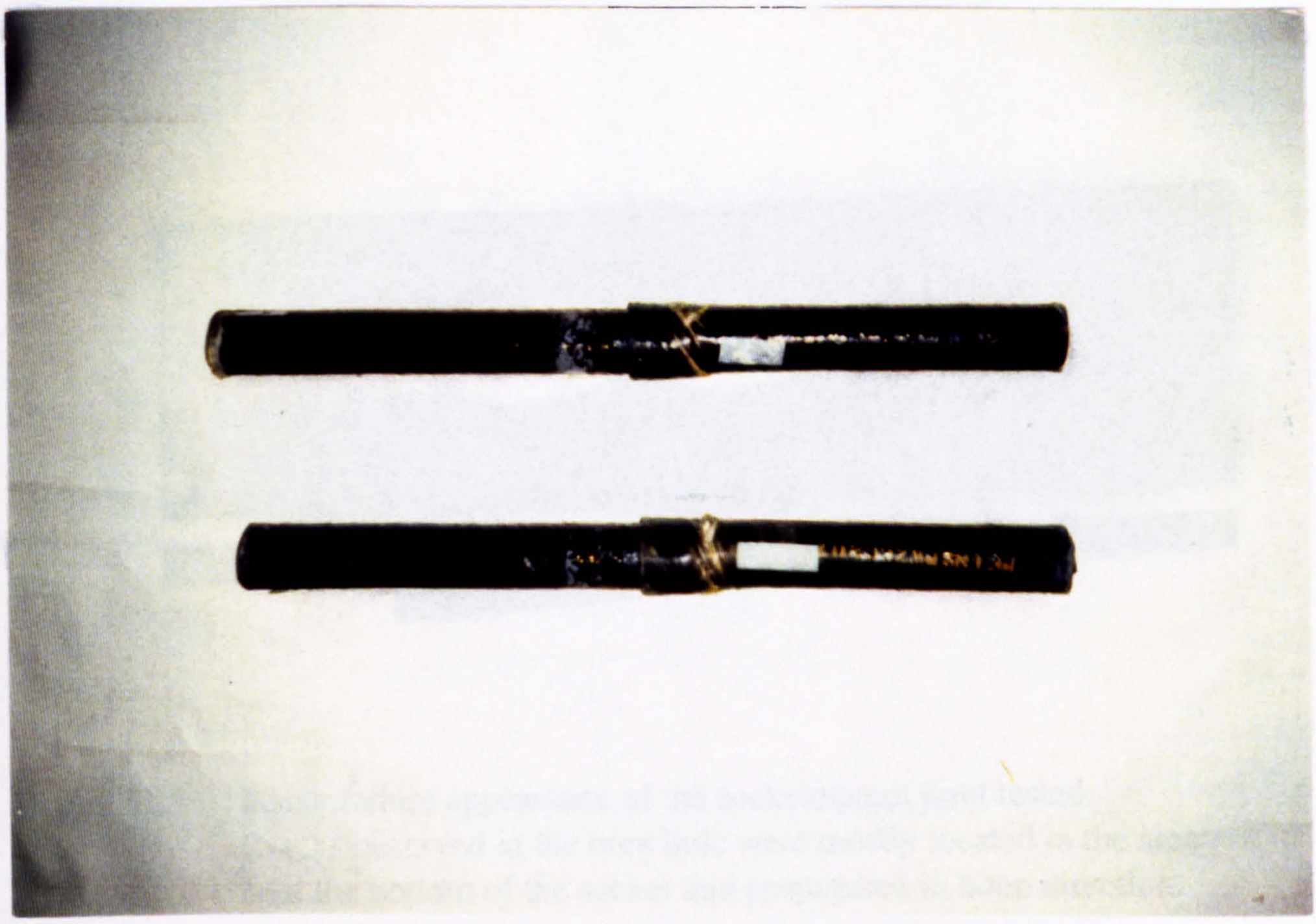

Figure 5.23 External failure appearance of the socket/spigot joints tested. Both modes of matrix cracking and fibre breakage were observed in the pipe wall.

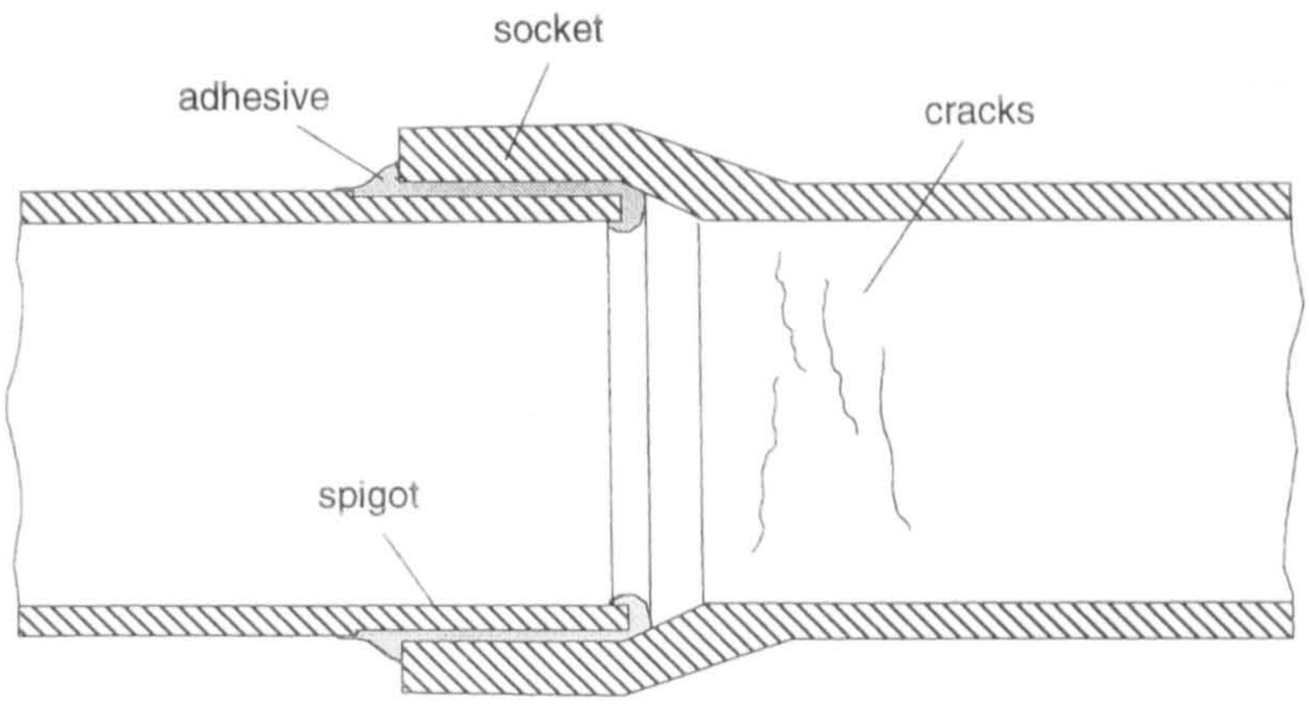

Figure 5.24 Cracks in resin-rich liner of a socket/spigot joint after weepage tests. These were located in the zone near the bottom of the socket and propagated in the hoop direction. They were probably induced by the high axial strain caused by local bending.

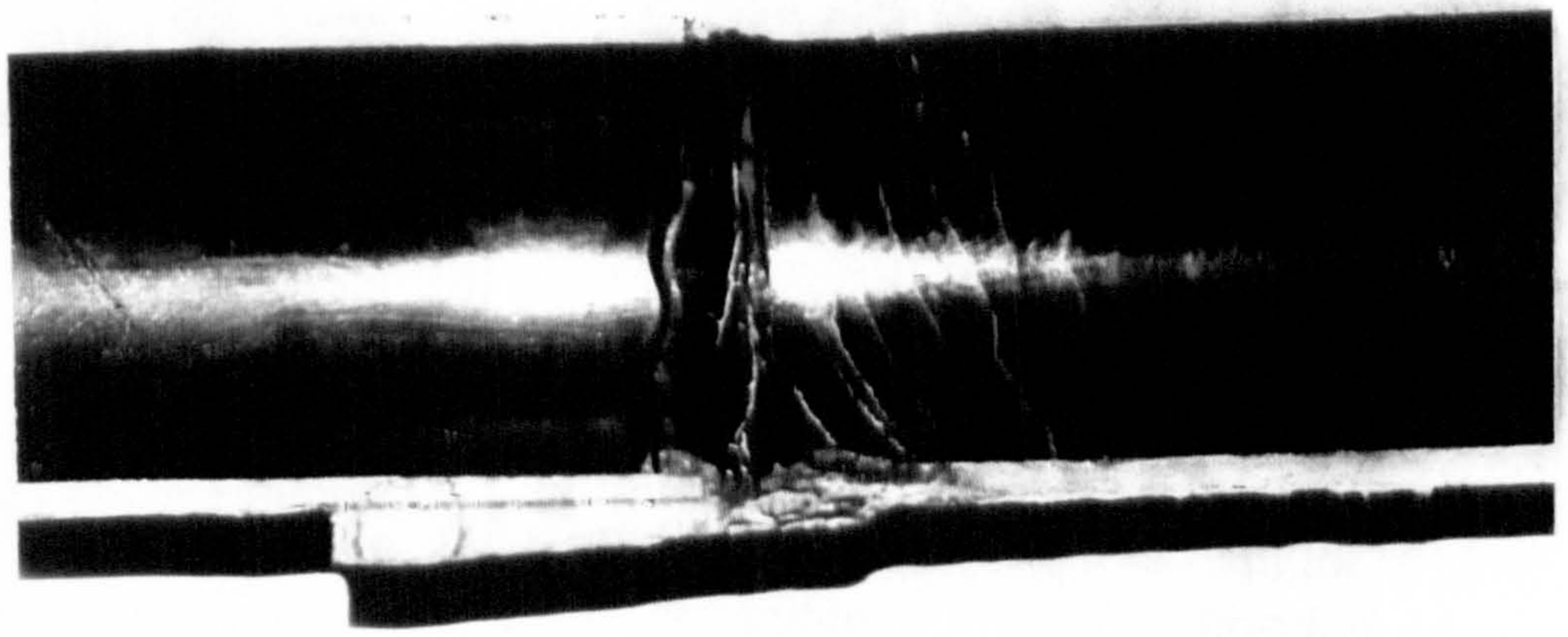

Figure 5.25 Inside failure appearance of the socket/spigot joint tested. Cracks observed in the bore hole were mostly located in the area near the bottom of the socket and propagated in hoop direction.

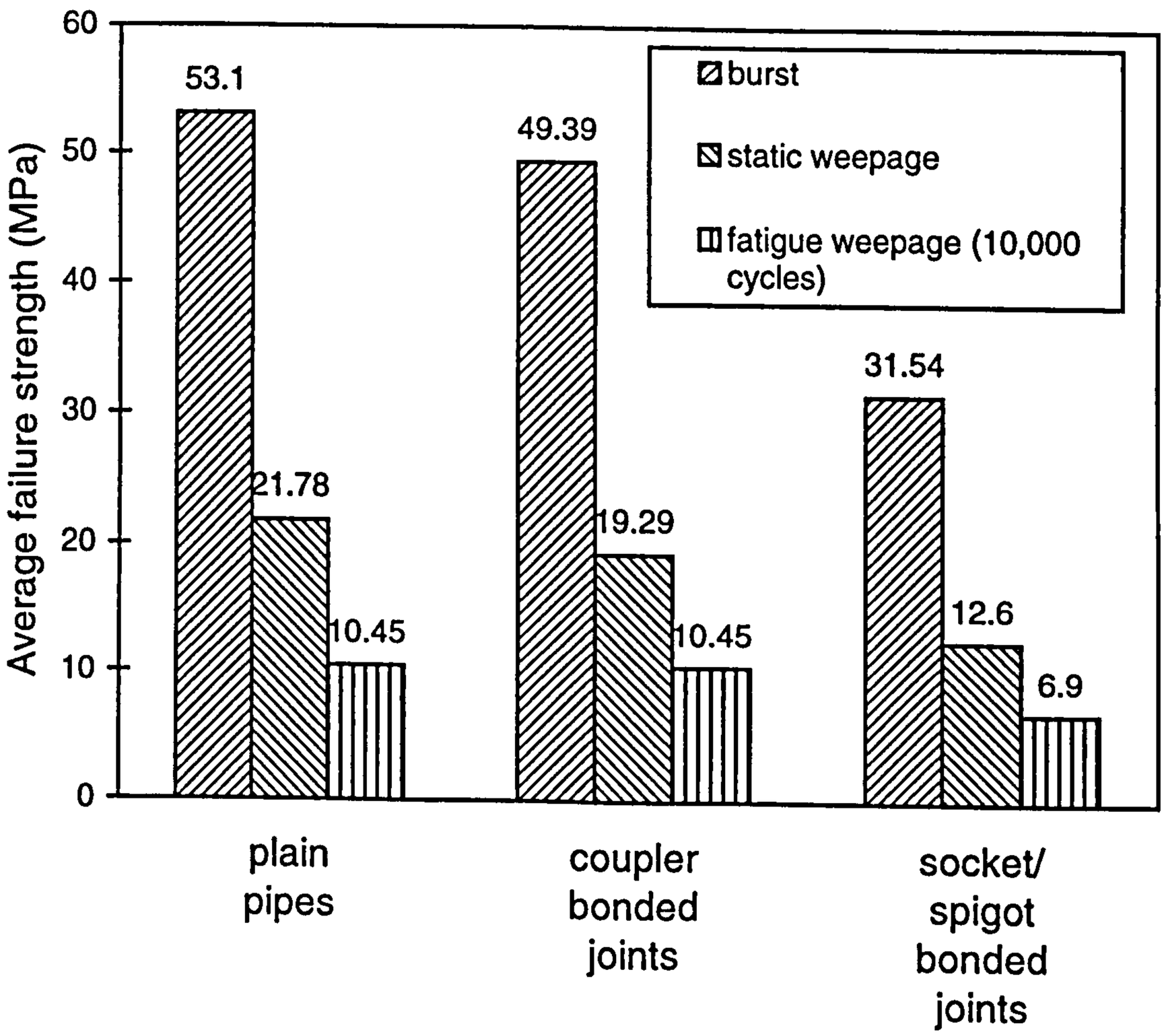

Figure 5.26 Comparison of average weepage and burst pressures for different types of specimens.

CHAPTER SIX

TESTS ON GLASS REINFORCED VINYL ESTER PIPES AND JOINTS

6.1 INTRODUCTION

Filament wound GRP pipe products based on vinyl ester resin are also being considered for use in offshore fire system because of their lower cost and comparable properties [1-3]. However, limited performance data are available to date for this type of pipes. The purpose of the study reported in this Chapter is to compare the properties of filament wound glass-fibre reinforced vinyl ester (GRVE) pipes and joints with those of glass reinforced epoxy (GRE) products discussed in Chapter 5, and to evaluate the potential for the utilisation of GRVE pipes in the offshore industry.

This Chapter describes the experimental investigation into the static and fatigue strengths of GRVE pipes subjected to internal hydraulic pressure. Tests were performed on three types of pipe specimens:

plain pipes,
central laminated joints,
central socket/spigot adhesively bonded joints,

as shown in Table 6.1. The specimens were all 50 mm nominal diameter, 20 bar nominal internal pressure pipes, manufactured by Sarplast (Italy). The results showed that the plain pipes tested can withstand a static hydraulic pressure of up to 20 MPa, whilst the joints failed at a load level of about half the pipe strength.

6.2 PLAIN PIPES

Specimens

A total of six plain pipe specimens were tested. These were all filament wound fibreglass reinforced vinyl ester resin pipes, having a nominal diameter of 50 mm, a nominal pressure of 20 bar. Table 6.2 gives the measured dimensions and the fibre contents for each specimen. Each specimen was 1 metre long and had a 690 mm gauge length after installing the end-caps. The gauge length was more than 10 times the pipe diameter. There were some small variations in the wall thicknesses of the pipes. The average pipe wall thickness was 3.6 mm, including a 1.5 mm resin-rich liner, 2.0 mm filament wound structural wall and 0.1 mm top coat. The structural wall was composed of 4 plies and wound at winding angle $\pm 55^{\circ}$. The fibre volume fraction in structural wall was 54.3±0.3%. Figure 6.1 shows a specimen which has been installed with end-caps and ready to be tested.

Experimental

Of the six plain pipes, two were used for static tests and four for fatigue tests. The specimens were numbered from VP01 to VP06. The test details are presented in Table 6.3. Specimens VP01 and VP02 were statically tested under quasi-static internal pressure. Specimens VP03 and VP04 were tested under a cyclic saw-tooth pressure of 0 - 10 MPa and VP05 and VP06 under a cyclic saw-tooth pressure of 0 - 11 MPa. After weepage tests, burst tests were carried out on three pipes, VP01-03. The experimental set-up was the same as in GRE pipe tests described in Chapter 4.

Results

Table 6.4 presents the results for the plain pipe tests. In all these tests, failures occurred in the gauge length and thus the results were valid. VP01 and VP02 gave static weepage pressures of 20.76 MPa and 20.97 MPa, having a average of 20.87 MPa. VP03 and VP04, being tested under cyclic pressure of 10 MPa, about 48% of the static strength, gave fatigue lives of 4,885 and 4082 cycles. VP05 and VP06 under cyclic pressure of 11 MPa, about 53% of the static

strength, gave fatigue lives of 2,362 and 2,068 cycles. These results showed that the strengths of the GRVE pipes were significantly reduced under fatigue loading. Burst tests on specimens VP01, VP02 and VP03 gave burst pressure from 24.75 to 27.39 MPa. The burst strength of VP03 was similar to these of VP01 and VP02, although they experienced different weepage loading. It appears that the damage developed during weepage had little effect on the burst strength. Comparing the weepage and burst pressures in Table 6.4, the burst pressures were just slightly higher than the weepage strengths, while the GRE pipes showed large differences between weepage and burst pressures (Table 5.3).

Figure 6.2 shows the cracks in a microscope photograph of the cross section of the pipe wall. During weepage tests, the failure modes of the GRVE plain pipes were fibre/matrix interface debonding, matrix cracking and delamination, which caused water to seep through the pipe wall.

6.3 LAMINATE-JOINTED PIPES

Specimens

Three central laminated joint specimens were tested, being numbered as VL01, VL02 and VL03. Figure 6.4 shows the three specimens ready to be tested, the ends of which were reinforced with GRE fabric laminates and bonded to aluminium collars (see Section 4.2). They were samples of commercial products with 50 mm nominal diameter and 20 bar nominal pressure, manufactured by Grouppo Sarplast. Each specimen was composed of two 500 mm long filament wound Glass-Reinforced Vinyl Ester (GRVE) pipes joined by CSM glass/vinyl ester lamination. The pipes were described in previous section.

Figure 6.3 shows the geometry and dimensions of the joint. The ends of the two pipes were tapered to an angle of 2°55'. Both pipes were correctly aligned to the pipe axis, before chopped strand mat was laid over the gap and liquid vinyl ester resin was worked into the fibres using brush and rollers. The laminated joint had an outer diameter of 65.2 mm. The ends of the laminate strap had a 22° taper angle.

Table 6.5 gives the measured dimensions and the fibre volume fractions of the specimens. In each case the internal diameter was exactly 50 mm. The wall thickness and external diameter varied slightly, although the difference was less than 0.6%. After the installation of end grips, the one metre long specimens were reduced to gauge lengths of 690 mm. The winding angle was ±54.3°. The fibre volume fractions in the structural wall of the GRVE pipe and in the CSM GRVE laminated strap were 54.3±0.3% and 17.6±0.5% respectively.

Experimental

Table 6.6 describes the details of the tests. Two specimens (VL01 and VL02) were tested to weepage by applying with quasi-static internal pressure. VL03 was tested under a cyclic pressure of 0 - 10 MPa. The frequency of the fatigue loading was 10 cycles per minute. After the weepage tests, burst tests were conducted on specimens VL01 and VL02 by applying

quasi-static internal pressure. The experimental set-up was the same as described in Sections 4.1.6 and 4.2.3.

Results

Table 6.7 presents the test results for the GRVE laminate-jointed pipes. Specimens VL01 and VL02 had an average static weepage pressure of 14.76 MPa and an average burst pressure of 23.30 MPa. The later was 1.58 times higher than the former.

All three specimens failed at the laminated joints. During the weepage testing, water seeped through the CSM laminate because of resin cracking and delamination in the laminated strap. Figure 6.5 shows the visible delamination crack of specimen VL03 after the fatigue failure. During the burst tests, failure also occurred at joints where fibres were broken in the CSM laminated strap. Figure 6.6 shows specimen VL01 after its burst test where it can be seen that a piece of the joint material has been blown off. The whitened areas close to the joint in the picture show severe delamination cracks.

6.4 SOCKET/SPIGOT BONDED PIPES

Specimens

Three central socket/spigot jointed pipe specimens were tested. Figure 6.7 shows a socket/spigot bonded specimen, along with a plain pipe and a laminate-jointed pipe. Each socket/spigot specimen comprised two 500 mm long, 50 mm internal diameter filament wound fibreglass reinforced vinyl ester resin pipes with a socket or a spigot. They were connected by adhesive bonding between the socket and the spigot. Figure 6.8 shows the construction and the dimensions of the joint. The nominal pipe wall thickness was 4.8 mm, thicker than those of the GRVE plain pipe and laminate-jointed specimens which were 3.6 mm thick and described in Sections 6.2 and 6.3. The pipe wall had a 1.5 mm resin-rich liner, 3.2 mm GRVE structural wall and 0.1 mm top coat. The structural pipe wall was wound with 6 plies of glass fibres at angles of $\pm 55^{\circ}$. The spigot and the socket were shaved to a taper angle of $6^{\circ}12'$. The spigot, which was 35 mm long, and the socket, which was 45 mm long, were bonded together by adhesive paste. The average thickness of the adhesive was 0.5 mm.

Table 6.8 gives the measured dimensions and fibre volume fractions of the three specimens which were marked with numbers VB01, VB02 and VB03. The inner diameters were exactly 50 mm but the outer diameters and wall thicknesses varied slightly. After the installation of the end grips, the one metre long specimens were reduced to a 690 mm gauge length. The fibre volume fraction in the structural wall was $55.1 \pm 0.3\%$.

Experimental

Table 6.9 shows the details of the tests. Two specimens (VB01 and VB02) were tested statically to weepage by applying quasi-static internal pressure. VB03 was tested under a cyclic saw-tooth pressure of 0 - 10 MPa. The frequency of the fatigue loading was 10 cycles per minute. After the weepage tests, burst tests were performed on VB01 and VB02 by installng rubber liners and applying quasi-static pressure. The experimental set-up was described in Chapter 4. Since the joint was expected to be weaker than the pipe and pipe ends, no reinforcement was needed at both ends before mounting the end-caps.

Results

Table 6.10 presents the test results for the GRVE socket/spigot jointed specimens VB01, VB02 and VB03. Specimen VB01 and VB02 gave an average static weepage pressure of 11.24 MPa and an average burst pressure of 47.49 MPa. The average burst pressure was four times higher than the average weepage pressure. In the fatigue test, specimen VB03 failed by water weepage after 971 cycles of an internal pressure of 0-10 MPa. All failures occurred at the bonded adhesive interfaces during both weepage and burst tests. Figure 6.9 shows the specimen VB01 which failed during a burst test due to the failure of the adhesive interface.

6.5 DISCUSSION

Weepage Tests

Figure 6.10 shows the results for the three types of GRVE specimen plotted in a pressure versus life diagram, compared with the results for GRE pipes obtained in Chapter 5. It was found that the GRVE plain pipes had a weepage pressure comparable to that of GRE pipes. This indicates that the use of cheaper vinyl ester-based pipes does not involve a very significant lose of pipe strength at large number of cycles. Figure 6.10 also shows that both types of the jointed GRVE pipes had lower weepage pressures than the GRE pipes and the plain GRVE pipes. Since all pipes (GRE and GRVE pipes) had the same wall thickness (3.6 mm) and the same nominal diameter (50 mm), except the GRVE socket/spigot jointed pipes which had a thicker pipe wall (4.8 mm), the nominal hoop stress - life diagram would be very similar to Figure 6.10.

Figure 6.11 shows the average static weepage pressures for the three types of GRVE specimen. Plain pipes had the highest weepage pressure. The socket/spigot bonded pipes gave the lowest average static weepage pressure of 11.24 MPa, approximately 54% of that of the plain pipes, even though the average pipe wall thickness of the former was 4.8 mm, 33% thicker than the latter. It is therefore apparent that in this case the joints are the weakest parts of the pipe. In order to make full use of the pipe strength, stronger joints would be desirable. Nevertheless, all specimens tested gave a static weepage pressure of more than five times the nominal pressure (20 bar) of this product series, which was probably acceptable.

Figure 6.12 shows the fatigue lives for the three specimen types when subjected to cyclic saw-tooth internal pressure of 0 - 10 MPa. It shows a similar relationship to that seen in Figure 6.11, the plain GRVE pipes having a longer fatigue life than the GRVE joints.

Since only four plain pipes, one laminated joint and one socket/spigot bonded joint were tested under cyclic pressure, the fatigue lives presented here might be of limited accuracy. The purpose of these tests on GRVE pipes was to examine and compare their static and fatigue strengths with those of similar GRE products. To build a complete P-N curve, more specimens would be needed.

Weepage Failure Modes

All of the GRVE specimens tested under static or cyclic internal pressure failed by weepage. With plain pipes, weepage occurred uniformly over the whole gauge length. As the applied pressure increased, the pipe wall first started to crack (indicated by acoustic emission), then delaminated (causing pipe wall whitening to be observed) and finally water seeped out. For the pipes jointed by CSM/vinyl ester laminate, weepage occurred through the laminated strap where delamination was observed during tests, as shown in Figure 6.5. Therefore, stronger joints (or longer and thicker laminated straps) may be desirable.

In the case of the central socket/spigot bonded joints, water sprayed out through the adhesively bonded interface between the socket and the spigot when the pressure reached its maximum value. The failure was presumably caused by the failure of bonded adhesive interface. No damage was observed on the thick-walled sockets, spigots and pipe wall. This indicates that a stronger bonded interface may be desirable.

Burst Tests

Figure 6.13 shows the average burst strengths for the three specimen types. The aim of the burst tests was to determine the full strength of the pipe wall laminate. Since the results in Chapter 5 showed that the pressure history experienced by pipes during weepage tests had almost no effect on the burst strength, the average burst pressures are calculated based on all the specimens tested. From Figure 6.13, the plain GRVE pipes had slightly higher burst pressures than those of the CSM laminate-jointed pipes. However, in contrast to the weepage tests, the socket/spigot jointed pipes had the highest burst strength, probably because of their thick pipe wall. These results indicated that the socket/spigot jointed pipes had the maximum potential strength.

Figure 6.14 shows examples of the burst specimens of the three types of GRVE specimens. The plain pipes burst at the gauge length of the pipe wall and the two jointed pipes failed at joints. The socket/spigot joint failed by the failure of adhesively bonded interface and the laminated joints by the failure of CSM/vinyl ester laminated strap.

The failures of the plain pipes in the pipe wall at reasonable distances from the ends showed that the end grips and the reinforcement did not induce significant stress concentrations. The joint failures in both of the jointed pipes indicate that they did not achieve their maximum strength and could be improved to obtain higher strength. The improvement can be: using a larger bonding area or a stronger adhesive material, and tapering the edge of the socket and spigot for socket/spigot joints; using a thicker and longer external laminate for the laminated joints. Finite element analysis was carried out to optimise the design of the joints which will be described in Chapter 7.

Comparison with GRE Pipes

Figure 6.15 compares the structures of the pipe wall of the GRVE plain pipes described in this Chapter and of the GRE pipes described in Chapter 5. Both had the same gross wall thickness of 3.6 mm, 0.1mm top coat and winding angle of $\pm 55^0$ in the structural wall. Although they were based on different matrix material systems and had different numbers of reinforced plies and different resin liner thicknesses, they all had similar weepage strengths (Figure 6.10).

Figure 6.16 compares the average static weepage and burst pressures of GRE and GRVE pipes. Since weepage was caused by fibre debonding and matrix cracking, weepage pressure mainly depended on the matrix and liner material. Thus, despite the different reinforcement thickness, both types of pipes had similar weepage pressures. The weepage pressure of the GRE pipes was slightly higher than that of the GRVE pipes. This might be because the former used stronger matrix material epoxy.

Different from the weepage pressures, the average burst pressure of GRE pipes was two times more than that of the GRVE pipes. Since the failure mode of pipe burst was fibre breakage, the burst strength was mainly dependant on the fibre reinforcement. GRE pipe had six reinforced layers, thicker than GRVE pipe, thus had higher burst pressure.

6.6 CONCLUSIONS

All three types of glass reinforced vinyl ester pipe specimens tested had a high static weepage strength, more than five times the nominal pressure (20 bar) of the products. In comparison with more expensive epoxy pipes, the vinyl ester pipes showed comparable static and fatigue weepage strength.

Both types of GRVE pipe joints showed lower weepage pressures than plain pipes and weepage failure occurred at joints. In order to make full use of the pipe strength, stronger joints may be desirable. These two types of joints may need to be modified. With the laminated joint, the modifications can be: increasing the length and the thickness of the CSM laminated strap. With the socket/spigot bonded joints, increasing the bonding length and reducing the taper angle of the socket and the spigot will increase the jointing strength.

The thick-walled socket/spigot bonded joint had the lowest weepage strength but gave the highest burst pressure than the other two types of specimens. This indicates that the socket/spigot joints had a high potential weepage strength which can be utilised by employing stronger joints.

REFERENCES

[1] Boothby,P.J., Glass Reinforced Plastics for Offshore Topside Seawater Pipework - The Current Position, ERS Report 4613, March 1991.

[2] Gibson,A.G., Composites in the Offshore Structures, pp.199-226, Composites materials in Marine Structures, Volume 2: Practical Considerations, Edited by Shenoi,R.A. and Wellicime,J.F., Cambridge University Press, 1993.

[3] Cheremisinoff,N.P. and Cheremisinoff,P,N., Fiberglass-Reinforced Plastics Deskbook, Chapter 3: FRP Pipe Products and Applications, Ann Arbor Science Publishers Inc., 1983.

Table 6.1 Nominal dimensions of the three types of GRVE pipe specimens tested.

Specimen type	Plain pipe 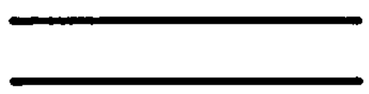	Central laminated joint 	Central socket/spigot bonded joint 
Number of specimen	6	3	3
Nominal diameter (mm)	50	50	50
Length (mm)	1000	1000	1000
Total pipe wall thickness (mm) ■ Resin liner ■ Reinforcement thickness ■ Top coat	3.6 1.5 2.0 0.1	3.6 1.5 2.0 0.1	4.8 1.5 3.2 0.1
Dimensions of joint (mm)	-	Strap length: 100.0 Strap thickness: 4.0	Socket end length: 45.0 Spigot end length: 35.0

Table 6.2 Measured dimensions of the GRVE plain pipes.

Pipe identifier	Outer diameter (mm)	Inner diameter (mm)	Total wall thickness (mm)	Inner resin-liner thickness (mm)	Gauge length (mm)	Total Length (mm)	Volume fraction (%) (Fibre reinforced layers)
VP01	57.19	50	3.595	1.5	690	1000	54.3±0.3
VP02	57.23	50	3.615	1.5	690	1000	54.3±0.3
VP03	57.20	50	3.600	1.5	690	1000	54.3±0.3
VP04	57.33	50	3.665	1.5	690	1000	54.3±0.3
VP05	57.17	50	3.535	1.5	690	1000	54.3±0.3
VP06	57.22	50	3.610	1.5	690	1000	54.3±0.3

Table 6.3 Test details for the GRVE plain pipes.

Pipe identifier	Type of tests	Type of loading	Frequency (cycles/min)	Cyclic pressure range (MPa)
VP01	static weepage & static burst	quasi-static internal pressure	-	-
VP02	static weepage & static burst	quasi-static internal pressure	-	-
VP03	fatigue weepage & static burst	saw-tooth cyclic internal pressure	10	0-10
VP04	fatigue weepage	saw-tooth cyclic internal pressure	10	0-10
VP05	fatigue weepage	saw-tooth cyclic internal pressure	9	0-11
VP06	fatigue weepage	saw-tooth cyclic internal pressure	9	0-11

Table 6.4 Results of the GRVE plain pipe tests.

Pipe identifier	Type of test	Weepage pressure (MPa)	Weepage cycles	Burst pressure (MPa)	Failure location
VP01	(a)static weepage (b)static burst	20.76 -	- -	- 24.75	gauge length gauge length
VP02	(a)static weepage (b)static burst	20.97 -	- -	- 27.39	gauge length gauge length
VP03	(a)fatigue weepage (b)static burst	- -	4,885 -	- 24.80	gauge length gauge length
VP04	fatigue weepage	-	4,082	-	gauge length
VP05	fatigue weepage	-	2,362	-	gauge length
VP06	fatigue weepage	-	2,068	-	gauge length
Average		20.87		25.65	

Table 6.5 Measured dimensions of the GRVE laminated joints.

Specimen identifier	Pipe outer diameter (mm)	Pipe inner diameter (mm)	Total pipe wall thickness (mm)	Pipe resin-liner thickness (mm)	Fibre volume fraction (%) (structural pipe wall)
VL01	57.23	50	3.615	1.5	54.3±0.3
VL02	57.19	50	3.595	1.5	54.3±0.3
VL03	57.20	50	3.600	1.5	54.3±0.3
Pipe identifier	Outer diameter of joint (mm)	Fibre volume fraction (%) (CSM laminated strap)	Total specimen length (mm)	Specimen gauge length (mm)	
VL01	65.51	17.6±0.5	1000	690	
VL02	65.30	17.6±0.5	1000	690	
VL03	65.23	17.6±0.5	1000	690	

Table 6.6 Test details for the GRVE laminated joints.

Pipe identifier	Type of test	Type of loading	Frequency (cycles/min)	Cyclic pressure range (MPa)
VL01	static weepage & static burst	static internal pressure	-	-
VL02	static weepage & static burst	static internal pressure	-	-
VL03	fatigue weepage	saw-tooth cyclic internal pressure	10	0-10

Table 6.7 Results for the GRVE laminated joints.

Pipe identifier	Type of test	Weepage pressure (MPa)	Weepage cycles	Burst pressure (MPa)	Failure location
VL01	static weepage & static burst	16.05	-	24.18	joint
VL02	static weepage & static burst	13.46	-	22.42	joint
VL03	fatigue weepage	-	1,217	-	joint
Average		14.76		23.30	

Table 6.8 Measured dimensions of the GRVE socket/spigot jointed pipes.

Pipe identifier	Outer diameter (mm)	Inner diameter (mm)	Total wall thickness (mm)	Inner resin-liner thickness (mm)	Gauge length (mm)	Total Length (mm)	Fibre volume fraction (%)
VB01	59.59	50	4.795	1.5	690	1000	55.1±0.3
VB02	59.63	50	4.815	1.5	690	1000	55.1±0.3
VB03	59.60	50	4.800	1.5	690	1000	55.1±0.3

Table 6.9 Test details for the GRVE socket/spigot jointed pipes.

Pipe identifier	Type of test	Type of loading	Frequency (cycle/min)	Cyclic pressure range (MPa)
VB01	static weepage & static burst	static internal pressure	-	-
VB02	static weepage & static burst	static internal pressure	-	-
VB03	fatigue weepage	saw-tooth cyclic internal pressure	10	0-10

Table 6.10 Results for the GRVE socket/spigot jointed pipes.

Pipe identifier	Type of tests	Weepage pressure (MPa)	Weepage cycles	Burst pressure (MPa)	Failure location
VB01	static weepage & static burst	11.34	-	46.08	adhesive interface
VB02	static weepage & static burst	11.13	-	48.90	adhesive interface
VB03	fatigue weepage	-	971	-	adhesive interface
Average		11.24		47.49	

Table 6.11 Comparison of the results of the static weepage tests.

Type of specimen	Number of tested specimens	Weepage pressures (MPa)	Weepage positions
Plain pipes	2	20.76 20.97	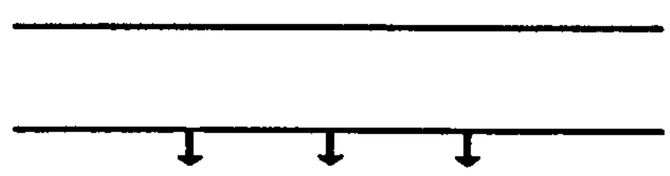 Water seeped through the resin cracks in the pipe wall. Failure occurred at the gauge length.
Central CSM-laminate joints	2	16.05 13.46	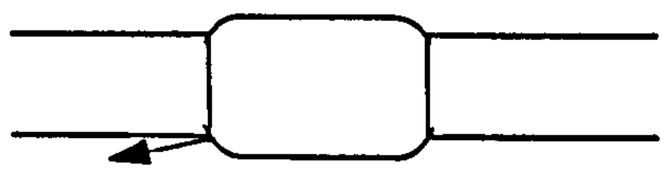 Water seeped through the cracks in the CSM laminated joints.
Central socket/spigot adhesively bonded joints	2	11.34 11.13	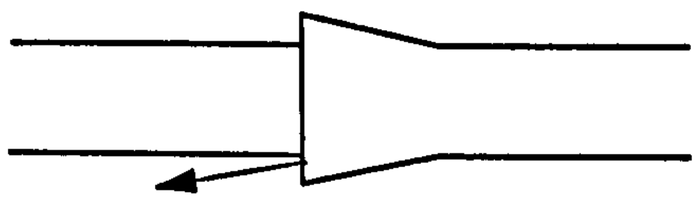 Water seeped through the cracks in the bonded interface.

Table 6.12 Comparison of the fatigue results for GRVE pipes.

Type of specimen	Number of tested specimens	Pressure cycles to weepage		Fatigue failure positions
		under 0-10 (MPa)	under 0-11 (MPa)	
Plain pipes	4	4,082 4,885	2,362 2,068	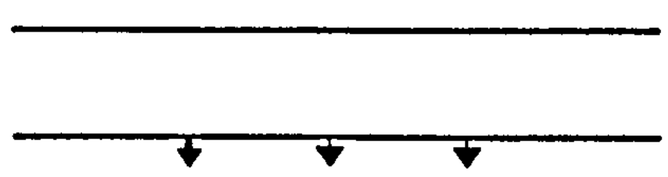 Water seeped through the resin cracks in the pipe wall. Failure occurred at the gauge length.
Central laminate joints	1	1,217	-	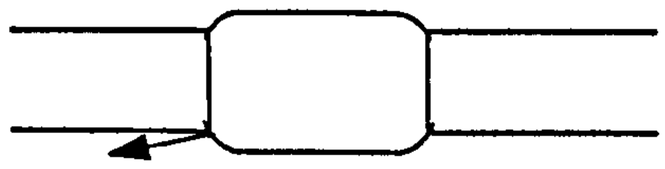 Water seeped through the cracks in the CSM laminated strap.
Central socket/spigot bonded joints	1	971	-	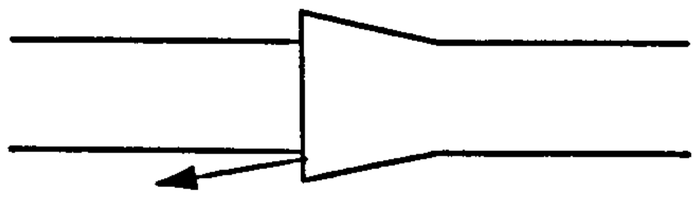 Water seeped through the cracks in the bonded interface.

Table 6.13 Comparison of the results of the static burst tests carried out after weepage tests.

Type of specimen	Number of burst specimens	Burst pressure (MPa)	Burst positions
Plain pipes	3	24.75 24.80 27.39	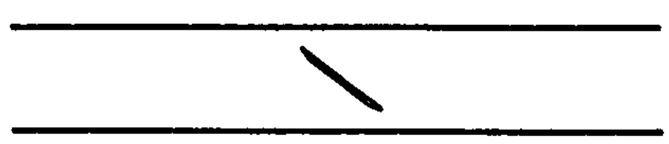 Burst occurred at the gauge length.
Central laminate joints	2	24.18 22.42	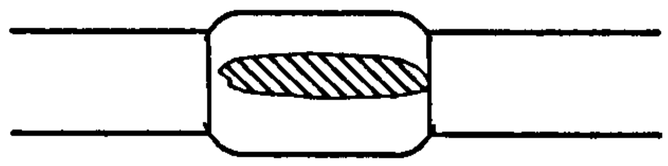 Burst occurred at the CSM laminate joints. At the centre of the joint, some of laminate material flew away.
Central socket/spigot bonded joints	2	46.08 48.90	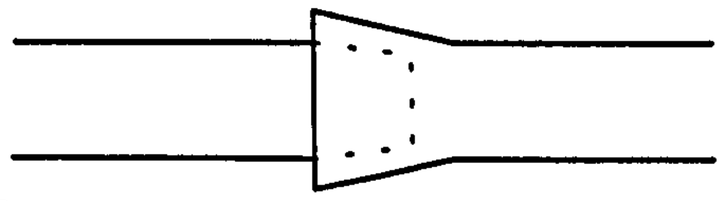 Joints were separated through the bonded interfaces.

Table 6.14 Comparison of the dimensions of the GRE and GRVE specimens.

	Glass reinforced epoxy pipes	Glass reinforced vinyl ester pipes
Nominal diameter (mm)	50.0	50.0
Specimen length (mm)	1000	1000
Total pipe wall thickness (mm)	3.6	3.6
Reinforcement thickness (mm)	3.0 (6 plies)	2.0 (4 plies)
Resin liner thickness (mm)	0.5	1.5
Top coat thickness (mm)	0.1	0.1

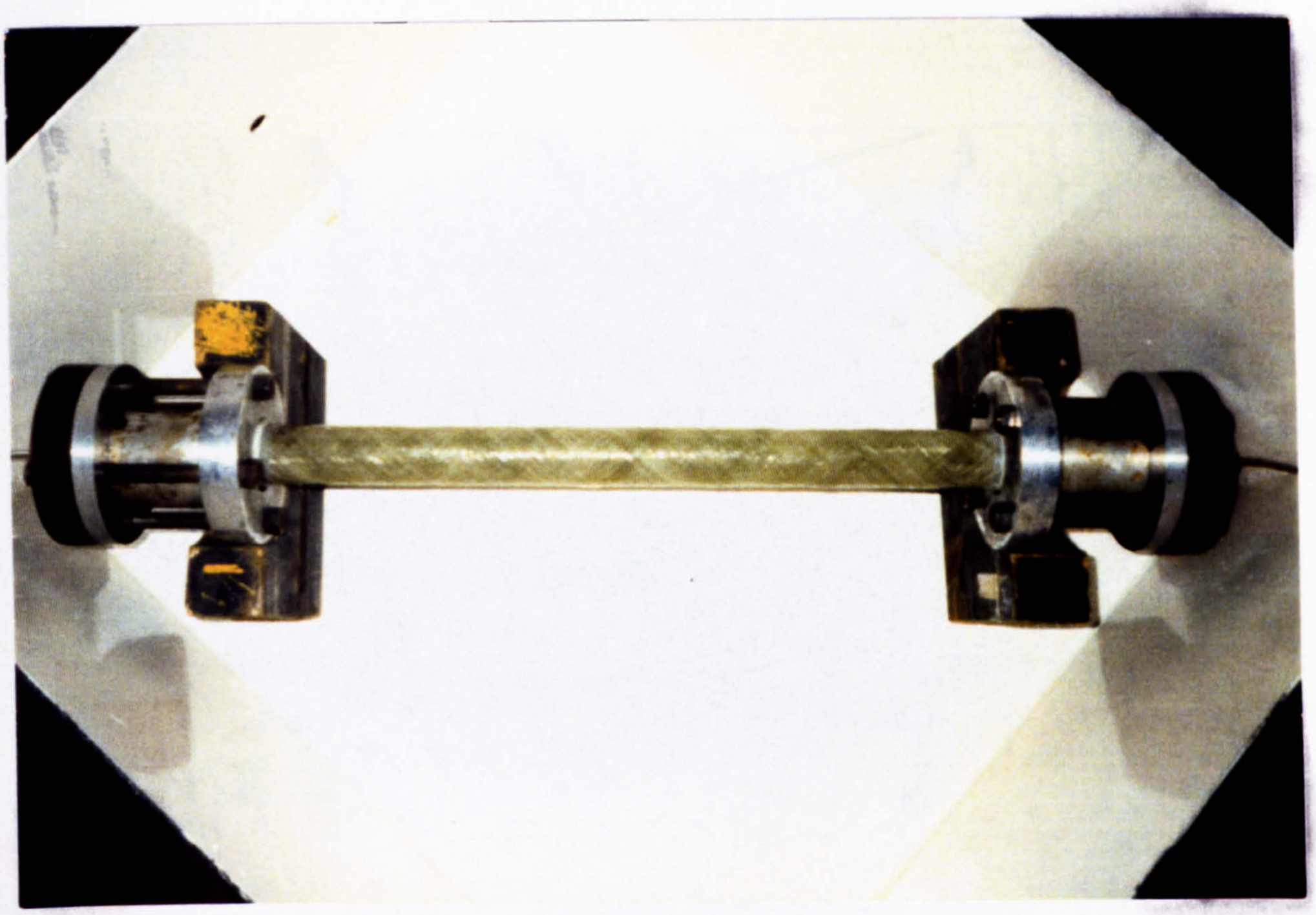

Figure 6.1 Glass-reinforced vinyl ester plain pipe installed with end-caps ready for testing in the safety enclosure.

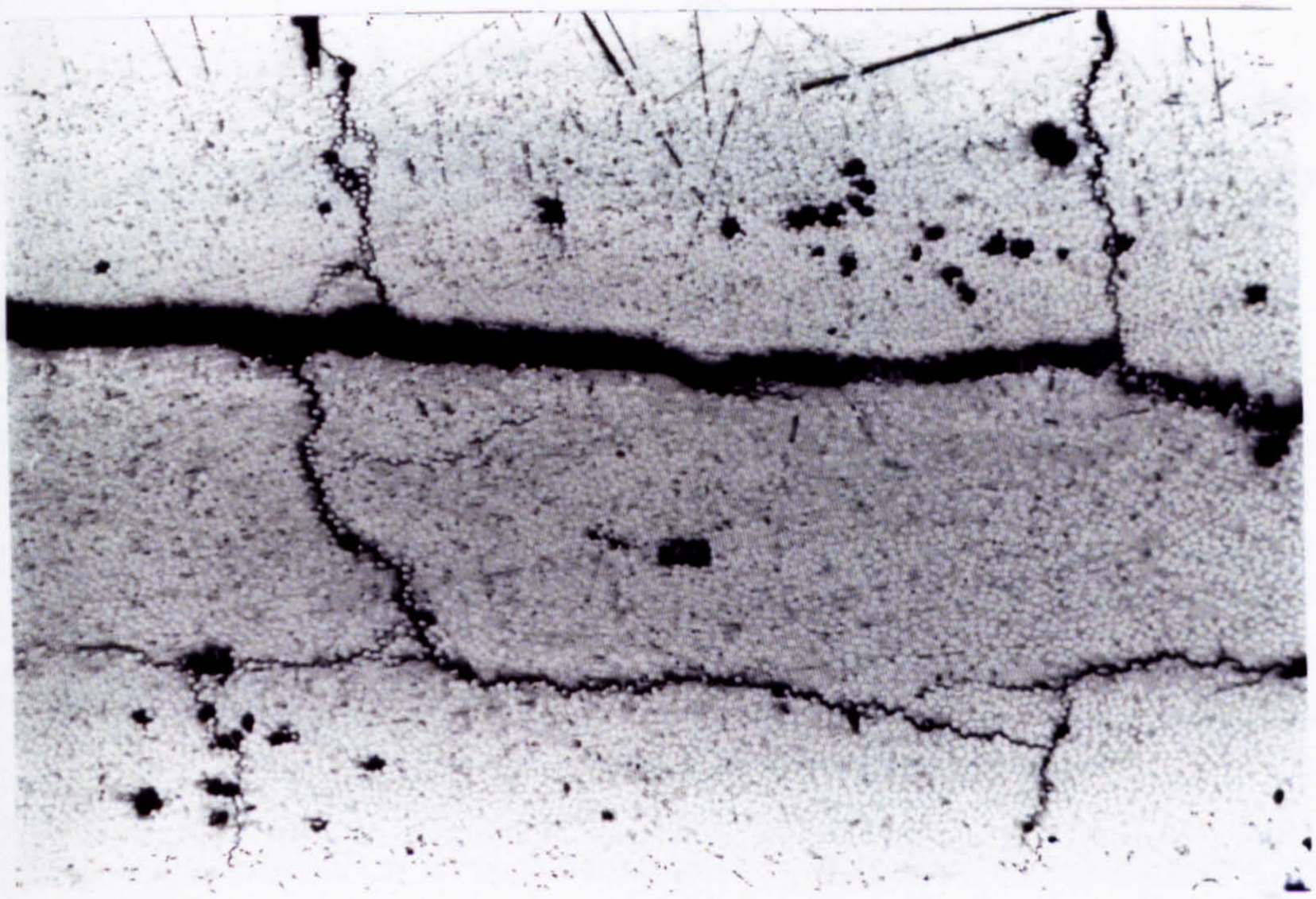

Figure 6.2 Resin cracks in the GRVE pipe wall. The cracks propagated through each ply by fibre/matrix interface debonding and matrix cracking, and were joined by delamination between the plies.

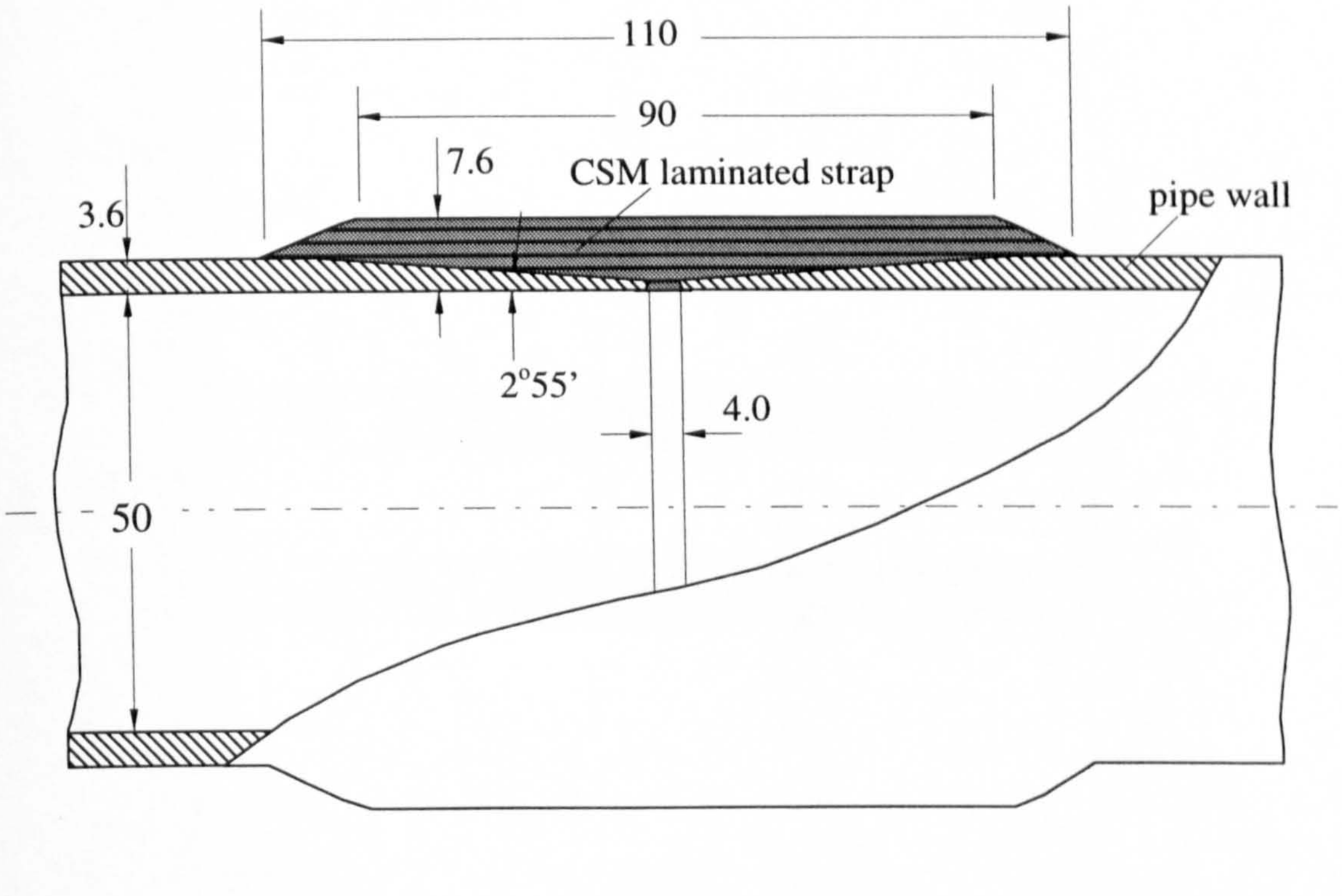

Figure 6.3 Illustration of a glass CSM/vinyl ester laminated joint (Units for dimensions: mm).

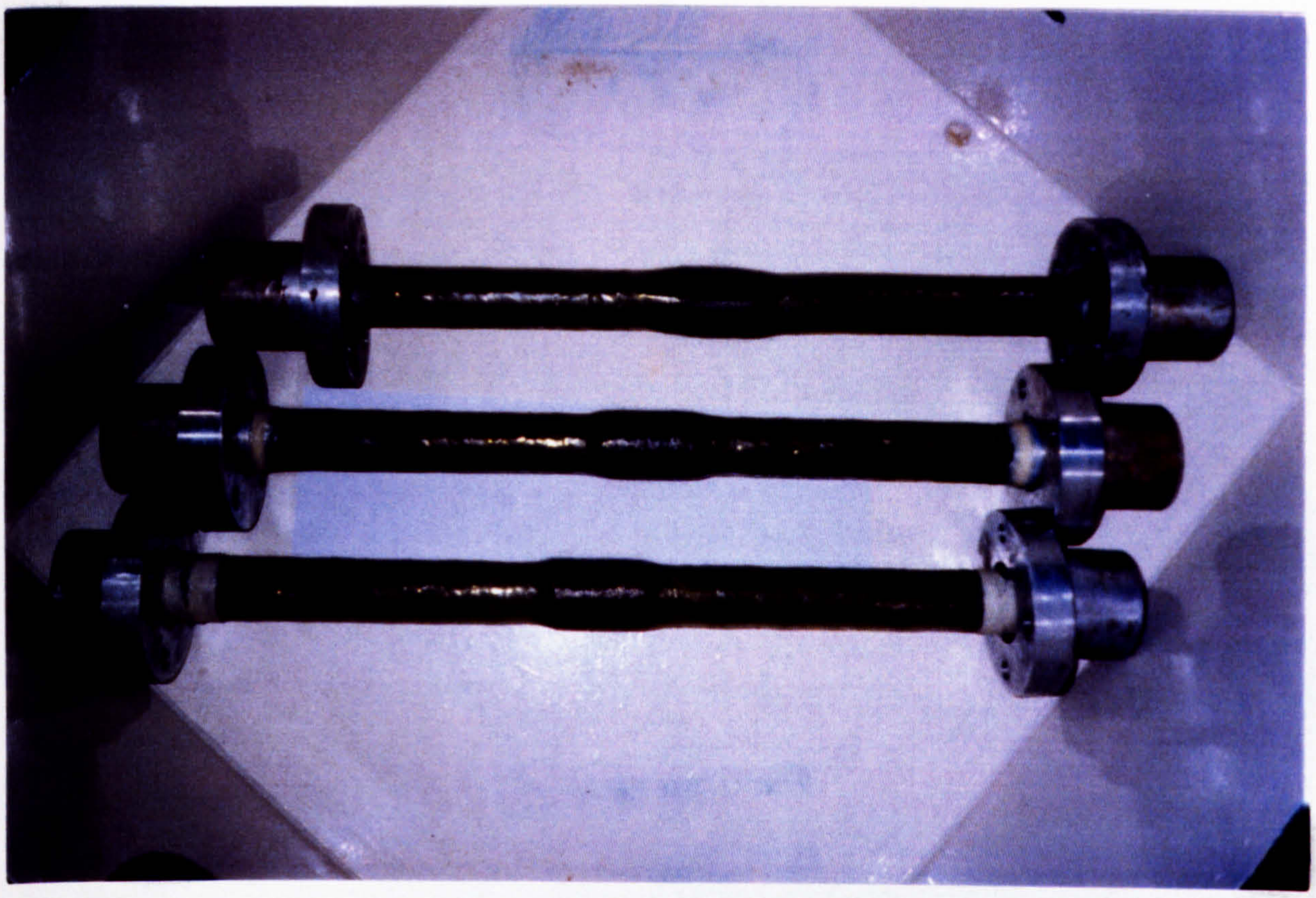

Figure 6.4 Central laminate-jointed 2-inch pipes equipped with end fittings ready to be tested.

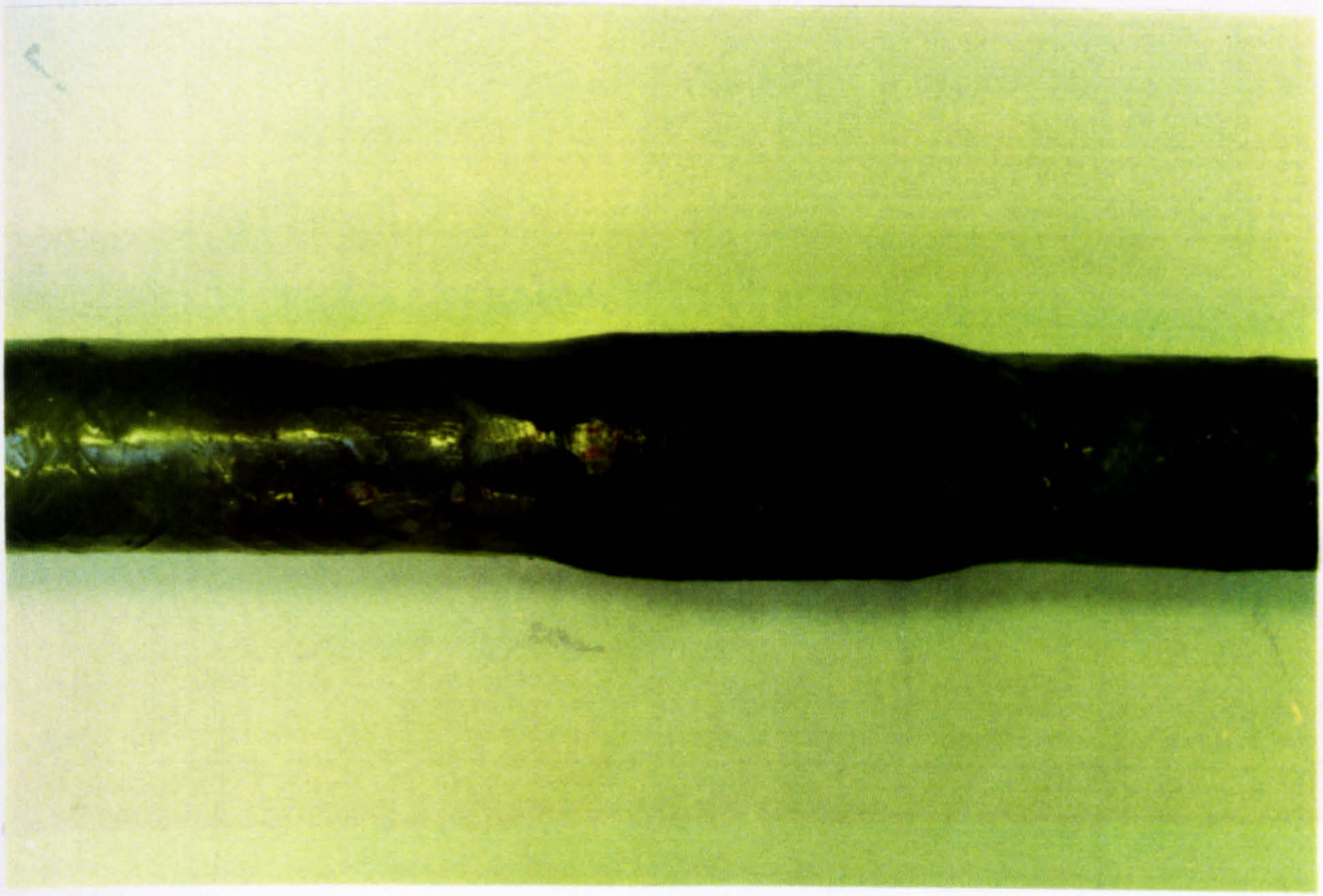

Figure 6.5 Delamination at the laminated joint of specimen VL03 during a fatigue test.

Figure 6.6 Laminate material was burst away during a burst test on specimen VL01.

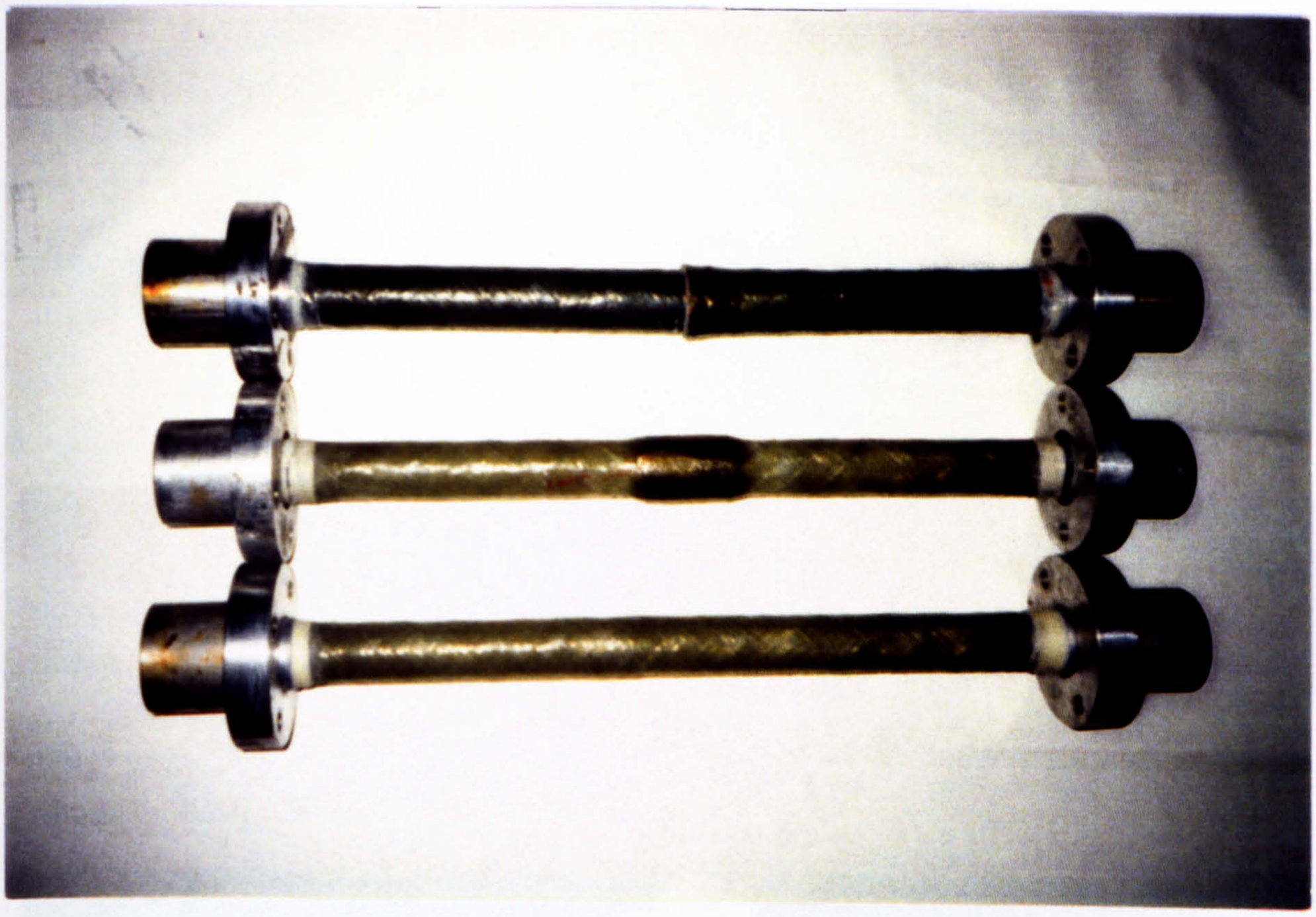

Figure 6.7 The three types of GRVE specimen equipped with end-caps ready for tests.

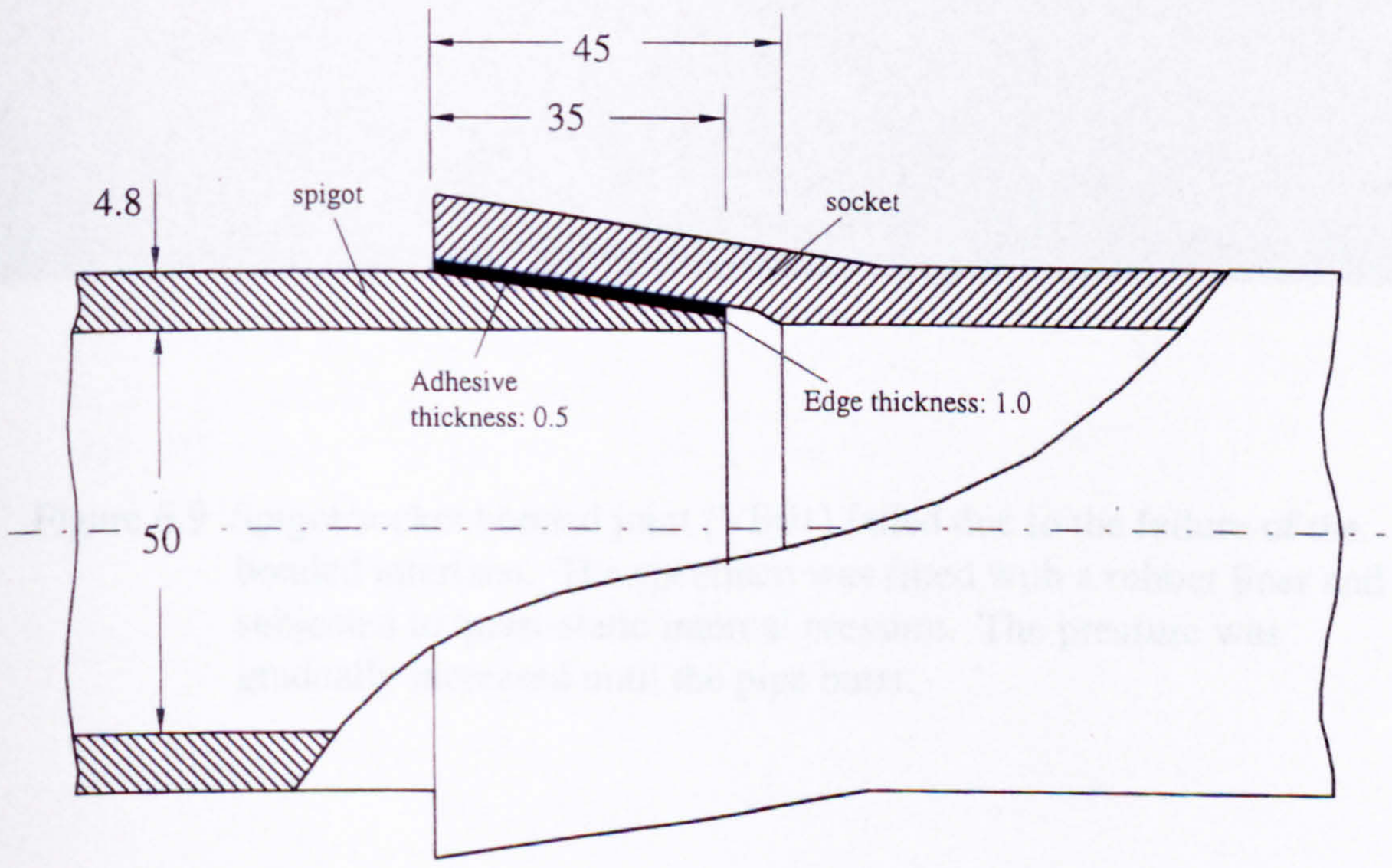

Figure 6.8 Illustration of a central socket/spigot (taper to taper) adhesively bonded joint (Units for dimensions: mm).

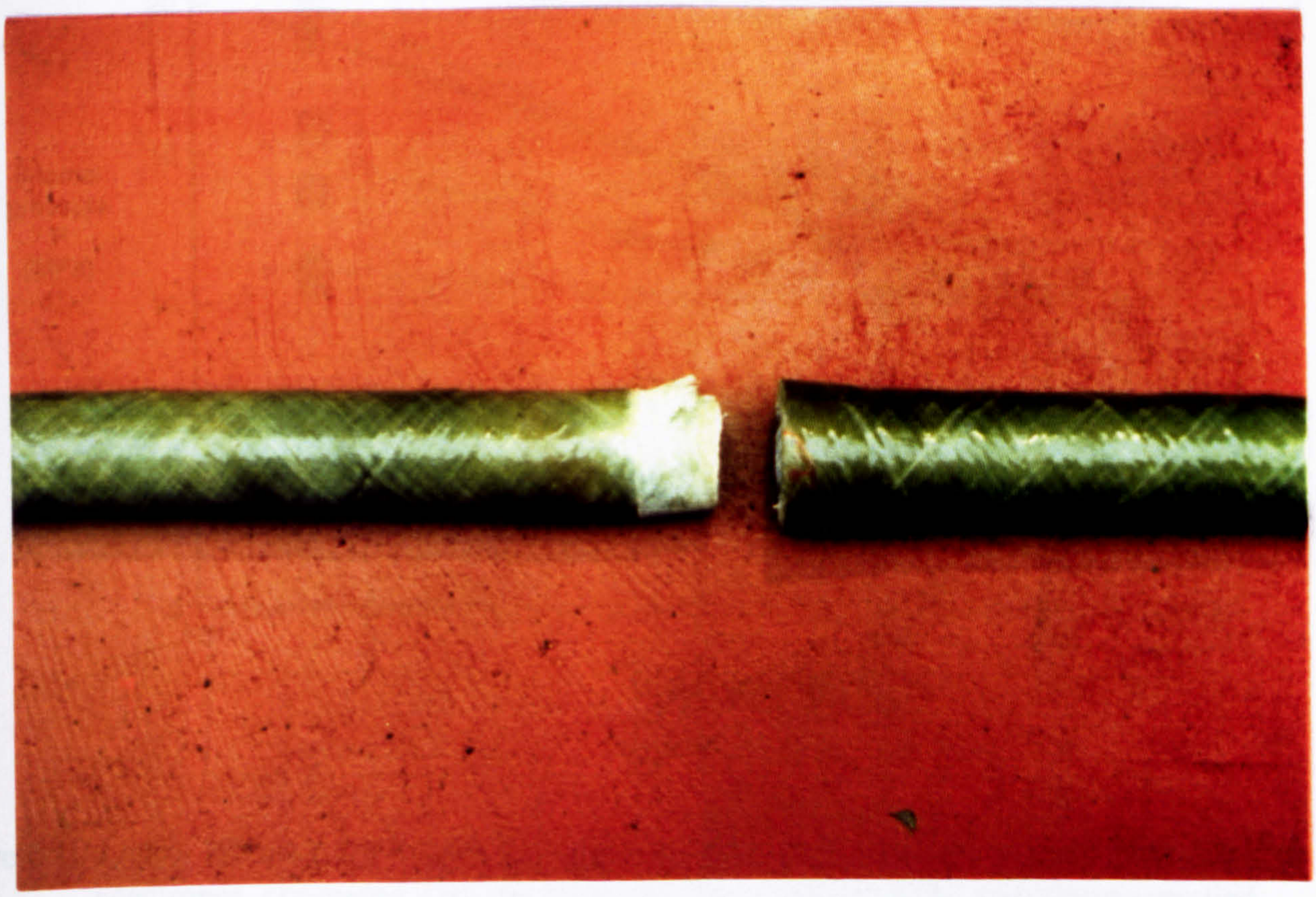

Figure 6.9 Spigot/socket bonded joint (VB01) failed due to the failure of the bonded interface. The specimen was fitted with a rubber liner and subjected to quasi-static internal pressure. The pressure was gradually increased until the pipe burst.

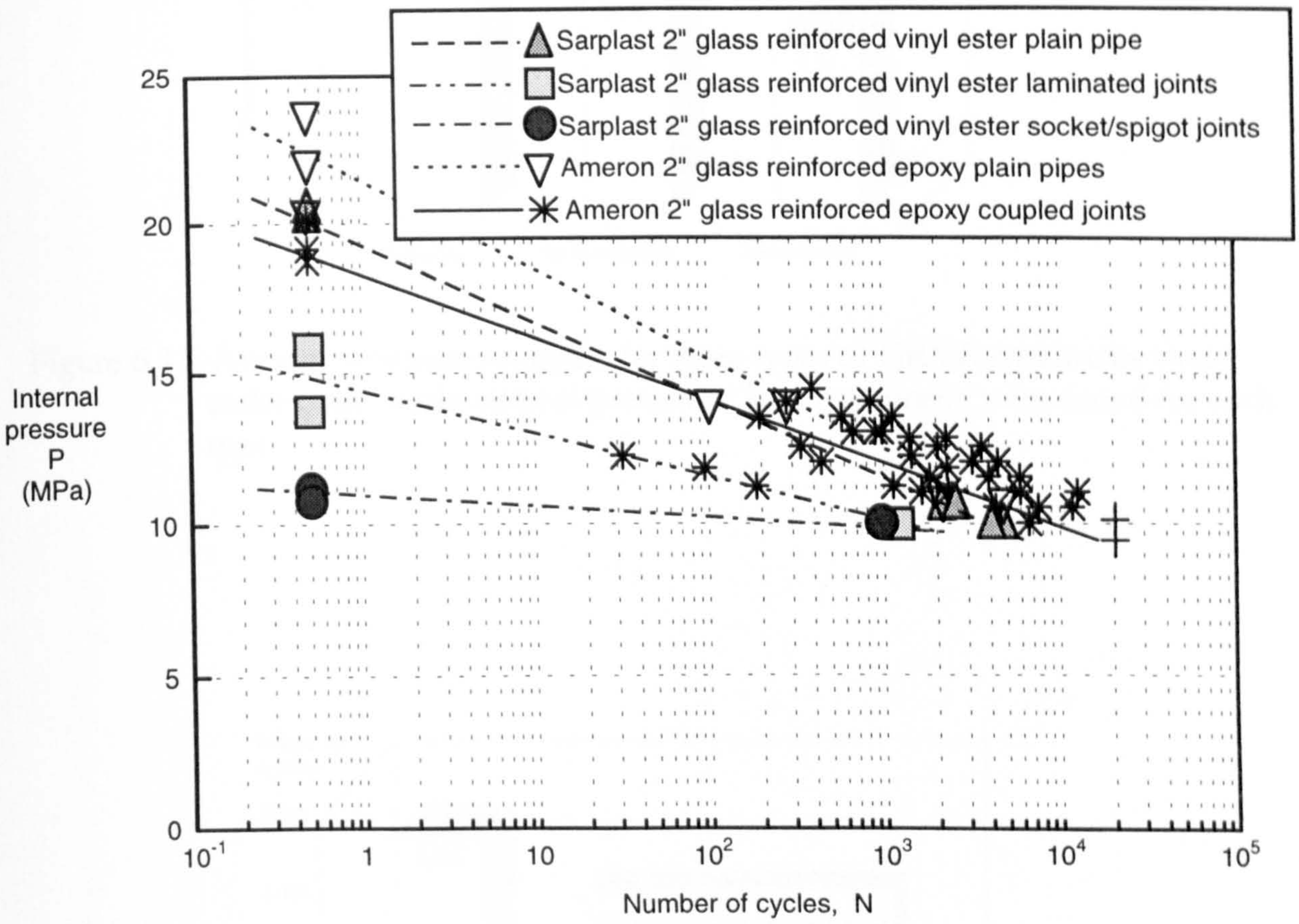

Figure 6.10 Load - life diagram for the three types of glass reinforced vinyl ester (GRVE) specimens, compared with the glass reinforced epoxy (GRE) specimens studied in Chapter 5. All specimens were subjected to cyclic saw-tooth internal pressure until water weepage. Plain GRVE pipes showed a comparable strength to that of the GRE pipes, but both types of GRVE joints gave lower strengths.

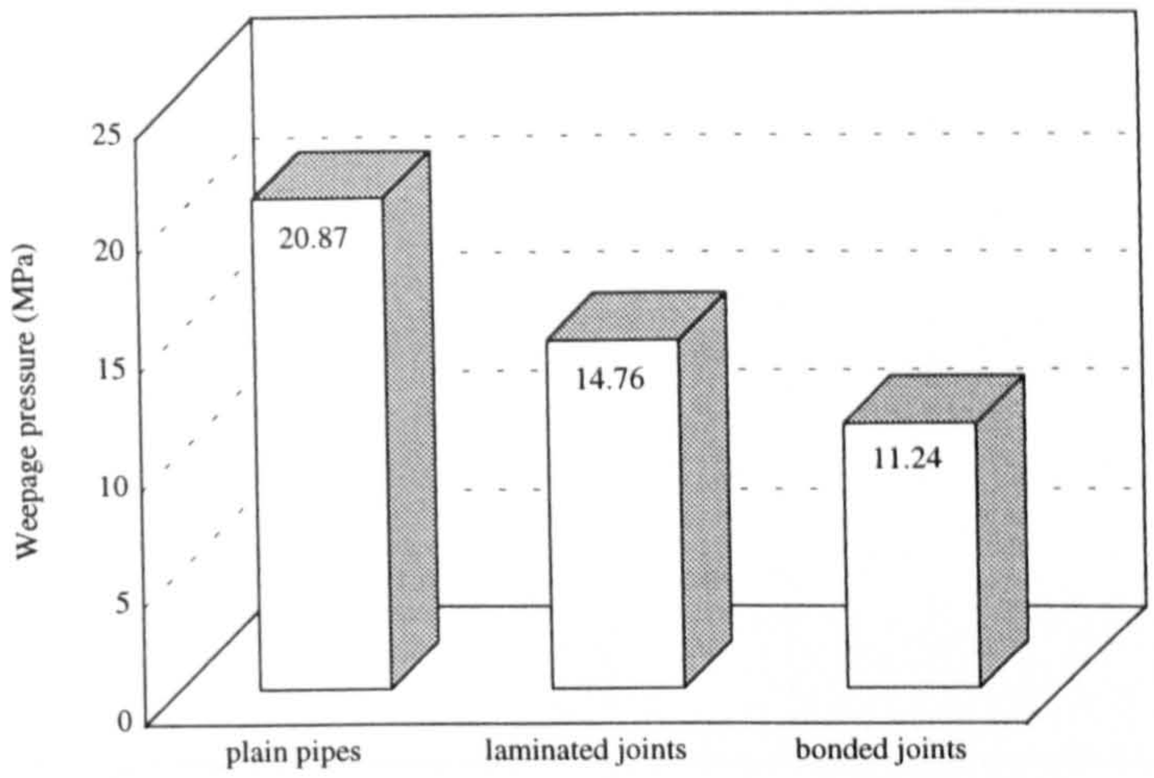

Figure 6.11 Average weepage strengths for three types of GRVE specimens tested under quasi-static internal pressure. Two specimens were tested for each type.

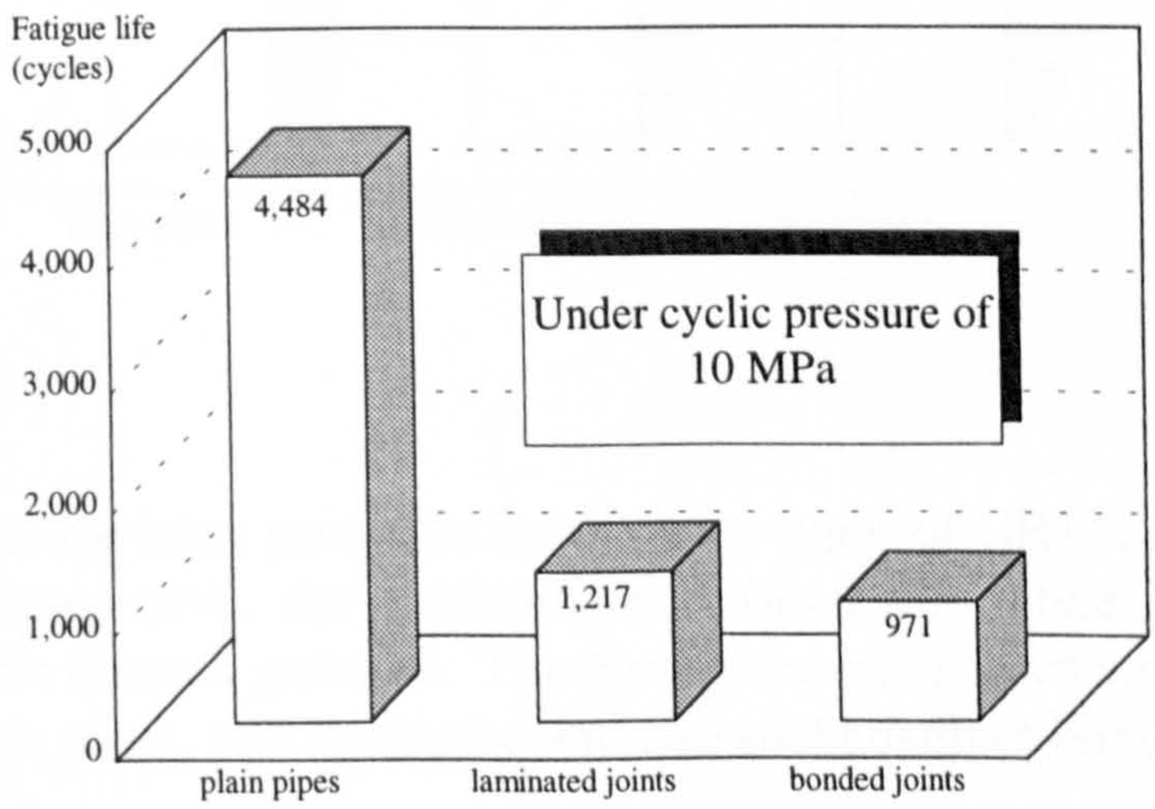

Figure 6.12 Fatigue life for three types of GRVE pipe specimens under cyclic internal pressure of 10 MPa. The fatigue life of plain pipes is the average of two specimens, VP03 and VP04. The fatigue life of the GRVE joints is apparently lower than that of the plain pipes.

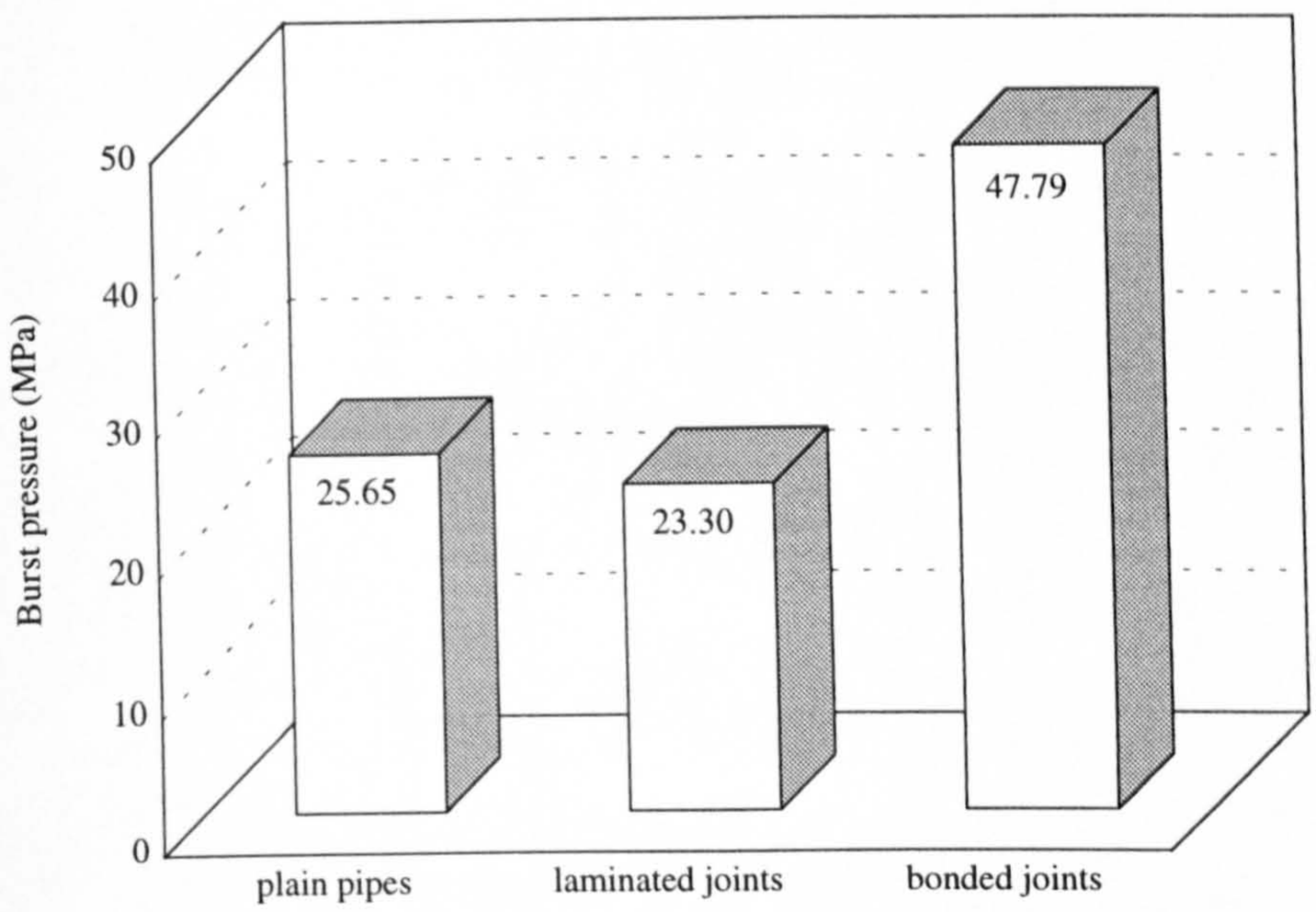

Figure 6.13 Average burst pressures for the three types of GRVE specimens. After the weepage tests, the specimens were fitted with rubber liners and tested under static internal pressure. The burst pressures shown were obtained from three plain pipes, two laminated and two socket/spigot bonded joints.

Figure 6.14 Examples of burst GRVE pipe specimens under internal pressure. The plain pipe burst at the gauge length. Both the laminated joint and socket/spigot bonded joint failed at the joints. With the laminated joint, a part of the joint material was burst away. The socket/spigot joint failed by the adhesive interface failure.

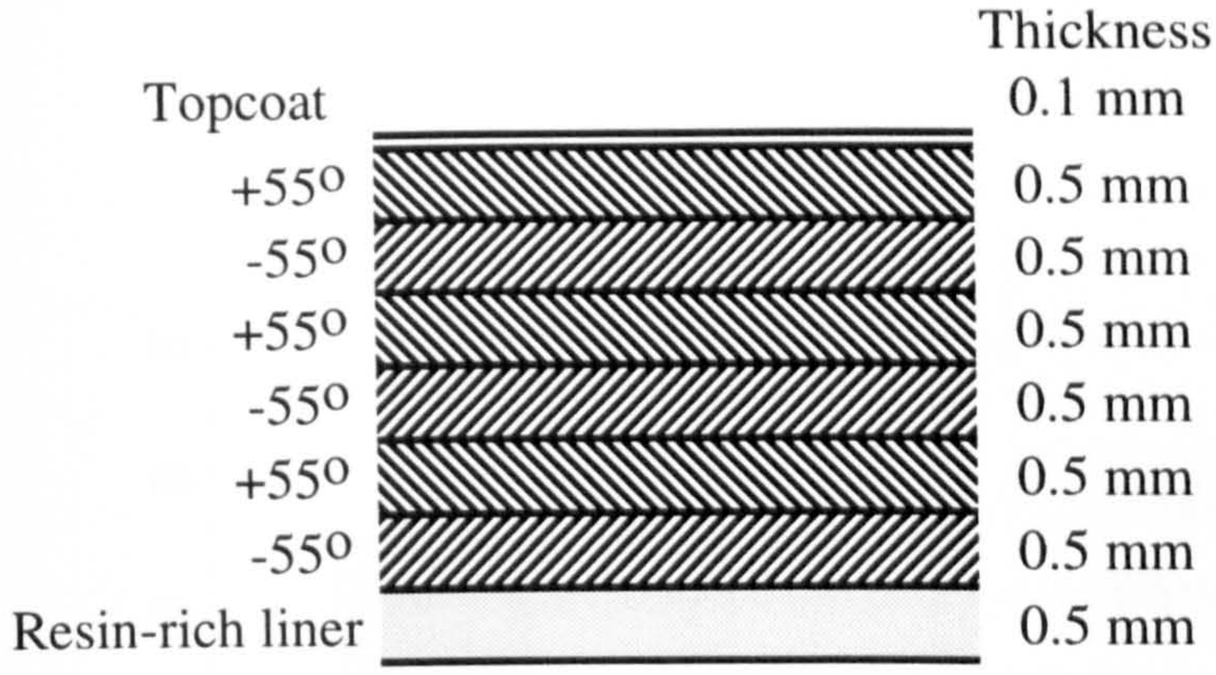

(a) GRE pipe

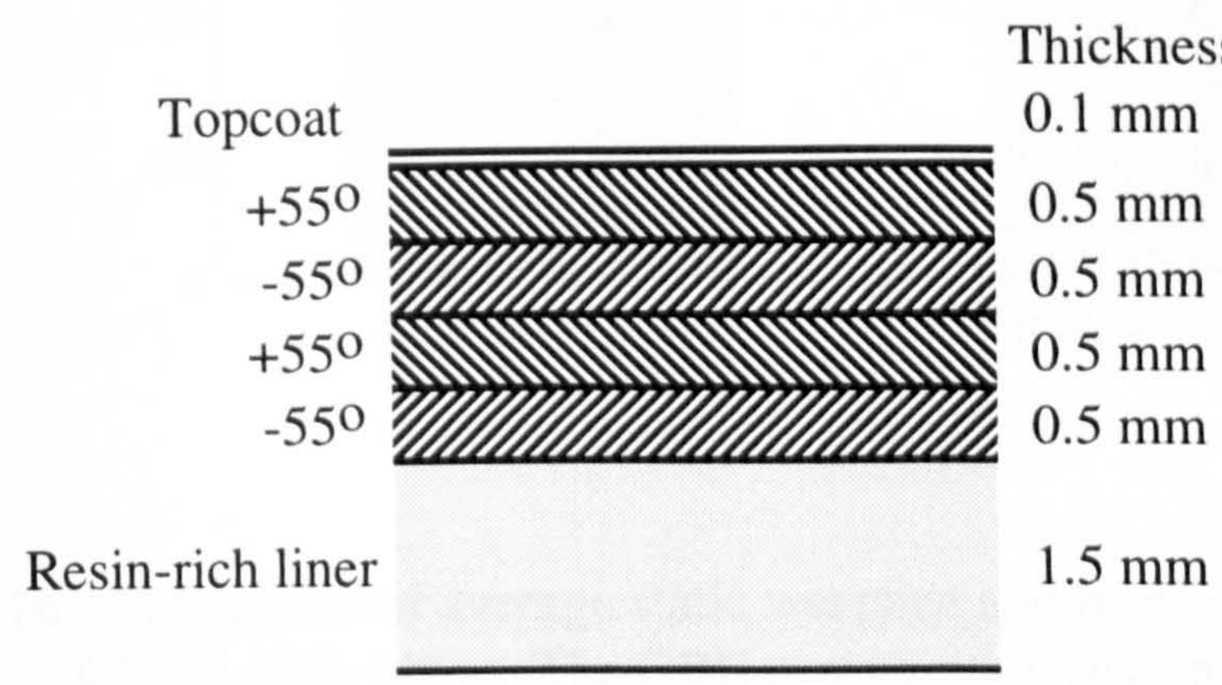

(b) GRVE pipe

Figure 6.15 Through-thickness structures of pipe wall laminate of GRE and GRVE plain pipes.

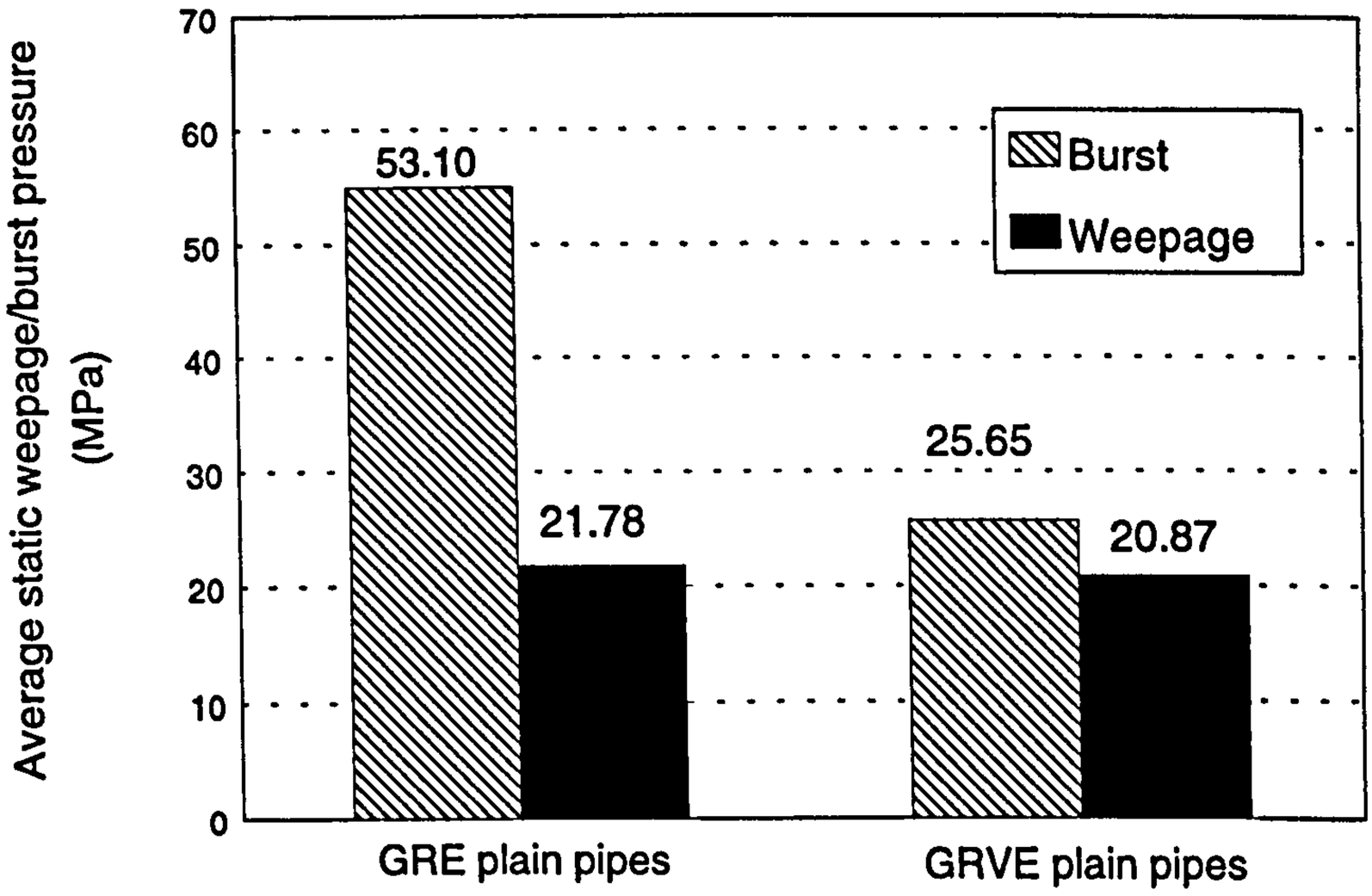

Figure 6.16 Comparison of average static weepage and burst pressures of GRE and GRVE plain pipes. The GRE pipes were tested in Chapter 5 and the GRVE in Chapter 6.

CHAPTER SEVEN

NUMERICAL ANALYSIS

7.1 INTRODUCTION

This chapter presents the results of the numerical investigation into the filament wound glass reinforced plastic (GRP) pipes and joints whose experimental results were described in Chapters 5 and 6. Ply strain and stress components and Tsai-Wu failure indexes [1,2] in the GRP pipes and adhesively bonded joints have been calculated by the finite element method using three dimensional laminated composite elements. The numerical results show a good agreement with the experimental results.

7.2 NISA SOFTWARE

The NISA (Numerically Integrated element for System Analysis) finite element analysis package [3] was used to model the stresses and deformation of the glass reinforced plastic pipes and joints subjected to internal pressure. The aim was to examine the capability of a PC-based finite element package to predict damage initiation and failure in a GRP pipework.

NISA is a general purpose finite element program used to analyse a wide spectrum of problems encountered in engineering. For filament wound glass reinforced plastic pipes, a model constructed of three dimensional laminated composite and adhesive brick elements was used. This was found helpful in interpreting the failure modes of the joints.

7.3 3-D LAMINATED COMPOSITE ELEMENT

A 3-D curved isoparametric composite brick element was used for modelling the structural pipe wall of filament wound GRP pipes and fittings. The element consists of a number of plies of perfectly bonded unidirectional laminae with different ply thicknesses and fibre directions. The element has 20 nodes, including 8 corner nodes and 12 side nodes. Each node has three translational degrees of freedom (u, v, w) and has no rotational freedoms. The state of stress is characterised by six stress components (σ_1, σ_2, σ_3, τ_{23}, τ_{31} and τ_{12}) in the principal material directions of each ply. The mechanical properties of the UD laminae and the thickness and orientation of each ply were defined in every element. The volume fraction and elastic properties of UD laminae used are listed in Table 7.1, in which the elastic constants were estimated by the Halpin-Tsai equations[6, pages 51-57]. For the E-glass/epoxy material system, the modulus of the fibres E_f=76 GPa, Poisson's ratio ν_f=0.2; the modulus of the matrix E_m=3.4 GPa and Poisson's ratio ν_m=0.4. In addition to the displacements, gross stresses, gross strains, ply stresses and ply strains, the stress ratios and the Tsai-Wu failure index were calculated for each ply referring to the maximum stress failure theory and the Tsai-Wu failure theory.

A general 20-node 3-D brick element was used for modelling adhesive layer in the bonded tubular joints and the aluminium end-caps. This element is similar to the laminated composite element except being homogeneous and having isotropic mechanical properties. The elastic constants and the shear strength of the epoxy adhesive layer are listed in Table 7.2.

The pipe was modelled with 36 elements in the hoop direction and one element through the thickness (covering all plies of the structural wall). Since the resin-liner had much lower stiffness than the structural wall, it was considered to have little influence on the stresses and strains of the reinforced layer. Therefore, the resin-liner was ignored in the calculation.

7.4 TSAI-WU CRITERION AND TSAI-WU FAILURE INDEX

The strength of a filament wound composite pipe is based on the strength of the individual plies within the pipe wall. Successive ply failures will occur in the pipe wall as the applied internal pressure increases. The first ply failure (FPF) is followed by other ply failures until the last ply failure (LPF), which corresponds to the ultimate failure of the pipe.

The interactive Tsai-Wu failure criterion was used for the strength prediction of unidirectional fibre composites. The layer failure was presumed to have occurred when the value of the Tsai-Wu failure index reached unity [1],

$$f = f_{11} \bullet \sigma_1^2 + f_{22} \bullet \sigma_2^2 + f_{33} \bullet \sigma_3^2 + f_{12} \bullet \sigma_1 \bullet \sigma_2 + f_{13} \bullet \sigma_1 \bullet \sigma_3 + f_{23} \bullet \sigma_2 \bullet \sigma_3 + f_{44} \bullet \tau_{23}^2 + f_{55} \bullet \tau_{13}^2 + f_{66} \bullet \tau_{12}^2 + f_1 \bullet \sigma_1 + f_2 \bullet \sigma_2 + f_3 \bullet \sigma_3 \qquad (7.1)$$

Of the 12 coefficients, nine can be obtained from the strength properties using simple tests,

$$f_{11} = 1/(F_{1t} F_{1c}), \quad f_{22} = 1/(F_{2t} F_{2c}), \quad f_{33} = 1/(F_{3t} F_{3c}),$$
$$f_{44} = 1/S_{23}^2, \quad f_{55} = 1/S_{13}^2, \quad f_{66} = 1/S_{12}^2,$$
$$f_1 = 1/F_{1t} - 1/F_{1c}, \quad f_2 = 1/F_{2t} - 1/F_{2c}, \quad f_3 = 1/F_{3t} - 1/F_{3c} \qquad (7.2)$$

where F_{1t} , F_{2t} and F_{3t} are uniaxial tensile strengths, F_{1c} , F_{2c} and F_{3c} the corresponding compressive strengths and S_{23} , S_{13} and S_{12} the shear strengths referring to the principal material directions (1,2,3), such that 1 is the fibre direction, 2 normal to 1 and 3 normal to the lamina.

The remaining coefficients f_{12} , f_{13} , and f_{23} reflect the interaction between the material principal directions, and must be obtained by some type of biaxial testing. The strength properties and coupling coefficients of the UD laminae in the GRE pipes are listed in Table 7.3, where the interactive coefficients f_{12} , f_{13} , and f_{23} were approximately calculated by[1],

$$f_{ij} = (-0.5) \cdot \sqrt{f_{ii} \cdot f_{jj}} \qquad (i, j = 1,2,3)$$

Similar calculations are also conducted for the glass reinforced vinyl ester pipes. More details of the analysis are described in the following sections.

7.5 STRESS ANALYSIS OF GRE PIPES AND JOINTS

7.5.1 Coupler Bonded Joint

FE Model

The joint shown in Figure 5.10 and 5.11 comprised two filament-wound fibreglass reinforced epoxy resin pipes and a coupler bonded with epoxy adhesive. The coupler and pipe ends were machined before the adhesive was applied. The dimensions of the joint are given in Table 5.1. The pipe had a 0.1 mm topcoat and a 0.5 mm resin liner. The load in the pipe wall was mainly carried by the 3 mm thick (6 plies) structural wall which consisted of epoxy resin reinforced by E-glass fibres. The volume fraction of the glass fibres in the structural wall was 50% and the winding angles were $\pm 55^{\circ}$. The outside diameter of the machined part of the pipe was 59.2 mm, compared with 60.4 mm for the pipe itself. A thickness of 0.6 mm of the pipe wall (i.e. the top coat and the outer ply) was machined off and the machined pipe ends only had 5 plies, $[(\pm 55^{\circ})_2/-55^{\circ}]$. According to the manufacturer's guidelines for pipe installation, the machined pipe length was 50 mm, 5 mm longer than the overlap with the coupler. This created a "groove" with a length of 5 mm and a depth of 0.5 mm between the pipe and the coupler. The "groove" was generally covered by adhesive.

Figure 7.1 shows the 3-dimensional finite element mesh which was constructed and analysed using the NISA finite element package. Half of the coupler connected joint was modelled and symmetric displacement boundary conditions were applied on the middle cross section of the coupler. The pipe wall and coupler were modelled by the 20-node composite brick elements described in Section 7.3 and the adhesive layer by 20-node isoparametric brick elements with isotropic mechanical properties. There were 36 elements in the hoop direction and one element in the thickness direction of the pipe wall (covering 6 plies). A finer mesh in the axial direction was used in the thickness changing zone ("shoulder" area). In the bonded overlap length, there were three elements though the thickness: one 3-D laminated composite element modelling the machined pipe wall (5 plies only, the top coat and outer ply were machined away), one isotropic 3-D element modelling the adhesive layer (0.5 mm thick) and one composite element for the coupler (12 plies, $[\pm 55^{\circ}]_6$), see Figure 7.1. Since the stiffness of the resin-liner was much smaller than that of the structural wall, the resin-liner was

considered that there was little influence on the stresses and strains in the structural wall and thus was ignored in the FE model.

Material Properties

The elastic constants of the GRE pipe wall were estimated using laminate theory. Appendix B gives the equations for estimating the elastic constants of the unidirectional lamina from the elastic constants of the fibres and matrix and the fibre volume fraction. Both the elastic constants in the laminate plane and the through thickness were estimated for 3-dimensional finite element analysis. For the E-glass/epoxy system [6],

Young's modulus of fibres: $E_f = 76$ GPa

Poisson's ratio of fibres: $\nu_f = 0.2$

Young's modulus of matrix: $E_m = 3.4$ GPa

Poisson's ratio of matrix: $\nu_m = 0.4$

For a unidirectional lamina of the GRE pipe with fibre volume fraction V_f=50%, the elastic constants in the principal material directions are calculated by equations in Appendix B (page 242) and listed in Table 7.1. Direction 1 is the fibre direction, 2 is the transverse direction in the lamina plane and 3 is normal to the lamina plane.

Table 7.3 gives the strength properties and coupling coefficients of the UD laminae in the GRE pipe wall. When running the finite element program NISA, both the elastic constants and strength properties in the principal material directions were input.

The isotropic elastic and mechanical properties of the epoxy adhesive are given in Table 7.2.

Results and Discussion

Figure 7.2 shows the distribution of the Tsai-Wu failure indexes (defined by Eq.7.1) in the structural wall of the filament wound GRE pipe subjected to an internal pressure of 15.6 MPa. The pipe wall was composed of six unidirectional GRE composite layers in stacking sequence $[\pm 55^0]_3$. Layer 1 represents the inner ply where fibres aligned in 55^0 direction to the pipe axis. Layer 6 represents the outer ply where fibres were in -55^0 direction. The internal

pressure of 15.6 MPa was the predicted failure load of plain pipe when the Tsai-Wu index equalled unity. The results show that all layers had high Tsai-Wu indexes in the region near the "groove". Layers 5 and 6 (outer plies) had very high values in the "groove" area. When the distance from the "groove" was greater than 30 mm, the Tsai-Wu indexes became constant and showed little influence of the joint. In the "remote" area, the inner ply (layer 1) had the maximum Tsai-Wu failure index. The FE results in Figure 7.2 implied that the damage (matrix cracking) started from the outer ply in the "groove" area. In the "remote" area (equivalent to plain pipes) the damage initiated from the first ply. In the area where the pipe was overlapped by the coupler, all plies of the pipe wall showed low failure indexes. Since the maximum value of the Tsai-Wu indexes in the "groove" area was 2.4 times higher than those in the "remote area", damage initiation was predicted to occur at an internal pressure of 6.5 MPa, which was rather low compared with the weepage pressure of 19.29 MPa measured during tests (in Chpater 5). The reason probably was that the predicted values were only for the first ply failure (FPF) while the test results were for the last ply failure (LPF). After the first ply failed, more loads were required to cause successive failures in the other plies. Therefore the first ply failure load was lower than the actual pipe strength. The other reason might be that progressive damage removed the stress concentration near the "groove" (when the top ply peeled off from the "groove", the local bending stresses in the "groove" area would be decreased). Therefore, although the stress concentration affected the strength for damage initiation, it had less effect on the weepage strength (i.e. last ply failure).

The prediction of the burst strength would be more difficult as the pipe wall was already damaged by matrix cracking and thus the stiffness of the laminae was degraded by the damages. Assumptions for stiffness degradation must be made and a step-by-step analysis must be conducted to simulate the damage propagation. Burst strength can finally be predicted by ply stress σ_1 reaching the tensile strength of the degraded UD laminae in fibre direction. In the present work, only the elastic analysis of the undamaged pipe wall was conducted and the predictions were only corresponding to the first ply failure. As the pipe wall was relatively thin comparing to its diameter, there were no large differences between the Tsai-Wu index in the first ply and that in the last ply for the plain pipes (or the "remote" area of the jointed pipes). Therefore, for plain pipes, the failure strength was approximately considered as the weepage strength. However, for jointed pipes, the first ply failure strength may be quite different from that of the last ply failure. Therefore, good predictions of the

weepage strength were not achieved in the current work, only the critical locations were identified by the results of the elastic FE analysis.

Figure 7.3 shows the shear stress distributions in the adhesive layer under the same internal pressure. The results showed shear stress concentrations at the edges of bonded interface. Under the internal pressure of 15.6 MPa, the Tsai-Wu indexes in the structural wall were greater than unity in the "groove" area (Figure 7.2) but the total shear stress in the adhesive was less than its shear strength, approximately 22 MPa for the epoxy adhesive (Figure 7.3). Therefore, no adhesive shear failure was predicted and the joint was expected to fail by the pipe wall failure near the joint in the "groove" area. It agreed with the experimental results in Chapter 5 that weepage and burst occurred predominantly in the zone close to the joint, as shown in Figure 5.15 and 5.16. In Figure 7.3, it also gave an anti-symmetric (radial-hoop) shear stress of up to 4 MPa in the adhesive which was caused by the unsymmetric laminate structures of the pipe wall. The tendency of the self-rotation of a filament wound pipe with unsymmetric laminated pipe wall will be discussed in Section 7.5.

Figure 7.4 shows the through-thickness variation of the Tsai-Wu failure indexes. In the cross section near the "shoulder" of the joint, the outer ply had the maximum value of the Tsai-Wu indexes and the value in the inner ply was smaller. In the remote area, the index in the inner ply was greater than that in the outer ply. The local bending moment might have caused this change. In the coupler-covered area, the index was very low indicating there was no damage predicted in this area.

Although the resin-liner did not carry much of the load, its ultimate tensile strain might influence the weepage strength of a GRE pipe, as shown in Figure 5.9(b). Calculations were also conducted by modelling the structural GRE pipe wall (composite laminate elements) and the resin liner (isotropic elements). The hoop and axial strains in the resin liner were examined in Figure 7.5, compared with the strains in outer surface of the pipes under internal pressure of 10 MPa (for comparing the measured strains under the same load). The measured strains in the outer surface of the GRE pipe (Section 4.5) are also shown in Figure 7.5. The predicted strains had a good agreement with the measured values in the outer surface. Both hoop strains (in top face and resin-liner) in the "groove" area near the coupler were slightly higher than those in the "remote" area, whereas the axial strains showed a quick variation,

which indicated an axial bending in the "groove" area. The hoop strains were higher than the axial strains, that probably was the reason why the resin-rich liner cracked in the direction of pipe axis during the tests (Chapter 5, Figures 5.4 and 5.18). In the overlapped area, strains were relatively low.

Although serious stress concentrations were predicted by the elastic analysis, coupler bonded pipes gave only slightly lower weepage and burst pressures than plain pipes during tests (see Figure 5.26). These stress concentrations caused the damage initiation at an early stage (delaminations were observed between outer ply (layer 6) and layer 5 from the the edge of the "groove") , but the damage propagation might have quickly removed the stress concentration. Therefore, a FE analysis was carried out on the pipe after the outer ply (layer 6) had completely peeled off. Figure 7.6 shows the distributions of Tsai-Wu indexes in a 5-ply pipe which had no "groove". Layer 5 (which is the outer ply in the new FE model) had the maximum value of the failure index of 1.8 in the region near the shoulder, which was lower than that before the peeling (2.4 in Figure 7.2). It demonstrates that the damage propagation reduced the stress concentration. However, since the pipe wall had an unbalanced number of plies in $+55^0$ and -55^0 directions, the anti-symmetric shear stress $\tau_{radial,hoop}$ in the adhesive layer was further increased.

Assuming that only the topcoats of the pipe ends were shaved without damaging the outer ply (layer 6) of the original reinforced structural wall before the joint was assembled as shown in Figure 7.7, the pipe wall had six balanced plies in the whole length, $[\pm 55^o]_3$ and had no "groove" near the joint. The maximum Tsai-Wu failure index of this assumed joint, as shown in Figure 7.7, was 1.2, only 45% of that for the thickly-machined pipe in Figure 7.2 and 67% of that for the 5-ply pipe (outer ply was completely peeled off) in Figure 7.6. In practice, however, it is difficult to achieve a uniform, thin and clean bonding interface by machining only the 0.1 mm topcoat as the commercial pipe has a considerable variation of pipe outside diameter.

7.5.2 Socket/Spigot Bonded Joint

The joint shown in Figure 5.20 was formed by a socket and a spigot and bonded by epoxy adhesive. A similar numerical model to that used for the coupler-connected joints described

in previous section was created and similar finite element analysis was carried out. Same reason as for the coupler bonded joints, only the structural wall (6 plies) was modelled. The heavily machined spigot (45 mm long) was modelled by 5-ply laminated elements. Figure 7.8 shows the Tsai-Wu failure indexes in the structural wall of the filament wound GRE pipes under internal pressure of 15.6 MPa. The solid lines were the indexes of the first ply (inner ply) and the dashed lines were of the outer ply. The Tsai-Wu index distributions in the spigot side were similar to that of the coupler-jointed pipe, as shown in Figure 7.2. As discussed in previous section, the high Tsai-Wu failure index in the "groove" area of the spigot would be reduced as the outer ply was peeled off from the "groove". The socket side, where had the radius variation, also showed high Tsai-Wu failure indexes. Unlike the spigot side, the maximum index occurred in the inner ply of the socket. Therefore, from these FEA results it was assumed that the damage initiated from the inner ply of the socket in the radius variation area. When the inner ply failed (the first ply failure), the second ply would carry the load released by the first ply. Failure would propagate quickly to the second and third plies, and finally penetrate the pipe wall and cause a failure (weepage). It appears to agree with the failure observed in the tests that weepage mainly occurred at the bottom of the socket (see Figure 5.22). The maximum index was approximately 2.5 times of those in the "remote" area. Therefore, the loading for the first ply failure (FPF) was predicted approximately 40% of that for the plain pipes, compared with the test result, the average weepage pressure corresponding to the last ply failure (LPF), which was 58% of the measured weepage pressure for the plain pipes. Figure 7.9 shows the shear stress in the adhesive of the bonding interface under the same internal pressure. At the ends of the bonding line, it showed shear stress concentrations. Under the internal pressure of 15.6 MPa while the maximum Tsai-Wu index equalled 2.5 (in the structural wall, Figure 7.8), the maximum shear stress in the adhesive was less than the adhesive shear strength, approximately 22 MPa for epoxy adhesive (Figure 7.9). Therefore, it was assumed that no adhesive shear failure occurred and the joint failed by the failure of the socket of the pipe.

7.5.3 Pipe End with Bonded End-Fittings

The specimen's end bonded with end-fittings, as shown in Figure 4.8, was also modelled by the finite element method. Numerical analysis was performed on the bonded joint of the pipe end with an aluminium collar when no extra end reinforcement was employed. Figure 7.10

shows the construction of the joint and the axial reactions in the pipe wall and in the aluminium collar to the internal pressure for "close-end" tests. The collar was 110 mm long and had an outer diameter of 100 mm. The pipe end and aluminium collar had a taper angle of 1°02'. A uniform adhesive layer of 0.5 mm thick was used. The resin-liner (0.5 mm thick) was also included in the FE model. The structural GRE pipe wall was modelled by 3-D laminated composite elements with different numbers of plies depending on the axial locations. The aluminium collar, the adhesive layer and the resin-liner were replaced by isotropic 3-D elements. Figure 7.11 shows the hoop stress distributions along the pipe axis when subjected to an internal pressure. The stresses were normalised by the applied internal pressure. In the structural wall, the hoop stresses became slightly higher in the "shoulder" area close to the aluminium collar. In contrast, the liner did not show much hoop stress concentration in this area. In the aluminium collar and the pipe wall of the overlapped area, the hoop stresses were relatively low, and the hoop stresses in the adhesive and the liner were compressive.

Axial stresses had the similar distributions, as shown in Figure 7.12. In the "shoulder" area near the aluminium collar, the axial stress in the outer surface became higher than that in the "remote" area. In the inner surface, the axial stress first became lower as it got closer to the collar, and then reached its maximum at the "shoulder". The variations of the axial stresses were caused by the axial bending of the pipe wall, because the thick-walled aluminium collar restricted the expansion of the GRE pipe. In the "remote" area, the axial stress in the inner surface was higher than that in the outer surface and both were constant. As it got closer to the collar, the pipe wall was first bent inwards and thus the axial stress in outer surface increased and that in the inner surface decreased. As it reached the edge of the collar, the pipe wall was bent outwards and thus the axial stress in the inner surface increased and that in the outer surface decreased. Inside the aluminium collar, the axial stresses became constant again. In order to reduce the stress concentrations, the pipe end was laminated with glass fabric/epoxy before mounting the aluminium collar, as shown in Figure 4.8. The experiments in Chapter 5 and 6 showed that increasing the thickness of the pipe wall in the "shoulder" area successfully avoided the plain pipes failing at the ends.

In Figure 7.13, the solid line shows the distribution of the normalised shear stress in the adhesive layer when the adhesive had a uniform thickness, as shown in Figure 7.10. At the

"shoulder" of the joint, there was a shear stress concentration. The maximum of the normalised shear stress is 1.05. In order to reduce the shear stress concentration, a modification was introduced by tapering the aluminium collar from inside and increasing the local adhesive thickness, as shown in Figure 7.14. The dashed line in Figure 7.13 shows that the maximum shear stress in the modified end joint was only 60% of that in the unmodified joint.

7.5.4 Thermal Residual Stresses in Filament Wound GRP Pipes

The manufacturing process of filament winding and subsequent resin curing introduces residual stresses in GRP pipes. The stresses are generated from the differences in thermal contraction between the individual plies comprising the pipe wall and the overall composite pipe during the cool down from the maximum cure to operating temperature (the residual stresses within a single ply due to different thermal contraction between the fibres and the matrix were not taken into account in the current calculation). With filament wound glass reinforced epoxy pipes, the difference between the cure and operating temperatures is typically, ΔT = -150°C. The linear thermal expansion coefficients of the unidirectional laminae are listed in Table 7.4.

Therefore, FE calculations were conducted to examine these thermal residual stresses and their influence on the strength of GRE plain pipes. Figure 7.15 shows the thermal residual stresses induced by curing (ΔT=-150 ^{0}C) in the first ply of the filament wound GRE pipe [$\pm\theta_3$] for various values of winding angle θ. When the winding angle is equal to 45^0, the thermal stress components S_{11} and S_{22} become the maximum compressive and tensile stresses respectively. When θ=22.5^0 and 67.5^0, the thermal shear stress S_{12} becomes a maximum.

Figure 7.16 gives the maximum Tsai-Wu failure indexes for the filament wound GRE pipe $[\pm 55°]_3$ (in the first ply) under different internal pressures when considering or not considering the thermal residual stresses. By assuming that the Tsai-Wu failure indexes equal unity, the estimated FPF internal pressures are 10.2 MPa when the thermal residual stresses are considered and 15.5 MPa when they are not taken into account. This produces an error of 35%.

Figure 7.17 shows the ply stresses in the first ply, which has the maximum Tsai-Wu failure index when the filament winding GRE pipe $[\pm 55^0]_3$ is subjected to various internal pressures. Solid lines represent the results obtained without consideration of the thermal residual stresses and dashed lines represent those with consideration of the thermal residual stresses. It was found that the curing residual stresses increased the ply stress component S_{22} and S_{12} but reduced S_{11}. The overall influence to the pipe strength is that the pipe strength is reduced as the Tsai-Wu failure index is increased, as shown in Figure 7.16.

7.5.5 Self-Rotation of Filament Wound GRP Pipes

Unlike pipes made from homogeneous materials, the filament wound composite pipes generally can not be treated as axi-symmetric problems even though axi-symmetric loads are applied. Rotation will occur when a filament wound composite pipe is subjected to internal pressure, as shown in Figure 7.18. This tendency to self-rotation induces extra hoop shear stress in the adhesive layer of the bonded joints (Figure 7.3). It is found that the symmetry of the lay-up of the pipe wall is the main parameter influencing the pipe rotation. Figure 7.19 shows the rotation angles of pipes with various numbers of unidirectional plies. The self-rotation of the pipes with an odd number of plies is more severe than for those with an even number of plies because of their imbalance of $+55^0$ and -55^0 reinforcements. As the number of plies increases, the balance is improved and the self-rotation becomes less severe. Figure 7.20 presents the maximum Tsai-Wu failure indexes in the pipe wall with differing numbers of plies in the sequence of ($+55^0/-55^0/+55^0/-55^0/\ldots\ldots$). It is found that the pipes with odd number of plies have higher Tsai-Wu failure indexes than those with even number of plies.

Figures 7.21 and 7.22 show the influence of the winding angle on the maximum Tsai-Wu failure index and self-rotation angle. Six ply $[\pm\theta]_3$ and five ply $[(\pm\theta)_2/+\theta]$ pipes are investigated. Figure 7.21 indicates that for both types of pipes a winding angle of 55° gives the lowest Tsai-Wu failure indexes under internal pressure thus the highest strengths, which agree with the results of netting analysis. However, Figure 22 shows that pipes with this 55^0 winding angle have the largest self-rotation angle, which will introduce additional hoop shear stresses in the pipe joints.

7.6 STRESS ANALYSIS OF GRVE PIPES AND JOINTS

7.6.1 Laminated Pipe Joint

FE Model

Similar to the previous treatments for GRE pipes, the GRVE pipes and joints tested in Chapter 6 (see Figure 6.7) were also modelled by finite element method. For the laminate joints shown in Figures 6.3 and 6.4, a finite element model was constructed using the NISA package, as shown in Figure 7.23. The pipe wall and the joining laminate were modelled by 20-node brick elements with orthotropic material properties. Static elastic calculations were performed under internal pressure and corresponding axial loading. For a "thin-wall" pipe with diameter D and wall thickness t, the corresponding tensile axial stress σ_{axial}, induced by internal pressure P in the 'close-end' pipe, equals

$$\sigma_{axial} = \frac{D}{4t} P \tag{7.3}$$

Elastic Properties

The orthotropic elastic properties in the three directions of the GRVE pipe wall are given in Table 7.5. These were estimated using equations of laminate theory, as described in Appendices B and C, and the corresponding FORTRAN program presented in Appendix A.

The elastic properties of a glass CSM /vinyl ester laminate can be estimated using the following empirical equations [5,6],

$$E = \frac{3}{8} E_1 + \frac{5}{8} E_2 \tag{7.4}$$

$$G = \frac{1}{8} E_1 + \frac{1}{4} E_2 \tag{7.5}$$

where E_1 and E_2 are calculated from the fibre modulus E_f, matrix modulus E_m and fibre volume fraction V_f by the equations,

$$E_1 = E_f V_f + E_m V_m \tag{7.6}$$

$$E_2 = E_m \frac{1+\xi\eta V_f}{1-\eta V_f} \tag{7.7}$$

where

$$\eta = \frac{E_f / E_m - 1}{E_f / E_m + \xi}$$

and the coefficient ξ is determined empirically. For the usual case of circular-section fibres, a value of ξ=2 was used[6]. For the E-glass/vinyl ester system used in the laminate pipe joint[6],

$$\begin{aligned} E_f &= 76{,}000\,MPa \\ E_m &= 3{,}400\,MPa \end{aligned} \tag{7.8}$$

and the fibre volume fraction V_f = 0.176. The estimated elastic constants of the CSM glass/vinyl ester laminated strap are listed in Table 7.6.

Results

Since the GRVE laminate joints tested in Chapter 6 failed by CSM laminated strap failure, the stresses in the laminated strap were examined by the finite element analysis. Figure 7.24 shows the stress contours in the glass CSM/vinyl ester laminate strap when the pipe is subjected to an internal pressure of 100 MPa. Graphs (a), (b) and (c) show the normal stress components in the axial, hoop and radial (or thickness) directions. Graph (d) shows the shear stress and (e) the Von-Mises stress. From these graphs, it was found that the middle part of the joint suffered high stresses. High stress concentrations also exist in the small local areas

of both tapered end-tips of the strap. These critical locations agree with experimental observations where matrix cracking and water weepage occurred.

A direct way to improve the joint is to increase the thickness of the laminated strap. Comparative FE calculations were performed for a GRVE joint with 4 mm thick CSM laminated strap (such as the specimens tested in Chapter 6) and for a hypothesised 8 mm thick strap. Figure 7.25 shows the hoop stresses in the CSM laminated strap (inner face). The results show that the thicker laminate joint has a lower hoop stress (dashed line). Both ends of the joint show stress singularities since an elastic continuous solid model was used, although the materials behave elastic-plastically in the real joint. The high stresses at the ends of the joint are also restricted to a very small local area. Figure 7.26 shows the axial stress components in the CSM laminated strap (inner face) for the two laminate thicknesses. Similar to the hoop stress, the thicker laminate joint has a lower axial stress. Therefore, the thicker laminate joint will have a higher strength.

7.6.2 Socket/Spigot Bonded Joint

FE Model

Similar to the CSM laminated joints discussed in the previous section, the adhesively bonded socket/spigot GRVE pipe joints tested in Chapter 6 (see Figure 6.8) were also modelled by the finite element method. Figure 7.27 shows the finite element mesh. The structural wall of the pipe was modelled by using 3-D 20-node brick elements with orthotropic material properties. As the stiffness of the resin liner was relatively low compared with the GRVE structural pipe wall, the resin liner was considered to have little influence on the stresses and strains in the structural pipe wall and was thus ignored in the FE model. The elastic constants of the filament wound GRVE pipe wall are listed in Table 7.5. The adhesive layer (0.5 mm thick) was modelled by isotropic elements, with Young's modulus E=3.4 GPa and Poisson's ratio ν=0.35.

Results

The tests described Chapter 6 showed that the failure of socket/spigot GRVE joints occurred at the joints by water weepage through the adhesive interfaces. The adhesive failure was possibly caused by the high shear stress in the adhesive layer. Therefore, in this section, only the adhesive shear stress was presented. Figure 7.28 shows the shear stress distributions in the adhesive layer from the socket mouth to the bottom (see Figure 6.8). The solid line is for the tested specimen with 35 mm bonding length. One simple method to improve the joint is to increase the bonding length. The dashed line is for an assumed joint with 70 mm bonding length, showing a lower adhesive shear stress. Therefore, increasing the bonding length reduces the shear stress in the adhesive layer and increases the strength of the joint.

From Figure 7.28, showing the results of elastic analysis, it is also found that there are high stress concentration factors at the ends of the bonding line. The middle zone of the bonding line suffered relatively low shear stress. Although the end high stresses are restricted to very

local areas, they will cause failure initiation which may propagate quickly under fatigue loading and cause the whole joint to fail completely. Hence, the author suggests a method to improve the joint by tapering the socket and spigot mouths and increasing the edge adhesive thickness, as shown in Figure 7.29. Finite element analysis was carried out on a joint which was tapered into a slope of 1:4 over 3 mm and having a local adhesive thickness of 1.25 mm, 2.5 times greater than the normal adhesive thickness (0.5 mm). Figure 7.30 shows the adhesive shear stress for the modified joint (solid line), compared to that of the untapered joint. An obvious reduction in stress concentration is found at the ends of the bonding line in the finite element analysis. However, only numerical simulation was carried out for this modification method, and experimental investigations are required before this approach can be used for pipe products in the future.

7.7 CONCLUSIONS

Finite element analysis using three dimensional laminated composite solid elements is a useful tool for the analysis of stress concentrations, the prediction of failure initiation and the interpretation of failure modes in filament wound composite pipes and joints.

Comparing the working pressure range of 3 MPa in practical offshore fire water systems and the product pressure rating of 4.4 MPa, numerical analyses and experimental investigation indicate that the glass reinforced epoxy pipes and joints have sufficient strength for their successful application.

Coupler bonded joints only slightly reduce the strength of plain GRE pipes but socket/spigot bonded joints reduce the strength significantly due to serious bending at the bell root.

It may be improper to analyse filament wound composite pipes by the use of an axisymmetric model even though they are subjected to an axisymmetric loading, because the effects of pipe rotation and hoop shear stress may not be negligible, especially when pipes have an odd number of plies.

It is worth paying attention to the thermal residual stresses induced by curing. The harmful residual stresses may not be negligible in certain cases.

REFERENCES

[1] S.W.Tsai and H.T.Hahn, Introduction to Composite Materials, Technomic Publishing Co. Inc., 1980, pp.277-327.

[2] D.Hull, An Introduction to Composite Materials, Cambridge University Press, 1981.

[3] User's Manual of the NISA Finite Element Analysis Software, 1993, pp.4.32.1 - 4.32.31.

[4] B.Jena and B.Pradhan, Analysis and Optimisation of Bonded Joints with FRP Composite Tubes. Proc. of Ninth Int. Conf. on Composite Materials (ICCM/9), Vol.IV, pp.82-88, Madrid, 12-16 July, 1993.

[5] B.D.Agarwal and L.J.Broutman, Analysis and Performance of Fiber Composites, Wiley, New York, 1980.

[6] C.S.Smith, Design of Marine Structures in Composite Materials, Elsevier Applied Science, 1990.

Table 7.1 Elastic constants of glass reinforced epoxy unidirectional laminae.

E_1 (MPa)	E_2 (MPa)	E_3 (MPa)	ν_{12}	ν_{23}
39700	7068	7068	0.30	0.16
ν_{13}	G_{12} (MPa)	G_{23} (MPa)	G_{13} (MPa)	V_f (%)
0.30	3308	3045	3308	50

Table 7.2 Elastic constants of the epoxy adhesive

Tensile Young's Modulus (MPa)	Poisson's ratio	Shear strength (MPa)
3400	0.35	22

Table 7.3 Strength properties and coupling coefficients[1] of the unidirectional GRE laminae composing the pipe wall [1,6].

F_{1t} (MPa)	F_{1c} (MPa)	F_{2t} (MPa)	F_{2c} (MPa)	F_{3t} (MPa)	F_{3c} (MPa)
1000	600	30	110	30	110
S_{23} (MPa)	S_{13} (MPa)	S_{12} (MPa)	f_{23} $(MPa)^{-2}$	f_{13} $(MPa)^{-2}$	f_{12} $(MPa)^{-2}$
35.	40.	40.	-1.51×10^{-4}	-1.12×10^{-5}	-1.12×10^{-5}

[1] Approximately calculated from F_{it}, F_{1c}, F_{2t}, F_{2c}, F_{3t} and F_{3c} by $f_{ij} = (-0.5)/\sqrt{F_{it}F_{ic}F_{jt}F_{jc}}$, $(i,j=1,2,3)$ [1].

Table 7.4 Thermal expansion coefficients of the unidirectional glass/epoxy lamina. (V_f=0.50)

Linear thermal expansion coefficient in fibre direction, α_1, ($1/^0C$)	7×10^{-6}
Linear thermal expansion coefficient in transverse direction, α_2, ($1/^0C$)	21×10^{-6}

Table 7.5 Elastic constants of glass/vinyl ester pipe wall.
(1 for fibre direction, 2 for transverse direction and 3 normal to the lamina plane; x for axial direction, y for hoop direction and z for thickness direction.)

E_{11} (MPa)	E_{22} (MPa)	E_{33} (MPa)	ν_{12}	ν_{23}
39700	7070	7070	0.30	0.16
ν_{13}	G_{12} (MPa)	G_{23} (MPa)	G_{13} (MPa)	
0.30	3300	3050	3300	
E_x (MPa)	E_y (MPa)	E_z (MPa)	ν_{xy}	ν_{yz}
8100	16100	7100	0.38	0.12
ν_{xz}	G_{xy} (MPa)	G_{yz} (MPa)	G_{xz} (MPa)	
0.12	9980	3220	3130	

Table 7.6 Elastic constants of glass CSM/vinyl ester laminate of the pipe joints.
(x for axial direction, y for hoop direction and z for thickness direction.)

E_x (MPa)	E_y (MPa)	E_z (MPa)	ν_{xy}	ν_{yz}
8700	8700	4210	0.41	0.36
ν_{xz}	G_{xy} (MPa)	G_{yz} (MPa)	G_{xz} (MPa)	
0.36	3080	1690	1690	

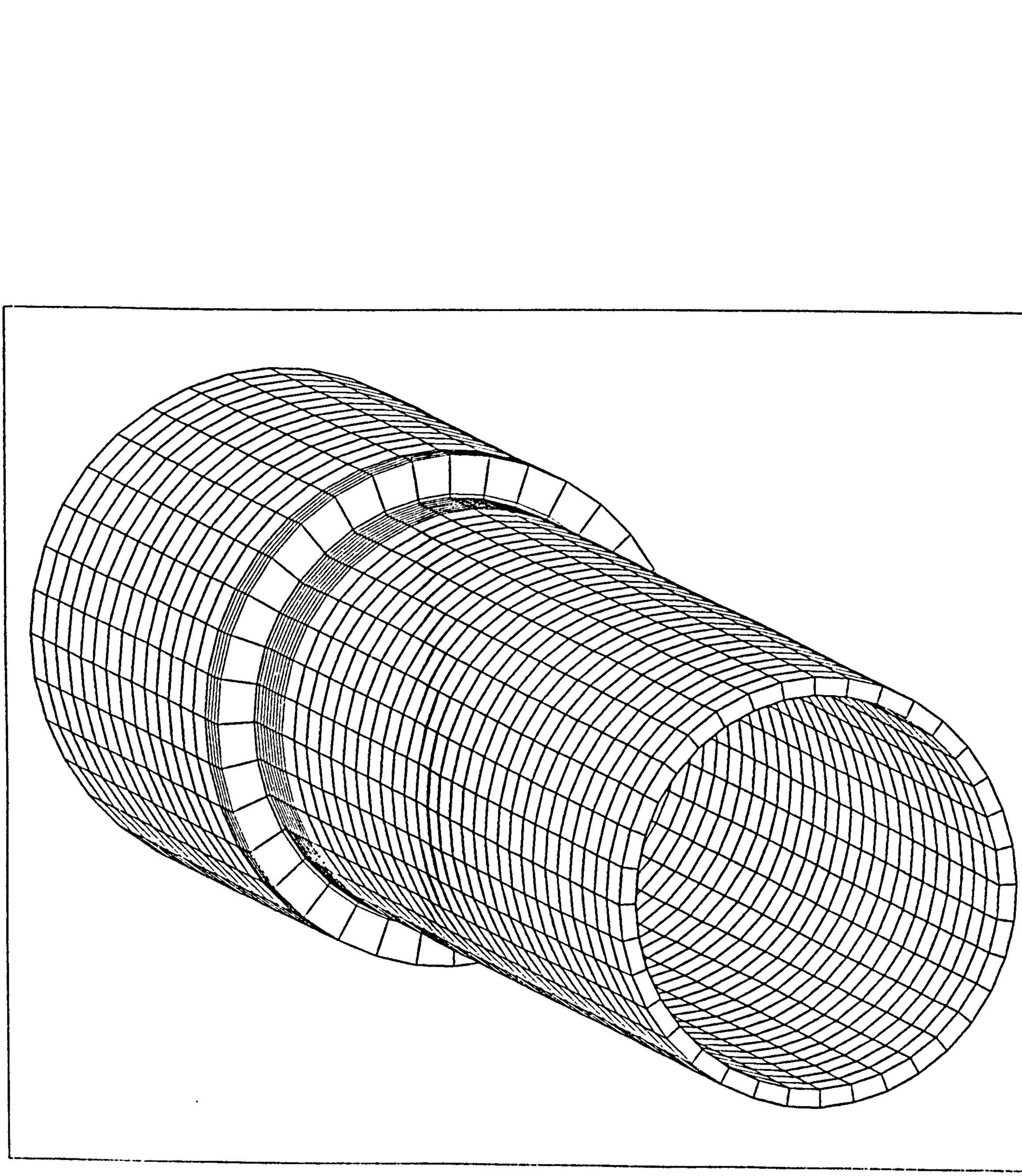

Figure 7.1 3-dimensional finite element mesh for half the coupler connected tubular joint.

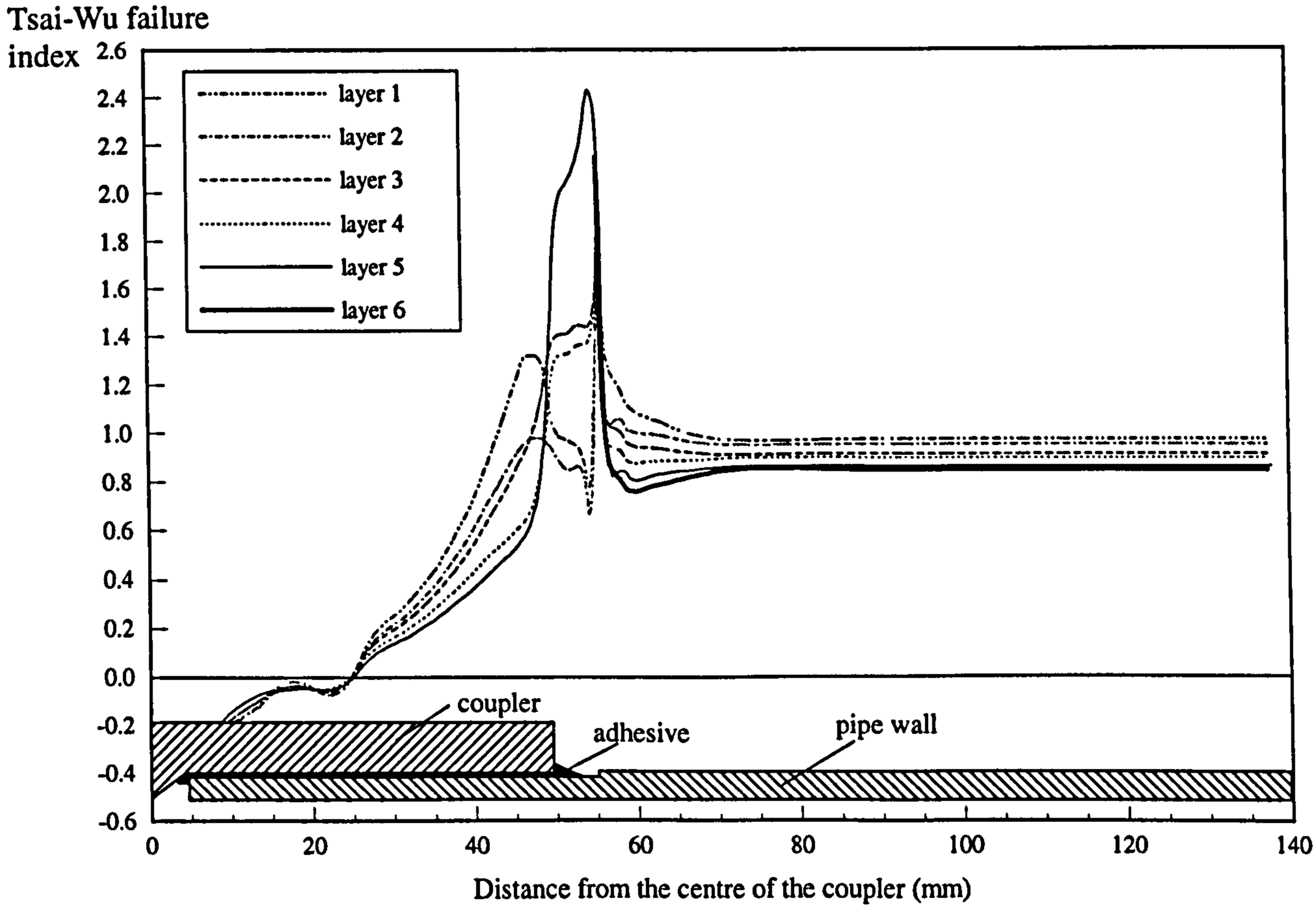

Figure 7.2 Tsai-Wu failure indexes in the structural wall of the filament wound GRE pipe $[\pm 55°]_3$ subjected to an internal pressure of 15.6 MPa. The outer ply of the pipe end was machined away for 50 mm of its length, only 5 plies [+55/-55/+55/-55/+55] was remained. Layer 1 represents the inner ply +55° and layer 6 the outer ply -55°. All plies near the "groove" have high Tsai-Wu failure indexes.

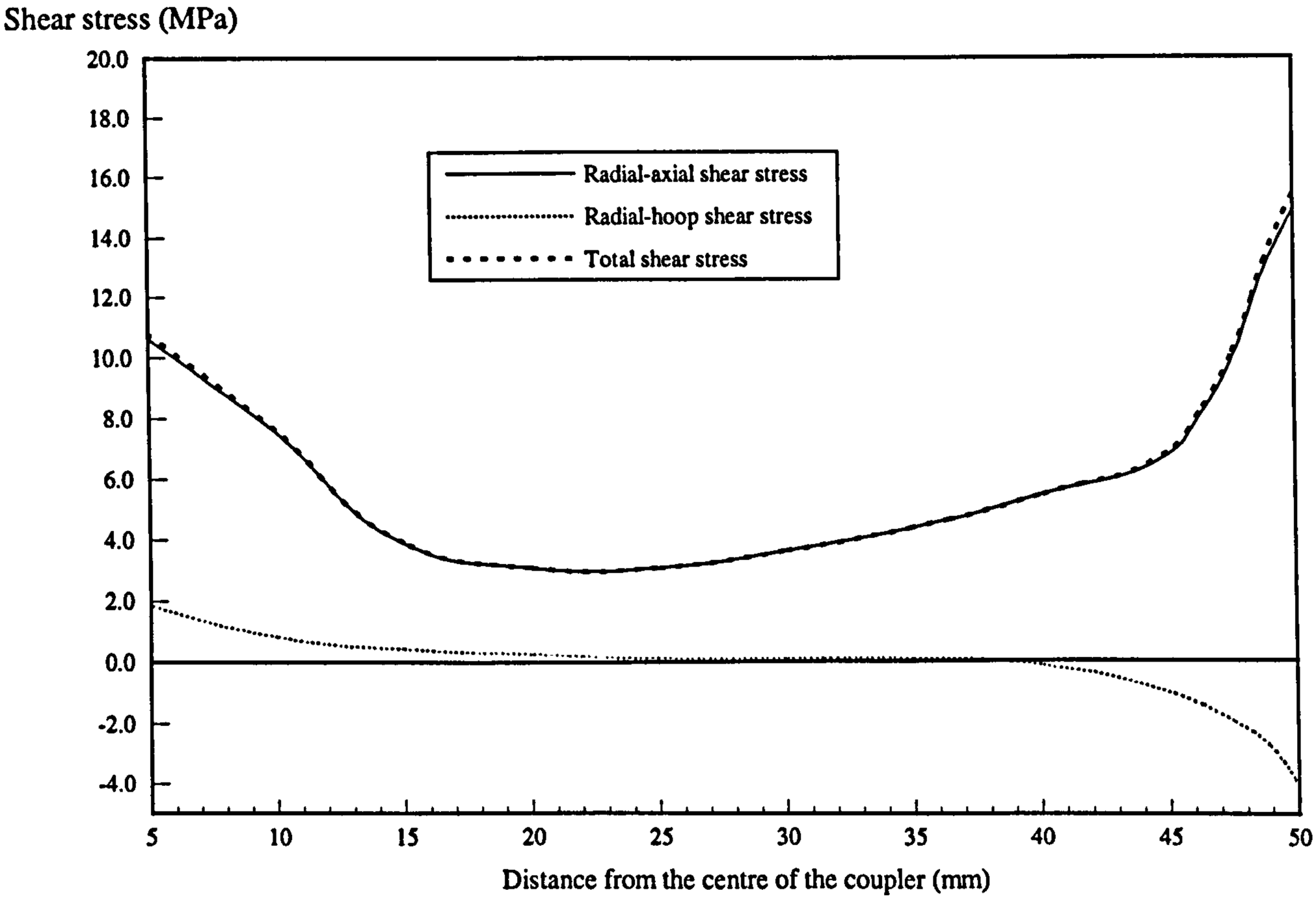

Figure 7.3 Shear stresses in the adhesive layer of the coupler-bonded joint under an internal pressure of 15.6 MPa.

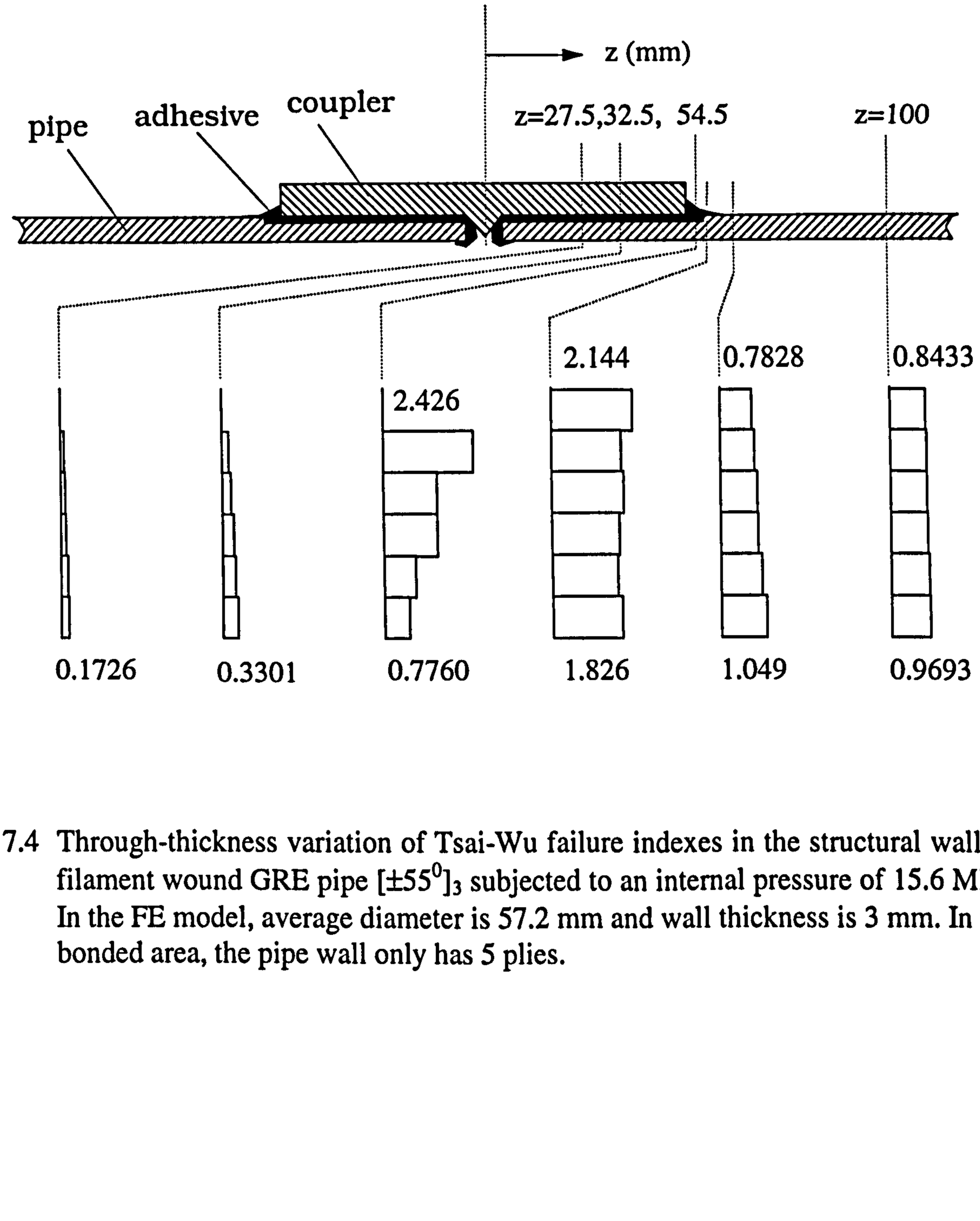

Figure 7.4 Through-thickness variation of Tsai-Wu failure indexes in the structural wall of filament wound GRE pipe $[\pm 55^0]_3$ subjected to an internal pressure of 15.6 MPa. In the FE model, average diameter is 57.2 mm and wall thickness is 3 mm. In the bonded area, the pipe wall only has 5 plies.

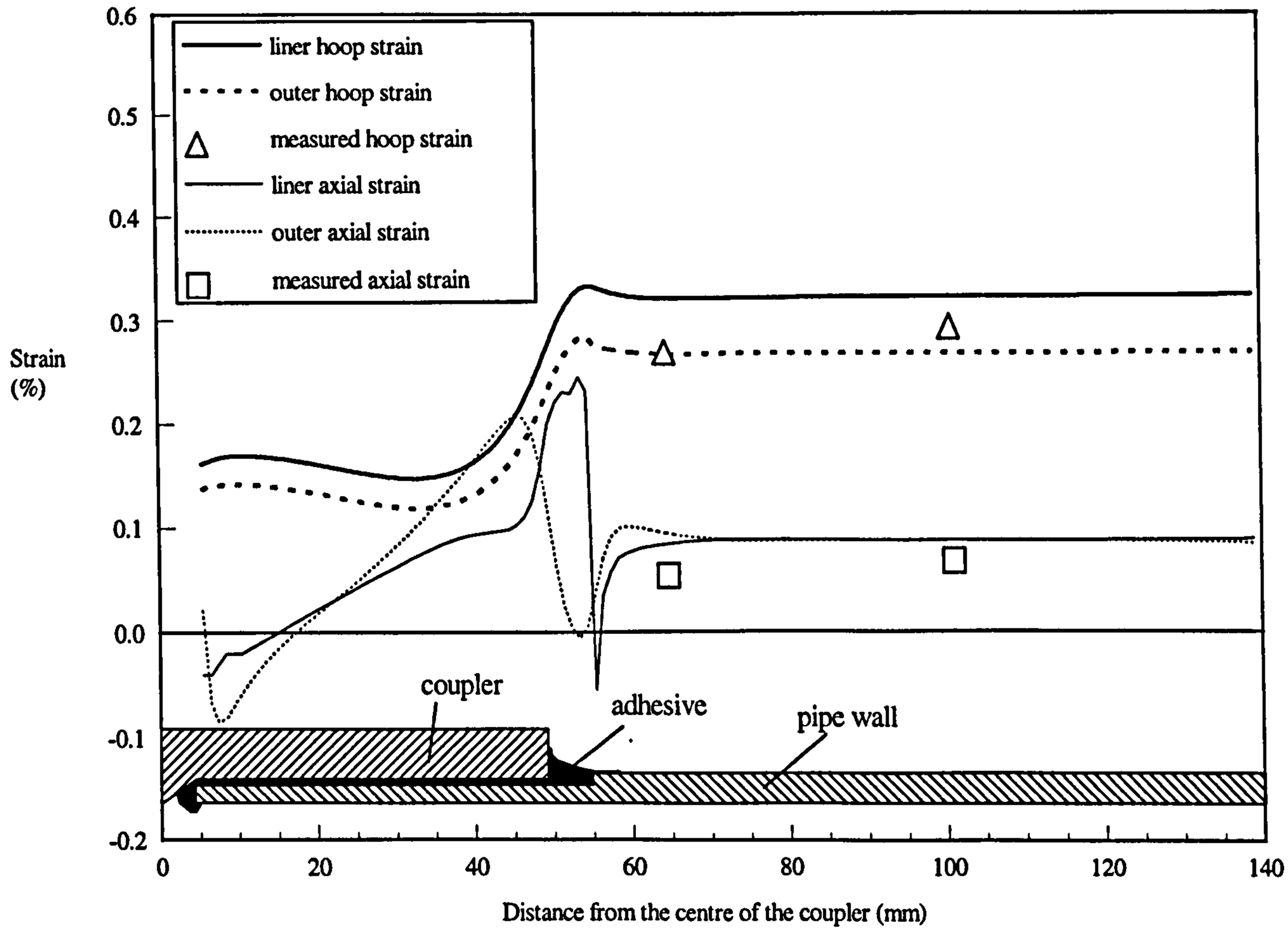

Figure 7.5 Strains in the inner and outer surfaces of the pipe under an internal pressure of 10 MPa. Hoop strains in the area close to the joint were slightly higher than those in the remote area. Hoop strains were higher than axial strains, which was probably the reason why the resin-rich liner cracked along the pipe axis.

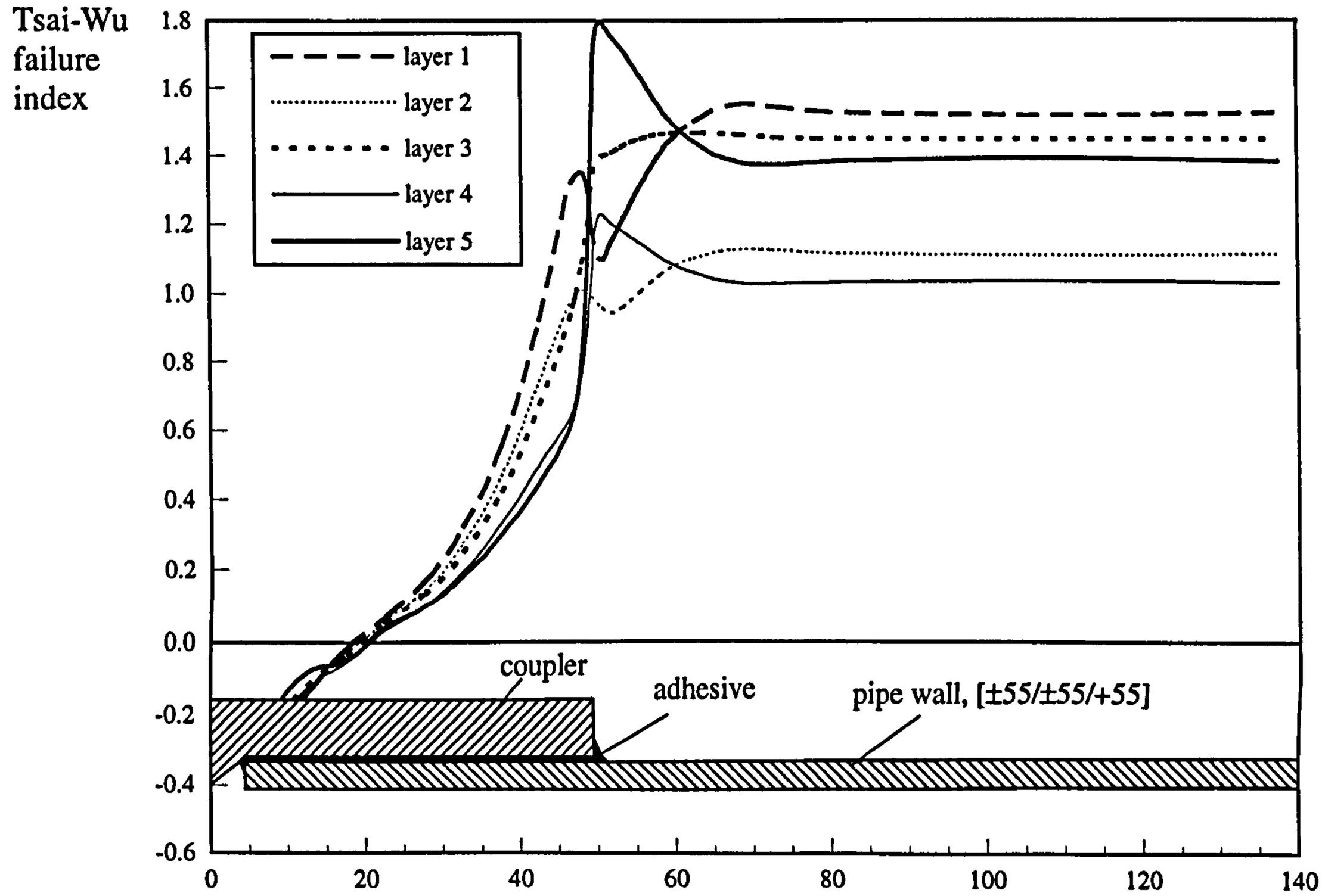

Figure 7.6 Distributions of Tsai-Wu failure indexes along the pipe length after the outer ply has peeled off. The pipe wall consists of five plies $[(\pm 55^{o})_{2}$ $+55^{o}]$. The outer ply corresponds to layer 5 and inner ply to layer 1. 3-D laminated element model was used for the GRE pipe which was subjected to an internal pressure of 15.6 MPa.

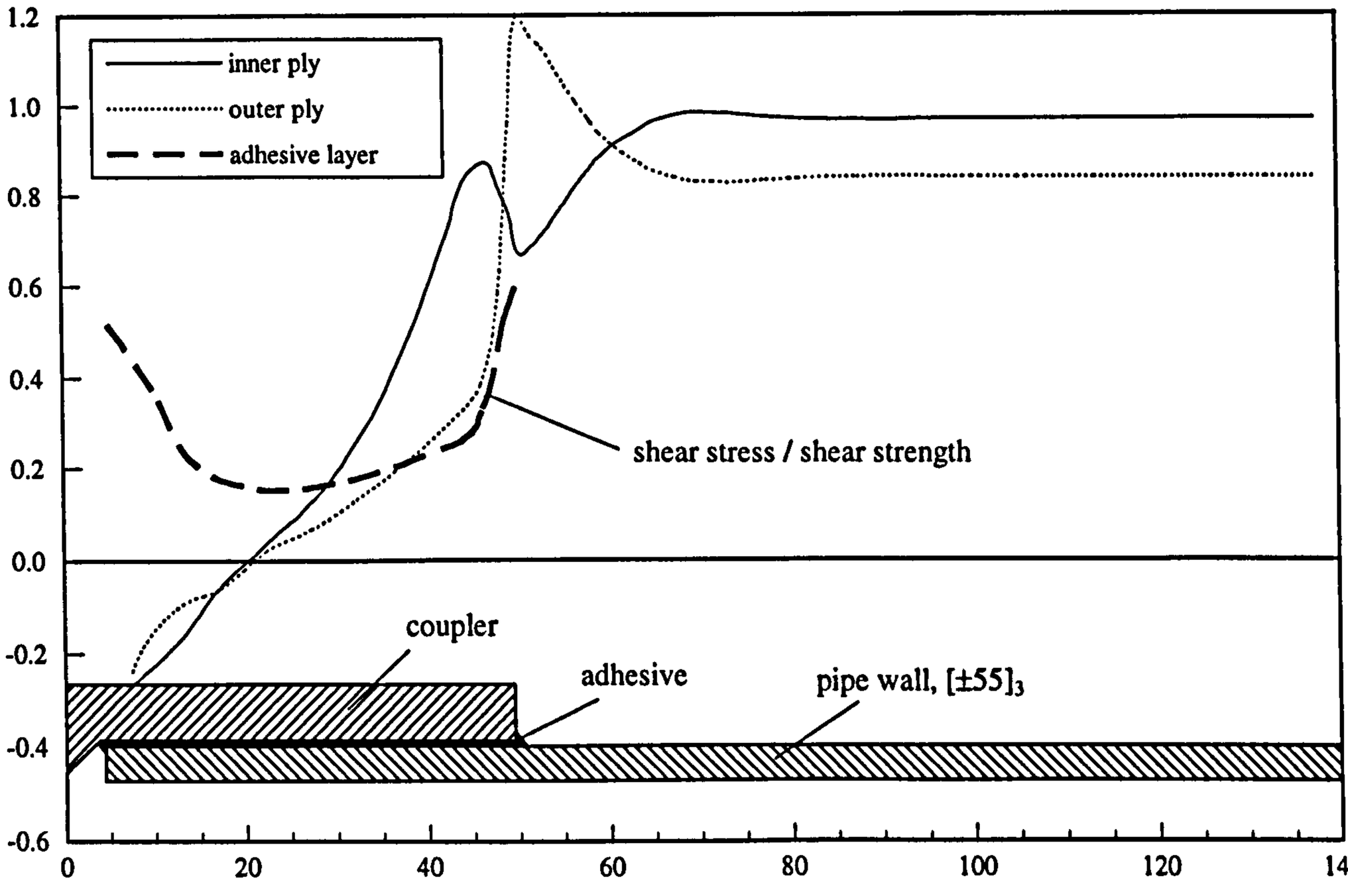

Figure 7.7 Tsai-Wu failure indexes in the structural wall of a six ply pipe $[\pm 55^{o}]_3$ subjected to an internal pressure of 15.6 MPa. The pipe ends were slightly shaved without damaging the outer ply before the joint was assembled.

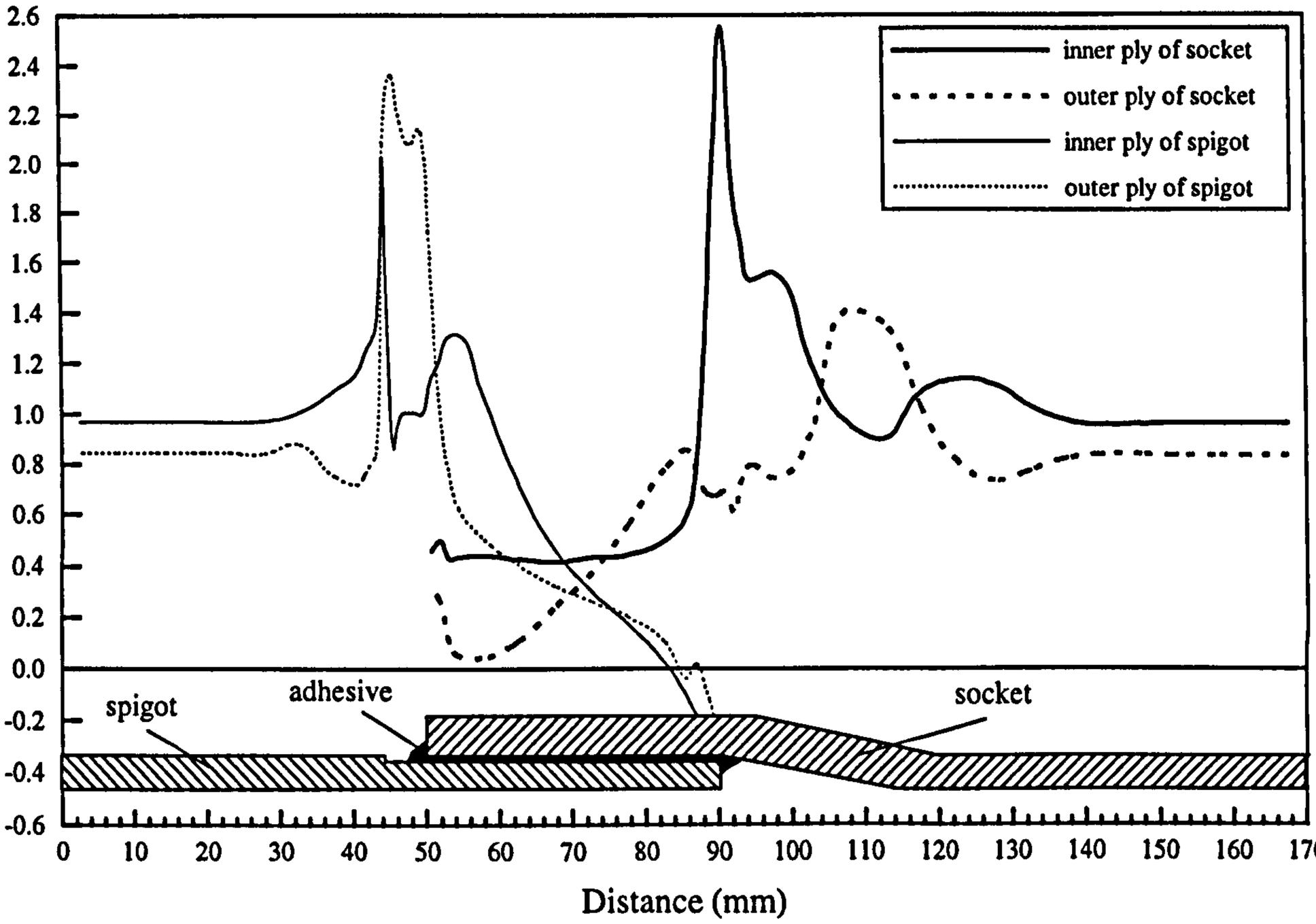

Figure 7.8 Tsai-Wu failure indexes in the structural pipe wall close to the socket/spigot bonded joint subjected to an internal pressure of 15.6 MPa. The pipes have higher Tsai-Wu failure indexes near to the joint than in the other areas.

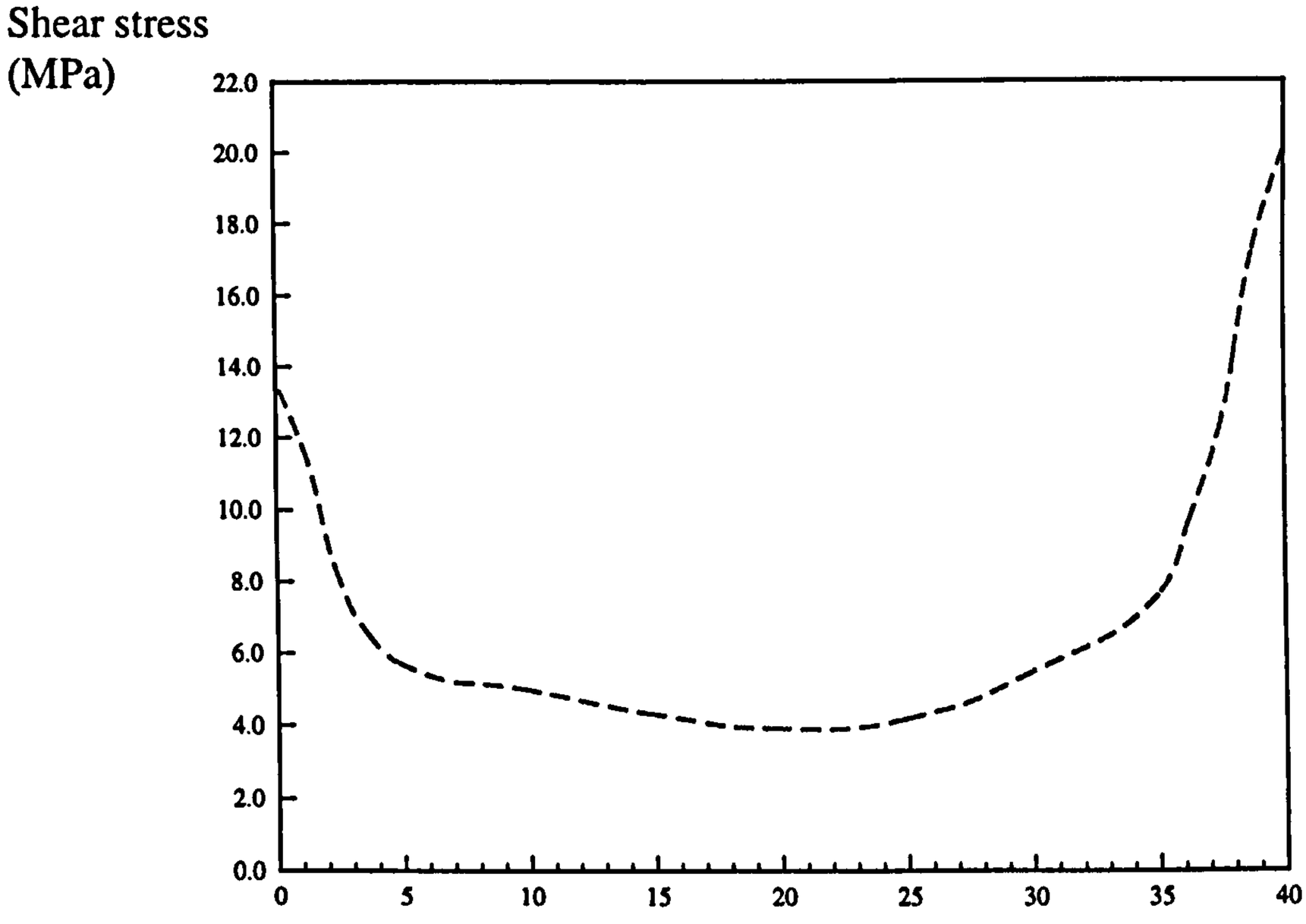

Figure 7.9 Shear stress in the adhesive layer of socket/spigot joint subjected to an internal pressure of 15.6 MPa. Both ends of the bonded interface gave much higher shear stress than the middle area.

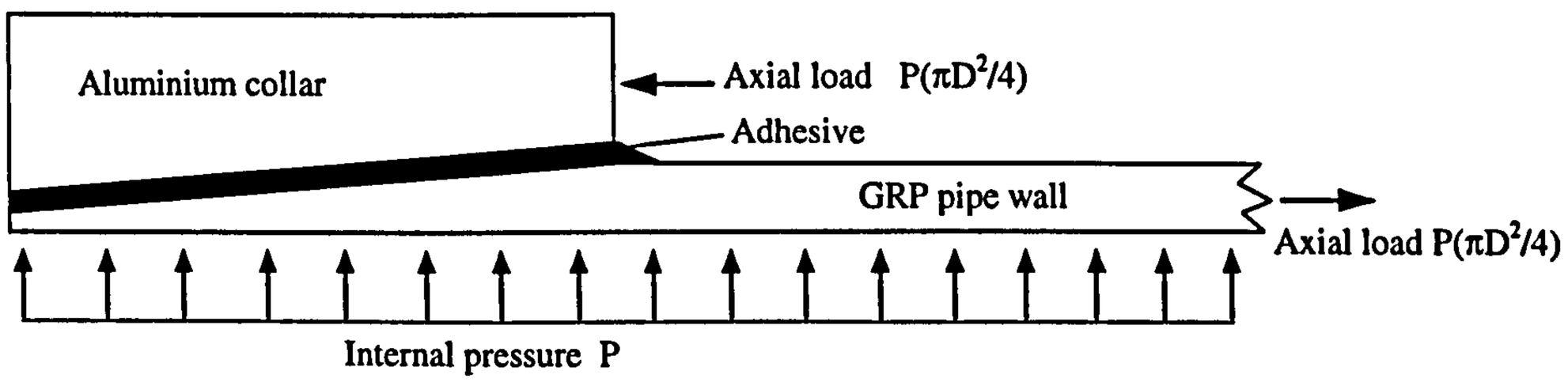

Figure 7.10 GRP pipe with end-fitting subjected to internal pressure. The pipe wall is subjected to a total axial load of $P(\pi D^2/4)$ for a "close-end" specimen.

Figure 7.11 Hoop stresses in the structural pipe wall, resin liner and adhesive layer. Slight stress concentrations appear in the area close to the collar.

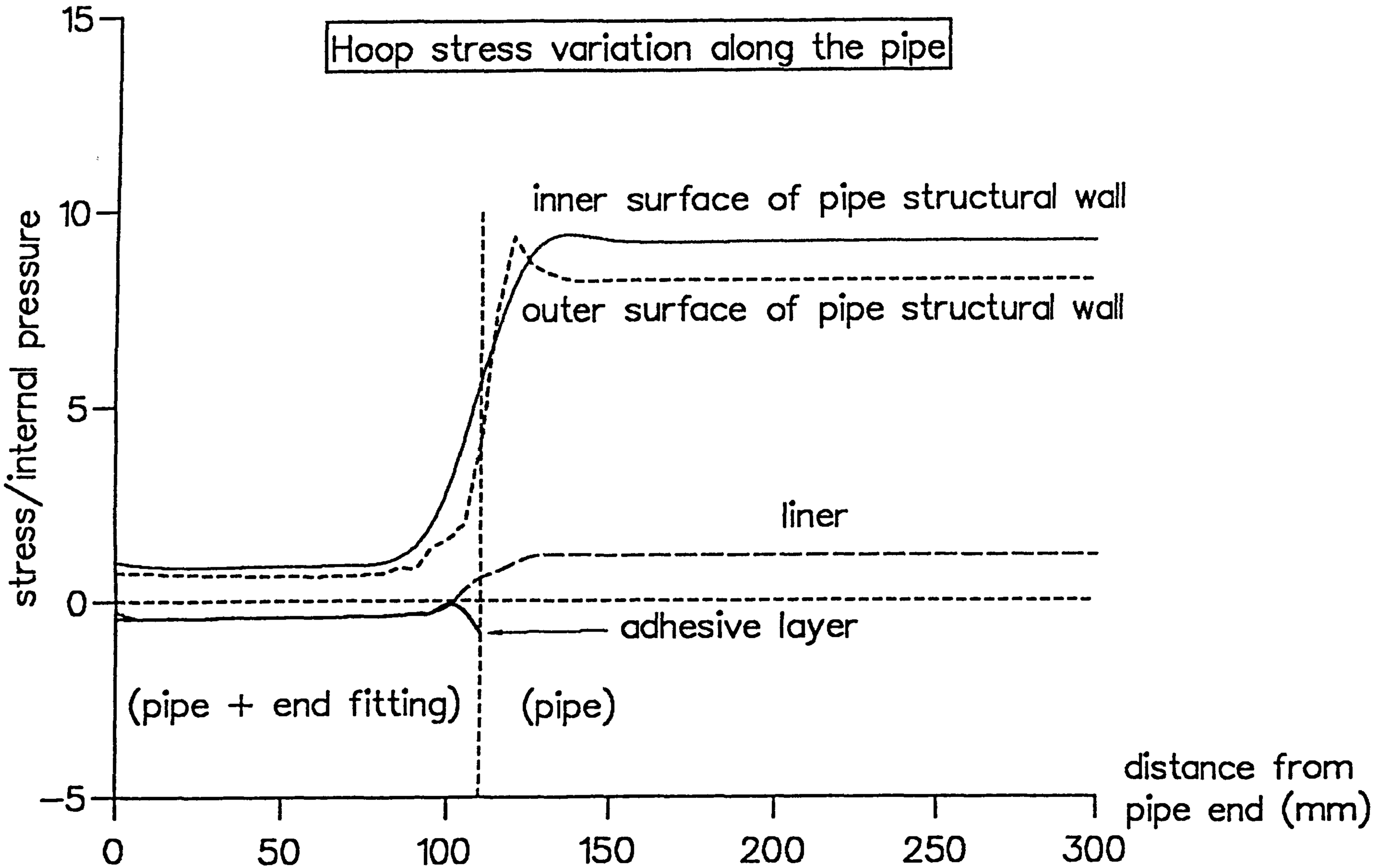

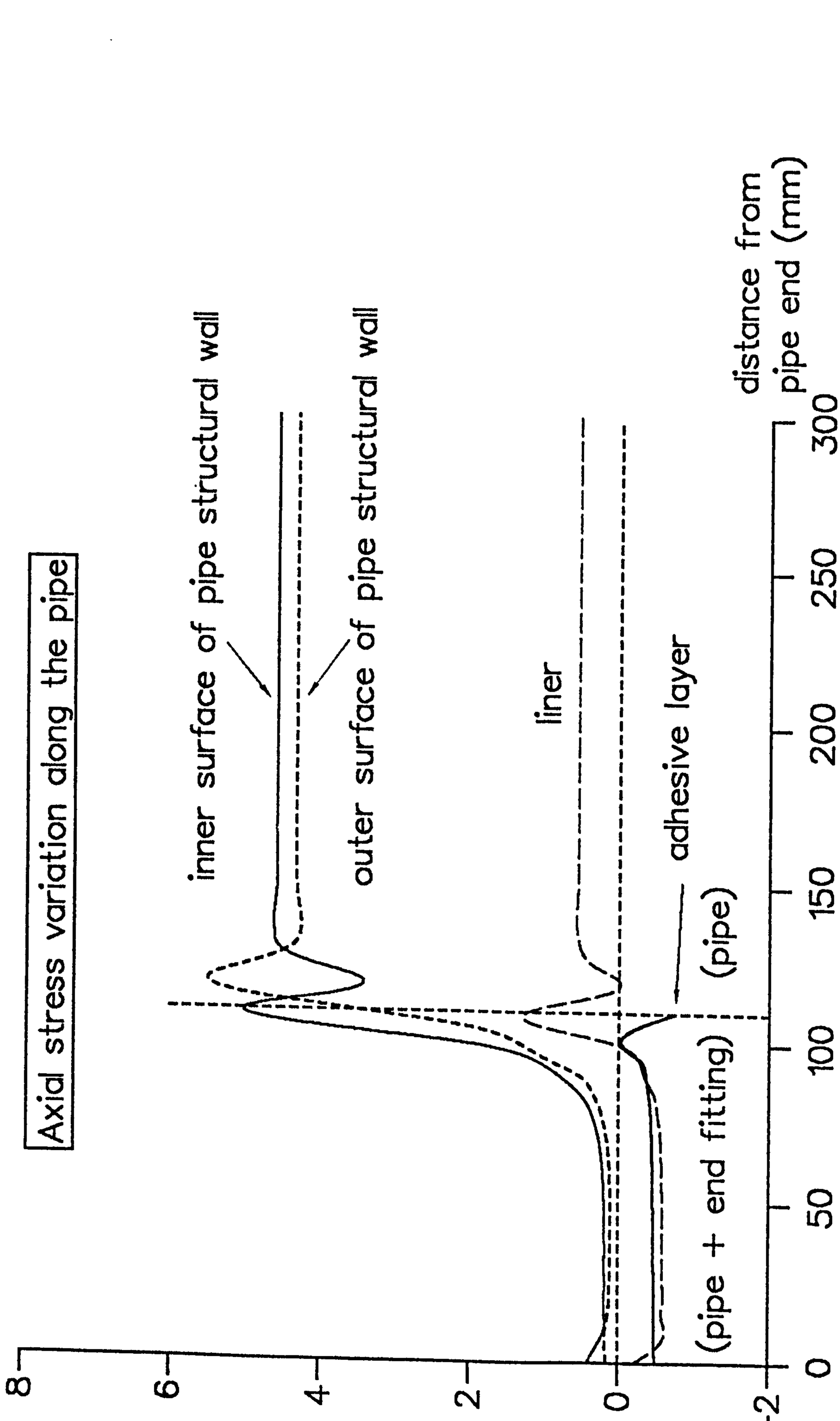

Figure 7.12 Axial stresses in the structural pipe wall, resin liner and adhesive layer. Slight stress concentrations appear in the area close to the collar.

Figure 7.13 Shear stresses in the adhesive layer. The maximum shear stress in the edge of the bonding interface is reduced when the aluminium collar is tapered from inside.

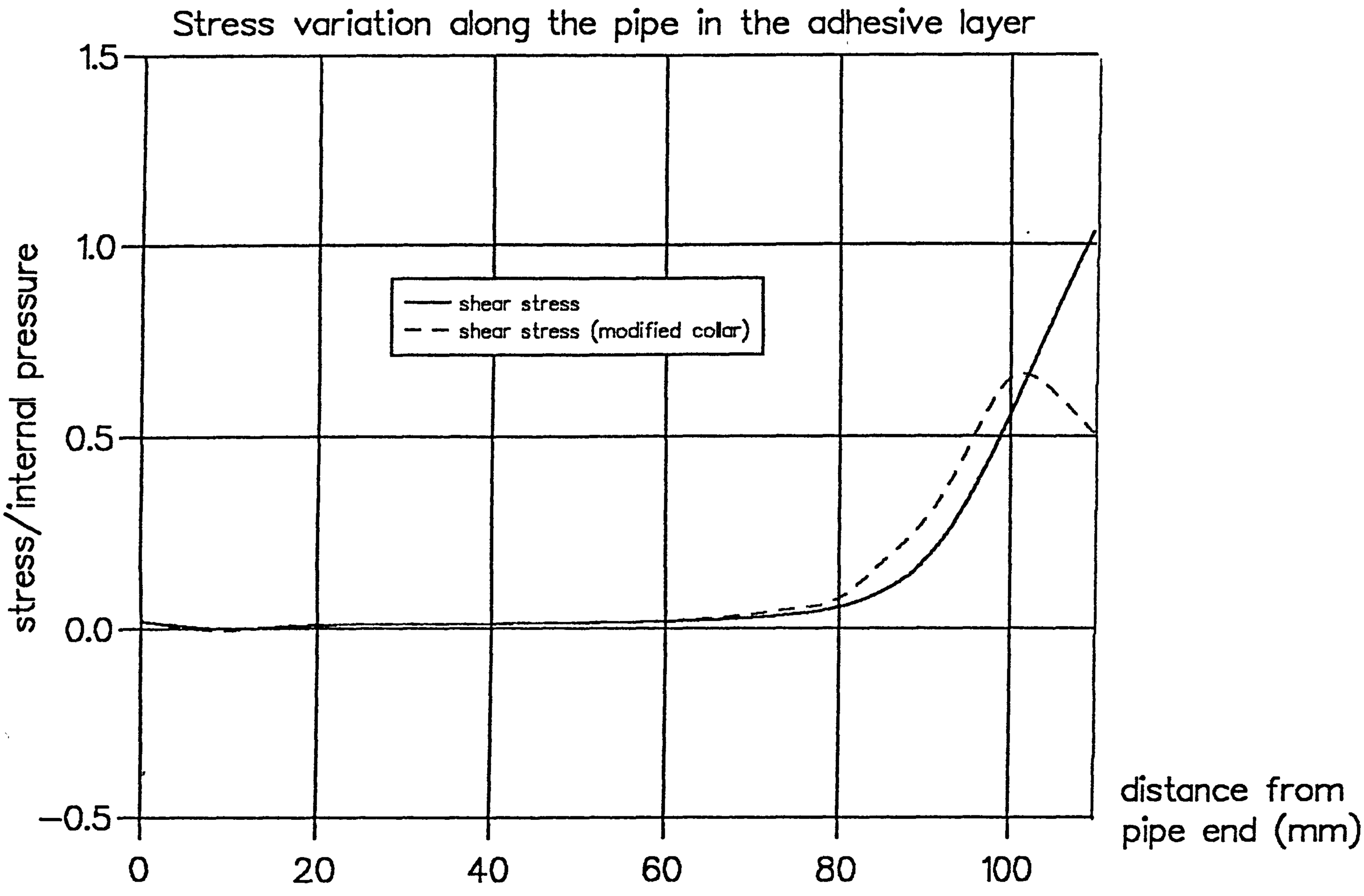

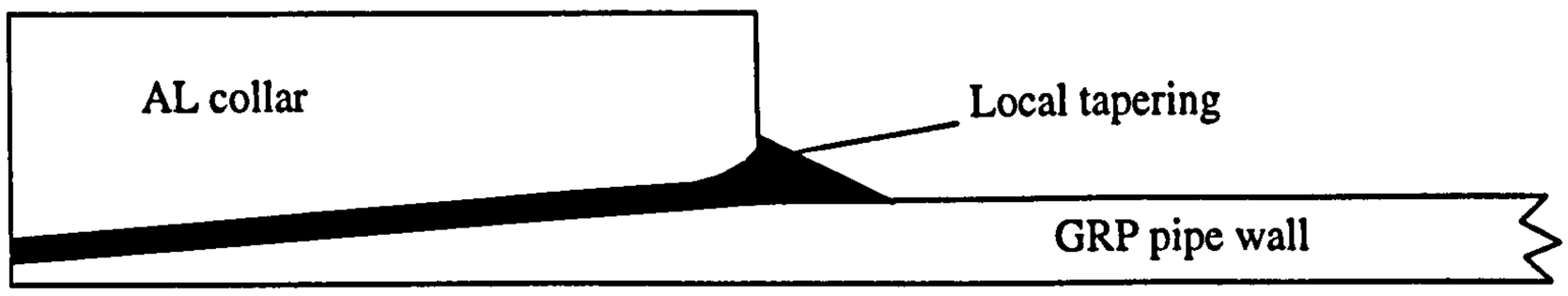

Figure 7.14 End-fitting modified by tapering the aluminium collar from the inside and thus increasing the adhesive thickness locally.

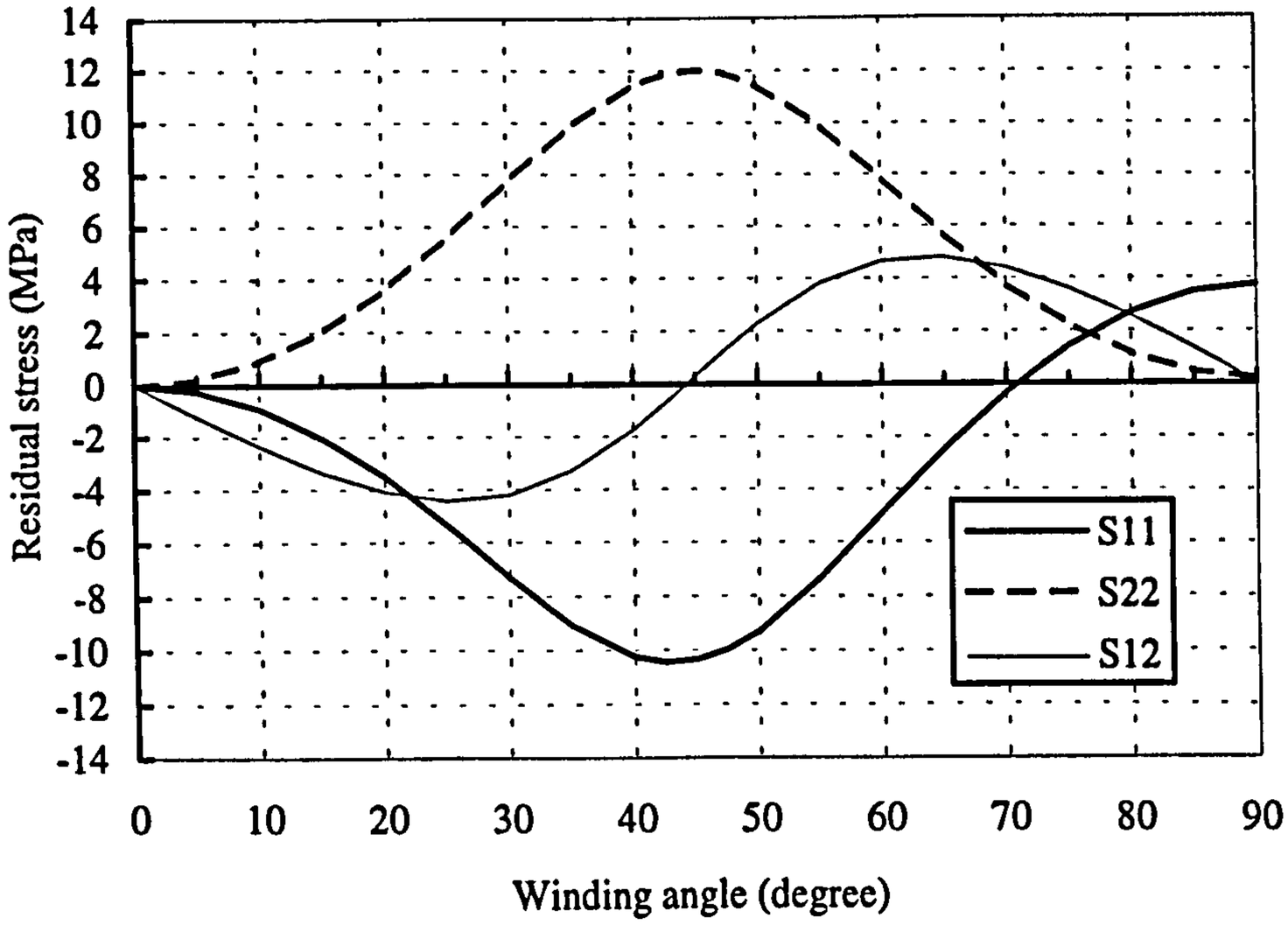

Figure 7.15 Thermal residual stresses induced by curing (ΔT=-150 ^{0}C) in the first ply of a filament wound GRE pipe $[\pm\theta]_3$ with various values of the winding angle θ. The average diameter is 57.2 mm and the wall thickness 3 mm. A pipe with $\pm 45^0$ winding angle has the maximum thermal residual normal stresses. For commonly used $\pm 55^0$ wound pipes, all residual stress components are therefore rather high.

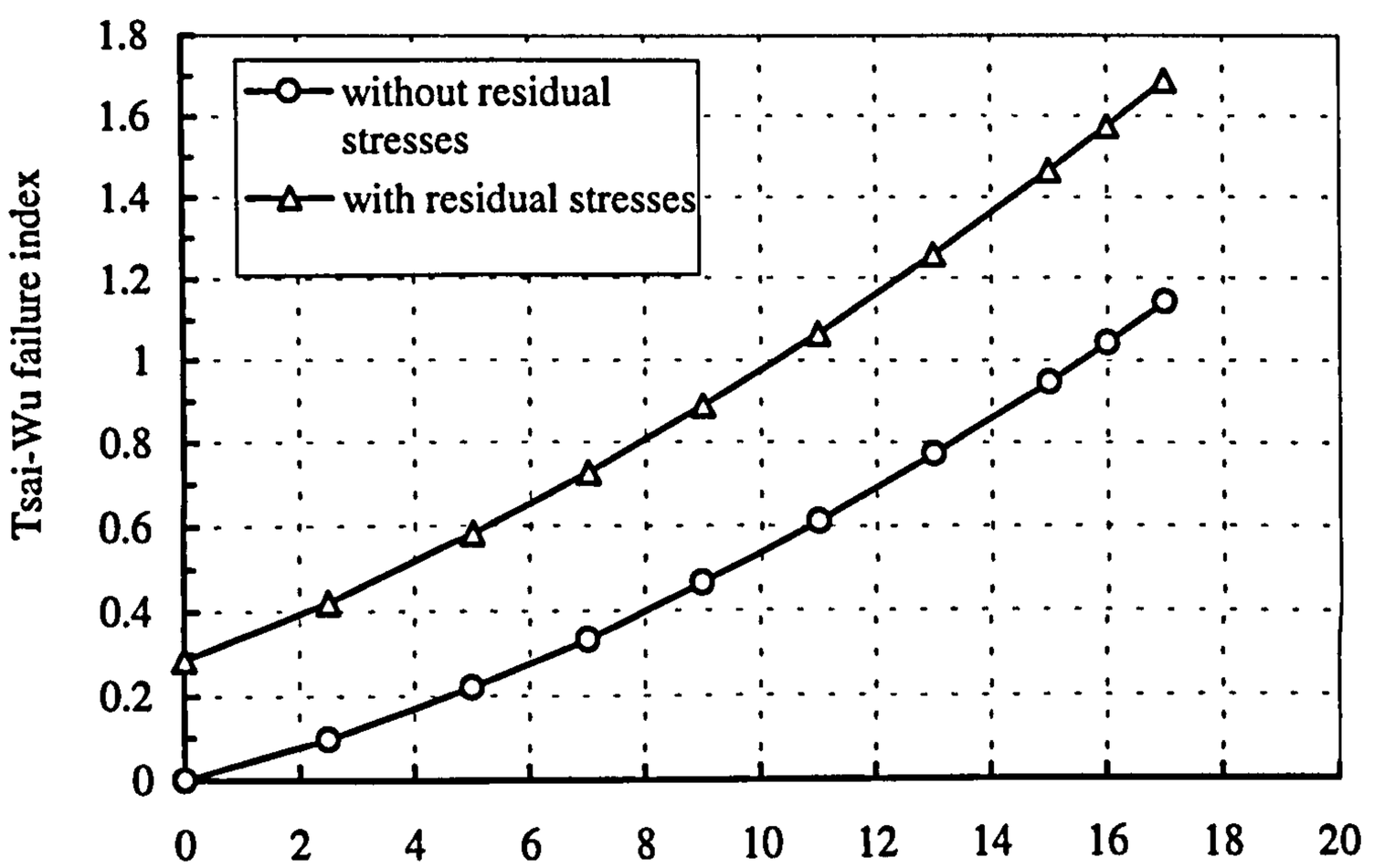

Figure 7.16 Maximum Tsai-Wu failure indexes for the filament wound GRE pipe $[\pm 55°]_3$ (in the first ply) subjected to differing internal pressures. The average diameter is 57.2 mm and wall thickness is 3 mm. According to the Tsai-Wu failure criterion, the failure internal pressure is 15.5 MPa when the thermal residual stresses are not considered, and only 10.2 MPa when the thermal residual stresses are considered. Without considering the thermal residual stresses, the pipe strength will therefore be overestimated.

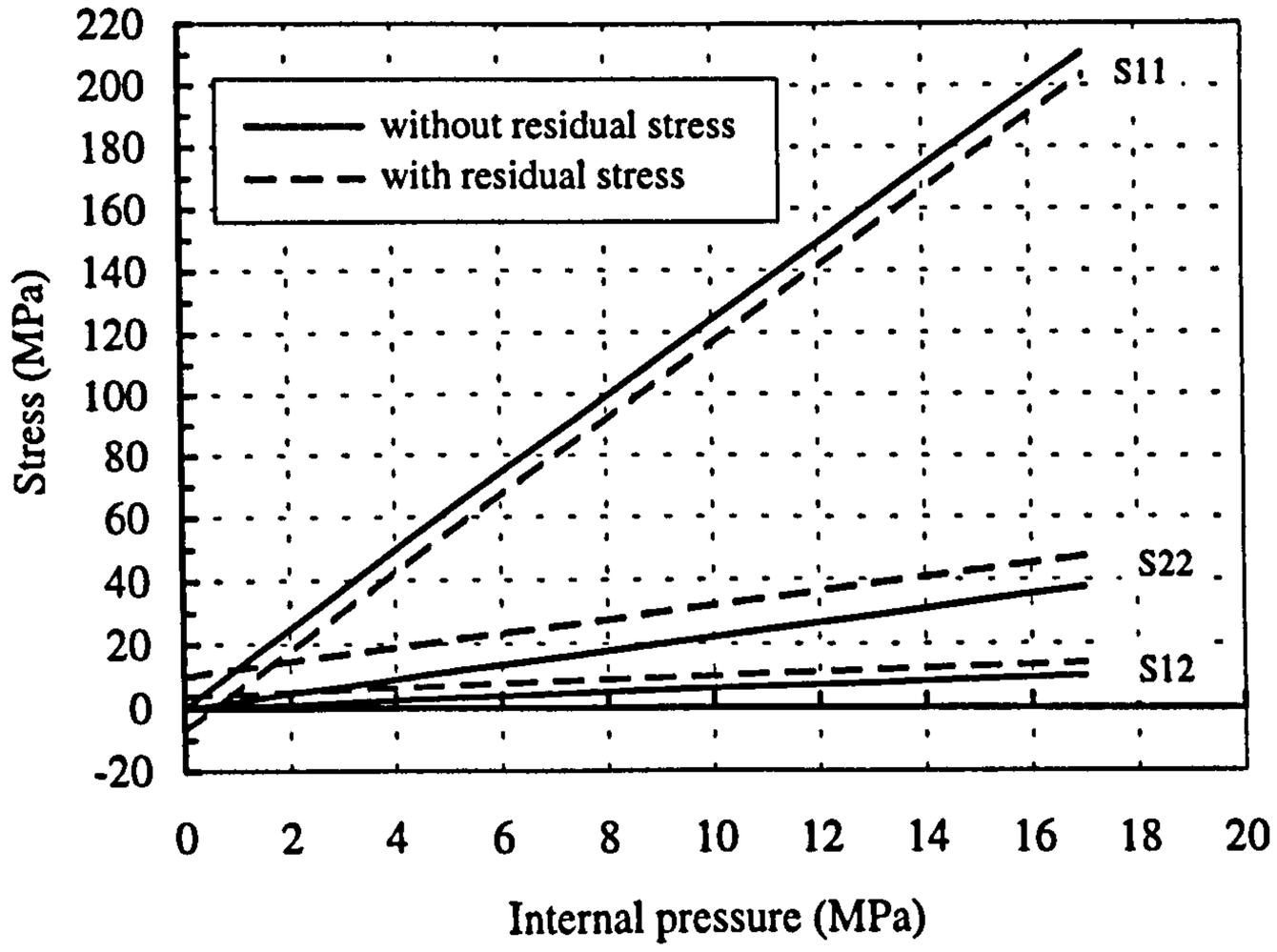

Figure 7.17 Stress components in the first ply of the structural wall of a filament wound GRE pipe $[\pm 55°]_3$ subjected to differing internal pressures. The first ply has the highest ply stresses. Solid lines represent the results obtained without consideration of thermal residual stresses and dashed lines represent those for which the residual stresses were considered. The pipe has an average diameter of 57.2 mm and wall thickness of 3 mm.

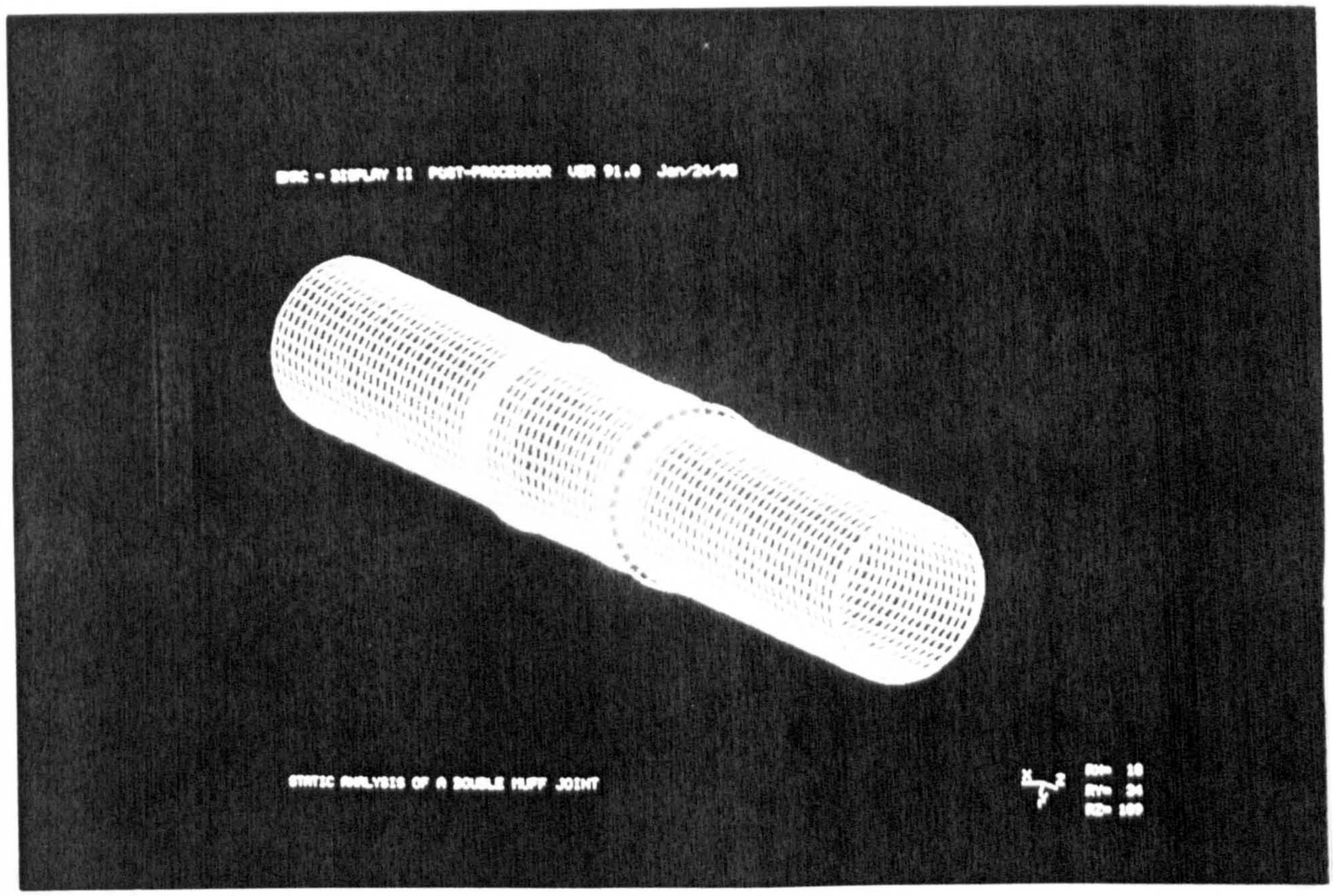

Figure 7.18 Rotation about the pipe axis occurring when a filament wound GRE pipe was subjected to internal pressure.

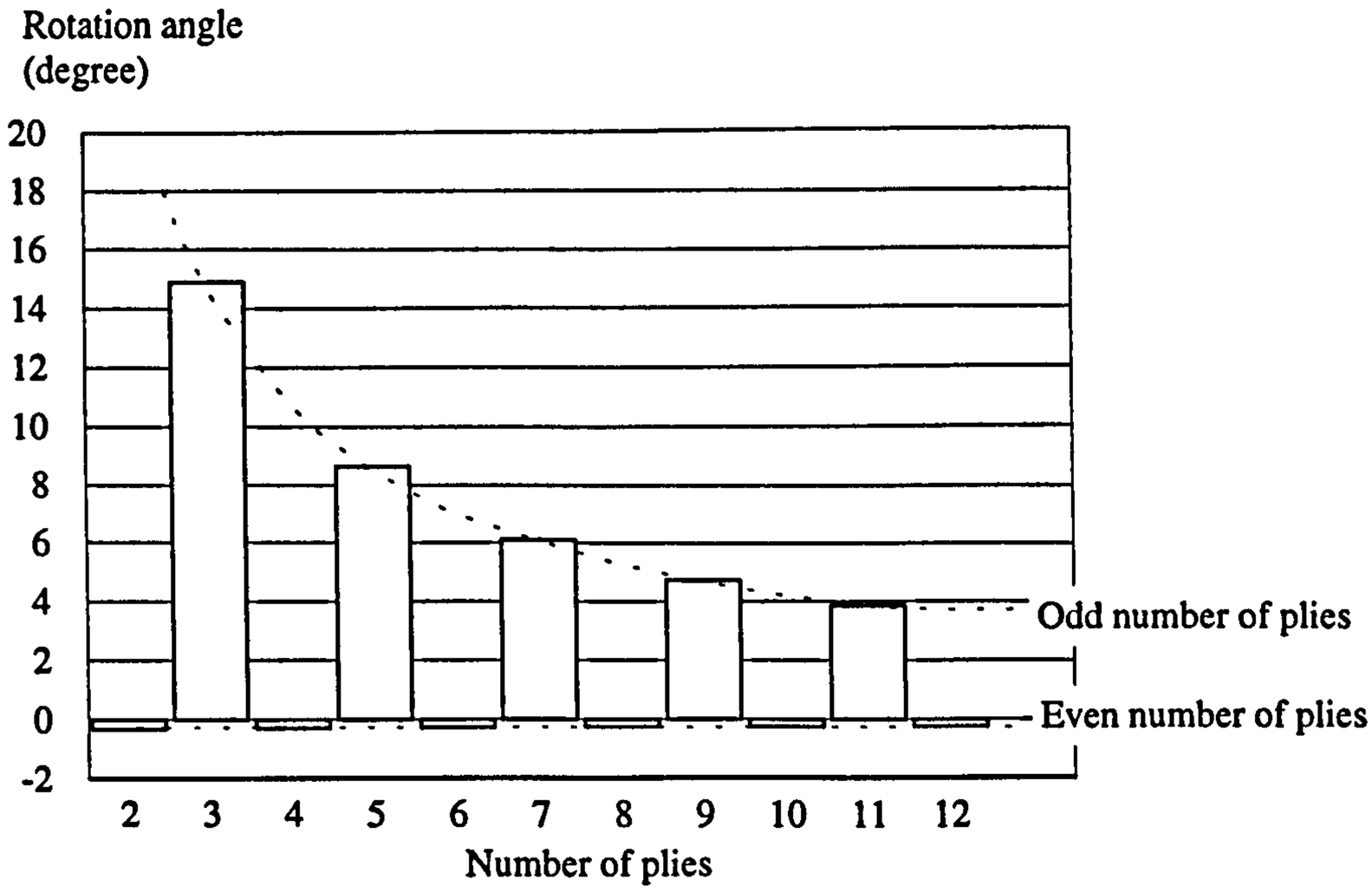

Figure 7.19 Rotation angles about the axis of the six metre long pipes with various numbers of plies ($+55^0/-55^0/+55^0/-55^0/\ldots\ldots$). All pipes had the same ply thickness of 0.5 mm, average diameter of 57.2 mm and nominal hoop stress of 148.7 MPa.

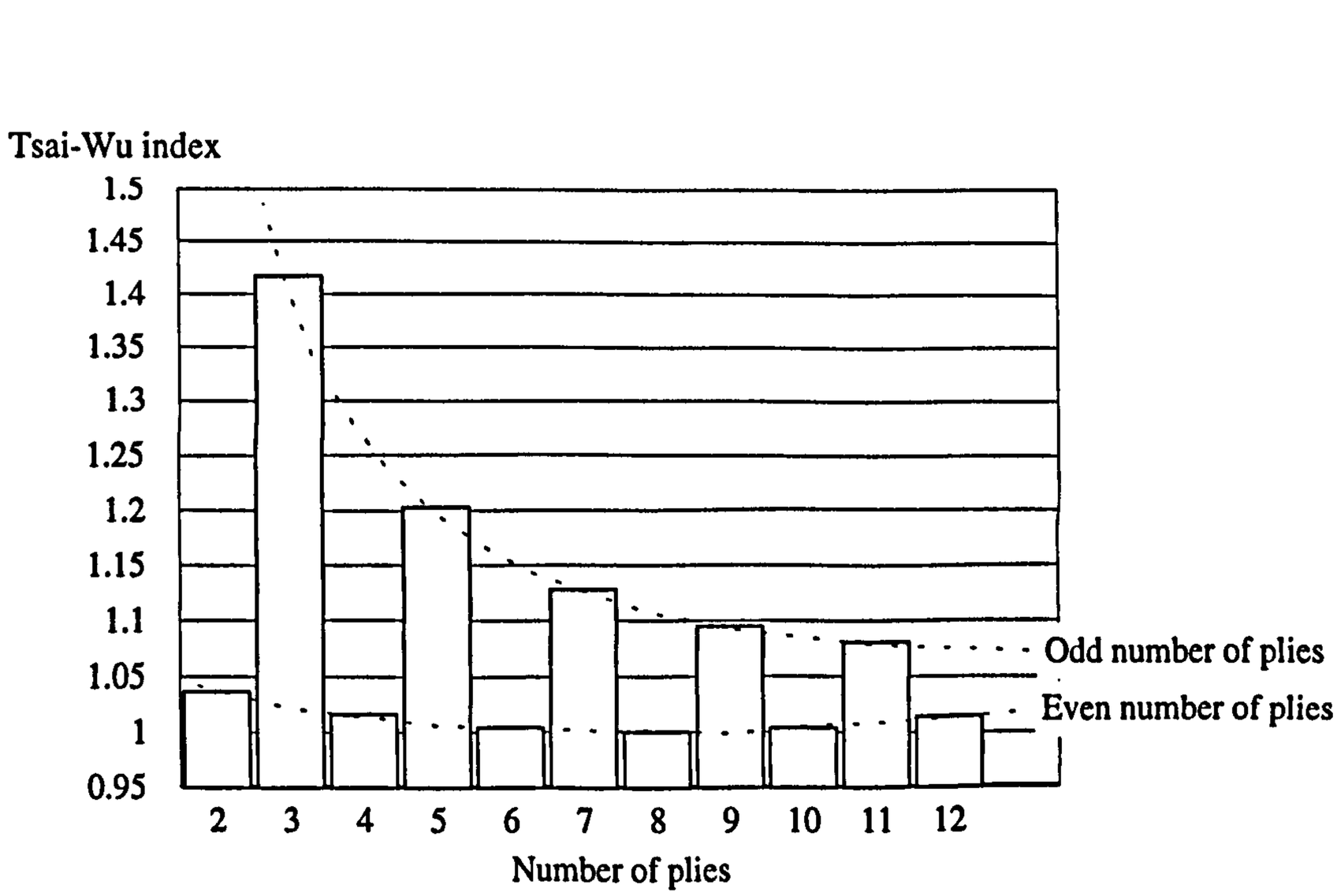

Figure 7.20 Tsai-Wu failure indexes in the structural wall of filament wound glass reinforced epoxy pipes with various numbers of plies ($+55^0/-55^0/+55^0/-55^0/\ldots\ldots$) and pipe wall thickness. Ply thickness was 0.5 mm, average diameter 57.2 mm and nominal hoop stress 148.7 MPa.

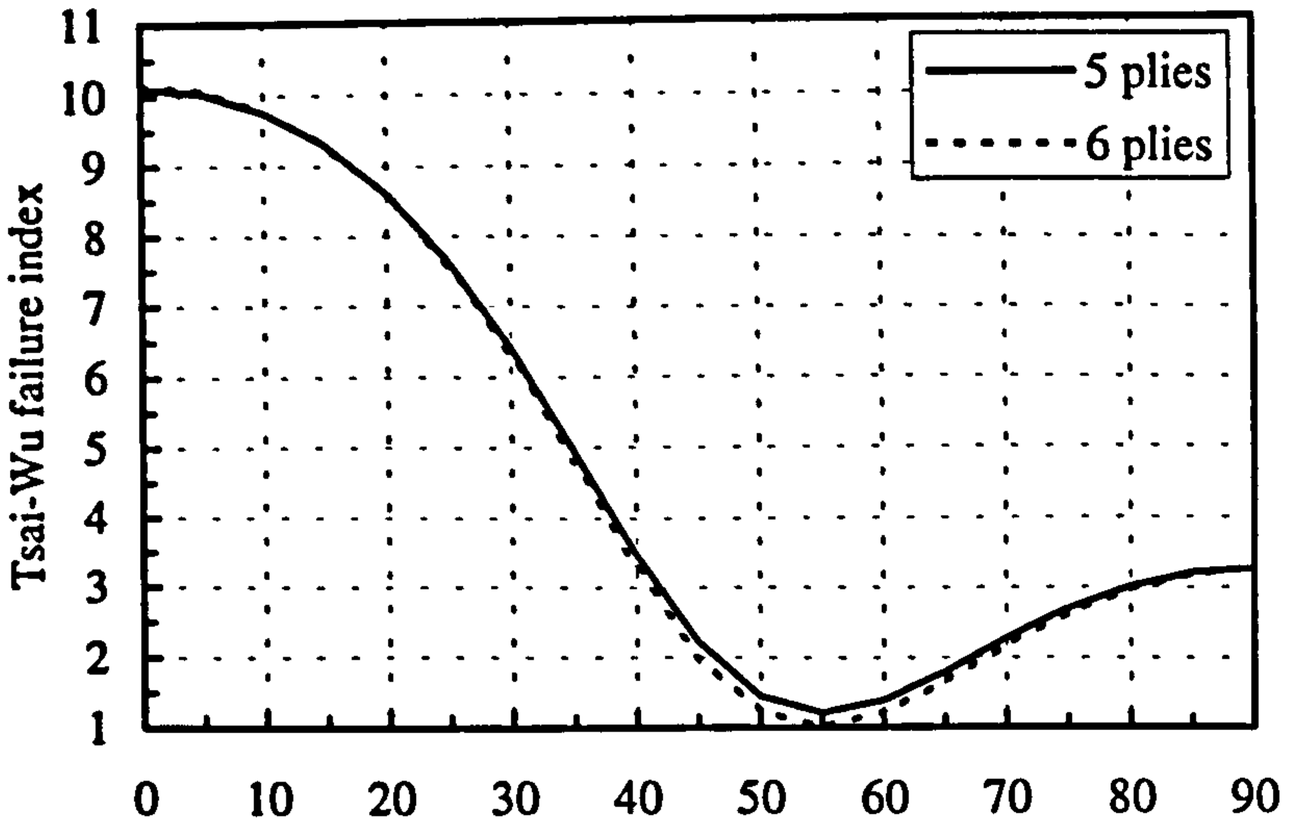

Figure 7.21 Tsai-Wu failure indexes in the structural wall of a filament wound GRE pipe $[\pm\theta]_3$ and $[(\pm\theta)_2/+\theta]$ with various winding angles. The pipes were subjected to an internal pressure and have the same nominal hoop stress of 148.72 MPa and nominal axial stress of 74.36 MPa. The average pipe diameter was 57.2 mm and ply thickness 0.5 mm.

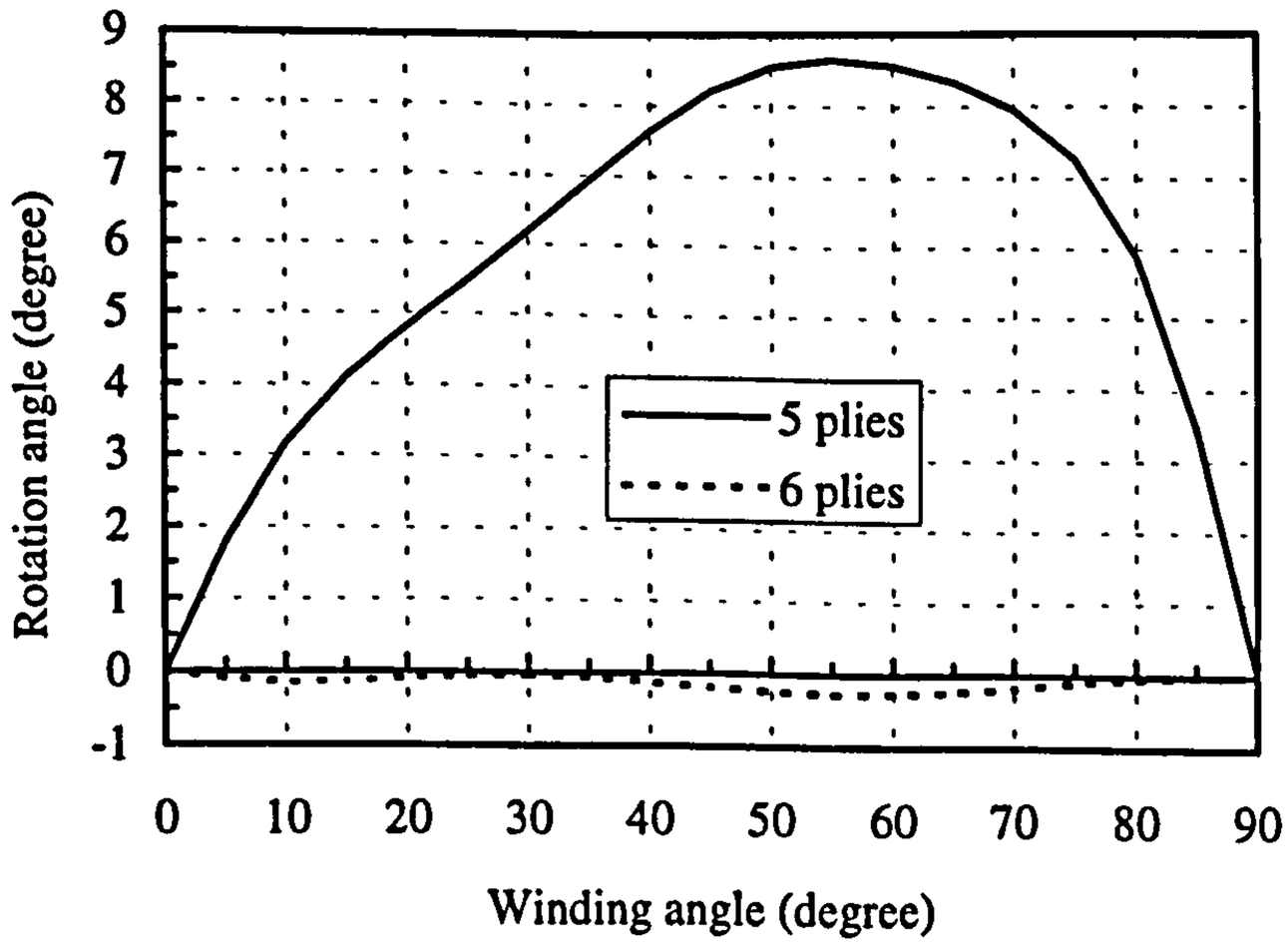

Figure 7.22 Rotation angle about the axis of the six metre long filament wound GRE pipes $[\pm\theta]_3$ and $[(\pm\theta)_2/+\theta]$ with various winding angles. All pipes were subjected to internal pressures and had a nominal hoop stress of 148.72 MPa and nominal axial stress of 74.36 MPa. The average pipe diameter was 57.2 mm and ply thickness 0.5 mm.

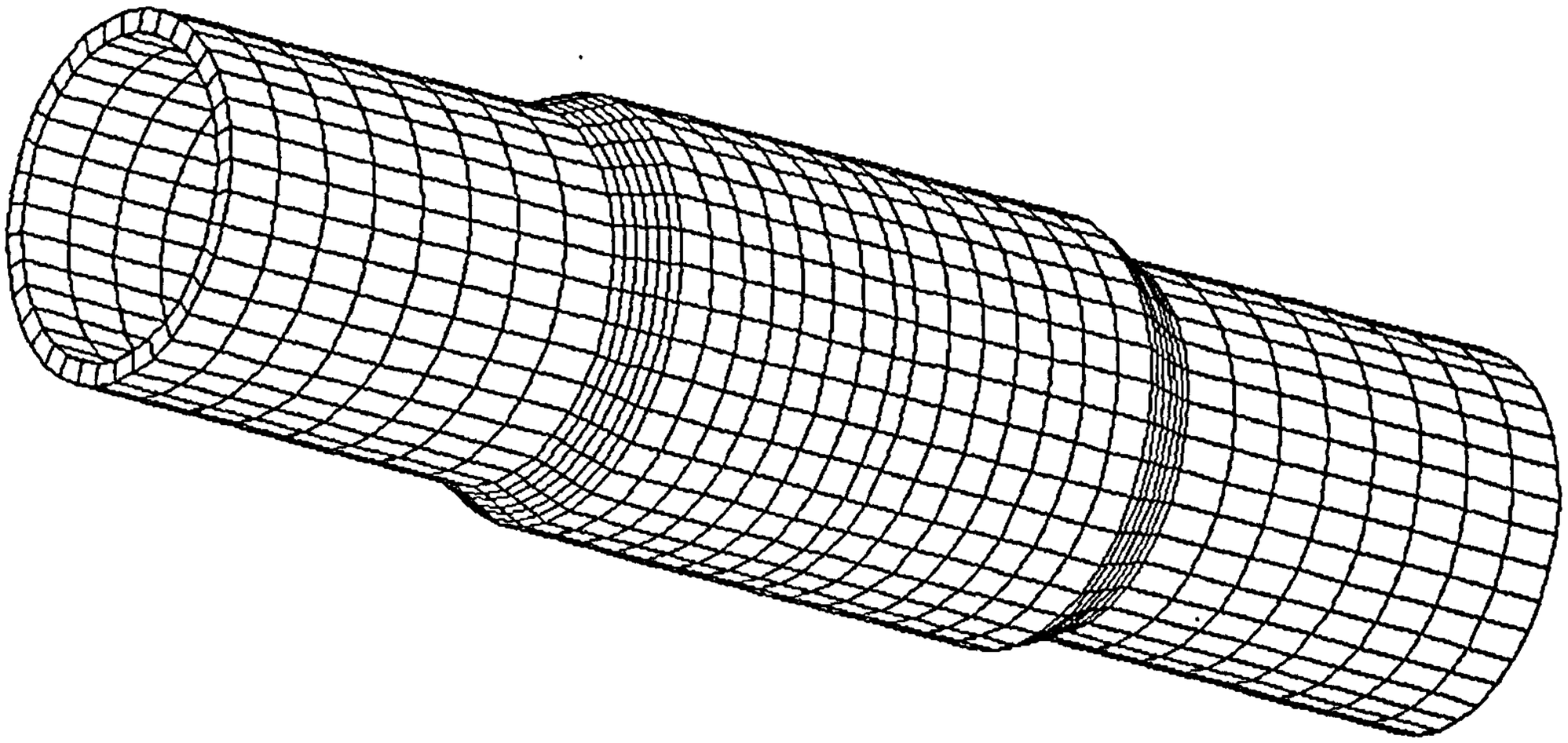

Figure 7.23 Finite element mesh for GRVE laminated joint.

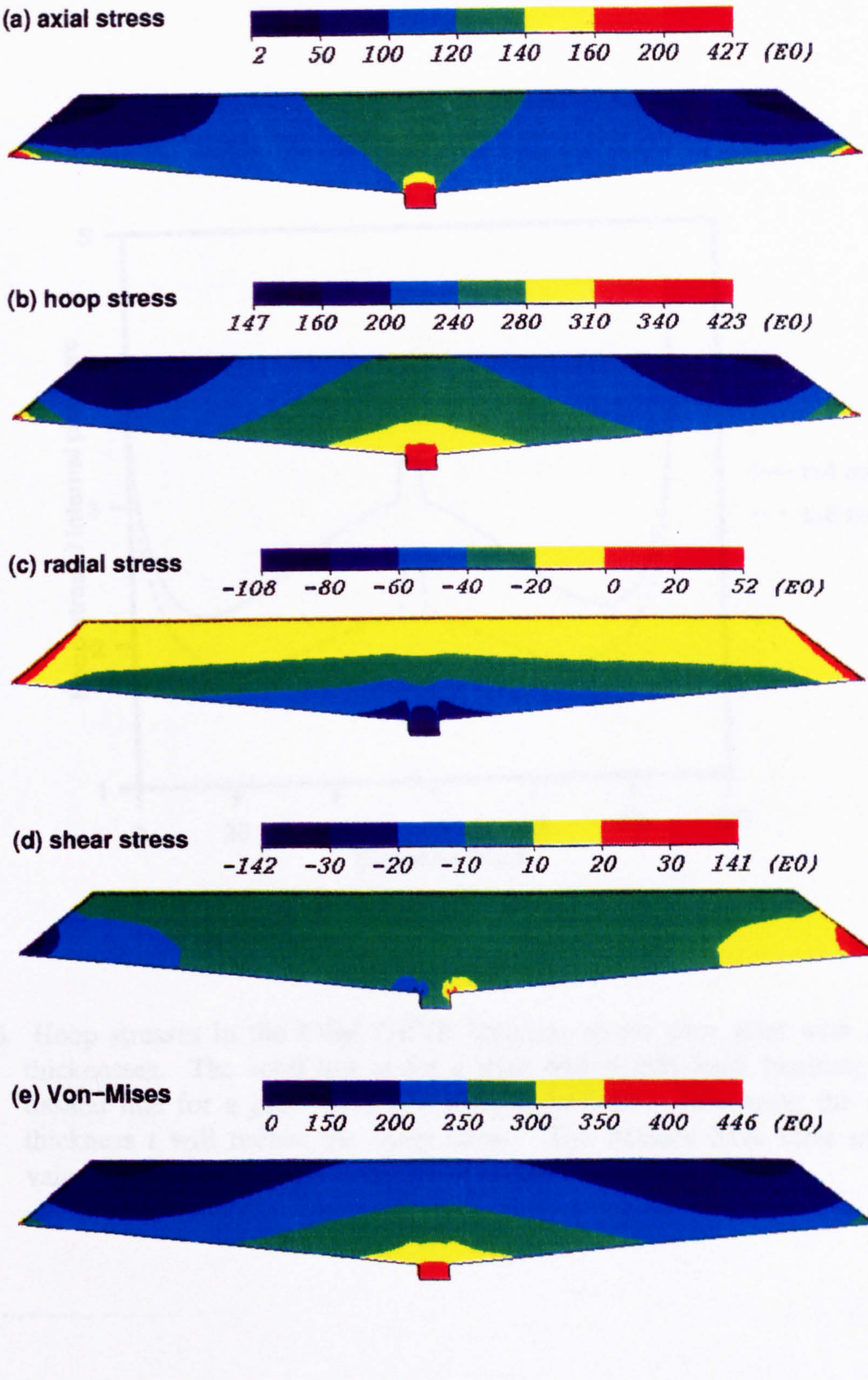

Figure 7.24 Stress component contours in the glass CSM/vinyl ester laminate when the pipe is subjected to an internal pressure of 100 MPa. It is found that the middle part of the joint suffers high stresses. High stresses also exist in the small local areas of both tapered end–tips of the joint.

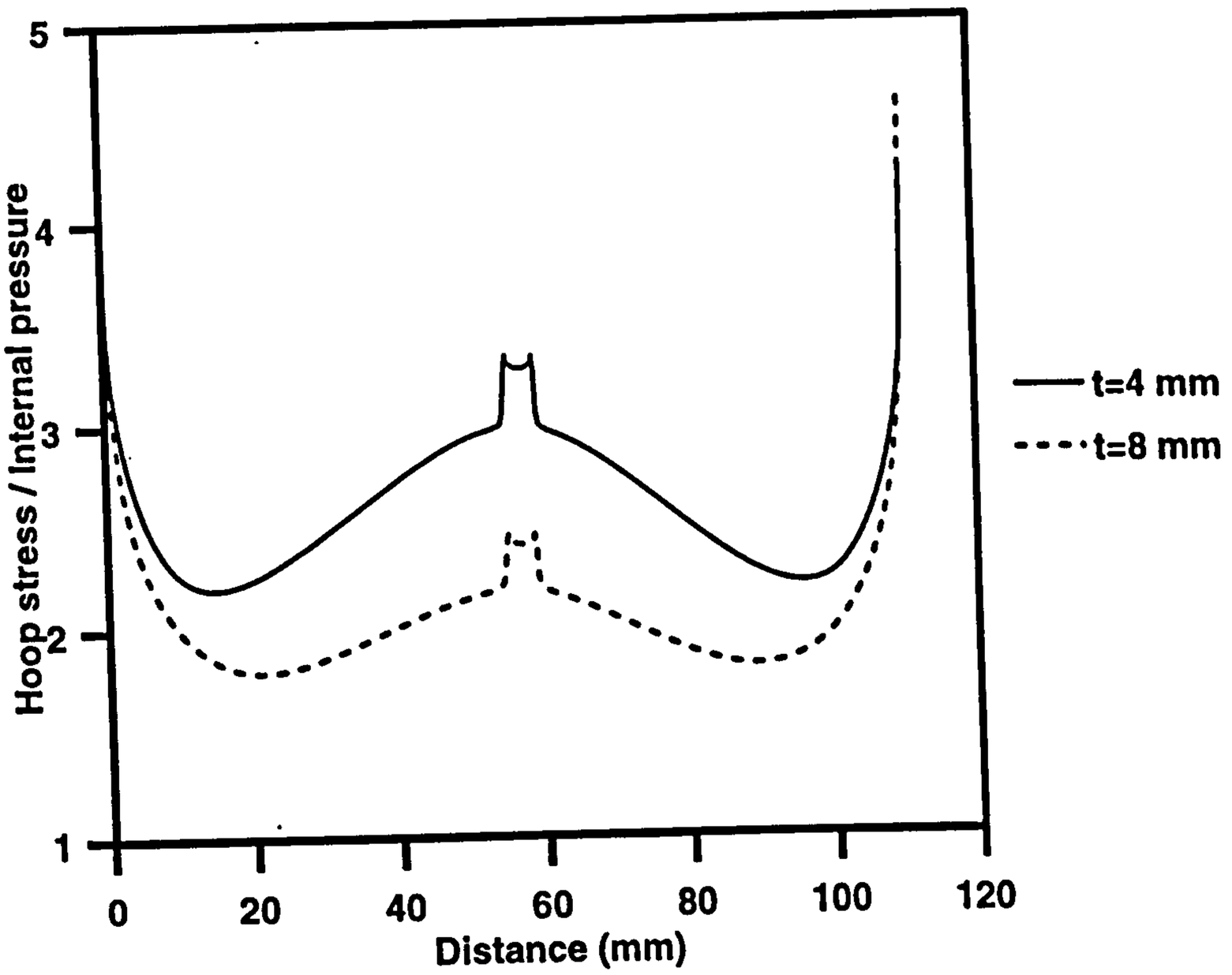

Figure 7.25 Hoop stresses in the CSM GRVE laminate of the pipe joint with different thicknesses. The solid line is for a joint with 4 mm thick laminate and the dashed line for a joint with 8 mm thick laminate. Increasing the laminate thickness *t* will reduce the hoop stress. The stresses have their maximum values at the inner layer.

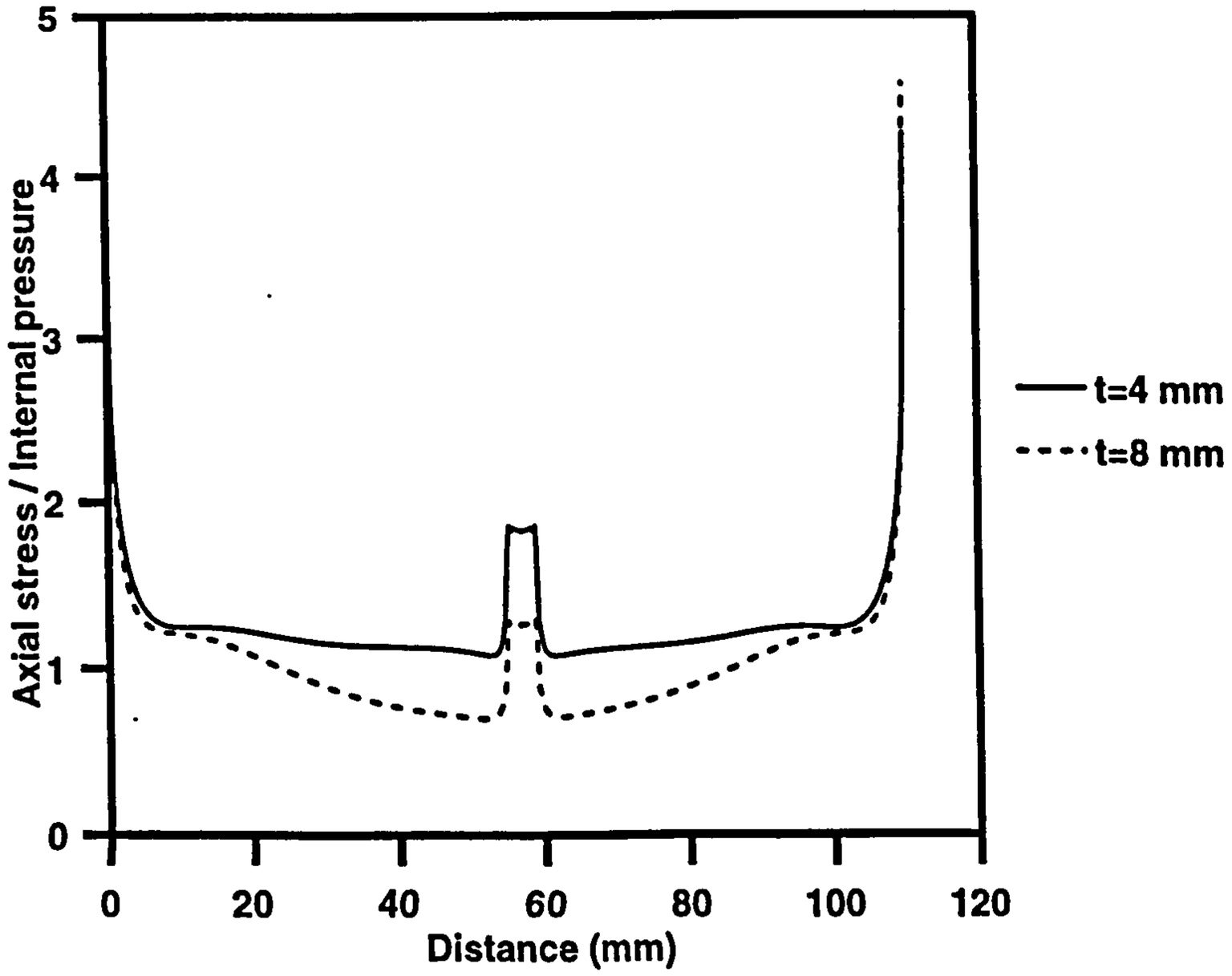

Figure 7.26 Axial stresses in the CSM GRVE laminate of the pipe joint with different thicknesses. The solid line is for a joint with 4 mm thick laminate and the dashed line for a joint with 8 mm thick laminate. Increasing the laminate thickness *t* will reduce the hoop stress. The stresses have their maximum values at the inner layer.

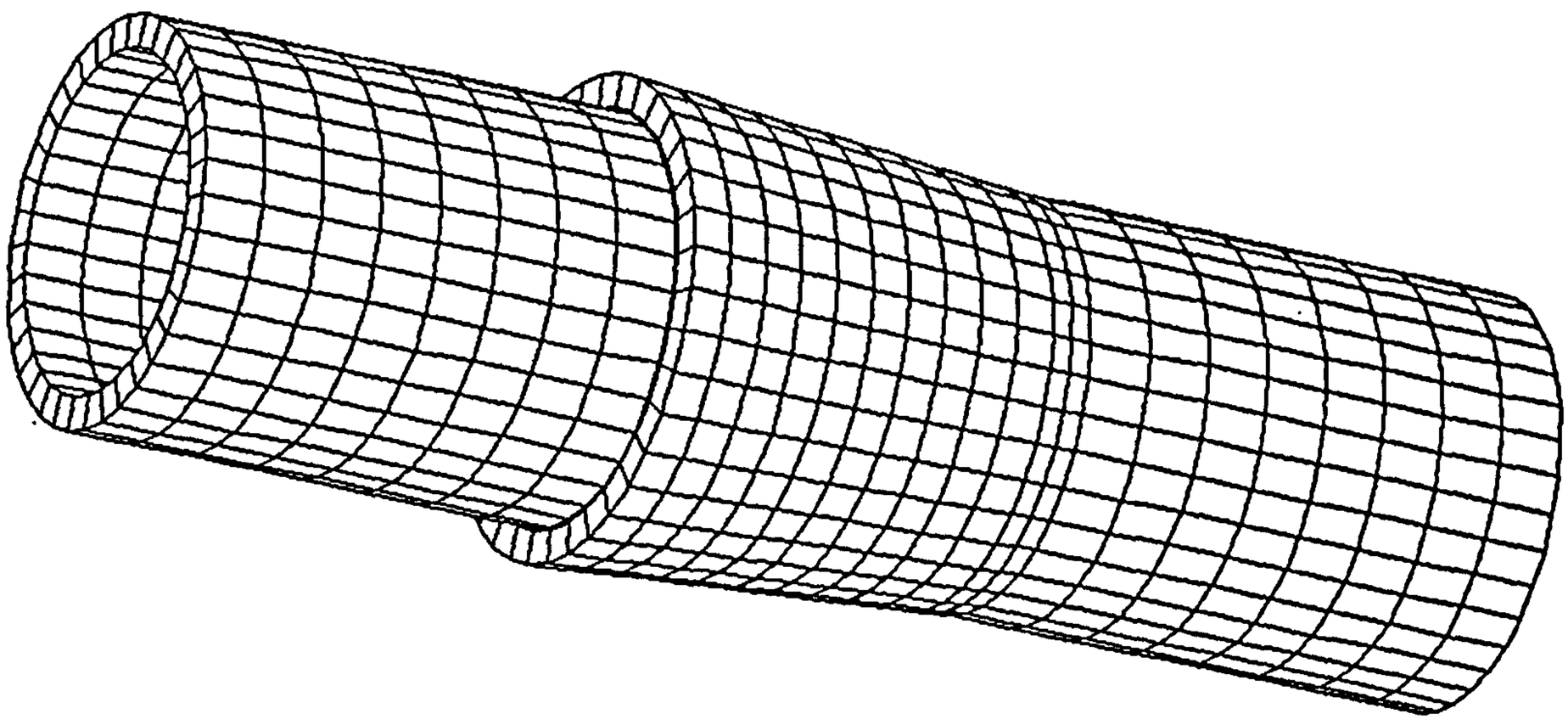

Figure 7.27 Finite element mesh for GRVE socket/spigot joint.

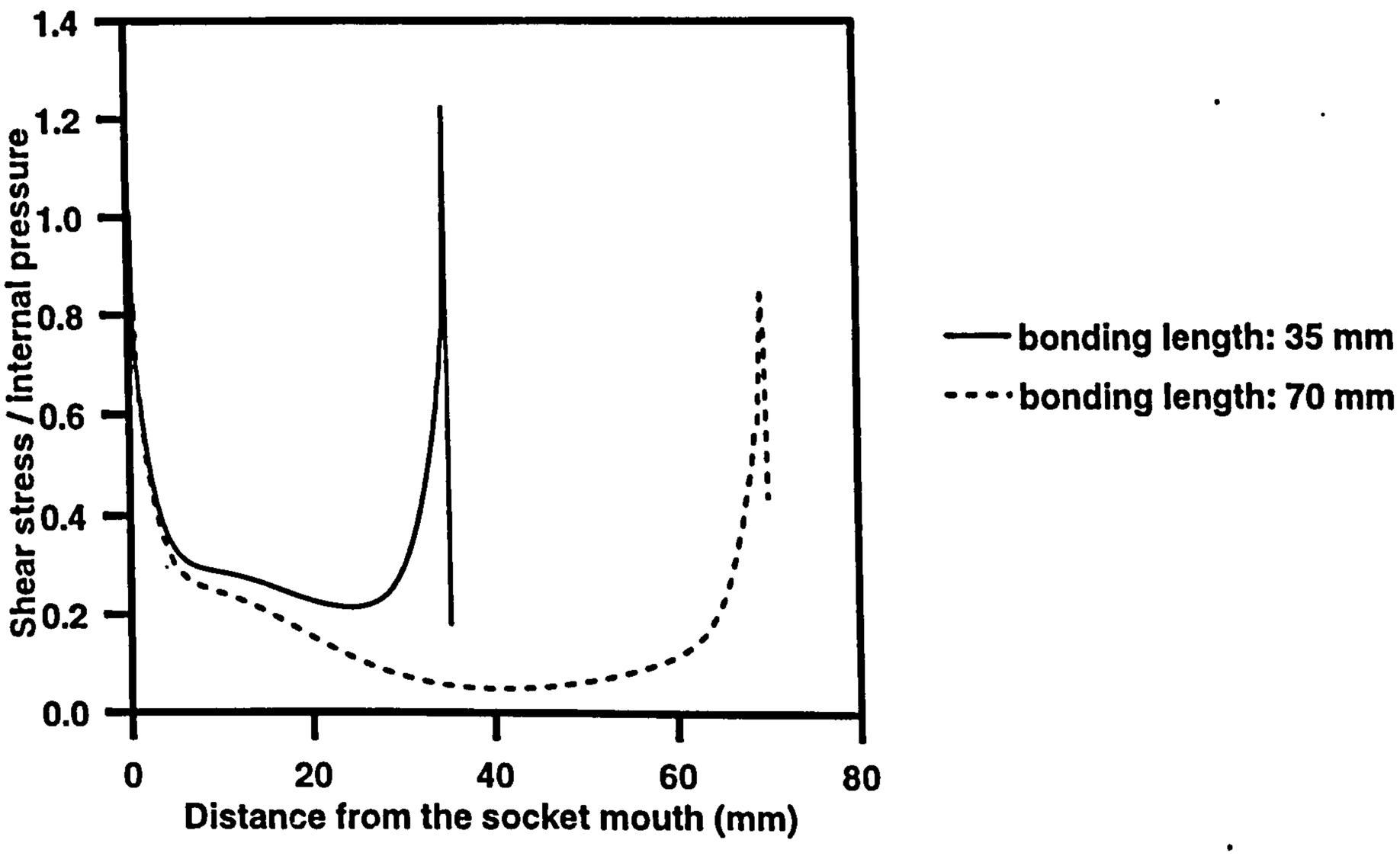

Figure 7.28 Shear stress distributions in the adhesive layers of the socket/spigot joints with different bonding lengths. The joint with a bonding length of 70 mm generally gives lower shear stresses than the joint with a shorter bonding length of 35 mm.

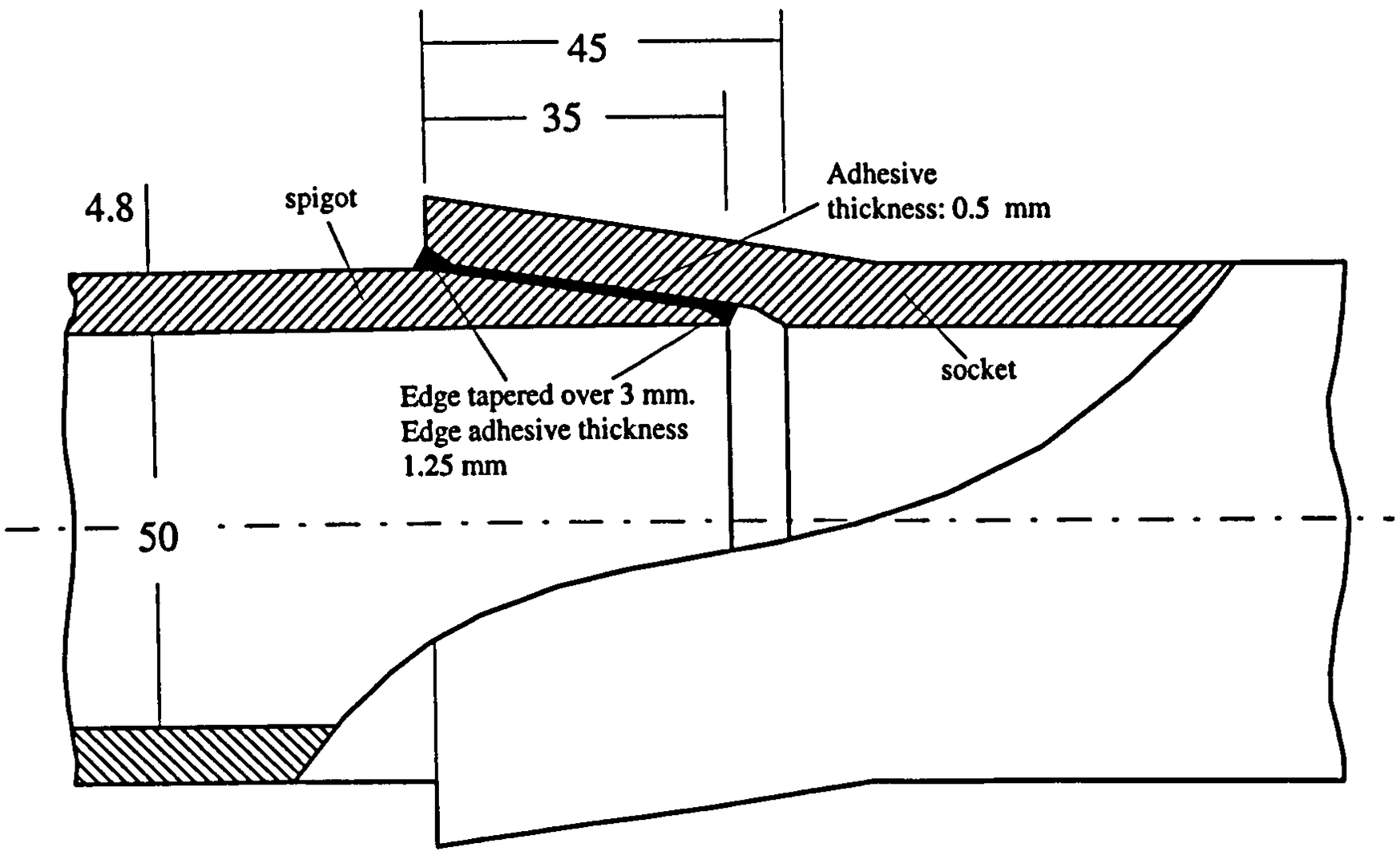

Figure 7.29 Suggested modification for socket/spigot (taper to taper) adhesively bonded joint. The socket and spigot mouths are tapered and the edge thickness of the adhesive are 2.5 times of the normal adhesive thickness. (Units for dimensions: mm)

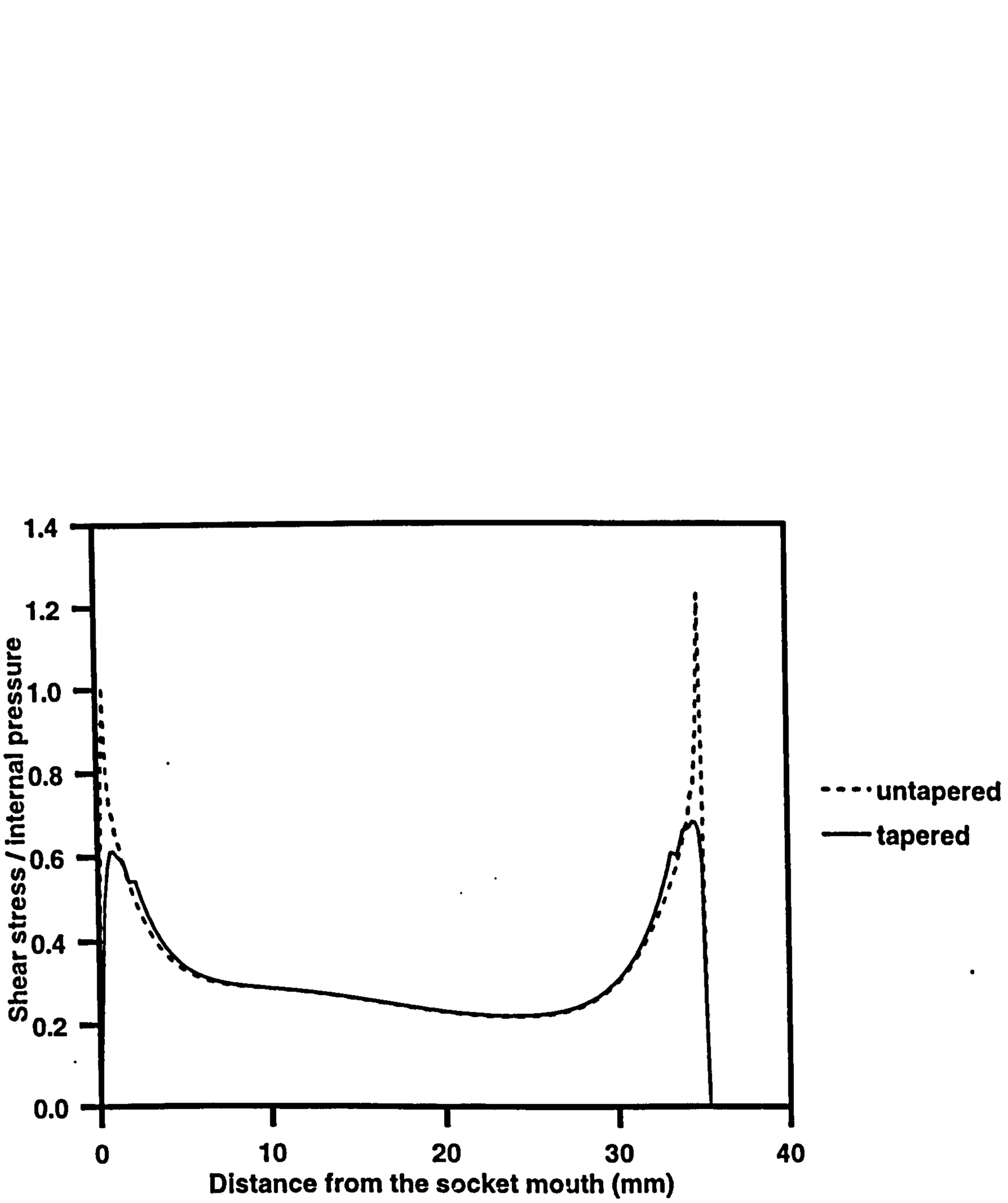

Figure 7.30 Shear stress distributions in the adhesive layers of the socket/spigot joints with or without modification. The dashed line shows the results for the untapered joint which has a uniform adhesive thickness (0.5 mm) over the whole bonding length, as shown in Figure 6.8. The solid line is for the tapered joint in which the socket and spigot mouths are tapered and the local adhesive thickness at the ends of the bonding line is 2.5 times the normal adhesive thickness (0.5 mm). The bonding length along the pipe axle is 35 mm.

CHAPTER EIGHT

CONCLUSIONS

Extensive experimental research has been carried out on filament wound glass reinforced plastic pipes and joints. The aims of these tests were to supply data for British Gas plc and to obtain confidence for the application of these products to offshore structures. Three dimensional finite element numerical analyses have also been conducted for these pipes and joints. The purposes of the numerical work were to understand the responses of the pipes and joints to internal pressure and to explain the damage and failure developed in them during the experiments.

The scheduled test programme was completed successfully and satisfactory experimental results were obtained. Fatigue tests were conducted for low cycles only (≤ 20,000 cycles) to simulate the loading conditions of fire systems on offshore platforms.

The following conclusions can be drawn from this work:

(I) Experimental Method

In this thesis, an experimental method has been developed for the static and fatigue tests of GRP pipes subjected to internal pressures. This method has been proved to be successful by a large number of tests on various pipes and joints.

Test Rig

Tests of GRP pipes subjected to internal pressure are generally much more difficult than conventional coupon specimen tests. Although a standard test method has been suggested in ASTM D2143, a special test rig is required to be built. Therefore, a fatigue test rig was

designed and built from scratch. This rig has been verified to be good by hundreds of hours of testing.

In the rig, a test fluid of some type must be used to transmit the pressure. A difficulty often encountered is the leakage of fluid which releases the system pressure. A precondition of a successful test is that the entire system has been perfectly sealed. However, the seal situation changes as the internal pressure and pressure cycle increase. Although the rig has been sealed very well at low pressure, fluid may leak under high pressure conditions or after a certain number of cycles due the pipe expansion and other deformations. Special sealing designs were in the rig which worked satisfactorily under high pressures of up to 70 MPa and for long time fatigue testing.

Another characteristic of the testing of GRP pipes subjected to internal pressure is the low loading speed for static tests or low loading frequency for fatigue tests. The pressurisation speed depends on the volume of the specimen and the size of the hydraulic pump. The rig built for the present work can achieve a maximum pressurisation speed of 100 MPa per minute for a pipe containing 2 litres of fluid. The pressure frequency also depends on the range of the pressure cycle. For a pipe with 2 litres of water, the maximum achievable frequency of cyclic pressure with a range of 0-10 MPa is 10 cycles per minute.

End Grips

Well-designed end grips were essential for successful tests on pipes, which should avoid end leakage and end failure. The cast resin style designs in the published literature were found to be unsuitable for the strong commercial pipes in the current test programme. The modified design using adhesive bonding used in this research was successful. In addition, the new design is more economical, time saving and is easy to manufacture.

Potential Risks

Since the tests involved hazardous equipment and operations, it was the responsibility of the user of the methods reported in this thesis to establish appropriate safety practices and to apply

limitations for certain cases. In order to help other workers avoid any potential risks, the user's experiences are summarised as follows:

(a) Incompressible fluid must be used as the medium of pressurisation. Air or other type of compressible media must be removed from entire system.

(b) A safety device or closure must be used to isolate the system, particularly the pipes to be tested, from any humans or equipment around.

(c) Safety valves should be used to release the pressure when it has reached the maximum working pressure of the rig.

(d) The rig should be operated strictly by well trained people.

(II) Experimental Results

All of the pipes and joints tested showed sufficient strengths for application to fire water systems on offshore platforms. The maximum working pressure range in offshore fire water systems is 3 MPa and the fatigue strengths of pipes and joints tested were greater than 7.5 MPa, i.e., 2.5 times the working pressure, over a test period of 20,000 cycles.

For the GRE pipes and joints reported in Chapter 5, the coupler joint showed a good strength which was almost as high as that of the plain pipes. Socket/spigot joints, however, gave lower strength due to local bending at the socket bottom. Therefore, the coupler is a good fitting for joining pipes not only because of its high strength but also for its ease and conveniences of installation.

The vinyl ester based pipes described in Chapter 6 showed comparable strengths to GRE pipes, although both types of joints gave lower strengths than GRVE plain pipes. Therefore, GRVE pipes should be used in the offshore industry since they are more economical. However, the two types of joints tested may need to be modified to achieve higher strength.

Failure Modes

Matrix cracking is the main failure mode of the GRP pipes subjected to internal pressure. As cracks initiated and propagated in the resin matrix and resin liner, sea water seeped through the

pipe wall and the system pressure was released. In general, when water weepage occurred, none of the fibres were broken.

For the GRE pipe joints tested, the coupler connected joint had a strong bonding interface and the coupler had superior strength. The socket/spigot bonded joint also had strong bonding but the bending moment at the bottom of the socket caused it to have a lower strength than the coupler-connected joint.

In the tests of GRVE pipe joints, both types failed at the joints. The laminated joint failed due to the failure of the laminate strap, whereas the socket/spigot joint failed by bonding adhesive failure. Water weepage occurred through the laminated strap or adhesive interface. Both designs may need to be modified simply by increasing the laminate thickness and overlap length.

Burst Tests

The burst tests involving the insertion of extra rubber liners gave the burst strength which reflected fibre breakage in the pipe wall. Although the burst strength was not the real strength of the pipe, it represented the potential or upper bound of the pipe strength which could be achieved by using a pipe liner with a high failure strain.

(III) Numerical Work

The finite element method is a power mathematical tool for the analysis of complex composite structures. Numerical models using 20-node composite laminate elements and 20-node brick elements have successfully simulated GRP pipes and joints.

(IV) Offshore Application

The cost effective GRP materials are attractive for offshore applications. From the fatigue tests described in this thesis, the GRP pipes and joints have sufficient fatigue strength for them to be used in the fire water systems of offshore platforms. Parallel projects are investigating their fire performance, impact properties, resistance to environmental exposure and so on. It is optimistic that GRP pipes will be used widely on offshore platforms in the future.

Suggestions for Future Work

As this work was restricted to 50 mm diameter pipes, the results obtained and the corresponding conclusions drawn can only be applied to small diameter pipe systems. The fatigue performance of bigger pipes needs to be examined.

As only a small number of types of joints have been investigated, further work is required on other types of joints, such as flanged joints, mechanical O-ring and key-lock joints, and other commonly used fittings, such as elbows and tees.

Only internal pressure load was considered in the current work. In certain conditions, however, bending moment and axial load are also important for fire pipes. Temperature variations during day and night may also introduce significant stresses. Further research is therefore required under more complex and severe loading and environmental conditions.

APPENDIX A :

A FORTRAN PROGRAM FOR CALCULATING THREE DIMENSIONAL ELASTIC CONSTANTS OF A LAMINATE

```
c--- Filename e3-lam.f
c--- A Fortran program for calculating three dimensional elastic
c---                    constants for multi-directional composites.
c--- 20/02/1996  -- by F.Z.Hu
c---
          dimension sd(6,6),qd(6,6),td(6,6),hd(6,6)
          dimension bq1(6,6),bq(6,6),bs(6,6),hwork(6)
          dimension h(200),ang(200)
          open(1,file='e3-out.dat',status='unknown')
c---
1         write(*,*)' Options for calculation : 1 --- from Ef,vf,Em,vm,Rf'
          write(*,*)'                                   (fibres and matrix)'
          write(*,*)'                           2 --- from UD lamina'
          read(*,*)index
          if(index.ne.1.and.index.ne.2)goto 1
          if(index.eq.2) goto 5
c---
c--- (1)calculate E1,E2,E3,G12,G13,G23,v12,v13,v23 ... from Ef,Em,vf,vm,Vf
c--- Ref. C.S.Smith, Design of Marine Structures in Composite Materials
c---          (pp.51-52,57-58)
c---    for unidirectional composites
c---
          write(*,*)' Fibre Youngs modulus :   Ef=?'
          read(*,*)ef
          write(*,*)' Fibre Poissons ratio :       vf=?'
          read(*,*)vf
          write(*,*)' Matrix Youngs modulus:  Em=?'
          read(*,*)em
          write(*,*)' Matrix Poissons ratio:       vm=?'
          read(*,*)vm
          write(*,*)' Fibre volume fraction:       Rf=?'
          read(*,*)rf
c--- Default input value
c--- (for E-Glass/Epoxy)
c         ef=76000.
c         em=3400.
c         vf=0.2
c         vm=0.4
c         rf=0.5
c--- (for E-Glass/Vinyl ester)
c         ef=76000.
c         em=3400.
c         vf=0.2
c         vm=0.4
c         rf=0.5
c--- (for T300/Epoxy)
c         ef=228000.
c         em=3400.
c         vf=0.2
c         vm=0.4
c         rf=0.65
c--- (for carbon/epoxy, TOHO BESLON HTA/913C CIBA-GEIGY )
c         ef=238000.
```

```
c       em=3390.
c       vf=0.33
c       vm=0.37
c       rf=0.60
c---
        gf=ef/(1.+vf)/2.
        gm=em/(1.+vm)/2.
c---
        e1=ef*rf+em*(1.-rf)
        v12=vf*rf+vm*(1.-rf)
c
        cs=0.2
        ata=(ef/em-1.)/(ef/em+cs)
        e2=em*(1.+cs*ata*rf)/(1.-ata*rf)
c
        cs=1.
        ata=(gf/gm-1.)/(gf/gm+cs)
        g12=gm*(1.+cs*ata*rf)/(1.-ata*rf)
c
        e3=e2
c
        akm=em/2./(1.-vm-2.*vm*vm)
        cs=(akm/gm)/(akm/gm+2.)
        ata=(gf/gm-1.)/(gf/gm+cs)
        g23=gm*(1.+cs*ata*rf)/(1.-ata*rf)
c
        g13=g12
        g31=g13
c
        v13=v12
        v21=v12*(e2/e1)
        v31=v13*(e3/e1)
        v23=e3/2./g23-1.
        v32=v23
c---
        write(1,*)' e1=',e1
        write(1,*)' e2=',e2
        write(1,*)' e3=',e3
        write(1,*)' g12=',g12
        write(1,*)' g13=',g13
        write(1,*)' g23=',g23
        write(1,*)' v12=',v12
        write(1,*)' v21=',v21
        write(1,*)' v13=',v13
        write(1,*)' v23=',v23
c
        write(*,*)' e1=',e1
        write(*,*)' e2=',e2
        write(*,*)' e3=',e3
        write(*,*)' g12=',g12
        write(*,*)' g13=',g13
        write(*,*)' g23=',g23
        write(*,*)' v12=',v12
        write(*,*)' v21=',v21
        write(*,*)' v13=',v13
        write(*,*)' v23=',v23
c---
        goto 6
c---
```

```
5       continue
        write(*,*)' E1  of UD lamina :  E1=?'
        read(*,*)e1
        write(*,*)' E2  of UD lamina :  E2=?'
        read(*,*)e2
        write(*,*)' G12 of UD lamina :  G12=?'
        read(*,*)g12
        write(*,*)' v12 of UD lamina :  v12=?'
        read(*,*)v12
        write(*,*)' G23 of UD lamina :  G23=?(0 for default 0.9G12)'
        read(*,*)g23
        write(*,*)' v23 of UD lamina :  v23=?(0 for default e3/2./g23-1)'
        read(*,*)v23
c---
        v21=v12*(e2/e1)
        e3=e2
        g13=g12
        g21=g12
        g31=g13
        v13=v12
        if(g23.eq.0.)g23=g12*0.9
        g32=g23
        if(v23.eq.0.)v23=e3/2./g23-1.
        v32=v23
        v31=v13*(e3/e1)
6       continue
c---
c--- (2)calculate Ex,Ey,Ez,vxy,vxz,vyz,Gxy,Gxz,Gyz for laminates with
c---    various lay-ups. (Laminate Theory).
c---    transformation of materials parameters to rotatation x-direction.
c---
7       write(*,*)' Total number of plies : Nt=?'
        read(*,*)nt
         if(nt.lt.1.or.nt.gt.200)then
          write(*,*)' Unreasonable --- Nt- ! Re-entry!'
          goto 7
         endif
        do ii=1,nt
         write(*,*)'   Angle for ply no. ',ii,' :'
         read(*,*)ang(ii)
         write(*,*)'   Thickness for ply no. ',ii,' :'
         read(*,*)h(ii)
        end do
c---
c---[S(6,6)]---
        do 10 i=1,6
        do 10 j=1,6
          td(i,j)=0.
          sd(i,j)=0.
10    qd(i,j)=0.
          sd(1,1)=1./e1
          sd(2,2)=1./e2
          sd(3,3)=1./e3
          sd(1,2)=-1.*v12/e1
          sd(1,3)=-1.*v13/e1
          sd(2,3)=-1.*v23/e2
          sd(2,1)=-1.*v12/e1
          sd(3,1)=-1.*v13/e1
          sd(3,2)=-1.*v23/e2
```

```
            sd(4,4)=1./g12
            sd(5,5)=1./g23
            sd(6,6)=1./g31
            write(1,11)((sd(i,j),j=1,6),i=1,6)
11          format(' ----sd(6,6)----'/,(6e12.4))

c---[Q(6,6)]---
            ddd=(1.-v12*v21-v23*v32-v31*v13-2.*v21*v32*v13)
            ddd=ddd/(e1*e2*e3)
c---
            qd(1,1)=(1.-v23*v32)/(ddd*e2*e3)
            qd(2,2)=(1.-v13*v31)/(ddd*e1*e3)
            qd(3,3)=(1.-v12*v21)/(ddd*e1*e2)
            qd(2,1)=(v21+v31*v23)/(ddd*e2*e3)
            qd(1,2)=(v12+v32*v13)/(ddd*e1*e2)
            qd(3,1)=(v31+v21*v32)/(ddd*e2*e3)
            qd(1,3)=(v13+v12*v23)/(ddd*e1*e2)
            qd(3,2)=(v32+v12*v31)/(ddd*e1*e3)
            qd(2,3)=(v23+v21*v13)/(ddd*e1*e2)
            qd(4,4)=g12
            qd(5,5)=g23
            qd(6,6)=g31
c
            write(*,12)((qd(i,j),j=1,6),i=1,6)
12          format(' ----qd(6,6)----'/,(6e12.4))
c--- Checking [S][Q]=[I] ?
            do 14 i=1,6
            do 14 j=1,6
            hd(i,j)=0.
            do 13 k=1,6
13          hd(i,j)=hd(i,j)+sd(i,k)*qd(k,j)
14          continue
            write(*,15)((hd(i,j),j=1,6),i=1,6)
15          format(' ----hd(6,6)----'/,(6e12.4))
            do 16 i=1,6
            if(abs(hd(i,i)-1.).gt.1.e-2) stop 1111
            do 16 j=1,6
            if(i.eq.j)goto 16
            if(abs(hd(i,j)).gt.1.e-2) stop 2222
16          continue

c---
c---[Q'(6,6)] for the entire laminates
            do 17 i=1,6
            do 17 j=1,6
17          bq(i,j)=0.0
            hh=0.
c---
            do 1000 kply=1,nt
c
c---[T(6,6)] & [Q1'(6,6)] for each ply
            do 18 i=1,6
            do 18 j=1,6
            td(i,j)=0.0
18          bq1(i,j)=0.0
c
            fi=ang(kply)
            sita=-1.*fi*3.1415926/180.
            am=cos(sita)
```

```
      an=sin(sita)
      td(1,1)=am*am
      td(2,2)=am*am
      td(1,2)=an*an
      td(2,1)=an*an
      td(1,4)=-2.*am*an
      td(2,4)=+2.*am*an
      td(4,1)=+1.*am*an
      td(4,2)=-1.*am*an
      td(4,4)=am*am-an*an
      td(3,3)=1.
      td(5,5)=am
      td(6,6)=am
      td(5,6)=+1.*an
      td(6,5)=-1.*an
c---
      do 21 i=1,6
      do 21 j=1,6
      hd(i,j)=0.
      do 20 k=1,6
20    hd(i,j)=hd(i,j)+qd(i,k)*td(j,k)
21    continue
      do 23 i=1,6
      do 23 j=1,6
      bq1(i,j)=0.
      do 22 k=1,6
22    bq1(i,j)=bq1(i,j)+td(i,k)*hd(k,j)
23    continue
      write(1,25)((bq1(i,j),j=1,6),i=1,6)
25    format(' ----bq1(6,6)----'/,(6e12.4))
c--- [Q'(6,6)]---
      do 37 i=1,6
      do 37 j=1,6
37    bq(i,j)=bq(i,j)+bq1(i,j)*h(kply)
c
      hh=hh+h(kply)
1000  continue
c-----------------[Q] for laminate -------------------------
      do 38 i=1,6
      do 38 j=1,6
38    bq(i,j)=bq(i,j)/hh
c
      write(1,39)((bq(i,j),j=1,6),i=1,6)
      write(*,39)((bq(i,j),j=1,6),i=1,6)
39    format(' --[Q`]--bq(6,6)----'/,(6e12.4))
c-----------------[S] for laminate -------------------------
      do i=1,6
       do j=1,6
        bs(i,j)=bq(i,j)
       enddo
      enddo
      n=6
      call SGJ1(n,bs,hwork,fail)
      if(fail.eq.1)then
        write(*,*)'***failed to obtain inverse matrix of [Q]'
      endif
      write(1,40)((bs(i,j),j=1,6),i=1,6)
      write(*,40)((bs(i,j),j=1,6),i=1,6)
```

```
40      format(' ----[S(6,6)]----'/,(6e12.4))
c---check [S']][Q']=[I] ?
        do 44 i=1,6
        do 44 j=1,6
        hd(i,j)=0.
        do 43 k=1,6
43      hd(i,j)=hd(i,j)+bs(i,k)*bq(k,j)
44      continue
        write(1,45)((hd(i,j),j=1,6),i=1,6)
45      format(' ----hd(6,6)----'/,(6e12.4))
        do 46 i=1,6
        if(abs(hd(i,i)-1.).gt.1.e-2)stop 3333
        do 46 j=1,6
        if(i.eq.j)goto 46
        if(abs(hd(i,j)).gt.1.e-2) stop 4444
46      continue
c----------Elastic constants for multi-directional laminate ----------
        gxy=1./bs(4,4)
        gyz=1./bs(5,5)
        gxz=1./bs(6,6)
        ex=1./bs(1,1)
        ey=1./bs(2,2)
        ez=1./bs(3,3)
        vxy=-1.*bs(1,2)/bs(1,1)
        vxz=-1.*bs(1,3)/bs(1,1)
        vyz=-1.*bs(2,3)/bs(2,2)
        vyx=ey*vxy/ex
c---
        do 47 i=1,6
        write(*,48) (bq(i,j),j=1,i)
        write(1,48) (bq(i,j),j=1,i)
47      continue
48      format(6f11.1)
        write(1,*)' Ex=',ex
        write(1,*)' Ey=',ey
        write(1,*)' Ez=',ez
        write(1,*)' vxy=',vxy
        write(1,*)' vyx=',vyx
        write(1,*)' vxz=',vxz
        write(1,*)' vyz=',vyz
        write(1,*)' Gxy=',gxy
        write(1,*)' Gyz=',gyz
        write(1,*)' Gxz=',gxz
c---
        write(*,*)' Ex=',ex
        write(*,*)' Ey=',ey
        write(*,*)' Ez=',ez
        write(*,*)' vxy=',vxy
        write(*,*)' vyx=',vyx
        write(*,*)' vxz=',vxz
        write(*,*)' vyz=',vyz
        write(*,*)' Gxy=',gxy
        write(*,*)' Gyz=',gyz
        write(*,*)' Gxz=',gxz
c---
        stop
        end
```

```
C--- INVERSE MATRIX OF A(N,N)--------
C--- OUTPUT: FAIL=0 --- SUCESSFUL;
C---        FAIL=1 --- FAILED
C---
          SUBROUTINE SGJ1(N,A,H,FAIL)
          DIMENSION A(N,N),H(N)
          M=-1
          DO 103 K=N,1,M
          P=A(1,1)
          IF(P.LE.0.0) GOTO 105
          DO 102 I=2,N
          Q=A(I,1)
          IF(I.LE.K)GOTO 100
          H(I)=Q/P
          GOTO 101
100       H(I)=-Q/P
101       DO 102 J=2,I
          A(I-1,J-1)=A(I,J)+Q*H(J)
102       CONTINUE
          A(N,N)=1/P
          DO 103 I=2,N
          A(N,I-1)=H(I)
103       CONTINUE
          DO 104 I=1,N-1
          DO 104 J=I+1,N
104       A(I,J)=A(J,I)
          FAIL=0
          RETURN
105       FAIL=1
          RETURN
          END
```

APPENDIX B :

EQUATIONS FOR ESTIMATING ELASTIC PROPERTIES OF UNIDIRECTIONAL LAMINA

The elastic constants for the components of the lamina are assumed as,

Young's modulus of fibres: E_f
Poisson's ratio of fibres: ν_f
Shear modulus of fibres: $G_f = E_f/[2(1+\nu_f)]$

Young's modulus of matrix: E_m
Poisson's ratio of matrix: ν_m
Shear modulus of matrix: $G_m = E_m/[2(1+\nu_m)]$

Considering a unidirectional composite lamina with a fibre volume fraction V_f, its elastic constants in the principal material directions can be estimated by ,

$$E_1 = E_f V_f + E_m(1-V_f)$$

$$\nu_{12} = \nu_f V_f + \nu_m(1-V_f)$$

$$E_2 = E_m \bullet \frac{1+\xi\eta V_f}{1-\eta V_f} \quad \text{where} \quad \eta = \frac{E_f/E_m - 1}{E_f/E_m + \xi} \quad , \quad \xi = 0.2$$

$$G_{12} = G_m \bullet \frac{1+\xi^*\eta^* V_f}{1-\eta^* V_f} \quad \text{where} \quad \eta^* = \frac{G_f/G_m - 1}{G_f/G_m + \xi^*} \quad , \quad \xi^* = 1.$$

$$\nu_{21} = \nu_{12} \bullet \frac{E_2}{E_1}$$

and its through thickness properties by,

$$E_3 = E_2$$

$$G_{23} = G_m \bullet \frac{1+\xi^{**}\eta^{**} V_f}{1-\eta^{**} V_f} \quad \text{where} \quad \eta^{**} = \frac{G_f/G_m - 1}{G_f/G_m + \xi^{**}} \quad ,$$

$$\xi^{**} = \frac{k_m}{G_m}\Big/\left(\frac{k_m}{G_m} + 2\right), \quad \text{and} \quad k_m = \frac{E_m}{2(1-\nu_m - 2\nu_m^2)}$$

$$G_{13} = G_{12}$$

$$\nu_{13} = \nu_{12}$$

$$\nu_{23} = \frac{E_3}{2G_{23}} - 1$$

$$\nu_{32} = \nu_{23}$$

APPENDIX C :

EQUATIONS FOR CALCULATING ELASTIC CONSTANTS OF MULTI-DIRECTIONAL LAMINATES

C1. Stress - Strain Relations of UD Lamina

Let the stress and strain vectors in the principal directions of a laminate,

$$\sigma = \{ \sigma_1, \sigma_2, \sigma_3, \tau_{12}, \tau_{23}, \tau_{31} \}^t$$

$$\varepsilon = \{ \varepsilon_1, \varepsilon_2, \varepsilon_3, \gamma_{12}, \gamma_{23}, \gamma_{31} \}^t$$

The stress - strain relations based on the Hooke's law are,

$$\varepsilon = S\,\sigma \qquad \text{or} \qquad \sigma = Q\,\varepsilon$$

where the coefficient matrices are,

$$S = \begin{bmatrix} \frac{1}{E_1} & \frac{-\nu_{21}}{E_2} & \frac{-\nu_{31}}{E_3} & & & \\ \frac{-\nu_{12}}{E_1} & \frac{1}{E_2} & \frac{-\nu_{32}}{E_3} & & & \\ \frac{-\nu_{13}}{E_1} & \frac{-\nu_{23}}{E_2} & \frac{1}{E_3} & & & \\ & & & \frac{1}{G_{12}} & & \\ & & & & \frac{1}{G_{23}} & \\ & & & & & \frac{1}{G_{31}} \end{bmatrix}$$

$$Q = \begin{bmatrix} Q_{11} & Q_{12} & Q_{13} & & & \\ Q_{21} & Q_{22} & Q_{11} & & & \\ Q_{31} & Q_{11} & Q_{33} & & & \\ & & & Q_{44} & & \\ & & & & Q_{55} & \\ & & & & & Q_{66} \end{bmatrix}$$

where E_1 , E_2 , ... are the elastic constants of the UD lamina.

$$Q_{11} = (1 - \nu_{23}\nu_{32}) / \Lambda E_1 E_2$$
$$Q_{22} = (1 - \nu_{13}\nu_{31}) / \Lambda E_1 E_3$$
$$Q_{33} = (1 - \nu_{12}\nu_{21}) / \Lambda E_1 E_2$$
$$Q_{12} = Q_{21} = (\nu_{12} + \nu_{32}\nu_{13}) / \Lambda E_1 E_2 = (\nu_{21} + \nu_{31}\nu_{23}) / \Lambda E_2 E_3$$
$$Q_{23} = Q_{32} = (\nu_{23} + \nu_{21}\nu_{13}) / \Lambda E_1 E_2 = (\nu_{32} + \nu_{12}\nu_{31}) / \Lambda E_1 E_3$$
$$Q_{13} = Q_{31} = (\nu_{13} + \nu_{12}\nu_{23}) / \Lambda E_1 E_2 = (\nu_{31} + \nu_{21}\nu_{32}) / \Lambda E_2 E_3$$
$$Q_{44} = G_{12}$$
$$Q_{55} = G_{23}$$
$$Q_{66} = G_{13}$$
$$\Lambda = (1 - \nu_{12}\nu_{21} - \nu_{23}\nu_{32} - \nu_{31}\nu_{13} - 2\nu_{21}\nu_{32}\nu_{13}) / E_1 E_2 E_3$$

Generally, S and Q are symmetrical, *i.e.*

$$\frac{\nu_{ij}}{E_i} = \frac{\nu_{ji}}{E_j} \qquad (i, j = 1,2,3)$$

Assuming the principal coordinate system 0-123 rotates an angle φ around axis 0-3, we get another coordidate system 0-1'2'3. The stress - strain relations in coordinate system 0-1'2'3 are

$$\varepsilon' = S'\,\sigma' \qquad or \qquad \sigma' = Q'\,\varepsilon'$$

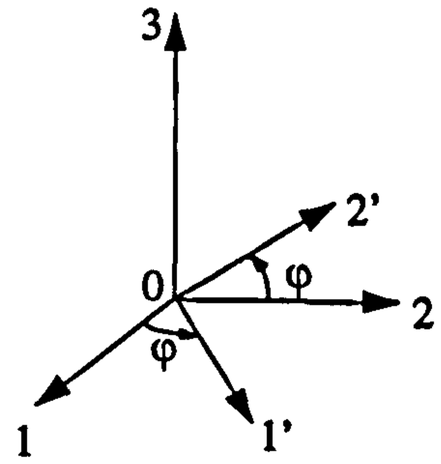

where the coefficient matrix ,

$$Q' = T\,Q\,T^t \qquad \text{(C1)}$$

$$T = \begin{bmatrix} m^2 & n^2 & & -2mn & & \\ n^2 & m^2 & & 2mn & & \\ & & 1 & & & \\ mn & -mn & & m & n & \\ & & & -n & m & \\ & & & & & m^2 - n^2 \end{bmatrix}$$

$m = cos\varphi$ and $n = -sin\varphi$

C2. Elastic Constants of Multi-Directional Laminates

For a laminate system [$\varphi_1/\varphi_2/\ldots\ \ldots/\varphi_n$] in which ply thickness is $t_1, t_2, \ldots\ \ldots, t_n$, the elastic coefficient matrix is,

$$Q' = \frac{1}{\sum_{i=1}^{n} t_i}(Q'_1 t_1 + Q'_2 t_2 + \ldots\ \ldots + Q'_n t_n) \qquad \text{(C2)}$$

where $Q'_1, Q'_2, \ldots\ \ldots, Q'_n$ can be obtained by substituting $\varphi_1, \varphi_2, \ldots\ \ldots, \varphi_n$ into equation (C1). And,

$$S' = [\,Q'\,]^{-1}$$

The engineering elastic constants,

$$E'_1 = 1/S'_{11} \qquad E'_2 = 1/S'_{22} \qquad E'_3 = 1/S'_{33}$$

$$G'_{12} = 1/S'_{44} \qquad G'_{23} = 1/S'_{55} \qquad G'_{31} = 1/S'_{66}$$

$$\nu'_{23} = -S'_{23}/S'_{22} \qquad \nu'_{31} = -S'_{31}/S'_{33} \qquad \nu'_{12} = -S'_{12}/S'_{11}$$

APPENDIX D:

LINEAR REGRESSION AND CONFIDENCE LIMITS

(Ref. ASTM Standard D2992, Standard method for obtaining hydraulic design basis for reinforced thermosetting resin pipe and fittings.)

D1. Method of Least Squares

The following symbols are used:

n	number of points on the plot of stress (or strain) versus cycles to failure;
f	stress or strain;
h	logarithm of cycles to failure;
F	arithmetic average of all f values;
H	arithmetic average of all h values.

By definition,

$$H = \frac{1}{n}\sum h$$
$$F = \frac{1}{n}\sum f \qquad \text{(D1)}$$

Fatigue test points are fitted by the following linear equation,

$$h = a + b(f\text{-}F) \qquad \text{(D2)}$$

where the parameter a and b are determined by the least squares calculation.

Let

$$\psi = \sum\left[h - a - b(f - H)\right]^2. \qquad \text{(D3)}$$

The above function can be rewritten as,

$$\psi = (V - \frac{W^2}{U}) + n(a - H)^2 + U(b - \frac{W}{U})^2 \qquad \text{(D4)}$$

where

$$U = \sum(f - F)^2 = \sum f^2 - nF^2$$
$$V = \sum(h - H)^2 = \sum h^2 - nH^2 \qquad \text{(D5)}$$
$$W = \sum(f - F)(h - H) = \sum fh - nFH$$

From Eq.(D4), ψ has the minimum when

$$a = H$$
$$b = W/U \qquad \text{(D6)}$$

Therefore, Eq.(D2) is the straight line which has the minimum total of the squares of errors with experimental data. If b is positive, the experimental data are unsuitable for evaluating the materials.

D2. Lower Confidence Limit of Fatigue Strength

Consider an assigned value for h, for example, h=4.3010, corresponding to a fatigue life of 20,000 cycles. Denote it by h_o. The problem is to evaluate the uncertainty of the corresponding value of f_o. The value f_o is evaluated by the Eq.(D2), i.e.,

$$f_o = F + (h_o - a)/b \tag{D7}$$

The lower confidence value of stress at h_o is given by, (See D4.)

$$f_{o,LowerLimit} = F + L_{LowerLimit} \tag{D8}$$

where

$$L_{LowerLimit} = \left[bD - ts\sqrt{(D^2/U) + (M/n)}\right]\Big/M \tag{D9}$$

$$D = h_o - H$$

t is the critical value of Student's t-distribution with (n-2) degrees of freedom and for the chosen level of significance. (The statistical table of Student's t-distribution at two-sided 5% level of significance is given in Section D5.)

$$s = \sqrt{\frac{1}{n-2}[V - W^2/U]}$$

$$M = b^2 - (t^2 s^2/U)$$

At two-sided 5% level of significance, 97.5% of the expected failures at h_o will be above the lower confidence limit of $f_{o,Lower\ Limit}$.

D3. Upper Confidence Limit of Fatigue Strength

The upper confidence value of stress at h_o is given by, (See D4.)

$$f_{o,UpperLimit} = F + L_{UpperLimit} \tag{D10}$$

where

$$L_{UpperLimit} = \left[bD + ts\sqrt{(D^2/U) + (M/n)}\right]\Big/M \tag{D11}$$

At two-sided 5% level of significance, 97.5% of the expected failures at h_o will be below the lower confidence limit of $f_{o,Lower\ Limit}$ and 95% will be between the lower and upper limits.

D4. Derivation of Formulas*

(* More details can be found in, [1].BS3518, Part 5: Guide to the Application of Statistics. [2] ASTM D2992: Standard Method for Obtaining Hydraulic Design Basis for Reinforced Thermosetting Resin Pipe and Fittings. [3] B.W.Lindgrem, Statistical Theory, 4th Ed., Chapman&Hall, 1993.)

Consider an assigned value of h, denoting as h_o. The problem is to evaluate the uncertainty of the corresponding value of f_o. The value f_o is evaluated by the Eq.(D2),

$$b(f_o - F) = h_o - H \tag{D12}$$

Let

$$z = b(f_o - F) - (h_o - H) \tag{D13}$$

Then the expected value of z is zero because of Eq.(D12) i.e.

$$E(z)=0 \tag{D14}$$

and the variance of z, $Var(z)$, is given by,

$$Var(z)=(f_o\text{-}F)^2 V(b)+V(H) \tag{D15}$$

By least squares theory we know that:

$$Var(H) = \sigma^2 / n \tag{D16}$$

and

$$Var(b) = \sigma^2 / U \tag{D17}$$

where σ^2 is the variance of the error in the determination of any single h value.

Introducing Eq.(D16) and (D17) into (D15), we have

$$Var(z) = \sigma^2\left[(f_o - F)^2 / U + 1/n\right] \tag{D18}$$

The estimate for σ^2 is:

$$s^2 = \frac{1}{n-2}\left[V - W^2 / U\right] \tag{D19}$$

and is evaluated with (n-2) degrees of freedom.

Consequently, an estimate for $Var(z)$ is given by:

$$\begin{aligned}\hat{V}ar(z) &= s^2\left[(f_o - F)^2 / U + 1/n\right] \\ &= \frac{1}{n-2}\left[V - W^2 / U\right]\left[(f_o - F)^2 / U + 1/n\right]\end{aligned} \tag{D20}$$

and the estimated standard deviation of z is:

$$s_z = s\sqrt{(f_o - F)^2 / U + 1/n} \tag{D21}$$

The quantity $[z\text{-}E(z)]/s_z$ has Student's t-distribution with $(n\text{-}2)$ degrees of freedom. The statistical table of Student's t-distribution at two-sided 5% level of significance is given in Section A5. Let t denote the critical value of Student's t for (n-2) degrees of freedom and for the chosen level of significance, α. Then the following inequity hold with probability equal to the applicable confidence coefficient, $(1\text{-}\alpha)$:

$$-t \le [z - E(z)]/s_z \le +t \tag{D22}$$

which is equivalent to:

$$[z - E(z)]^2 / \hat{V}ar(z) \le t^2 \tag{D23}$$

The limits of this interval are given by:

$$[z - E(z)]^2 = t^2 \hat{V}ar(z) \tag{D24}$$

which, in view of Eq.(D14) and (D20), becomes:

$$z^2 = t^2 s^2 \left[(f_o - F)^2 / U + 1/n \right] \tag{D25}$$

Introducing Eq.(D13), Eq.(D25) can be written:

$$\left[b(f_o - F) - (h_o - H) \right]^2 = t^2 s^2 \left[(f_o - F)^2 / U + 1/n \right] \tag{D26}$$

Writing

$$L = f_o - F \tag{D27}$$

$$D = h_o - H \tag{D28}$$

and solving Eq.(D26) for L, we obtain:

$$L = \frac{bD \pm ts\sqrt{\left[b^2 - (t^2 s^2 / U) \right]/n + (D^2 / U)}}{b^2 - (t^2 s^2 / U)} \tag{D29}$$

Let

$$M = b^2 - (t^2 s^2 / U) \tag{D30}$$

Then, the lower limit for L is given by:

$$L_{LowerLimit} = \left[bD - ts\sqrt{(D^2 / U) + (M/n)} \right] / M \tag{D31}$$

and the upper limit:

$$L_{UpperLimit} = \left[bD + ts\sqrt{(D^2 / U) + (M/n)} \right] / M \tag{D32}$$

Consequently, in view of Eq.(D27), the lower limit for f_o is:

$$f_{o,LowerLimit} = F + \left[bD - ts\sqrt{(D^2 / U) + (M/n)} \right] / M \tag{D33}$$

and the upper limit:

$$f_{o,UpperLimit} = F + \left[bD + ts\sqrt{(D^2 / U) + (M/n)} \right] / M \tag{D34}$$

D5. Statistical Table of Student's *t*-Distribution

Degrees of Freedom, n-2	Student's "*t*"[A]	Degrees of Freedom, n-2	Student's "*t*"[A]	Degrees of Freedom, n-2	Student's "*t*"[A]
1	12.7062	46	2.0129	91	1.9864
2	4.3027	47	2.0117	92	1.9861
3	3.1824	48	2.0106	93	1.9858
4	2.7764	49	2.0096	94	1.9855
5	2.5706	50	2.0086	95	1.9853
6	2.4469	51	2.0076	96	1.9850
7	2.3646	52	2.0066	97	1.9847
8	2.3060	53	2.0057	98	1.9845
9	2.2622	54	2.0049	99	1.9842
10	2.2281	55	2.0040	100	1.9840
11	2.2010	56	2.0032	102	1.9835
12	2.1788	57	2.0025	104	1.9830
13	2.1604	58	2.0017	106	1.9826
14	2.1448	59	2.0010	108	1.9822
15	2.1315	60	2.0003	110	1.9818
16	2.1199	61	1.9996	112	1.9814
17	2.1098	62	1.9990	114	1.9810
18	2.1009	63	1.9983	116	1.9806
19	2.0930	64	1.9977	118	1.9803
20	2.0860	65	1.9971	120	1.9799
21	2.0796	66	1.9966	122	1.9796
22	2.0739	67	1.0060	124	1.9793
23	2.0687	68	1.9955	126	1.9790
24	2.0639	69	1.9949	128	1.9787
25	2.0595	70	1.9944	130	1.9784
26	2.0555	71	1.9939	132	1.9781
27	2.0518	72	1.9935	134	1.9778
28	2.0484	73	1.9930	136	1.9776
29	2.0452	74	1.9925	138	1.9773
30	2.0423	75	1.9921	140	1.9771
31	2.0395	76	1.9917	142	1.9768
32	2.0369	77	1.9913	144	1.9766
33	2.0345	78	1.9908	146	1.9763
34	2.0322	79	1.9905	148	1.9761
35	2.0301	80	1.9901	150	1.9759
36	2.0281	81	1.9897	200	1.9719
37	2.0262	82	1.9893	300	1.9679
38	2.0244	83	1.9890	400	1.9659
39	2.0227	84	1.9886	500	1.9647
40	2.0211	85	1.9883	600	1.9639
41	2.0195	86	1.9879	700	1.9634
42	2.0181	87	1.9876	800	1.9629
43	2.0167	88	1.9873	900	1.9626
44	2.0154	89	1.9870	1000	1.9623
45	2.0141	90	1.9867	∝	1.9600

[A] Two-sided 5% level of significance.